SITE C CLEAN ENERGY PROJECT

VOLUME 2 APPENDIX K

TECHNICAL DATA REPORT: MICROCLIMATE

FINAL REPORT

Prepared for:

BC Hydro Power and Authority
333 Dunsmuir Street
Vancouver, BC
V6B 5R3

Prepared by:

RWDI AIR Inc.
830 – 999 West Broadway
Vancouver, BC
V5Z 1K5
Tel: (604) 730-5688 Fax: (604) 730-2915

December 2012

Document Number 06-110

CONSULTING ENGINEERS
& SCIENTISTS

Prepared for BC Hydro Power and Authority

SITE C CLEAN ENERGY PROJECT

TECHNICAL DATA REPORT: MICROCLIMATE

FINAL REPORT

Prepared by RWDI AIR Inc.

December 2012

Lead Author: Jeff Lundgren, M.Sc., Technical Director

Section Contributors: Christian Reuten, Ph.D., Senior Engineer/Scientist

Andres Soux, M.Sc., Senior Engineer/Scientist

EXECUTIVE SUMMARY

The purpose of the microclimate modelling study was to evaluate quantitatively how the construction of the proposed Site C dam and formation of the reservoir might influence the local and regional microclimate. To quantify potential changes in microclimate induced by the potential Site C reservoir formation, RWDI examined two model scenarios, the existing Baseline Case and a Future Case with the Project, using the Weather Research and Forecasting (WRF) numerical meteorological model. The WRF model combines large-scale weather information and geophysical description of the Earth's surface to simulate local-scale meteorology. By running the model for periods of a year or longer one can develop monthly, seasonal and annual average estimates of the average meteorological conditions and hence climate of a given region. The results of the model study allow site-specific estimates of changes in local microclimate well in advance of actual construction.

The region around Fort St. John experiences a continental subarctic climate characterized by long, cold and dry winters with short, mild summers. Normal daily average temperatures range from -14.2 °C in January to 15.7 °C in July with normal total annual precipitation totalling 465 millimetres, of which 65% falls between May and September.

Long-term climate information is available from a station located at the Fort St. John Airport. This station has been in operation since 1942 and is run by Environment Canada. Climate normals from 1971 through 2000, the most recent 30-year period for which Environment Canada has published them, were reviewed. In addition, the standard deviations of these normals were calculated to evaluate annual and monthly climate variability. Over the length of record there was a 1.5 °C increase in mean annual temperature. The record shows no change in mean annual total precipitation. The trend for wind speed shows a decrease over the period of record of approximately 6 km/h, while the trend for relative humidity also shows a decrease over the same time period of approximately 7%.

The technical study area covered the Peace River valley upstream of Hudson's Hope to downstream of Taylor, including the predicted extent of the reservoir and Fort St. John Airport. This length of the study area included a rectangular buffer, with outer boundaries between 10 and 20 km away from the proposed reservoir's water surface. The area measured 108 km east to west by 68 km north to south, corresponding to a 108 x 68 km WRF model grid..

To support an evaluation of the microclimate within the Technical Study Area, BC Hydro installed a network of seven climate stations in the Peace River Valley between Hudson's Hope and the future dam site. These stations measure a range of climate parameters and were installed across a number of different geographical settings (such as grassland, agricultural), different elevations and different distances from the future reservoir shore. The first full year of climate measurements at all stations was completed in January 2012. This first year of record was warmer, wetter and had higher wind speeds than a normal year as measured at Fort St. John Airport. There were small differences in temperature between stations and wind speed and direction were influenced by local topography.

Potential future microclimate changes were simulated using the WRF model. The model was run for a one year period from October 2004 through September 2005. This model year was chosen by selecting a recent consecutive 12-month period that was considered hydrologically normal in terms of water flows and comparing the chosen period with 30 year climate normals. A statistical comparison of the model period to the historical record of meteorological observation at Fort St. John Airport confirmed that the model year was representative of typical meteorological conditions within the area.

The one kilometre domain was run in two configurations: a Baseline Case to reflect the existing river valley and a Future Case with the Project to simulate the valley after the formation of the proposed Site C reservoir. The Future Case with the Project model run was developed by editing the terrain elevation and land-cover characterization within the model to represent the changes to the physical environment that would result from reservoir formation. The temperature and ice cover of the proposed reservoir surface were included in the model simulation by incorporating outputs from the Hydrodynamics in Three Dimensions (H3D) lake circulation model that was run as part of the EIS for the proposed Site C Project (EBA 2012) into the WRF model input files.

The differences between the two model runs were used to investigate changes in meteorology and microclimate that might result from the formation of the Site C reservoir. A statistical analysis of the predicted changes was conducted to quantify the probability that the model predictions represent a statistically significant change.

To confirm the model performance, the output data from the WRF model for October 2004 through September 2005 model year were evaluated against observations at Fort St. John Airport for the same period. The model was capable of predicting observed temperature differences from the long-term climate record. The model produced wind speeds and directions similar to those observed at Fort St. John Airport. Model predicted precipitation during the 2004 – 2005 model year was closer to the long-term climate mean at Fort St. John Airport than the typical year-to-year variability observed in the long-term climate record. The WRF model is not sensitive enough to predict these small differences from the mean, but the results indicate that model predictions for precipitation were within historic norms.

To further confirm model performance, the WRF model was also run using the Baseline Case terrain elevation and land-cover characterization inputs (no reservoir) for one year from January 2011 through January 2012 corresponding to the first full year of observations from the Site C climate station network. The meteorological observations collected during the first year at the field stations located along or near the proposed reservoir were similar to the observations at Fort St. John Airport for the same period. The evaluation shows that the WRF model reproduced the monthly, seasonal and annual observations at the climate stations. Any biases in model predictions apply to both cases and cancel when the difference is calculated.

The differences between the Baseline Case and Future Case with the Project the WRF model runs were examined to evaluate local meteorological changes after the formation of the reservoir. The WRF model predicted that there would be no changes more than one kilometre

from the proposed reservoir that are statistically distinguishable from year-to-year variations. Statistically significant changes were predicted only in some sections within one kilometre of the proposed reservoir for parts of the year for temperature, wind, and humidity. In some sections along the proposed reservoir, in the fall and winter, mean-temperature changes predicted by the WRF model resulting from the presence of the reservoir and regional mean-temperature increases expected from global climate change were found to be of similar strength. At other times and elsewhere, predicted changes due to the reservoir were smaller and sometimes partly cancel regional temperature increases.

For areas within one kilometre of the reservoir, annual average temperatures were predicted to increase by a maximum of one degree Celsius. Extreme temperatures were predicted to be moderated, with warmer minimum temperatures in winter and cooler maximum temperatures in summer. Largest short-term changes in temperature were predicted in winter during periods when H3D, the lake circulation model, predicted a portion of the water surface would be ice free.

Fog frequency and density were evaluated at the locations of the seven BC Hydro Site C climate stations, Taylor Bridge, and Fort St. John Airport. The number of normal and heavy fog hours was predicted to decrease at most locations with the addition of the proposed Site C reservoir. The number of normal fog hours was predicted to decrease at five out of the nine locations, with increases at Fort St. John Airport (seven hours per year), Taylor Bridge (eight hours per year), Hudson's Hope (one hour per year), and Attachie Flat Lower Terrace (nine hours per year) locations. The number of heavy fog hours decreases at most locations except Fort St. John Airport, where an increase of six hours per year was predicted, and Taylor Bridge where an increase of 118 hours was predicted.

Mixing ratio, the mass of water vapour divided by mass of dry air in a given volume of (moist) air, at elevations above ground level was also examined as this may be of concern to some transportation activities. At all levels where data were extracted, increases or decreases predicted by the WRF model are less than 0.04 grams of water per kilogram dry air, which is less than 1% of the saturated mixing ratio and at most a few percent of typical mixing ratios at these levels. Such differences would be unobservable in measurement and therefore should not represent any meaningful change in mixing ratio.

Visibility was examined to determine the potential for change at the Fort St. John Airport as a result of the Site C reservoir. The combined total number of clear hours with visibility greater than 20 kilometres and hours with visibility 10 to 20 kilometres was predicted to be reduced by 15 hours over the year, while the number of hours with visibility in the range of one to 10 kilometres was predicted to increase by eight hours over the year. The number of poor visibility hours (less than 500 metres) was predicted to increase by six hours per year with the addition of the reservoir.

Estimate of changes in temperature were compared to expected changes due to global climate change. For most of the Technical Study Area the magnitude of predicted changes in microclimate would be statistically insignificant when compared to global climate change.

List of Acronyms

A1B ..... A particular SRES scenario
ASTER ..... Advanced Spaceborne Thermal Emission and Reflection Radiometer
BC ..... British Columbia
FYO ..... First Year of Observations
GCM ..... General Circulation Model
GDEM ..... Global Digital Elevation Model
GHG ..... Greenhouse Gas
H3D ..... Hydrodynamics in Three Dimensions
IPCC ..... Intergovernmental Panel on Climate Change
NARR ..... North American Regional Reanalysis
NCAR ..... National Center for Atmospheric Research
NCEP ..... National Centers for Environmental Prediction
MB ..... Mean Bias
MG ..... Geometric Mean Bias
RE ..... Reduction-of-Error (score)
RMSE ..... Root Mean Square Error
SRES ..... Special Report on Emissions Scenarios
RWDI ..... RWDI AIR Inc.
USGS ..... United States Geological Service
VG ..... Geometric Variance
WRF ..... Weather Research and Forecasting model
WPS ..... WRF Preprocessing System

TABLE OF CONTENTS

1.0 INTRODUCTION 1

1.1 Scope and Objectives 1

1.1.1 Objectives 1

1.1.2 Temporal Boundaries 2

1.1.3 Spatial Boundaries 2

1.2 Processes Influencing Microclimate 4

2.0 METHODOLOGY 9

2.1 Review of Existing Information 9

2.1.1 Meteorological Data Sets 9

2.1.2 Weather Research and Forecasting Model Inputs 13

2.2 Numerical Modelling Approach 13

2.3 Weather Research and Forecasting Model Methodology 14

2.3.1 Initial Conditions 15

2.3.2 Spatial Nesting 15

2.3.3 Input Data 16

2.4 Simulating Land-Cover Changes in the Weather Research and Forecasting Model 19

2.5 Incorporation of H3D Lake Circulation Model Water Temperature 19

2.6 Weather Research and Forecasting Model Outputs 27

2.6.1 Basic WRF model outputs 27

2.6.2 Fog Estimation 27

2.6.3 Visibility at Fort St. John Airport 28

2.6.4 Evaporation over Future Water Surface 29

2.7 Statistical Methods 29

2.8 Quality Assurance and Quality Control Procedures 31

3.0 EXISTING CONDITIONS 32

3.1 General Climate 32

3.1.1 Previous Studies of Climate in the Peace River Valley 32

3.1.2 General Climate of the Peace River Valley 33

3.2 Microclimate 38

3.2.1 First Year of Observations 38

3.2.2 Temperature and Wind 38
3.2.3 Precipitation 39
3.2.4 Summary 40
4.0 WEATHER RESEARCH AND FORECASTING MODEL EVALUATION 52
4.1 TEMPERATURE 53
4.1.1 Representativeness of the Baseline Period at Fort St. John Airport 53
4.1.2 Model Skill at Fort St. John Airport Relative to the Climatologic Mean 54
4.1.3 Modelling of Extremes 55
4.1.4 Model Time Series Comparisons at Fort St. John Airport 55
4.1.5 Model Skill at the Field Stations Relative to Fort St. John Airport 56
4.2 PRECIPITATION 70
4.2.1 Representativeness of the Baseline Period at Fort St. John Airport 70
4.2.2 Model Skill at Fort St. John Airport Relative to the Climatologic Mean 71
4.2.3 Model Time Series Comparisons at Fort St. John Airport 72
4.2.4 Model Skill at the Field Stations Relative to Fort St. John Airport 72
4.3 WIND 81
4.3.1 Comparisons of Model Output with Observations at Fort St. John Airport 81
4.3.2 Comparisons of Model Output with Observations at the Field Stations 82
4.4 CONCLUSIONS 86
5.0 ESTIMATED PROJECT MICROCLIMATE INFLUENCES 87
5.1 TEMPERATURE 88
5.2 PRECIPITATION 103
5.3 WIND 109
5.4 MIXING RATIO 125
5.5 FOG 136
5.6 VISIBILITY AT FORT ST. JOHN AIRPORT 140
5.7 EVAPORATION FROM PROPOSED RESERVOIR 142
6.0 LIMITATIONS OF STUDY 143
6.1 NON-PROJECT RELATED MICROCLIMATE CHANGES 144
6.2 LIMITATIONS OF MODELLING APPROACH 149
6.2.1 Spatial Scales 149
6.2.2 Temporal Scales 150

7.0 REFERENCES 151

7.1 LITERATURE CITED 152

7.2 INTERNET SITES 153

7.3 PERSONAL COMMUNICATIONS 153

LIST OF TABLES

Table 2.1.1 BC Hydro Site C climate network station locations and elevations 9

Table 2.1.2 BC Hydro Site C climate stations with parameters measured 10

Table 2.7.1 Likelihood terminology and associated probability used in statistical analysis (IPCC, 2007) 31

Table 3.1.1 1971 through 2000 climate normals for Fort St. John Airport[1] 35

Table 3.2.1 Summary of measured climate parameters during First Year of Observation 40

Table 4.1.1 WRF model prediction skill for temperatures at Fort St. John Airport 54

Table 4.1.2 WRF model prediction skill for temperatures at the field stations 57

Table 4.2.1 WRF model prediction skill for precipitation at Fort St. John Airport 70

Table 4.2.2 WRF model prediction skill for precipitation at the field stations 73

Table 5.1.1 Seasonal change in daily average temperature 90

Table 5.1.2 Seasonal change in daily minimum temperature 90

Table 5.1.3 Seasonal change in daily maximum temperature 91

Table 5.1.4 Seasonal change in extreme minimum temperature 93

Table 5.1.5 Seasonal change in extreme maximum temperature 93

Table 5.2.1 Seasonal change in total precipitation 103

Table 5.3.1 Seasonal change in wind speed 110

Table 5.3.2 Seasonal change in maximum hourly wind speed 111

Table 5.4.1 Seasonal change in water vapour mixing ratio 125

Table 5.5.1 Predicted change in fog from Baseline Case to Future Case with the Project 137

Table 5.5.2 Predicted change in heavy fog from Baseline Case to Future Case with the Project 137

Table 5.6.1 Predicted changes in visibility at Fort St. John Airport 142

Table 5.7.1 Predicted evaporation from proposed reservoir for Future Case with the Project 142

LIST OF FIGURES

Figure 1.1.1 Microclimate Technical Study Area 3

Figure 1.2.1 Boundary layer growth over change in surface (Voogt 2012) 7

Figure 1.2.2 Profile of internal boundary layer (Epifanov 2012) 8

Figure 2.1.1 Meteorological stations in the vicinity of the Project 12

Figure 2.3.1 WRF model nested model domains 17

Figure 2.3.2 WRF model input streams 18

Figure 2.5.1 H3D lake circulation model points and corresponding WRF model grids 23

Figure 2.5.2 WRF model one-kilometre terrain elevation and land-cover characterization 24

Figure 2.5.3 Example WRF model lake surface inputs 25

Figure 2.5.4 WRF model daily lake temperature and ice cover 26

Figure 3.1.1 Mean annual temperature and precipitation at Fort St. John Airport 36

Figure 3.2.1 Mean daily temperatures at climate stations and Fort St. John Airport 41

Figure 3.2.2 Wind rose for Station 1 during first year of operation 42

Figure 3.2.3 Wind rose for Station 2 during first year of operation 43

Figure 3.2.4 Wind rose for Station 3 during first year of operation 44

Figure 3.2.5 Wind rose for Station 4 during first year of operation 45

Figure 3.2.6 Wind rose for Station 5 during first year of operation 46

Figure 3.2.7 Wind rose for Station 6 during first year of operation 47

Figure 3.2.8 Wind rose for Station 7 during first year of operation 48

Figure 3.2.9 Wind rose for Fort St. John Airport during first year of operation 49

Figure 3.2.10 Seasonal and annual precipitation totals at climate stations and Fort St. John Airport... 50

Figure 3.2.11 Hourly precipitation measured by two different gauges at Station 1 51

Figure 4.1.1 Observed, predicted, and climate-normal mean temperatures at Fort St. John Airport.. 59

Figure 4.1.2 Observed, predicted, and climate-normal maximum temperatures at Fort St. John Airport 60

Figure 4.1.3 Observed, predicted, and climate-normal minimum temperatures at Fort St. John Airport 61

Figure 4.1.4 Observed and predicted extreme maximum temperatures at Fort St. John Airport..... 62

Figure 4.1.5 Observed and predicted extreme minimum temperatures at Fort St. John Airport..... 63

Figure 4.1.6 One year of observed and predicted daily mean temperatures at Fort St. John Airport . 64

Figure 4.1.7 One winter week of observed and predicted hourly temperatures at Fort St. John Airport. 65

Figure 4.1.8 One summer week of observed and predicted hourly temperatures at Fort St. John Airport..... 66

Figure 4.1.9 WRF versus Fort St. John Airport predictions of mean temperature at field stations..... 67

Figure 4.1.10 WRF versus Fort St. John Airport predictions of maximum temperature at field stations 68

Figure 4.1.11 WRF versus Fort St. John Airport predictions of minimum temperature at field stations 69

Figure 4.2.1 Observed, predicted, and climate-normal precipitation at Fort St. John Airport..... 75

Figure 4.2.2 Observed, predicted, and climate-normal rainfall at Fort St. John Airport..... 76

Figure 4.2.3 Observed, predicted, and climate-normal snowfall at Fort St. John Airport 77

Figure 4.2.4 One summer week of observed and predicted daily precipitation at Fort St. John Airport... 78

Figure 4.2.5 One winter week of observed and predicted daily precipitation at Fort St. John Airport. 79

Figure 4.2.6 WRF versus Fort St. John Airport predictions of precipitation at field stations..... 80

Figure 4.3.1 Observed and predicted wind roses at Fort St. John Airport..... 83

Figure 4.3.2 Observed and predicted wind-speed frequencies at Fort St. John Airport..... 84

Figure 4.3.3 Observed and predicted wind-speed frequencies at field stations 85

Figure 5.1.1 Predicted changes in temperatures – annual 94

Figure 5.1.2 Likelihoods of statistically significant changes in temperatures – annual..... 95

Figure 5.1.3 Change in daily average temperature..... 96

Figure 5.1.4 Predicted changes in mean temperatures – monthly 97

Figure 5.1.5 Likelihoods of statistically significant changes in mean temperatures – monthly..... 98

Figure 5.1.6 Predicted changes in maximum temperatures – monthly..... 99

Figure 5.1.7 Likelihoods of statistically significant changes in maximum temperatures – monthly 100

Figure 5.1.8 Predicted changes in minimum temperatures – monthly..... 101

Figure 5.1.9 Likelihoods of statistically significant changes in minimum temperatures – monthly 102

Figure 5.2.1 Predicted changes in precipitation – monthly 105

Figure 5.2.2 Predicted changes in rainfall – monthly 106

Figure 5.2.3 Predicted changes in snowfall – monthly..... 107

Figure 5.2.4 Predicted changes in precipitation – annual 108

Figure 5.3.1 Wind rose of Baseline Case and Future Case with the Project at Fort St. John Airport 113

Figure 5.3.2 Wind rose of Baseline Case and Future Case with the Project at Station 1 – Attachie Flat Upper Terrace 114

Figure 5.3.3 Wind rose of Baseline Case and Future Case with the Project at Station 2 – Attachie Flat Lower Terrace 115

Figure 5.3.4 Wind rose of Baseline Case and Future Case with the Project at Station 3 – Attachie Plateau 116

Figure 5.3.5 Wind rose of Baseline Case and Future Case with the Project at Station 4 – Bear Flat 117

Figure 5.3.6 Wind rose of Baseline Case and Future Case with the Project at Station 5 – Hudson's Hope 118

Figure 5.3.7 Wind rose of Baseline Case and Future Case with the Project at Station 6 – Farrell Creek 119

Figure 5.3.8 Wind rose of Baseline Case and Future Case with the Project at Station 7 – Site C Dam 120

Figure 5.3.9 Predicted changes in wind speeds – monthly 121

Figure 5.3.10 Likelihoods of statistically significant changes in wind speeds – monthly 122

Figure 5.3.11 Predicted changes in wind speeds – annual 123

Figure 5.3.12 Likelihoods of statistically significant changes in wind speeds – annual 124

Figure 5.4.1 Changes in daily average water vapour mixing ratio 128

Figure 5.4.2 Predicted changes in mixing ratio – monthly 129

Figure 5.4.3 Likelihoods of statistically significant changes in mixing ratio – monthly 130

Figure 5.4.4 Predicted changes in mixing ratio – annual 131

Figure 5.4.5 Likelihoods of statistically significant changes in mixing ratio – annual 132

Figure 5.4.6 Estimated changes in mixing ratio 2640 feet a.s.l. – monthly 133

Figure 5.4.7 Estimated changes in mixing ratio 3000 feet a.s.l. – monthly 134

Figure 5.4.8 Estimated changes in mixing ratio 3300 feet a.s.l. – monthly 135

Figure 5.5.1 Predicted changes in monthly river temperature, reservoir surface temperature and evaporation 139

Figure 6.1.1 Project influences versus regional climate projections for temperature 147

Figure 6.1.2 Project influences versus regional climate projections for precipitation 148

LIST OF APPENDICES

Appendix A ..... Appendix A Glossary of Terms

Appendix B ..... Appendix B Bayesian Two-Sample Comparison

Appendix C ..... Technical Memo – Climate and Air Quality Station Installation Summary

Appendix D ..... Fort St. John Airport Climate Normals

1.0 INTRODUCTION

Operation of the Site C Clean Energy Project (the Project) has the potential to influence local and regional climate (henceforth the term 'microclimate' will be used for the small scale regional climatic variation within the Technical Study Area). The formation of the reservoir would alter local topography by decreasing the depth of the valley. Furthermore, the surface characteristics of flooded areas would change, in particular greater moisture content, higher albedo (reflectivity), and less surface roughness. Global climate change and anthropogenic land-use changes, independent of the influence of the reservoir, would change regional microclimate in the Technical Study Area over the operational lifetime of the Project. This report does not consider the influence of these global long-term trends on the local microclimate. The focus of this study is the magnitude and statistical significance of the changes caused by filling the reservoir in relation to natural inter-annual variability.

1.1 SCOPE AND OBJECTIVES

The Project component that might potentially alter microclimate is the reservoir. The purpose of the Weather Research and Forecasting (WRF) modelling study was to provide a quantitative estimate of potential changes to the microclimate of the Peace River Valley that might result from formation of the proposed Site C reservoir. This study focuses primarily on changes that a reservoir at full storage capacity would cause under currently observed large-scale weather patterns, as reflected in the chosen model year. No further changes to microclimate are expected with ongoing operation of the dam and reservoir.

1.1.1 Objectives

The two main objectives of this study were to:

1. Predict the change in common meteorological parameters within the Peace River Valley due to operation of the Project compared to existing conditions. Common meteorological parameters that were examined include:

- Air temperature
- Humidity
- Wind speed and direction
- Fog frequency and density
- Precipitation

2. Provide estimates of the changes in meteorological and microclimatic variables of interest to other discipline areas. Examples of metrics from other disciplines that directly depend on microclimate include:

- Agricultural crop drying
- Growing degree days
- Fog
- Visibility at Fort St. John Airport and Taylor Bridge

- Icing and precipitation on highways and roads
- Icing on downstream infrastructure

These objectives were achieved by:

- Describing the microclimate in the Technical Study Area
- Examining terrain relief and land-cover characteristics and large-scale meteorological conditions over a twelve-month baseline period that is representative of current microclimate
- Determining changes of terrain relief and land-cover characteristics caused by the filling of the reservoir
- Establishing current microclimate at the Project site for terrain relief and land-cover characteristics and large-scale meteorological conditions during the baseline period
- Evaluating future microclimate at the Project site for large-scale meteorological conditions during the baseline period incorporating the expected new terrain relief and land-cover characteristics after the reservoir is filled

1.1.2 Temporal Boundaries

The temporal boundaries for the microclimate study consist of the current conditions prior to construction of the dam and after the reservoir has been filled to capacity. The scenarios are denoted as the Baseline Case and the Future Case with the Project, respectively. The model period for the Baseline Case, referred to hereafter as the baseline period, was chosen to be the twelve consecutive months from October 2004 through September 2005. This model year was chosen by selecting a recent 12 consecutive month period that was considered hydrologically normal by BC Hydro in terms of water flows and comparing the chosen period with 30 year climate normals. The Future Case with the Project was defined by using the same baseline period but with the surface geography of the Peace River changed to reflect the reservoir at full storage capacity. Only changes in surface characteristics pertaining to formation of the reservoir were modelled; changes caused by other factors, e.g., global climate change and anthropogenic land-use changes independent of the Project, were not considered.

1.1.3 Spatial Boundaries

The position of the Technical Study Area within the greater Peace River Valley is shown in Figure 1.1.1. The Technical Study Area, which encompassed the entire reservoir, is 108 kilometres east to west, by 68 kilometres north to south, corresponding to a 108 x 68 one-kilometre WRF model grid. Located within the Technical Study Area are a long-term climate station at Fort St. John Airport and seven climate monitoring stations within the BC Hydro Site C climate network. The climate station at Fort St. John Airport within the Technical Study Area is shown in Figure 2.1.1. The potential influence of the reservoir on the microclimate was examined using output from the numerical atmospheric WRF model over the Technical Study Area.

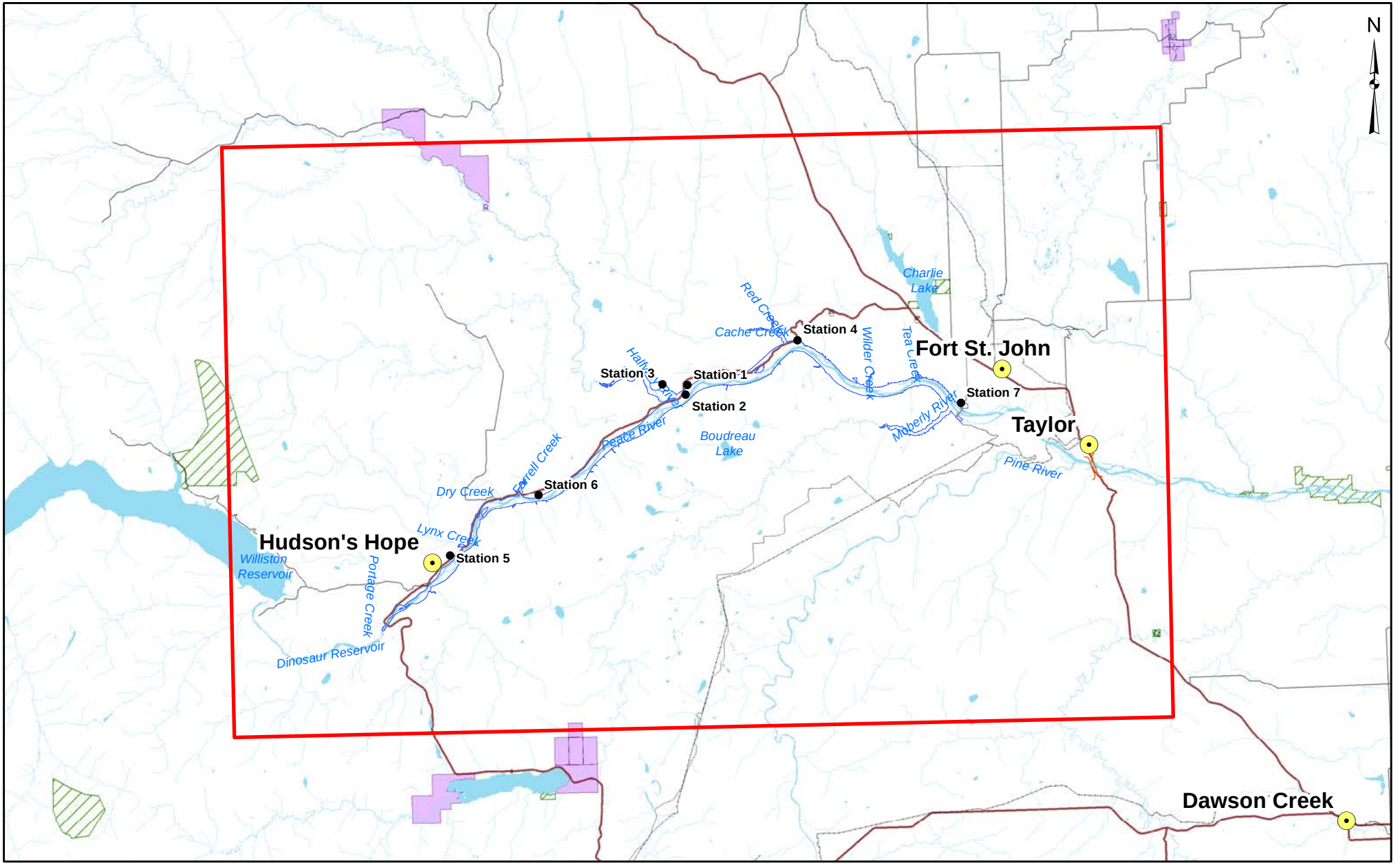

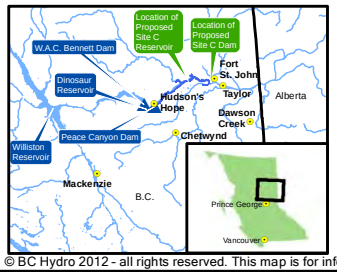

Technical Study Area for WRF Microclimate Study.
The extent of TSA correpsonds to WRF 1 km grid.

Map Notes:
1. Datum/Projection: NAD83/UTM Zone 10N.
2. Proposed Reservoir Area (461.8 m maximum normal elevation) from Digital Elevation Models (DEM) generated from LiDAR data acquired July/August 2006.

Legend

- BC Hydro - Site C Stations
- City/District Municipality
- Fort St. John and Taylor Bridge
- Technical Study Area
- Proposed Reservoir
- Protected Areas, Provincial Parks, Regional Parks and Ecological Reserves
- Indian Reserve
- Existing Road
- Existing Highway
- Existing Railway

1:600,000

0 20 km

SITE C CLEAN ENERGY PROJECT

RWDI BC hydro

Figure 1.1.1
Microclimate technical study area

DATE	Dec. 3, 2012	1016-C14-A5497	R 0

© BC Hydro 2012 - all rights reserved. This map is for information purposes only and accuracy is not guaranteed.

Construction of the Site C Clean Energy Project is subject to required regulatory approvals including environmental certification

1.2 PROCESSES INFLUENCING MICROCLIMATE

The term “microclimate” normally refers to climates that exist over spatial scales from 10^{-2} to 10^{3} metres (Oke, 1987). In the context of this report “microclimate” is used to describe climates from the micro to meso-scale and was chosen as it conveys to the non-expert the smaller scale being represented by the Peace River Valley.

In fact, there is no single microclimate for the Technical Study Area. Each location will have its own microclimate based on local vegetation, elevation, terrain aspect, drainage on so on. The climate of the Technical Study Area is thus an amalgamation of numerous microclimates, and the climate of the area as a whole is more properly termed ‘meso-climate’.

Along these lines, each grid cell of a local climate model application may be considered to be the solution for the microclimate of the area represented by that grid cell. Therefore, by examining the model results for different model grid cells, changes to the microclimate of various locations within the Technical Study Area may be examined.

The formation of the reservoir would influence the microclimate of the Technical Study Area by changing the physical characteristic of the Earth’s surface and the resulting energy balance that takes place at the Earth-atmosphere boundary. A portion of the existing Peace River Valley would change from a mix of agricultural, grassland and forests to a water surface. That water surface would be liquid or ice depending on location and time of year.

The proposed water surface would change the Earth-atmosphere balance in several ways. In general, the water would absorb less sunlight and cause more evaporation of water. This would increase atmospheric water vapor and reduce surface heating from the sun. The water surface has a larger thermal mass than the land surface so it would tend to have less of a temperature range than a land surface, with warmer minimum temperature and cooler maximum temperature.

The water surface would be less rough than a land surface. This would reduce surface friction for wind and tend to result in higher wind speed. In addition the change in elevation would change the topographic influence on local winds, though the result of this in terms of wind speed would depend on the specific location.

In broad terms it is expected that the proposed reservoir would moderate temperature by creating cooler summers and warmer winters, increase atmospheric humidity and potentially change the occurrence of precipitation, and create higher wind speeds over and close to the water surface.

The lowest layer of the atmosphere directly above the Earth’s surface is known as the boundary layer. It is so named because the atmospheric properties of this layer, (temperature, humidity etc.) are strongly determined by the properties of the underlying surface.

Any changes to the atmosphere that may result from changes to the underlying surface, such as when an air mass moves from over water to over land, are first transferred to the boundary layer.

When this occurs, the atmosphere develops a new boundary layer, which grows inside the previous one, that is adapted to the different surface, and the boundary between the air mass that was adjusted to the old surface and the boundary that is adjusting to the new surface is termed an internal boundary layer. After a sufficient distance, the new boundary layer will approach a stable height that is characteristic of the surface/atmosphere energy balance.

Figure 1.2.1 illustrates this for the transition from a rural to an urban land surface. The change between water and land is analogous. As a new boundary layer grows over the new surface, it will erode the previous layer, and the characteristics of that layer will be mixed into the new one.

Changes to the atmosphere, and thus the climate, resulting from the proposed Site C reservoir would occur by creating a boundary layer that is adjusted to the reservoir surface. The distance over which these changes persist away from the proposed reservoir would be determined by the distance for which the internal boundary layer that is adapted to the reservoir persists downwind over land. In turn, the distance for which the boundary layer persists would depend, in some part, on the size of the surface that created it.

In the simplest terms, the depth of the internal boundary layer that will form over a new surface is proportional to the size of the surface feature and inversely proportional to wind speed (Garratt, 1992). The size of the surface feature acts to create the layer and the wind speed acts to erode it through turbulence. An idealized depiction of the process showing the typical growth of the layer along with the wind and turbulence profiles is shown is Figure 1.2.2.

When the proposed Site C reservoir is examined in this context, it is seen that the reservoir forms a smaller surface compared to the land area which surrounds it. If the characteristic width of the reservoir is approximately one kilometre, then the height of the resulting internal boundary layer caused by the reservoir would be proportional to this length. Garratt (1992) suggests this internal boundary layer grows with the square root of the distance from the land-reservoir discontinuity.

Similarly, once the air mass leaves the reservoir and passes back over land, the new internal boundary layer that forms over land would reach approximately the height of the previous internal boundary layer that was adjusted to the reservoir, in approximately the same distance. Thus, the internal boundary layer formed by the one kilometre width of the reservoir should be completely replaced by a new internal boundary layer of equivalent height once it has been over land for approximately one kilometre. There would still be a layer, modified by the reservoir, above the internal boundary layer created as air moves from the reservoir back over land. The distance from the reservoir where the boundary layer is fully adjusted to the land surface and hence exhibiting no characteristics of the reservoir is dependent on the change in surface roughness between the reservoir and land and the stability of the atmosphere.

One complication to this example is that the distance an air mass might spend over the reservoir water surface depends on the angle of its path over the water and could be longer than the typical reservoir width of one kilometre. This suggests that the expected distance from the reservoir where changes may be observed within the internal boundary layer could be greater than one kilometre. Also, although the internal boundary layer created by the land may be fully adjusted to the surface below, above this internal boundary layer the atmosphere may still exhibit the influence of the previous reservoir-created internal boundary layer. Hence, the effect of the reservoir may extend well beyond the distance of the typical width of the reservoir.

However, the residual influence of the reservoir boundary layer would be a second order effect compared to the dominant influence of the underlying surface. Therefore it is reasonable to assume that the residual influence would be not be of a larger order of magnitude than the original influence of the reservoir which would suggest an upper bound of around 10 km is a reasonable estimate for the extant of the reservoir influence.

In a previous study of climate in the Peace River, Thurber Consultants (1979) used a bulk analysis to estimate the change in temperature over land resulting from a hypothetical reservoir. They estimated that a 10 degree difference in water/land temperature could cause up to a maximum of a 2 degree change in the air temperature compared to current conditions for locations near the reservoir's edge. The water/land temperature difference for the proposed reservoir would vary both during each day and over the course of the year, but it was expected that the WRF model study would provide results within this rough estimate.

Local wind speeds would be altered by the change in surface roughness. However, as argued above, the expected extent of reservoir influences would not be enough to change the synoptic conditions that drive large scale wind speeds. This means that the reservoir would cause higher speeds at low levels but would not change the wind experienced by the upper atmosphere. Thus it would be expected that winds would be increased by a percentage of the current wind speed but would not increase so much as to reflect a change in large scale wind speeds.

It is possible to use physical arguments such as the above to deduce the expected general influence of the reservoir on local climate. However, meteorology and climate are complex phenomena and the response of the atmosphere to the proposed reservoir will not necessarily be linear. Increases and decreases in the parameters of interest are possible depending on the time of year, the water-land temperature difference, reservoir ice cover and valley elevation and slope with the proposed reservoir water surface. The use of an atmospheric model is required to examine the influence of all these factors for all conditions that may exist in a typical year.

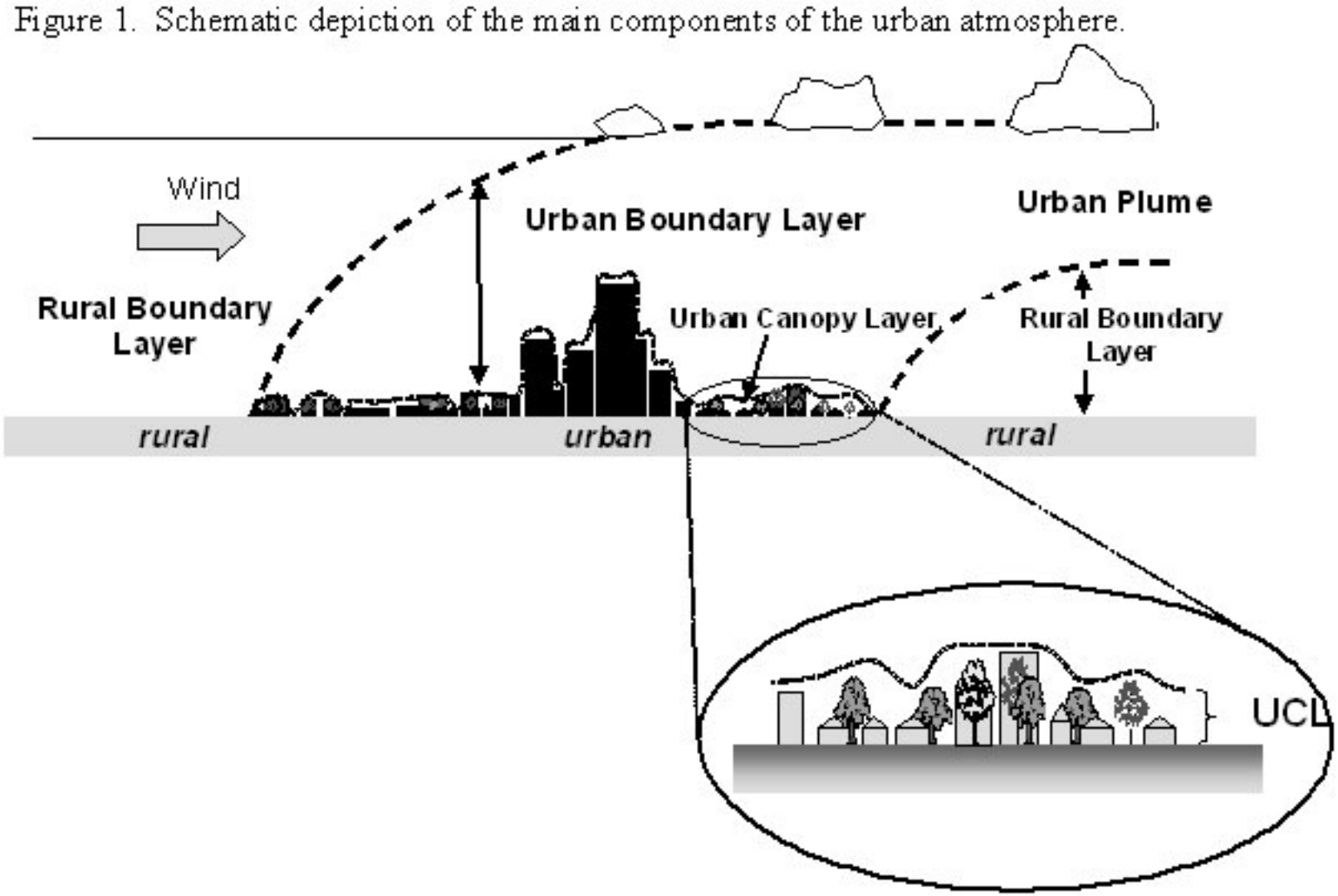

Example of boundary layer growth over differing surface characteristics.
Example shows an urban/rural interface. A land/water interface will behave in a similar manner.

SITE C CLEAN ENERGY PROJECT		RWDI BC hydro	**Figure 1.2.1 Boundary layer growth over change in surface (Voogt 2012)**
DATE	Dec. 3, 2012		R 0

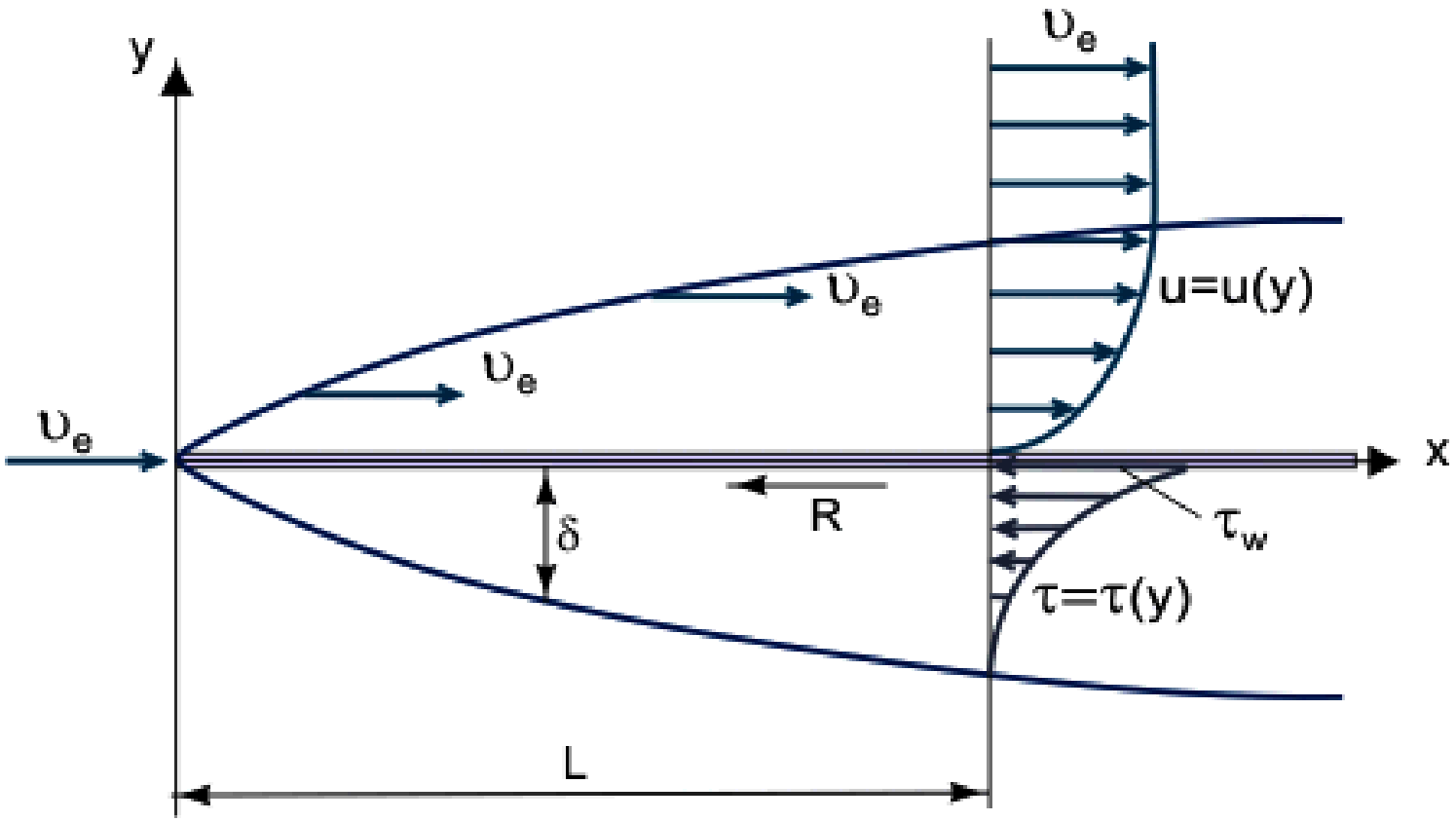

Idealized formation of internal boundary layer from wind flowing over change in surface.

SITE C CLEAN ENERGY PROJECT		RWDI BC hydro	**Figure 1.2.2 Profile of internal boundary layer (Epifanov 2010)**
DATE	Dec. 3, 2012		R 0

2.0 METHODOLOGY

This section describes the information and methods that were used for the microclimate analysis. Sources of data include historical meteorological observations, data from measurement field studies and geophysical databases of terrain and land-cover characteristics. This section also describes the numerical modelling methodology and the statistical methods used to analyze model results.

2.1 REVIEW OF EXISTING INFORMATION

This subsection lists and describes the meteorological data sets that were used to characterize the Baseline Case and summarizes how the data were used. In addition, the WRF model inputs for the Baseline Case are discussed.

2.1.1 Meteorological Data Sets

Meteorological stations in the Technical Study Area are operated by Environment Canada, BC Ministry of Environment (MOE), BC Ministry of Forest (MOF), BC Ministry of Transportation (MOT) and BC Hydro (see Figure 2.1.1). There are also a number of historical stations near the Project area that are no longer operational that recorded daily observations

To support an evaluation of the microclimate of the study area, BC Hydro installed a network of climate stations in the Peace River Valley. This network has been active since 2011. Figure 2.1.1 shows the station locations with in Technical Study Area. Table 2.1.1 and Table 2.1.2 show locations and parameters measured at these stations. The BC Hydro Site C monitoring network also includes one additional station, located at Old Fort, which measures air quality only. As there are no meteorological measurements at this station it was not included in the Microclimate Study.

Other meteorological stations inside the Technical Study Area are Fort St. John Airport (Environment Canada), Taylor South Hill (MOE), Taylor Townsite (MOE), PMD (BC Hydro), and Hudson's Hope (MOF). Fort St. John Airport is located 12 kilometres east of the proposed Site C reservoir and is the closest station with a long measurement record (several decades); Taylor South Hill and Taylor Townsite are about 15 kilometres downstream of the proposed Site C reservoir.

Table 2.1.1 BC Hydro Site C climate network station locations and elevations

Station	UTM NAD 83 (m)	Latitude, Longitude (decimal degrees)	Elevation (m)
Station 1 - Attachie Flat Upper Terrace	597983 E, 6232938 N	56.23N, -121.41W	461
Station 2 – Attachie Flat Lower Terrace	597721 E, 6231898 N	56.22N, -121.42W	441
Station 3 – Attachie Plateau	595065 E,	56.23N, -121.46W	648

Station	UTM NAD 83 (m)	Latitude, Longitude (decimal degrees)	Elevation (m)
	6233032 N		
Station 4 – Bear Flat	610669 E, 6238135 N	56.27N, -121.21W	431
Station 5 – Hudson's Hope	570577 E, 6213303 N	56.05N, -121.86W	562
Station 6 – Farrell Creek	580779 E, 6220238 N	56.12N,-121.70W	470
Station 7 – Site C Dam	629517 E, 6230875 N	56.20N, -120.91W	648
Fort St. John Airport	640053 E, 6234872 N	56.24N, -120.74	695

Table 2.1.2 BC Hydro Site C climate stations with parameters measured

Station	Air Temp. and RH	Wind Speed and Direction	Precipitation	Snow Depth	Barometric Pressure	All Radiation Components	Solar Radiation	Turbulent Fluxes	Visibility	Soil Temperature	Soil Moisture	Soil heat Flux
Station 1 - Attachie Flat Upper Terrace	X	x	x	x	X	X		x	x	x	x	x
Station 2 – Attachie Flat Lower Terrace	X	x	x	x	X	x		x		x	x	x
Station 3 – Attachie Plateau	X	x	x	x	X		x					
Station 4 – Bear Flat	X	x	x	x	X	x		x		x	x	x
Station 5 – Hudson's Hope	X	x	x	x	X		x					
Station 6 – Farrell Creek		x										
Station 7 – Site C Dam	X	x	x	x	X		x					

Prior to the installation of the climate stations, a network of five wind stations installed and maintained by BC Hydro was in place beginning in February 2009. The wind stations measured only wind speed and direction. The wind stations were located at the current sites for Stations 1, 4, 5, 6 and 7.

Meteorological data from 1971 to 2000 from Fort St. John Airport, compiled and provided by Environment Canada, were used to characterize the general climate characteristics in the Technical Study Area, determine inter-annual variability, evaluate the performance of the WRF

model, and establish a relationship between observations at the airport station and at the Site C climate network stations.

Data from the seven meteorological stations in the BC Hydro Site C climate network collected from January 2011 through January 2012 were used to characterize the existing microclimate in the Peace River Valley. Data from these field sites were compared to data from the Fort St. John Airport station over the field period to characterize inter-annual variability along the Peace River Valley. Furthermore, observations from six of these stations from January 16, 2011 through January 15, 2012 were used to provide detailed spatial information to evaluate the WRF model's ability to model microclimate differences at spatial scales of a few kilometres.

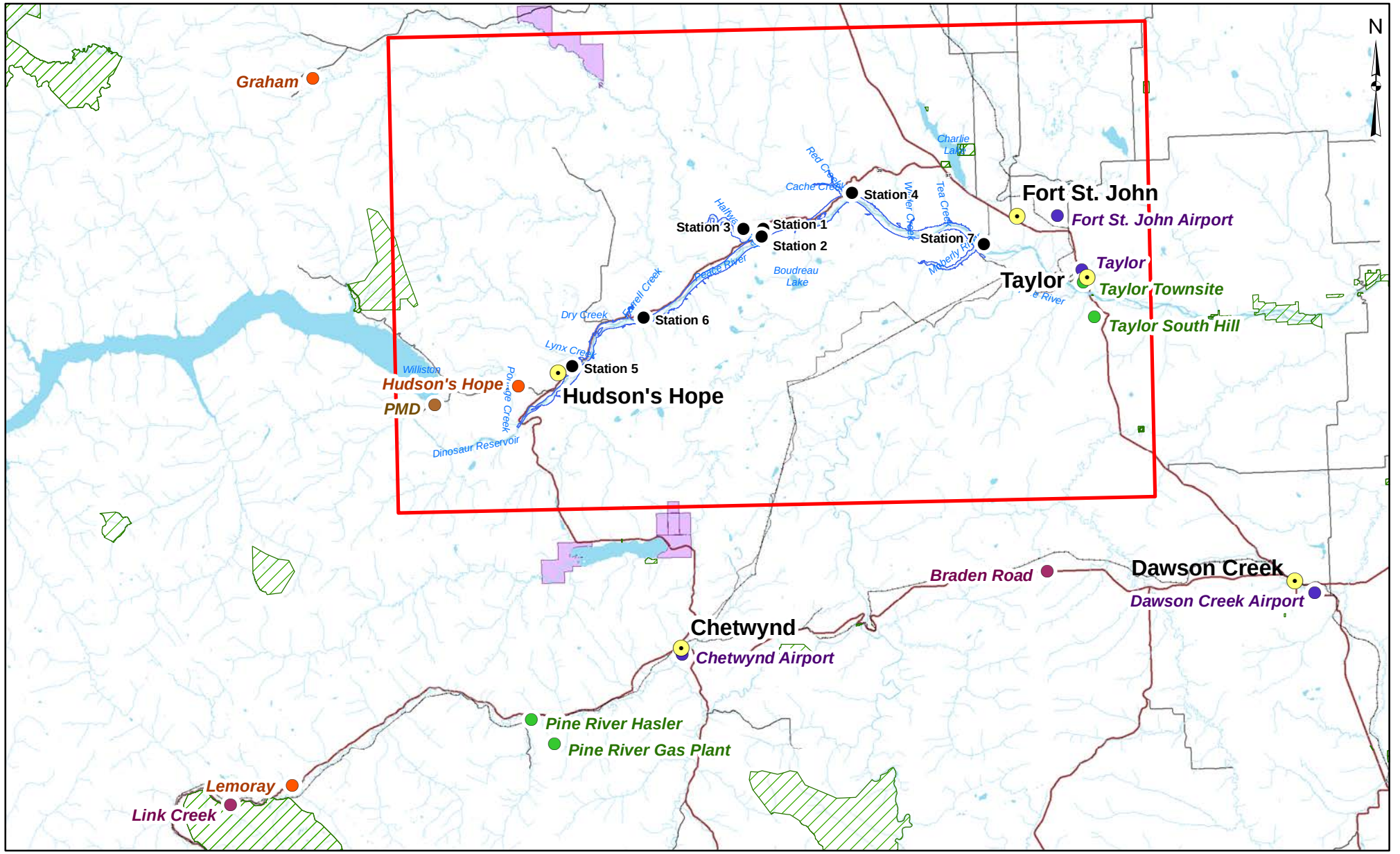

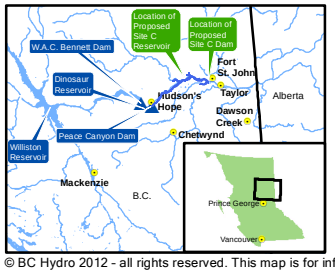

Map Notes:
1. Datum/Projection: NAD83/UTM Zone 10N
2. Proposed Reservoir Area (461.8 m maximum normal elevation) from Digital Elevation Models (DEM) generated from LiDAR data acquired July/August 2006.

© BC Hydro 2012 - all rights reserved. This map is for information purposes only and accuracy is not guaranteed.

Legend

- City/District Municipality
- Technical Study Area
- Proposed Reservoir
- Indian Reserve
- Protected Areas, Provincial Parks, Regional Parks and Ecological Reserves
- Existing Railway
- Existing Road
- Existing Highway

Meteorological Stations

- BC Hydro
- Environment Canada
- Ministry of Environment
- Ministry of Forest, Lands and Natural Resource Operations
- Ministry of Transportation and Infrastructure
- BC Hydro - Site C Stations

1:750,000

0 20 km

SITE C CLEAN ENERGY PROJECT

RWDI BC hydro

Figure 2.1.1
Meteorological stations in in the vicinity of the Site C project

DATE	Dec. 7, 2012	1016-C14-A5502	R 0

Construction of the Site C Clean Energy Project is subject to required regulatory approvals including environmental certification

2.1.2 Weather Research and Forecasting Model Inputs

Potential future microclimate changes were simulated using the WRF meteorological model (version 3.2.1, released August 2010). Model inputs were developed using the WRF Pre-processing System (WPS), also version 3.2. This was the most recent model release at the time the study commenced and was frozen for the duration of the model effort.

The WRF model has two main input streams: the meteorological inputs that set the initial and domain boundary conditions for the model, and the geophysical inputs that define the land-cover characterization and terrain elevation of the Earth's surface in the model.

Initial and boundary conditions for the WRF model simulation were set for each model day using the North American Regional Reanalysis (National Centers for Environmental Prediction 2011). These data are three-dimensional snapshots of the state of the atmosphere produced by the National Centers for Environmental Prediction. They are derived by taking the output from numerical weather forecasting and subsequently adjusting (or 're-analyzing') the data fields by assimilating actual observations for the time of the forecast. Sources of data that are assimilated include measurements from surface stations, upper air profiles, satellite observations, and overwater data from ships and buoys. The data are available at 32 kilometre resolution every three hours over most of North America. These were processed for each WRF model day using WPS.

Geophysical inputs, such as land-cover characterization and terrain elevation, were set using the geophysical database that is distributed along with the WRF model codes. The database is comprised of global geophysical data compiled by United States Geological Service at 30 second spatial resolution. The data were processed by the WPS and assembled on to the WRF model 12-kilometre, four-kilometre and one-kilometre grids.

Higher resolution terrain elevation data for the Peace River region are available from the Advanced Spaceborne Thermal Emission and Reflection Radiometer Global Digital Elevation Model (ASTER GDEM 2011). To increase terrain resolution within the WRF model, the terrain elevations from the United States Geological Service data in the WRF model input files were replaced by elevation data from Advanced Spaceborne Thermal Emission and Reflection Radiometer Global Digital Elevation Model.

2.2 NUMERICAL MODELLING APPROACH

The WRF model is a computer program used by meteorological forecasters to predict future weather over periods from hours to days. It can also be used as a research tool, to examine past weather events based on meteorological observations, including estimation of meteorological responses to land and water surface characteristics. It is the latest numerical weather forecasting model to be adopted by the United States National Weather Service as well as the United States military and private meteorological services. The WRF model is also being adopted by meteorological services worldwide, as seen in the television weather forecasts that

show computer-animated changes in cloud cover, indicating frontal movements over hours or days.

The WRF model solves the fundamental equations of atmospheric motion on a three-dimensional grid. In either the historical or forecast mode, the WRF model makes use of terrain data and land-use information. When applied in its reanalysis mode, the WRF model also makes use of actual observations of meteorology. The model incorporates parameters that influence atmospheric conditions, such as turbulence, convection and cloud formation, precipitation, radiation, surface heat transfer, and moisture. Thus, the WRF model is able to simulate various weather conditions, including wind shears, mountain and valley drainage flows, and other topographically induced wind flow patterns.

In simpler terms, the WRF model provides a three-dimensional estimate of the state of the atmosphere at any point in time. The model can produce a complete three-dimensional estimate of the wind, temperature, humidity and several other variables for each hour throughout the period modelled. The model output provides hourly estimates of weather conditions at any three-dimensional point within the model domain. By contrast, a meteorological station, though it is a direct measurement of actual meteorology, can only provide information for a single point in space. When applied over a period of a year or longer, WRF model results can provide an estimate of long-term average meteorological conditions, i.e., the climate of an area.

2.3 WEATHER RESEARCH AND FORECASTING MODEL METHODOLOGY

This section provides an overview of the settings used in the WRF model and how large-scale information was scaled down to one kilometre resolution. This includes:

- Initial conditions, nudging, model-run durations, and definition of spin-up time
- Spatial boundary conditions and nesting
- Meteorological and land-use input data
- Description of the new surface characteristics as a result of the filling of the reservoir
- Incorporation of results of lake temperature and ice cover modelling with H3D

WRF modelling was performed because it represents the best means by which to estimate climatic response to land-cover characteristics that do not yet exist. One might qualitatively estimate changes to local climate, but that would be based on scientific opinion rather than an objective quantitative analysis. Alternatively one might construct a simplified quantitative analysis, but to make such a study manageable it would need to be based on an a priori selection of the dominant atmospheric processes and on a subset of a small number of possible conditions that might occur. The only feasible means to quantitatively and objectively estimate changes to climate from future land-cover changes for all combinations of reservoir temperature, ice cover and of atmospheric conditions that are likely to occur in an average year is to use some type of physical or numerical model that can represent both the before and after land-cover characteristics and include consideration of multiple atmospheric process interacting at the same time.

The WRF model is commonly used to estimate meteorological responses to surface characteristics and, in fact, the model itself includes several options to investigate specific examples, such as changes to urban land cover (Grossman-Clarke et. al. 2010, Lopez-Espinoza et Al. 2012), changes to winds caused by surface roughness from wind turbines (Adams and Keith 2007) and changes to surface energy balances from groundwater (Hong et. al 2009). It has also been used in other locales specifically to investigate meteorological response due to lake and water bodies (Galvez et. al. 2006, Grim et. al. 2012). In addition, modellers have used WRF and other meteorological models to investigate how other phenomena such as photochemical smog would respond to changes in the urban land surface (Hudischewskyj et. al. 2001, Jiang et. al. 2008).

The before and after land-cover scenarios for the proposed Site C reservoir can similarly be represented by changing the physical inputs to the model. It thus provides a means to objectively investigate potential climatic changes resulting from the filling of the reservoir.

2.3.1 Initial Conditions

The WRF model was applied for one year, from October 2004 through September 2005, to examine annual meteorological conditions in the region of the proposed Site C reservoir. This year was selected because it is recent and is a normal year in terms of precipitation and water flows in the Peace River system. The chosen year was then checked to ensure that it was also climatologically normal. The representativeness of this year is evaluated in Section 4.0. One year is the shortest period that can demonstrate annual variation of ambient meteorology and thus provide an estimate of the climate in the area. The model year was constructed by restarting the model each day and then linking the individual days' outputs together over the full year. WRF requires several hours of model time for the simulated atmosphere to 'spin-up' and become adjusted to the inputs. Each day was constructed by performing a 30-hour run. The first six hours or each run were discarded as spin-up and the last 24 hours were retained.

2.3.2 Spatial Nesting

Modelling was performed using a nested domain, in which horizontal model resolution increases as one moves from the outer edges of the model domain inward to the interior, centered over the reservoir site. By this method, model results on a larger domain are used to provide boundary conditions to a smaller domain 'nested' within. The purpose of this is to provide increasingly detailed model parameter estimates close to the area of interest without having to incur the processing time and storage costs of using a fine resolution everywhere in the spatial domain, while allowing for a smooth transition from the coarse-scale inputs on the model boundaries to the fine-scale results in the middle of the domain. This is a common practice for application of three-dimensional atmospheric grid model such as the WRF model.

The WRF modelling was performed using nested grids of 12 kilometres, four kilometres and one kilometre resolution. In this configuration, model results which provide meteorology at 12-kilometre spacing are used as a boundary for a smaller domain that provides model results

every four kilometres. In turn, the four-kilometre outputs are used to drive the innermost 'nest' which provides meteorological model results at one kilometre spacing.

The 12 kilometre and four kilometre grids were run using 'two-way nesting'. In this configuration, the domains are run simultaneously and information can flow both ways between the domains. That is, the 12-kilometre grid is used as input to the four-kilometre nest, and the results from the four-kilometre nest are passed back to adjust the 12-kilometre parent. The one-kilometre run was performed separately as a 'one-way' nest. In a one-way nest, the information between the parent grid and nest is only passed in one direction. In this case, the four-kilometre model results were used to drive the one-kilometre nest, but the results of the one-kilometre nest were not used to adjust the four-kilometre parent. A one-way nest was chosen because it allows for multiple one-kilometre scenario runs to be spawned from the four-kilometre model results without having to re-run the coarser scale grids each time.

Figure 2.3.1 shows a map of the model domain for the 12-kilometre, four-kilometre and one-kilometre resolution domains. The innermost domain is comprised of a 108 x 68 one-kilometre grid cells covering the proposed Site C reservoir area. The one-kilometre domain corresponds to the Technical Study Area shown in Figure 1.1.1.

2.3.3 Input Data

Meteorological observations, terrain and land-use information are required as input to the WRF model in research mode. The terrain and global land-cover characterization information are contained in the model library while the meteorology was downloaded from the National Centre for Atmospheric Research (NCAR). The observed meteorology used in the model contains data observed from weather balloons, weather satellites, and surface weather stations. The meteorology was used to set the starting conditions for the 12-kilometre and four-kilometre model runs and to reset periodically the outer boundaries of the domain during the model run.

The input information was formatted in a pre-processor that produces input files that are accepted by the WRF model. The model was then executed to produce three-dimensional meteorological predictions for the modelled period. A flow chart of the modelling process is presented in Figure 2.3.2. The WRF model has the ability to estimate numerous meteorological variables including air temperature; wind speed and direction; water vapour; precipitation; sensible, latent and ground heat flux; incoming and outgoing radiative components; soil moisture content; and soil temperature.

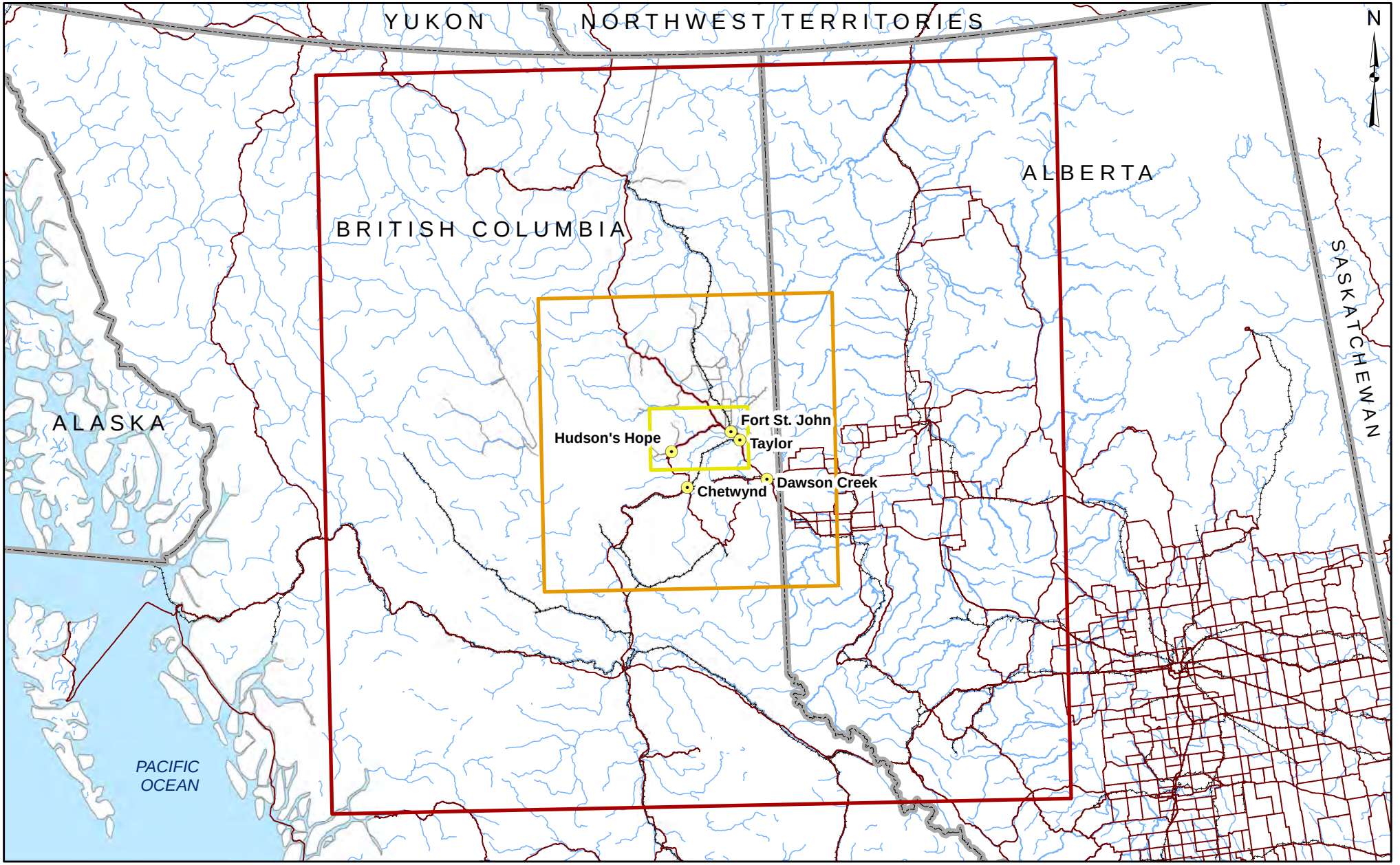

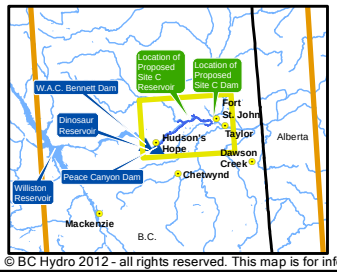

Regional Map of Western Canada showing the spatial coverage of the 12 km, 4 km and 1 km Weather Research and Forecasting Model (WRF) nested model domains

Map Notes:
1. Datum/Projection: NAD83/UTM Zone 10N.
2. Proposed Reservoir Area (461.8 m maximum normal elevation) from Digital Elevation Models (DEM) generated from LiDAR data acquired July/August 2006.
3. Ocean and Continent outline layer from Esri basemaps 2012.
4. Highways from Esri dataset v10.
5. Some railways and rivers from Geogratis.

Legend

- City/District Municipality
- Model Domain at 1 km Resolution
- Model Domain at 4 km Resolution
- Model Domain at 12 km Resolution
- Provincial/Territory Boundary
- Existing Highway
- Existing Railway

1:5,750,000

0 200 km

RWDI BC hydro

SITE C CLEAN ENERGY PROJECT

Figure 2.3.1
Weather Research and Forecasting model domains

DATE	Dec. 3, 2012	1016-C14-A5498	R 0

© BC Hydro 2012 - all rights reserved. This map is for information purposes only and accuracy is not guaranteed.

Construction of the Site C Clean Energy Project is subject to required regulatory approvals including environmental certification

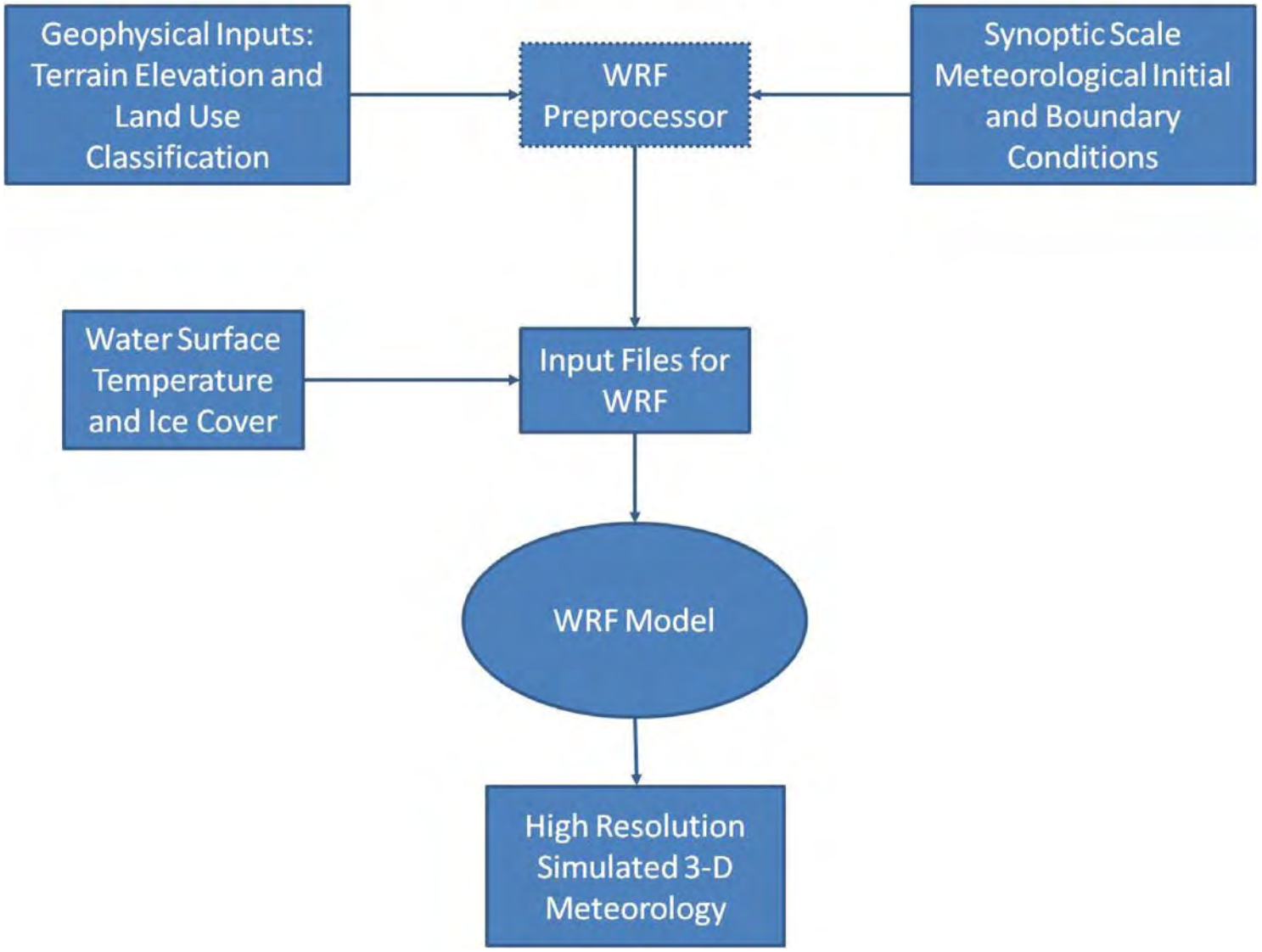

Flow chart showing how the geophysical information (elevation and land use), large scale meteorology and H3D lake model results are incorporated in the the Weather Research and Forecasting Model (WRF) model.

SITE C CLEAN ENERGY PROJECT

RWDI BC hydro

Figure 2.3.2
Weather Research and Forecasting model input streams

DATE	Dec. 3, 2012		R 1

Path: E:\00 - Large Project Folders\0920007 - Site C\GIS - CAM\Climate\1 - Climate Figures\0920007A - Confidential BC Hydro Climate_Figure_2.3.2_R1.mxd

2.4 SIMULATING LAND-COVER CHANGES IN THE WEATHER RESEARCH AND FORECASTING MODEL

Local-scale meteorology is influenced by the topography and land-cover characteristics of a given locale. Land-cover characterization refers to the geomorphology of the earth surface. The land surface is given a particular classification (such as grassland, mixed forest, urban, water and others) that determines processes such as the amount of heat that is absorbed and re-emitted, water that is evaporated, and the influence of surface friction on low-level wind speed. By changing the land-cover characterization supplied to the WRF model to correspond to what would result from constructing the proposed Site C reservoir (e.g., converting the land-cover category of reservoir grid cells to water rather than crops or forest), an estimate of the change in local-scale meteorology can be obtained. As climate is the long-term average of meteorology, the WRF model results for altered land-cover characterization can be used to infer how the proposed reservoir might influence the local microclimate.

The one-kilometre, one-way nested run was performed for two cases: a Baseline Case that uses terrain and land-cover characterization that presently exist; and the Future Case with the Project, with terrain height and land-cover characterization adjusted to reflect the changes due to the proposed Site C reservoir.

The Baseline Case was prepared using the WRF pre-processors and the USGS database for terrain height and land-cover characterization that are supplied with the model. The terrain elevations in the WRF input files derived from the USGS database were edited manually to incorporate the higher resolution ASTER GDEM elevation data.

The WRF model inputs for the Future Case with the Project were prepared by first determining which model grid cells would be subject to changes in terrain height and land-cover characterization from construction of the Project. Second, these cells were edited manually in the WRF model geophysical files. The terrain height of each of these model grid cells was set to the proposed water surface elevation of 461.8 metres above sea level, which is the water level height of the reservoir surface at full capacity. The land-cover characterization categories and other surface characteristics were edited to reflect the change from a valley bottom to a water surface. These surface characteristics include the reflectivity of the surface, the fraction of the surface covered by vegetation, and the surface skin temperature. The methodology for the determination of WRF model grid cells corresponding to the proposed reservoir is described further in the Section 2.5.

The WRF model was run for 12 consecutive months for both the Baseline Case and the Future Case with the Project. Changes in local meteorology between the two model runs were investigated by examining the differences in model outputs such as temperature, wind speed, mixing ratio and precipitation.

2.5 INCORPORATION OF H3D LAKE CIRCULATION MODEL WATER TEMPERATURE

The circulation of water within the proposed Site C reservoir was modelled with H3D in a separate study (Volume 2 Appendix H Reservoir Water Temperature and Ice Regime Technical

Data Report). The results of that study provide estimates of the surface water temperature and ice cover of the proposed reservoir. The results of that study were used to set the surface temperature and ice cover of the Future Case with the Project.

To define the proposed reservoir in the WRF model, the grid cells corresponding to the future reservoir were first changed to water and their elevation set to the water level height of the reservoir surface after the reservoir has been filled to capacity (461.8 metres above sea level). Though the height of the reservoir would change due to operations, the steep reservoir banks, and small reservoir operating range mean the water surface area would only change by a small fraction of the total area and any changes that do occur during operation would result in a smaller reservoir area than what was modeled, so using the full capacity height represents a conservative estimate of any resulting changes.

This was done by mapping the lake circulation model grid locations on to the one-kilometre WRF model grid. The mapping was accomplished by overlaying the lake circulation model grid points onto the WRF model grid and counting the number of lake circulation model points within each WRF model grid cell. If a certain number of lake circulation models points were found within a WRF model grid, the WRF model grid was set to reservoir. There are 6,328 grid points covering the reservoir surface as shown in the left panel of Figure 2.5.1. Various thresholds for determination of an ice surface were attempted, until the configuration that provided the best combination of a continuous reservoir in the WRF model while minimizing the overestimation of the reservoir surface was found. The resulting WRF model cells are shown in the right panel of Figure 2.5.1. This process resulted in 124 WRF model grid cells being classified as corresponding to the proposed reservoir surface.

The WRF model geophysical input files were edited to set the reservoir cell to the correct elevation and change the land-cover classification to a water body. The one-kilometre domain terrain elevation and land-cover characterization for both the Baseline case and Future Case with the Project are shown in Figure 2.5.2. With a grid dimension of one kilometre, this means the WRF model simulated reservoir has a surface area of 12,400 hectares. At full capacity, the proposed reservoir would have a surface area of 9,330 hectares. Thus the WRF model over-represents the future water surface area.

It should be noted that the one kilometre resolution is not capable of fully capturing the terrain features of either the Baseline Case or the Future Case with the Project. This is because the one kilometer grid resolution is not that much different from the width of the valley itself, so each one kilometer cell averages out some of the sub one kilometer terrain variation. As a result, in some locations the depth of the existing valley is not fully captured in the Baseline Case and for many of the grid locations that would become reservoir, the terrain represented in the WRF model is actually higher than what would be the future reservoir surface. This is a predictable artifact of trying to represent the valley with a one kilometer grid. This effect is compounded by the fact that the size of the reservoir is overestimated, which may also cause the reservoir to be mapped on the grid cells that have terrain elevations in the Baseline Case that are above the future water surface.

However, after the required WRF model grid locations are set to reservoir, it does not make physical sense to have adjacent water cells with differing elevations because the water should represent a flat surface. Therefore, all WRF model grid cells that were set to water were also set to the elevation of the future reservoir, even when this meant a decrease in elevation. The effect is that representing the reservoir in the WRF model requires filling in some locations and 'hollowing out' of others. Again this is a predictable artifact of both the one kilometer grid resolution and the overestimation of the reservoir surface area. The consequence of this overestimation is that it means the model results present a conservative overestimate of that component of the model results that are attributable to the size of the water surface.

For incorporation into the WRF simulations, the hourly lake circulation model results were first averaged over each day. Then, for each WRF model grid cell that was deemed to be reservoir, the daily average results over the lake circulation model grid points lying in the given WRF model grid were spatially summed and averaged. At the same time the number of points that the lake circulation model deemed to be frozen ice or open water within each WRF model grid were counted and the WRF model grid was set to either ice or water surface accordingly. Reservoir grids cells that were defined as open water were set to the average temperature calculated from the lake circulation model. Cells that were deemed frozen were set to the fresh water freezing point of 273.15 degrees Kelvin.

For each day of the WRF model run, the input files created by the WRF pre-processing system were manually edited to include the daily average lake circulation model results for water temperature and ice cover. Examples of the surface temperature and ice coverage for a winter and a summer day are shown in Figure 2.5.3. The plots show how the temperature of the water surface differs from the surrounding land surface during the different seasons. During winter, the open water surface is warmer than its surroundings, particularly at night when ambient temperatures are coldest. The opposite is true in summer when the water surface is cooler than the land surface.

The WRF model treats water surface and land surface differently. Water temperatures, especially over the open ocean, usually vary much more slowly than land surface temperatures. In fact, sea surface temperatures are a very strong driver of atmospheric conditions. As such, the WRF model is configured by default to treat water surface temperature as a constant, while land surface temperature varies over the model run. This means that once the surface temperature of the reservoir surface was set in the input file, it remained constant for that model day. However, once a surface is set to ice, it is treated in the model in the same manner as any other land surface and the surface temperature is allowed to vary. For ice surfaces, although the initial surface temperature was set to 273.15 degrees Kelvin, as the model progressed the temperature adapted to that of the surrounding land grid cells within the WRF simulation. Once the initial conditions for the WRF model were set to include the predicted water temperature and ice cover, the model simulation for the Future Case with the Project was allowed to run in the same manner as was previously done for the Baseline Case.

Figure 2.5.4 shows a daily time series of the water temperature as modelled by H3D from a location in the middle of the reservoir and the percent ice cover of the entire reservoir over the

model year. The water temperature ranges from more than 15 degrees Celsius during the summer months to frozen during the winter. Ice begins forming in late October. Starting in early December the reservoir is greater than half-frozen until late March, with greater than 80% ice coverage through January and February. In general the ice builds from the dam location westward. The extreme southwest portion of the reservoir remains ice free throughout the year.

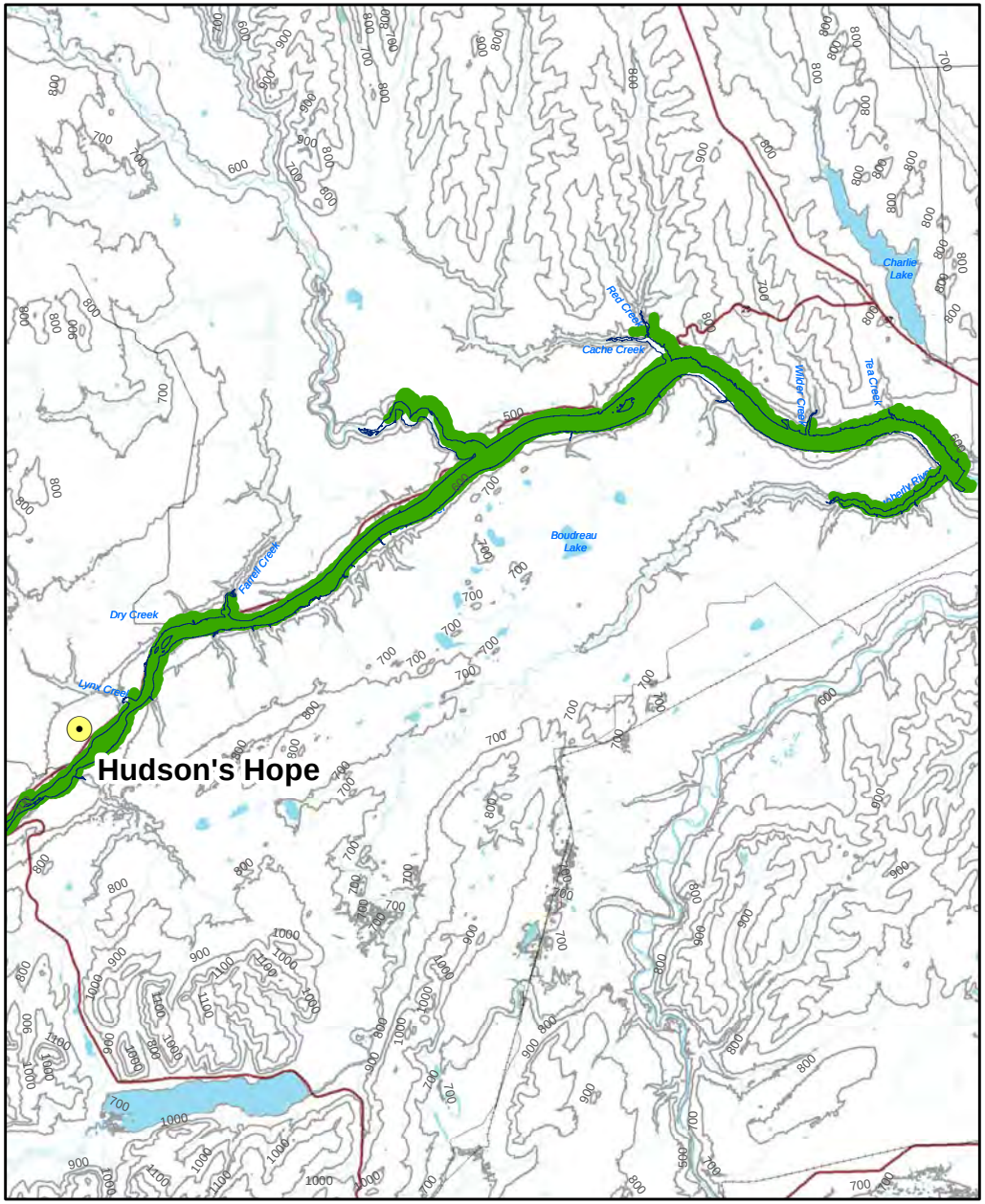

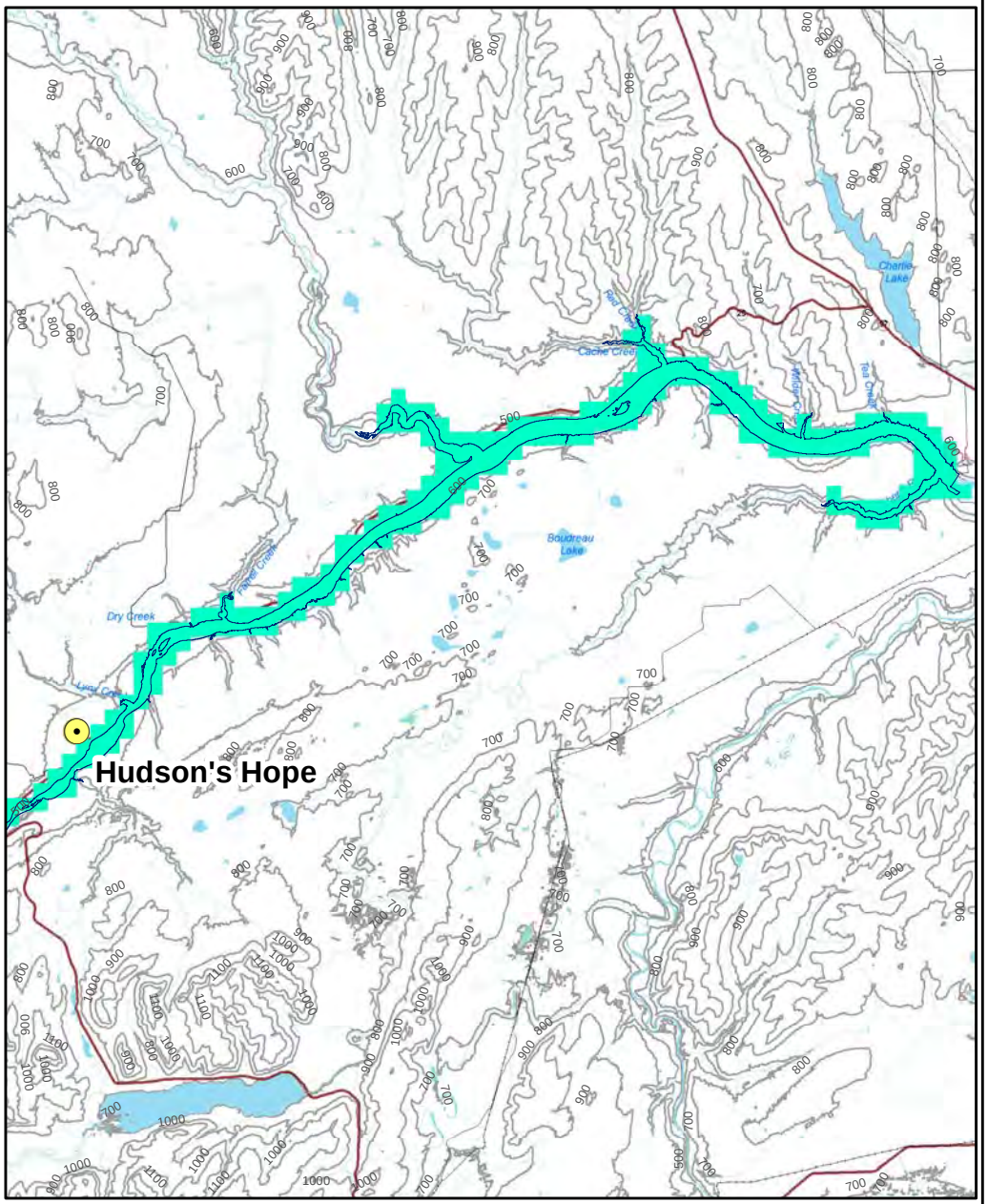

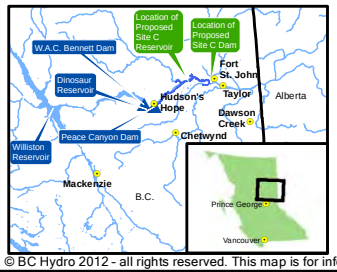

Map Notes:
1. Datum/Projection: NAD83/UTM Zone 10N.
2. Proposed Reservoir Area (461.8 m maximum normal elevation) from Digital Elevation Models (DEM) generated from LiDAR data acquired July/August 2006.

© BC Hydro 2012 - all rights reserved. This map is for information purposes only and accuracy is not guaranteed.

Legend

- HD3 Lake Circulation Model Points
- City / District Municipality
- WRF 1km Grid Points
- Proposed Reservoir
- Existing Road
- Existing Highway
- Existing Railway

N

1:500,000

0 20 km

SITE C CLEAN ENERGY PROJECT

RWDI BC hydro

Figure 2.5.1
H3D lake circulation model points and corresponding Weather Research and Forecasting model grids

DATE	Dec. 3, 2012	1016-C14-A5499	R 0

Construction of the Site C Clean Energy Project is subject to required regulatory approvals including environmental certification

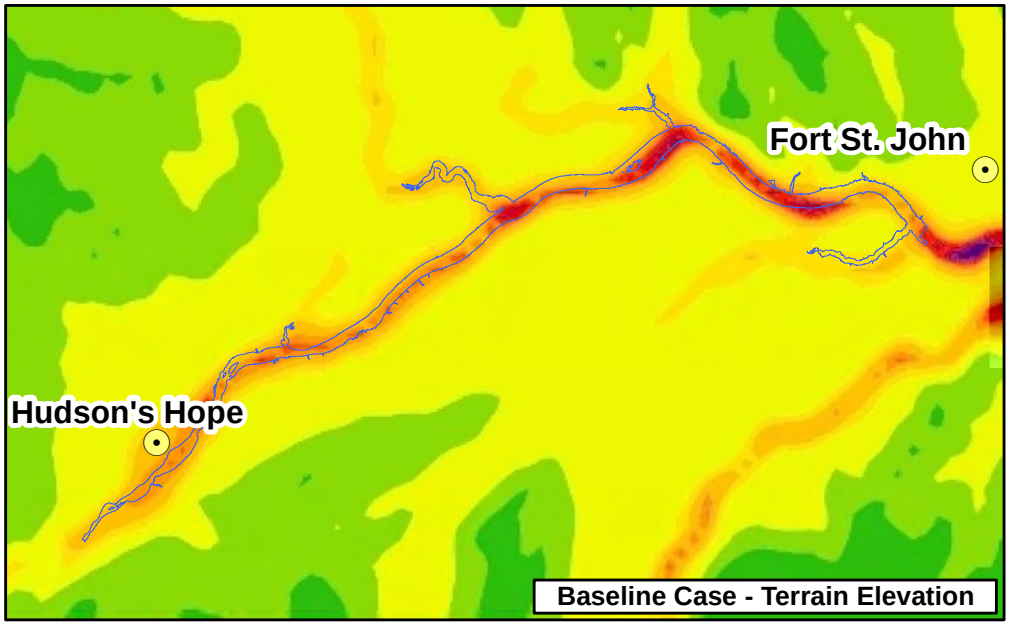

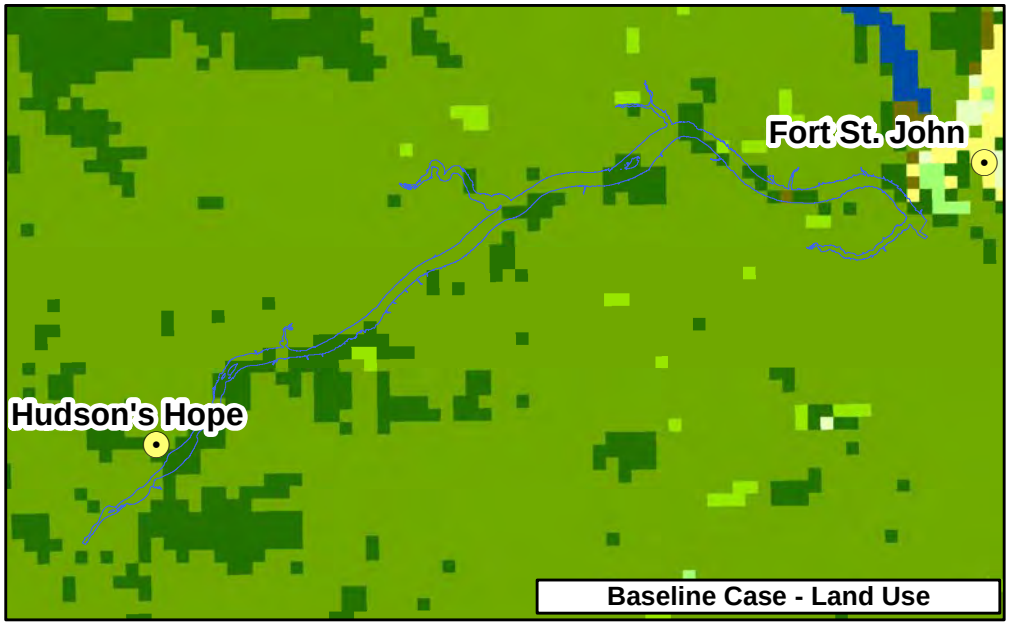

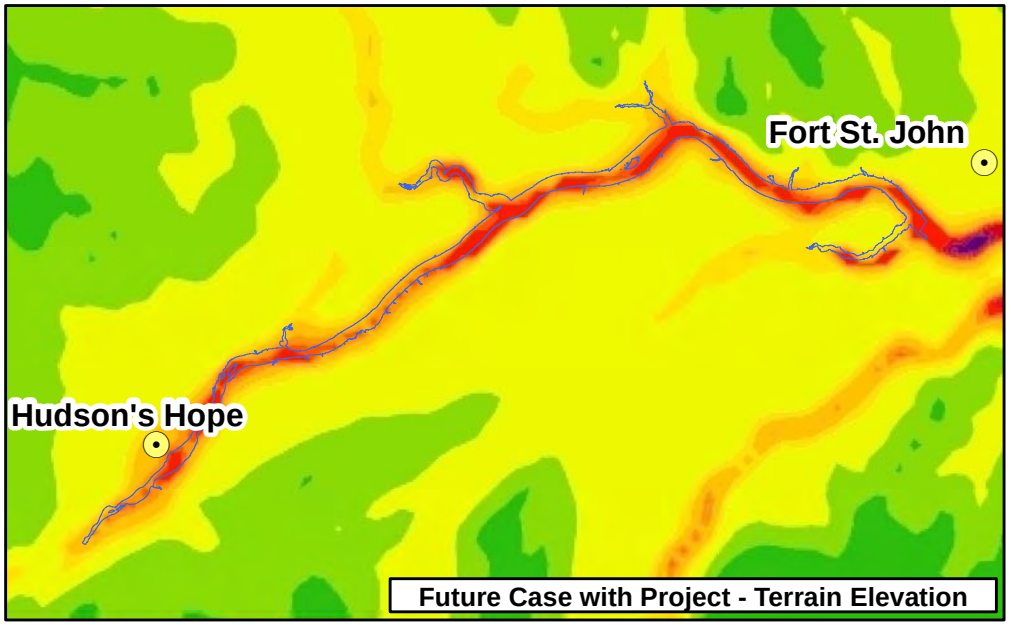

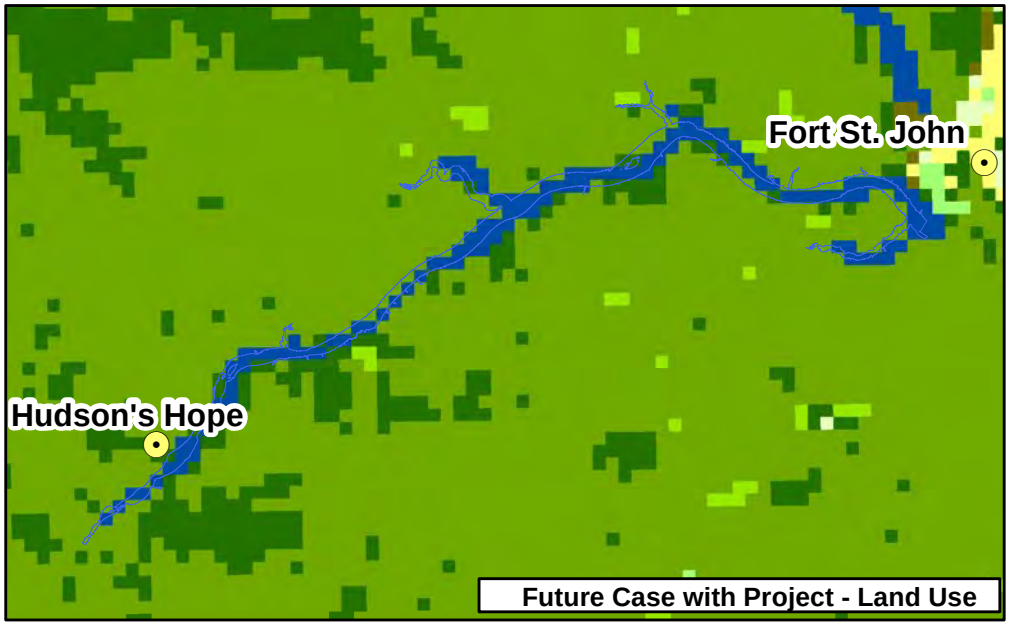

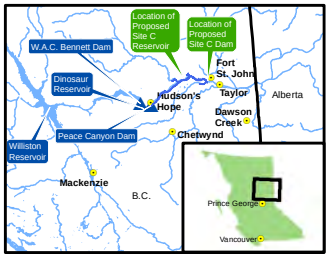

Map Notes:
1. Datum/Projection: NAD83/UTM Zone 10N
2. Proposed Reservoir Area (461.8 m maximum normal elevation) from Digital Elevation Models (DEM) generated from LiDAR data acquired July/August 2006.

Legend

- City / District Municipality
- Proposed Reservoir

Terrain Elevation (m)

- 1000
- 800
- 700
- 600
- 550
- 500
- 480
- 470
- 460
- 450
- 440

Land Use Classification

- Drylnd Crop. Past.
- Crop./Grs. Mosaic
- Crop./Wood Mosc
- Grassland
- Decids. Broadlf.
- Evergrn. Needlf.
- Mixed Forest
- Water Bodies
- Ice

N

1:600,000

0 20 km

SITE C CLEAN ENERGY PROJECT

RWDI BC hydro

Figure 2.5.2
Weather Research and Forecasting model one-kilometre terrain elevation and land-cover characterization

DATE	Dec. 3, 2012	1016-C14-A5500	R 0

© BC Hydro 2012 - all rights reserved. This map is for information purposes only and accuracy is not guaranteed.

Construction of the Site C Clean Energy Project is subject to required regulatory approvals including environmental certification

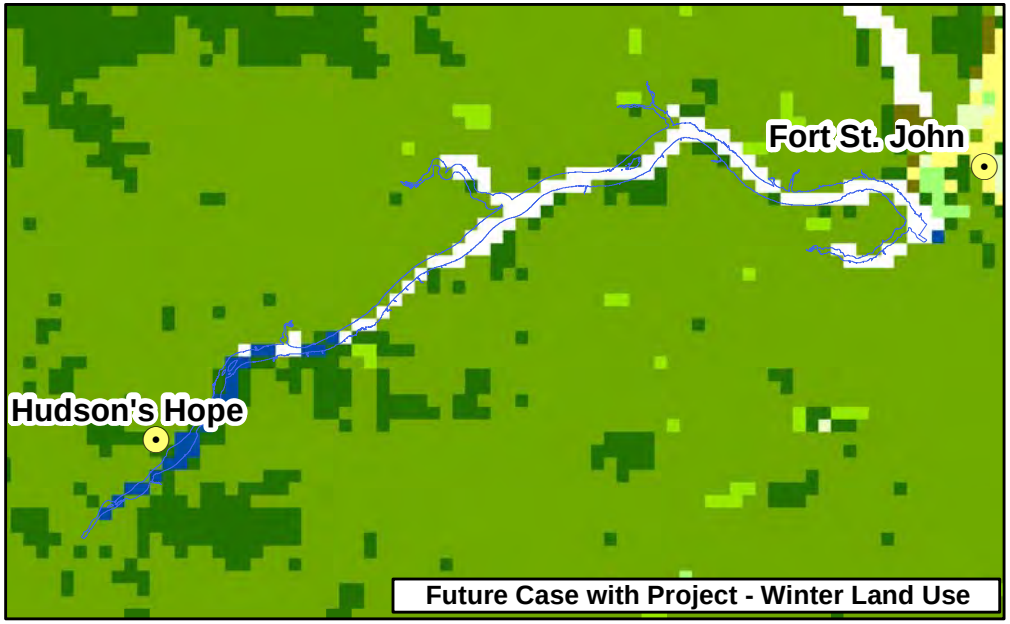

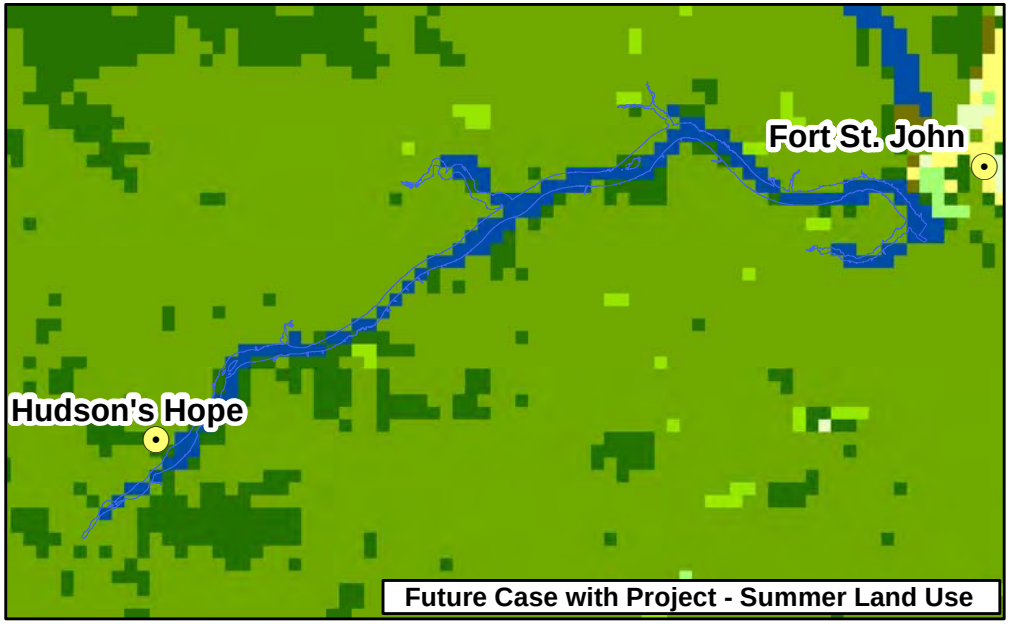

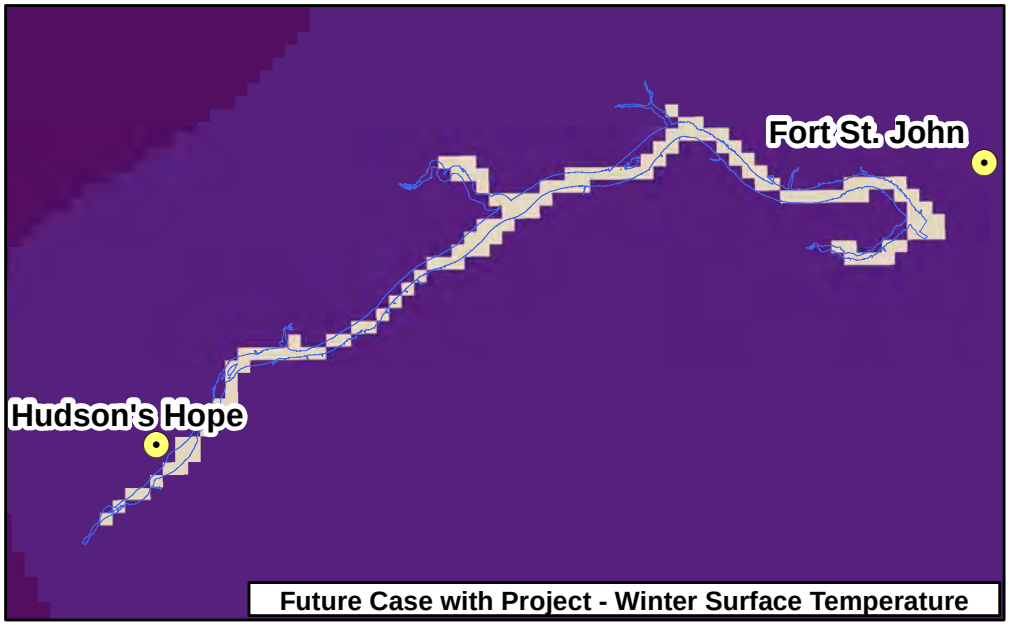

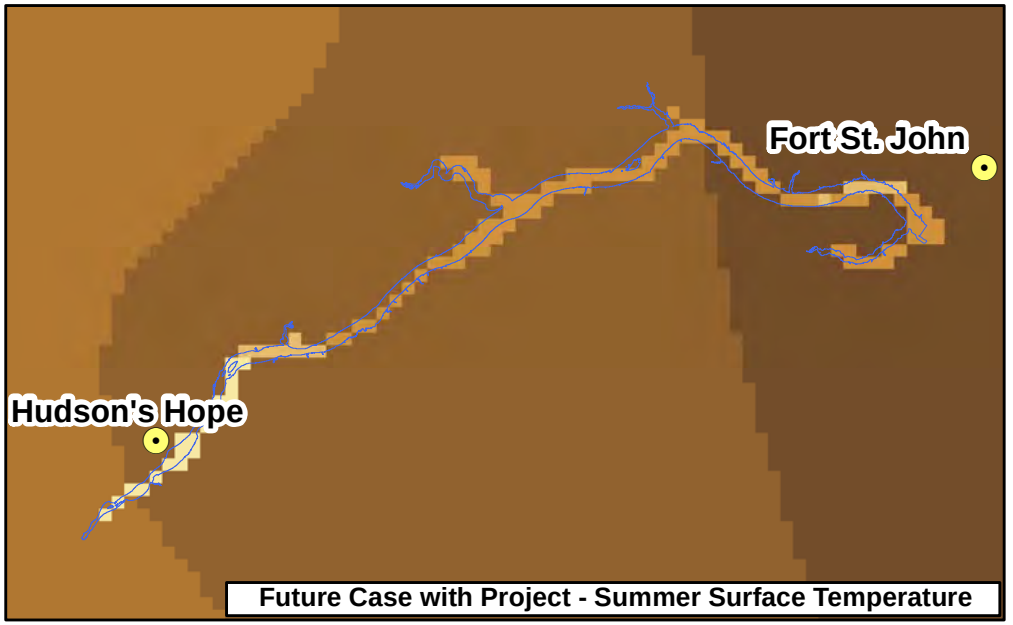

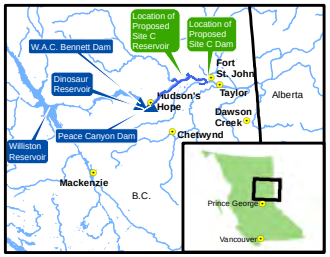

Map Notes:
1. Datum/Projection:Customized Lambert Conformal Conic.
2. Proposed Reservoir Area (461.8 m maximum normal elevation) from Digital Elevation Models (DEM) generated from LiDAR data acquired July/August 2006.

© BC Hydro 2012 - all rights reserved. This map is for information purposes only and accuracy is not guaranteed.

Legend

- City / District Municipality
- Proposed Reservoir

Land Use Classification

- Drylnd Crop. Past.
- Crop./Grs. Mosaic
- Crop./Wood Mosc
- Grassland
- Decids. Broadlf.
- Evergrn. Needlf.
- Mixed Forest
- Water Bodies
- Ice

Temperature (°K)

- 300
- 290
- 280
- 270
- 260
- 250

N

1:600,000

0 20 km

SITE C CLEAN ENERGY PROJECT

RWDI BC hydro

Figure 2.5.3
Example Weather Research and Forecasting model lake surface inputs

DATE	Dec. 3, 2012	1016-C14-A5501	R 0

Construction of the Site C Clean Energy Project is subject to required regulatory approvals including environmental certification

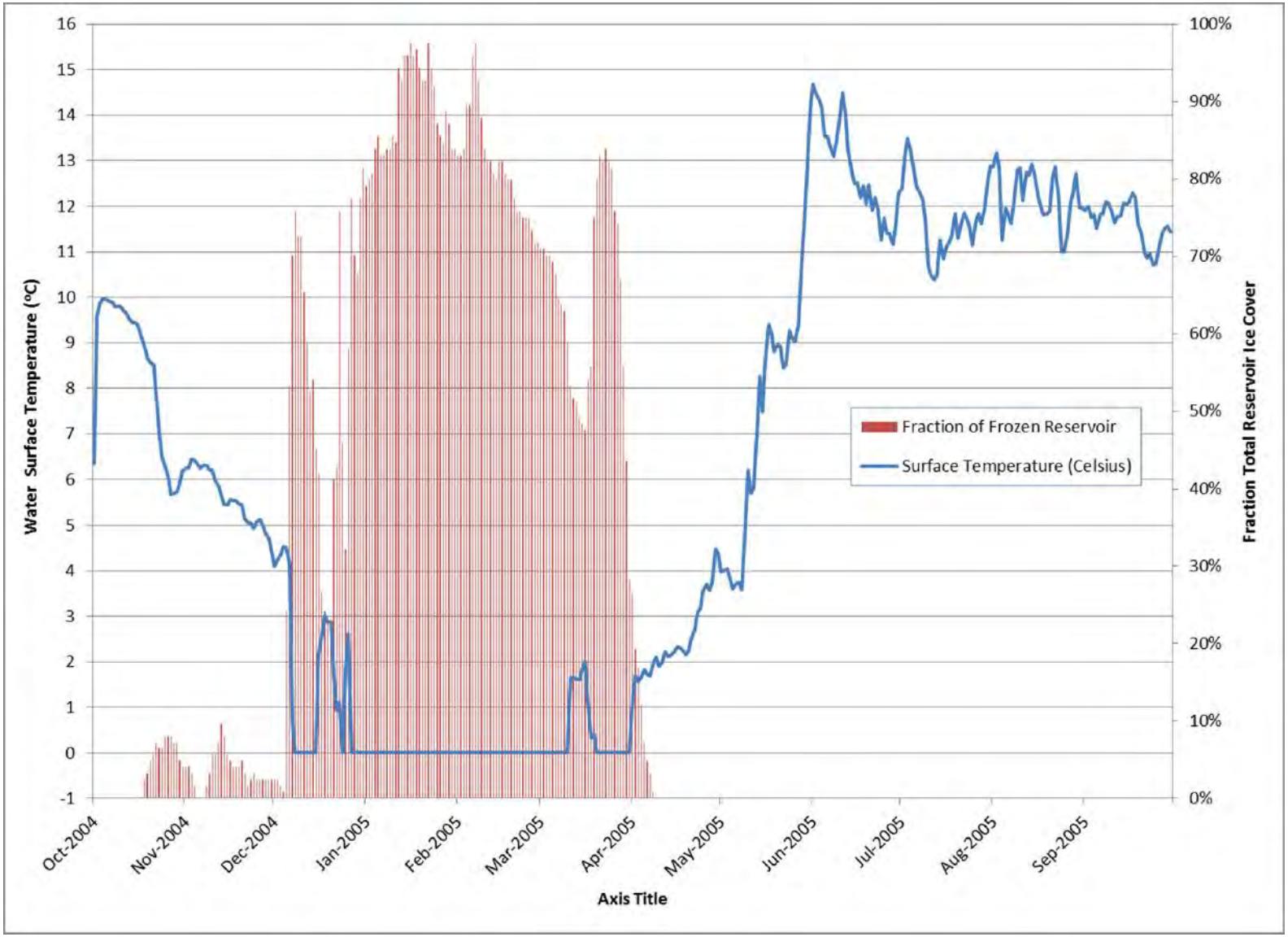

SITE C CLEAN ENERGY PROJECT

RWDI BC hydro

Figure 2.5.4
Weather Research and Forecasting model daily lake temperature and ice cover

DATE	Dec. 3, 2012		R 0

2.6 WEATHER RESEARCH AND FORECASTING MODEL OUTPUTS

2.6.1 Basic WRF model outputs

Basic WRF model outputs are those parameters that are directly predicted by the model and do not require any further calculation other than to extract from the output files and calculate metrics over the required averaging period. These parameters include temperature, mixing ratio, wind speed and precipitation. For example, to calculate the annual average temperature only requires extracting from the model and averaging over the year.

Results from the WRF model were extracted in two ways. First, time series of model variables may be extracted from specific cells within the three-dimensional model grids. WRF model outputs for the locations of the Site C climate network stations and Fort St. John Airport were extracted in this manner. Secondly ‘snapshots’ of the WRF model outputs at a single time across the entire domain were extracted. This method provides a spatial map of the given quantity across the Technical Study Area.

Arithmetic may also be performed on the full model files by applying post-processing tools designed specifically for use with WRF model output files. This allows a user to perform calculations such as maximum, minimum and averages over multiple files or even for the entire model year. Seasonal, monthly and annual metrics of model outputs were calculated thusly. The tools also allow for subtraction between two entire model files. The differences between the WRF model runs for Baseline Case and Future Case with the Project were derived in this manner.

The WRF model simulates many atmospheric quantities over a three dimensional grid from the surface through to the upper atmosphere. For this study, the analysis was limited to those quantities that are commonly associated with the perception of climate. Specifically, near-surface temperature, humidity and wind speed were examined as well as precipitation.

2.6.2 Fog Estimation

The general term 'fog' refers to degradation of near-surface visibility due to the presence of liquid water in the lower atmosphere. If the amount of water vapour present in the atmosphere exceeds the amount that the atmosphere can hold at a given temperature, liquid water droplets would condense to form clouds. As the number and size of these cloud droplets increases, the clouds become thicker. When the water droplets become large, they collide and coalesce into even larger droplets and eventually fall as rain.

When these clouds form near the surface, they constitute what is commonly called fog. Liquid cloud-water droplets in the surface fog and liquid rain drops falling from higher altitudes absorb and scatter visible light thereby reducing visibility. Fog occurrence is not directly predicted by the WRF model, but the model is capable of predicting both the liquid-cloud-water and rain-water contents and thus can be used to estimate fog formation.

If visibility is considered as the distance at which an illuminated object can no longer be seen, then the visibility, defined in units of kilometres and denoted as *VIS*, can be related to the extinction of light, β_{ext}, by the following equation (Stoelinga and Warner 1999):

$$\mathrm{VIS} = -\ln(0.02)/\beta_{ext} \qquad (2.7.1)$$

For visibility reduction due to fog, β_{ext} is the extinction of light by liquid water content of the fog. (Gultepe, et al. 2006) provide the following parameterization for extinction, β_{ext}, from liquid water content, LWC:

$$\beta_{ext} = 44.7 \cdot \mathrm{LWC}^{-0.88} \qquad (2.7.2)$$

The LWC is the value of the liquid water content in grams of water per cubic metre of dry air. Substitution of (2.7.2) into (2.7.1) provides a generalized parameterization for VIS in terms of LWC:

$$\mathrm{VIS} = 0.027 \cdot \mathrm{LWC}^{-0.88} \qquad (2.7.3)$$

The value of LWC for equation (2.7.3) is taken as the sum of the cloud water content and rain water content predicted by the WRF model in units of grams water per cubic metre of dry air.

Though in general terms fog is present whenever there is liquid water present in the atmosphere, more specifically fog is often defined as visibility, VIS, of less than one kilometre while dense fog refers to a value for VIS of less than 500 metres (Friedlein 2004).

Using equation (2.7.3), VIS was calculated for each hour of the model run to quantify the occurrence and density of fog for the Baseline Case and Future Case with the Project.

2.6.3 Visibility at Fort St. John Airport

The International Civil Aviation Organization document *Meteorological Service for International Air Navigation Annex 3* defines visibility as the greatest distance at which a black object of suitable dimensions, situated near the ground, can be seen and recognized when observed against a bright background. In clean air environments the visibility can be up to 70 to 100 kilometres. However, visibility is often reduced somewhat by air pollution and high humidity. In this study, the change in visibility was determined and the frequency of poor visibility was calculated. Examination of visibility at Fort St. John Airport followed a similar methodology to that defined for the examination of fog using equation (3) presented in Section 2.7. Visibility was calculated in units of kilometres using the relationship to the liquid water content as predicted in the WRF model. Since aircraft operations may be altered by changes in visibility over scales greater than one kilometre, the visibility analysis examined changes in the values of visibility over the entire WRF model time series rather than just those hours defined as fog (VIS less than one kilometre) or dense fog (VIS less than 500 metres).

2.6.4 Evaporation over Future Water Surface

The term evaporation refers to the movement of water to the air from sources such as water bodies, soil and canopy interception. Although the process occurs over any surface that contains moisture, a greater portion of evaporation occurs by evaporation of water over open water surfaces such as lakes and oceans.

The inundation of the reservoir would create an area of open water. Evaporation off this surface would increase the flux of water into the atmosphere compared to the existing conditions and would also act to decrease the total water volume held in the reservoir. Thus the rate of evaporation would influence the total amount of water flow available for power generation.

Evaporation is commonly given in unit of total mm of water. That is, how far would the level of a surface of water drop over a given time span due to evaporation at the water surface. The WRF model calculates upward moisture flux at the surface for each grid cell, denoted as, QFX, in units of kg/m^2s. Evaporation for a given period as calculated by the WRF model is then

$$E = 1000 * QFX/\rho * \Delta t \qquad (2.9.1)$$

Where:

E = total evaporation in mm

QFX = upward moisture flux from the WRF model in kg/m^2s

ρ = density of water in kg/m^3

ΔT = time in seconds

WRF model outputs are hourly, so for each output time step, E is given by:

$$E = (1000 *3600/\rho) * QFX \qquad (2.9.2)$$

Using this relation the hourly evaporation over all the WRF model grid cells representing the proposed reservoir surface was calculated. Results were then summed over monthly and annual time periods. For each period, the spatial average over all reservoir grid cells as well as the maximum at any grid cell was reported.

2.7 STATISTICAL METHODS

This section describes the statistical methods that were employed in this study.

Representativeness of the baseline period (October 2004 through September 2005) was evaluated by counting how often monthly parameter averages or totals were greater than one standard deviation of the inter-annual variability during the 1971 through 2000 climate-normal period. In addition, Bayesian two-sample comparisons were performed to compute probabilities

that the baseline period is a good representation of the climate normals. Explicitly, the odds were calculated in favour of equal means and in favour of different standard deviations. High odds indicate a representative baseline period. The technical details of these two analyses are described in Appendix B. Numerical probabilities are expressed using the terminology in IPCC (2007, Box TS.1 on page 23), which is repeated in Table 2.7.1 below.

The WRF model outputs were compared to observations at Fort St. John Airport for the Baseline Case. In particular, the WRF model's modelling skill was evaluated by comparing WRF model outputs with climate normals at Fort St. John Airport as predictors of observations for the Baseline Case. The equations and interpretations of statistics are provided in the sections where they are applied.

Model output from WRF for the Baseline Case was compared with WRF model output for the Future Case with the Project, and the differences were displayed in spatial plots. Bayesian two-sample comparisons were used to determine the statistical significance of the changes in microclimate that occur in the model due to the formation of the Site C reservoir, and to display these in spatial plots.

Results from the WRF model were compared to observations at the field stations for the first year of observations (January 16, 2011 through January 15, 2012). The WRF model skill was evaluated by comparing WRF model output with Fort St. John Airport observations as predictors of observations at the field stations. The following statistics were used.

Absolute differences were calculated for annual total precipitation.

Root mean square errors for N monthly average temperatures from climate normals $T_{CN,i}$ and from baseline observations $T_{obs,i}$ in month i is defined as:

$$RMSE = [\ \Sigma_i\ (T_{CN,i}-T_{obs,i})^2 / N\ ]^{1/2},$$

where Σ_i denotes a summation over all N=12 months. Root mean square errors were calculated for monthly and daily data and for various parameters, observations, WRF model output, and climate normals,

Reduction-of-error scores are calculated as:

$$RE = 1 - (RMSE_{WRF}/RMSE_{CN})^2,$$

where $RMSE_{WRF}$ and $RMSE_{CN}$ are the RMSE of the WRF model and climate normals, respectively. Values close to one represent higher WRF model skill, values close to zero represent similar skills, and negative values represent higher climate-normals skill. The corresponding formula was applied with $RMSE_{CN}$ replaced by $RMSE_{Fort\ St.\ John}$ when comparing WRF model output with observations at Fort St. John Airport.

Mean Bias (MB) is the average of differences between station observations and WRF model output or Fort St. John Airport observations (as labelled). Values closer to zero represent higher skill.

Geometric Mean Bias is used for precipitation and defined as:

$$MG = \Sigma_i R_i^2 / N,$$

where R_i is the ratio between Fort St. John Airport observations and WRF model output or climate normals for month i; the summation Σ_i is performed over N=12 months. The same formula is applied where R_i is the ratio between station observations and WRF model output or Fort St. John Airport observations.

Geometric Variance is used for precipitation and defined as:

$$VG = \Sigma_i \exp[(\ln R_i)^2] / N,$$

where R_i is the ratio between Fort St. John Airport observations and WRF model output or climate normals for month i; the summation Σ_i is performed over N=12 months. The same formula is applied where R_i is the ratio between station observations and WRF model output or Fort St. John Airport observations.

Table 2.7.1 Likelihood terminology and associated probability used in statistical analysis (IPCC, 2007)

Likelihood Terminology	Likelihood of the Occurrence/Outcome
Virtually certain	> 99% probability
Extremely likely	> 95% probability
Very likely	> 90% probability
Likely	> 66% probability
More likely than not	> 50% probability
About as likely as not	33 to 66% probability
Unlikely	< 33% probability
Very unlikely	< 10% probability
Extremely unlikely	< 5% probability
Exceptionally unlikely	< 1% probability

2.8 QUALITY ASSURANCE AND QUALITY CONTROL PROCEDURES

All model input and output files were checked in accordance with RWDI internal protocols in a manner appropriate for a modelling study of this type. The checks included:

- Spatial plots of the geophysical files to ensure that elevation and land-cover characterization are properly represented for both the Baseline Case and the Future Case with the Project;
- Plots of the H3D lake circulation model temperature and ice cover, both before and after incorporation into the WRF model ;

- Sample time series, spatial plots and animations for select periods of the model year to ensure the model ingested inputs and ran correctly; and
- Examination of model output log files and output file sizes to ensure the model ran to completion for all days in the model year.

In addition, a preliminary stage of the modelling study was subject to an independent third party review (Leung 2009, pers. comm.). This review confirmed that the WRF model was a suitable tool for this type of study and also confirmed that the model was run using appropriate inputs and user-selected options. Aside from the incorporation of water temperatures, this current study was performed using the WRF model in the same configuration as that which was subject to the review.

Once the model runs were finished, the model outputs were scrutinized to ensure that the model files were complete and error free and that model results were with the bounds of what is expected for a meteorological simulation in this context. The WRF simulations were subject to a rigorous evaluation, outlined in Section 4.0, to ensure model performance was acceptable. The model results presented in Section 5.0 were examined to make sure that all extractions from the WRF model output files were performed correctly and that model predictions were reasonable.

All metrics derived from the WRF model results were checked by the senior scientist and technical director. Model analyses were subject to quality assurance checks by both the senior scientist and technical director prior to being submitted to the client to ensure completeness, and accuracy. The final Technical Data Report was reviewed by both the technical director and senior consultant to ensure that the requirements outlined in the EIS Guidelines were met.

3.0 EXISTING CONDITIONS

This section describes the existing microclimate of the Peace River Valley. This was done by examining long term meteorological records, reviewing previous reports and field studies in the region and analyzing observations for the Site C climate network stations.

3.1 GENERAL CLIMATE

3.1.1 Previous Studies of Climate in the Peace River Valley

In August 2008, Dr. Stanton Tuller developed an annotated bibliography of reports that discuss the microclimate of the Peace River and estimate the potential influence of the Site C project (Tuller 2008). Rather than replicating Dr. Tuller's work here, the focus of this brief literature review is on descriptions of local microclimates within the Peace River Valley.

Environmental studies performed since the 1970s have included climate descriptions of the Peace River Valley and evaluation of the potential influences of a reservoir created by a dam at Site C. The majority of the reports that described the microclimate of the Peace River Valley were limited by the lack of general climate data observed in the region. Climate observations at Fort St. John Airport provided substantial high quality data for several of the studies; however, since Fort St. John Airport is located outside the Peace River Valley, only limited conclusions

could be drawn about the specific microclimates within the valley. The most detailed climate data set that has been collected in the Peace River Valley was collected over three five-day periods in the fall of 1976 and the winter and spring of 1977 along transects in the Peace River Valley (Thurber Consultants 1977). This data set was later updated to include measurements from the summer of 1977, which were reported in subsequent studies.

Possible additional studies are mentioned in the Tuller report, including the expansion of the existing climate data base by implementing a program of additional observations within the Peace River Valley (Tuller 1991). The report comments that an observational program that concentrates on climate parameters for which little or no data are available would make the greatest contribution to impact-assessment improvement. Specific locations for potential climate stations are identified in the report including areas on the terraces and downstream in Taylor. Attachie Flat is specifically mentioned as a site that has easy access, is a location of previous data collection and is an agricultural area where micro climatic change is of concern. The report also suggests Taylor would be the best site for a downstream station because of its settlement density, economic importance and ease of access.

With these suggestions in mind, BC Hydro installed a climate network in the Peace River Valley that began operating in 2011. These stations measure the parameters listed in Table 2.1.1 and provide climate data that has been heretofore unavailable.

The instrumentation and siting of the BC Hydro Site C climate station network are described in detail in Appendix C.

3.1.2 General Climate of the Peace River Valley

The climate of the Peace River Valley is continental subarctic and characterized by long, cold winters and short, warm, moist summers. The main flow of air is from the southwest (Environment Canada climate normals). While very cold, dry masses of Arctic air dominate in winter, these are occasionally replaced by somewhat warmer and moister air from the west. Although the flow of Arctic air continues through the summer, weather conditions during this season tend to be considerably moister and warmer due to the transfer of heat from the earth's surface to the lower levels of the atmosphere. The Peace River Valley also experiences an infrequent influx of modified maritime air from the Pacific Ocean. Very warm air from the southern regions of the continent rarely penetrates to these latitudes.

Climate normals are defined as the mean value of a specified parameter (i.e., air temperature) over a given 30-year period. For Fort St. John Airport, the most recent climate normals published by Environment Canada are from 1971 through 2000. A complete climate normal summary for Fort St. John Airport is given in Table 3.1.1.

Early spring generally has the lowest precipitation. Rainfall levels peak in summer and decrease to relatively low levels in fall and winter. Virtually all of the precipitation that occurs between November and March falls as snow. Typically, by early February, about 31 centimetres of snow has accumulated on the ground in the Fort St. John area.

During winter it is usual to have periods of arctic weather, with low temperatures between -29 and -40 degrees Celsius. Extreme minimum temperature at Fort St. John Airport is -47 degrees Celsius and extreme maximum temperature is 34 degrees Celsius. The lowest average daily temperature is -14 degrees Celsius in January and the highest is 16 degrees Celsius in July.

Table 3.1.1 displays climate normals in addition to the standard deviation of a range of climate parameters. The full set of climate normals for Fort St. John Airport is provided in Appendix D. Standard deviations are presented for both monthly and annual time frames. The standard deviation values provide an estimate of the variability within both the annual and monthly climate normals.

Figure 3.1.1 shows a time series of mean annual temperature and total annual precipitation from 1943 to 2010 at Fort St. John Airport. Also displayed are the linear trends of both of these parameters. For both time series, the two most obvious trends are the year-to-year variability and the overall 67-year trend. The overall temperature trend shows a warming of approximately 1.5 degrees Celsius over the length of the record. The precipitation trend shows no increase or decrease over the length of the record. The year-to-year variability in temperature and precipitation is typical for a continental location.

Hourly measurements of wind speed and relative humidity are available from Fort St. John Airport for the period from 1953 – 2010. Annual mean wind speed and annual mean relative humidity were calculated for each year over this period. The time series of annual averages for both is shown in Figure 3.1.2 along with the linear trend of both parameters. The trend for wind speed shows a decrease over the period of record of approximately 6 km/h. The trend for relative humidity also shows a decrease over the same time period of approximately 7%.

Table 3.1.1 1971 through 2000 climate normals for Fort St. John Airport[1]

	Jan	Feb	Mar	Apr	May	Jun	Jul	Aug	Sep	Oct	Nov	Dec	Year
Temperature													
Daily Average (°C)	-14.2	-10.5	-4.4	4.0	10.0	13.8	15.7	14.6	9.9	3.9	-6.7	-12.1	2.0
Standard Deviation	5.7	5.6	3.6	2.2	1.7	1.1	1.1	1.5	2.0	2.0	4.5	5.3	1.3
Daily Maximum (°C)	-9.9	-6.0	0.3	9.3	15.7	19.2	21.2	20.2	15.1	8.2	-2.9	-8.0	6.9
Standard Deviation	5.8	5.6	3.6	2.6	2.1	1.4	1.4	2.0	2.4	2.3	4.4	5.1	1.3
Daily Minimum (°C)	-18.4	-15.0	-9.1	-1.3	4.1	8.2	10.2	8.9	4.6	-0.4	-10.4	-16.2	-2.9
Standard Deviation	5.6	5.6	3.7	1.9	1.3	0.9	1.0	1.2	1.6	1.7	4.7	5.5	1.2
Extreme Maximum (°C)	11.6	12.8	18	27.9	31.8	31.7	33.3	33.6	30	25.6	18.3	11.4	33.6
Extreme Minimum (°C)	-47.2	-42.2	-36.7	-28.9	-10.6	-0.6	0.7	-2.9	-12.8	-25	-39.2	-44.6	-47.2
Precipitation													
Rainfall (mm)	0.4	0.5	0.7	8.8	35.5	70.9	83.2	56.1	41.1	11.5	3.4	0.6	312.6
Standard Deviation	1.0	1.4	1.3	9.5	24.4	37.2	44.3	34.1	25.8	9.1	4.1	2.0	81.8
Snowfall (cm)	32.2	28.3	25.3	10.6	4.1	0.4	0.0	0.8	4.8	16.5	30.3	32.4	185.6
Standard Deviation	23.9	19.8	18.2	7.6	6.3	2.2	0.1	3.8	9.7	12.4	23.4	21.8	60.4
Precipitation (mm)	26.0	21.9	21.4	18.8	39.7	71.4	83.2	56.9	45.7	25.8	28.5	26.5	465.6
Standard Deviation	19.9	16.6	16.4	13	26.3	37.6	44.3	34.1	28.1	15.3	20	16.9	103.7
Average Snow Depth (cm)	30	31	25	6	0	0	0	0	0	1	9	20	10
Standard Deviation	25.3	27.9	23.1	0.9	0.0	0.0	0.0	0.0	1.8	4.3	16.0	19.8	6.7
Wind Speed													
Speed (km/h)	13.7	14.3	13.8	14.4	14.3	13.6	12.3	11.9	13.0	15.4	13.8	13.7	13.7
Standard Deviation	3.3	2.8	1.7	2.5	2.0	2.2	1.5	1.8	1.6	2.1	2.3	2.9	1.4

NOTES:

[1](Environment Canada 2012)

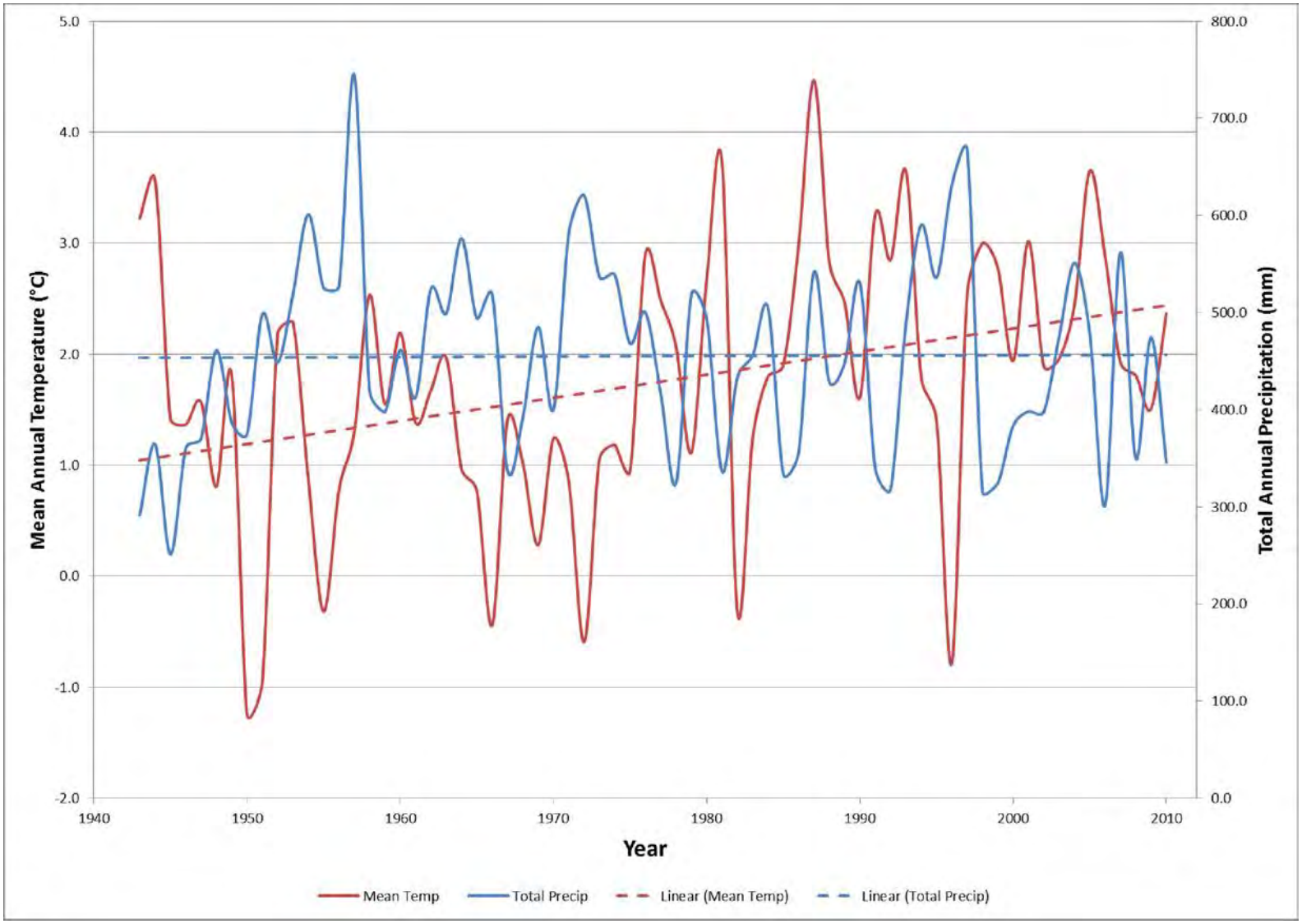

Mean annual temperature and precipitation at Fort St. John

SITE C CLEAN ENERGY PROJECT

RWDI BC hydro

Figure 3.1.1
Mean annual temperature and precipitation at Fort St. John Airport

DATE	Dec. 7, 2012		R 0

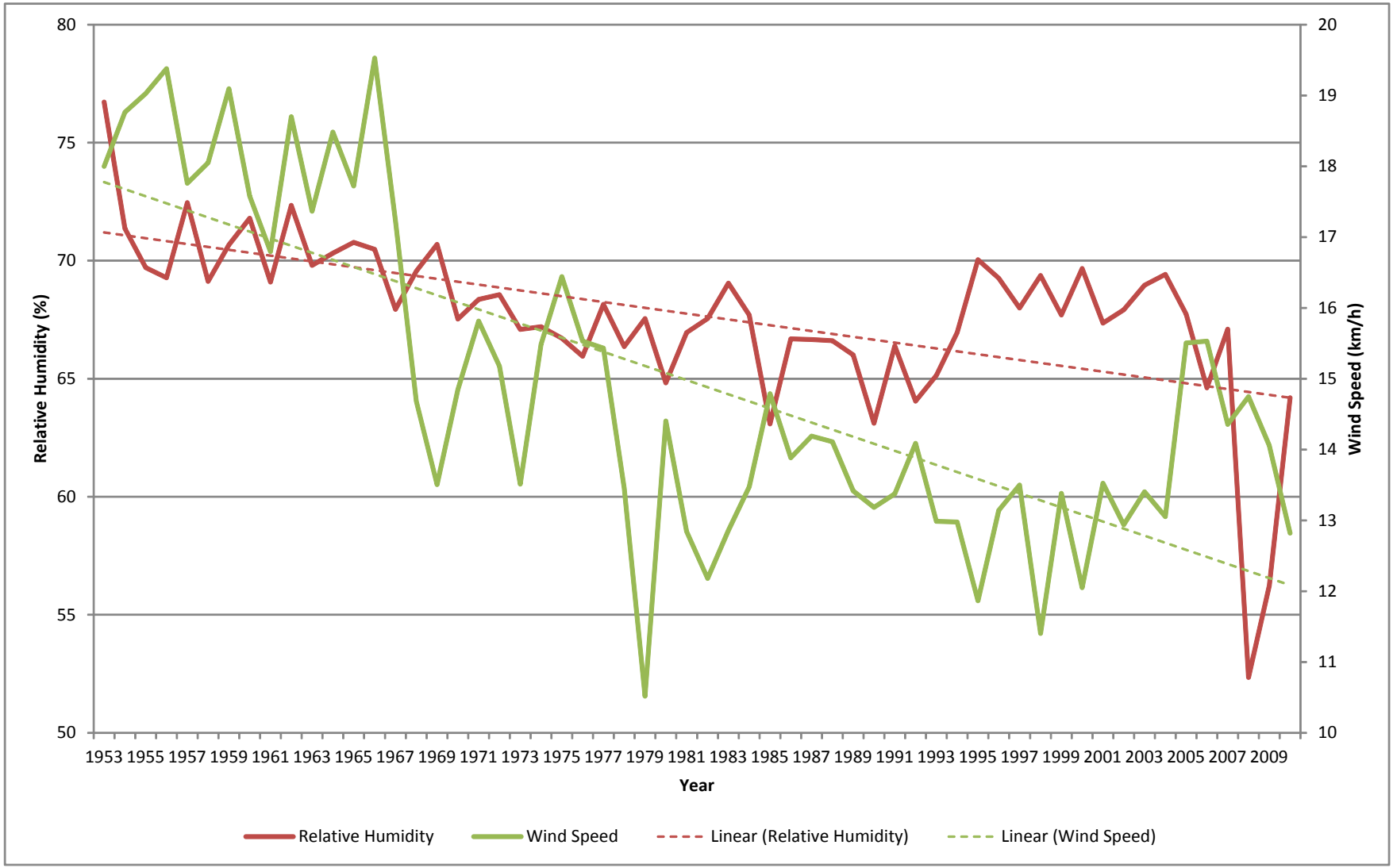

Mean annual wind speed and relative humidity at Fort St. John.

SITE C CLEAN ENERGY PROJECT		RWDI BC hydro	**Figure 3.1.2 Mean annual wind speed and relative humidity at Fort St. John Airport**
DATE	Dec. 7, 2012		R 0

3.2 MICROCLIMATE

As part of the Project, a network of climate stations was established in late 2010 and early 2011 (Figure 2.1.1). These stations were installed to be able to measure the current microclimate of the Peace River Valley and provide a baseline against which potential future microclimate change as a result of the Project could be evaluated. A range of climatically important parameters is measured at the climate stations (Table 2.1.1) that can be used to monitor any potential microclimate changes in the future. In addition, the location of the stations was chosen to represent a wide range of climatic zones within the Technical Study Area. Field measurements taken at sites along the proposed reservoir from January 2011 to February 2012 were used to provide more detailed spatial information on the existing microclimate at the Project site.

3.2.1 First Year of Observations

The first year of observations (FYO) at the seven Site C climate stations established by BC Hydro in the Peace Valley covered January 16, 2011 to January 15, 2012. At this point, all stations had a minimum of one complete year of observations. Data collected during the FYO was used, along with contemporaneous measurements taken at Fort St. John Airport by Environment Canada, to look at the spatial variability of climate parameters in the Technical Study Area.

It is not practical to present the results of all parameters measured at the Site C climate stations during the FYO (Table 2.1.1) here but a few of the more common parameters are presented below. These include air temperature, wind speed, wind direction and precipitation. These common climate parameters are also recorded at Fort St. John Airport and provide a basis to compare against climate normals measured there. The FYO at Fort St. John Airport was warmer (2.9 degrees Celsius vs. 2.0 degrees Celsius), wetter (626 millimetres vs. 466 millimetres) and had lower mean annual wind speed (2.9 metres per second vs. 3.8 metres per second) than normals.

3.2.2 Temperature and Wind

Figure 3.2.1 shows a time series plot of temperature at all the Site C climate stations as well as Fort St. John Airport. There are two main features of this plot that are important. The first is that the plot shows the annual trend in mean daily temperatures. Winter displays the greatest variability in temperatures due to the frequent passage of fronts that bring different air masses with distinct temperature characteristics. In the summer, the cold arctic air masses present in winter are much farther north, resulting in less extreme temperatures.

The second important feature of Figure 3.2.1 is the small differences that exist between the stations. The maximum average annual temperature difference during the FYO between any two stations is 1.0 degrees Celsius (Table 3.2.1). Therefore, the spatial differences in temperature between stations are less than the standard deviation of annual temperatures at Fort St. John Airport (Table 3.1.1). It is not surprising that this is the case as there is only a 70-

kilometre difference between Fort St. John Airport and the furthest station away (Station 5 – Hudson's Hope). In addition, although some stations are within the Peace River Valley, the maximum difference in station elevations is from 431 metres at Bear Flat to 648 metres at Attachie Flat. (Figure 3.1.1 Mean annual temperature and precipitation at Fort St. John Airport) The Peace River does not appear to influence temperatures differentially at the climate stations as there is no relationship between proximity of the river and average annual temperature. The differences between stations are likely a result of small scale differences in surface characteristics.

Wind speed and direction was also measured at all stations. Figure 3.2.2 through Figure 3.2.9 show wind roses for all stations including Fort St. John Airport. Mean annual wind speed ranges between 1.6 and 2.8 meters per second at the BC Hydro stations. Fort St. John Airport has the highest mean wind speed of 4.3 metres per second. (Table 3.2.1) Like temperature, the standard deviation of annual wind speed at Fort St. John Airport is smaller than the spatial difference in annual wind speed at all climate stations. The differences in wind speed and direction that do exist and are apparent in the wind roses are attributed to differences between small scale surface features such as proximity of trees and local topography to the climate station and location within the meandering Peace River Valley. Also, the higher wind speed at Fort St. John Airport is due to this station being on the plateau above the Peace River Valley and its very open location with a large fetch.

3.2.3 Precipitation

Unlike temperature and wind speed, total annual precipitation shows differences between stations over all seasons (Figure 3.2.10 and Table 3.2.1). The maximum difference between stations of 212 millimetres, which exists between Fort St. John Airport and Station 4, is larger than the standard deviation of annual precipitation at Fort St. John Airport, which is 104 millimetres. This suggests that there is a spatial dependence on precipitation in the Technical Study Area. On an annual basis, this does not make sense as there are no large topographical differences between stations and a horizontal range of only 70-kilometres is unlikely to result in large precipitation differences. Due to the consistently lower precipitation at all Site C climate stations relative to Fort St. John Airport it was decided to investigate whether there could be another reason for the differences.

At Fort St. John Airport, rain is recorded daily by a using a funnel and graduated cylinder. Snowfall is measured using a Nypher gauge to capture snow, which is melted into a graduated cylinder and also measured daily. At all the Site C climate stations, precipitation (both liquid and solid) is measured by a tipping bucket type gauge with an alter windshield. During periods of temperatures below freezing, antifreeze is added to the gauges to melt the snow and allow the tipping bucket to continue to function.

Due to the consistently lower precipitation measurements at the Site C climate stations relative to Fort St. John Airport, it was decided to temporarily install a different type of gauge to determine if there is undercatch occurring at these stations. An identical gauge to Fort St. John

Airport was not possible as it would require personnel to be onsite daily. Therefore, an automated Ott Pluvio weighing gauge was installed at Station 1 adjacent to the previously installed tipping bucket gauge. The Pluvio gauge also had a wind screen. Over the course of three months during the winter in 2011-2012, the Pluvio gauge consistently recorded higher precipitation than the existing tipping bucket gauge (Figure 3.2.11). Over the three months of comparison, the Pluvio recorded 33.2 millimetres versus 26.9 millimetres for the tipping bucket gauge. It is therefore likely that the tipping bucket gauges are under recording precipitation. The differences that are seen between Fort St. John Airport and the Site C climate stations are likely not as high as measured. The implications of this in terms of the model study are discussed in model evaluation in the model evaluation for precipitation in section 4.2.

Table 3.2.1 Summary of measured climate parameters during First Year of Observation

	Mean Temp (°C)	Max Temp (°C)	Min Temp (°C)	Total Precipitation (mm)	Mean wind speed (m/s)
Station 1	3.1	29.9	-33.5	447	2.5
Station 2	3.1	30.6	-35.6	415	2.3
Station 3	3.3	28.6	-34.2	509	2.8
Station 4	2.9	29.3	-35.4	414	1.6
Station 5	3.7	30.8	-36.3	521	1.9
Station 6	—	—	—	—	1.8
Station 7	3.9	29.2	-33.1	541	2.8
Fort St. John Airport	2.9	27.7	-32.9	626	4.3
Max. difference in values	**1.0**	**3.1**	**3.4**	**212**	**2.7**

NOTES:
— indicates no data collected

3.2.4 Summary

Although there are relatively small differences in measured climate parameters between stations in the FYO the differences that are present demonstrate that each station exists in its own microclimate. Differences in factors such as elevation, moisture availability, surface cover, topography and local roughness all contribute to the differences seen between stations. Until the record of measurement becomes longer it is not known if the differences in measured parameters, and hence the range of microclimates, seen in the FYO are typical in the long term. This is related to the general limitation for this study of using a single year of observations or a single model year to estimate a long term phenomenon such as climate. As with the model year, the FYO is expected to be close to the long term average, but year-to-year variation cannot be confirmed until there is a longer data record.

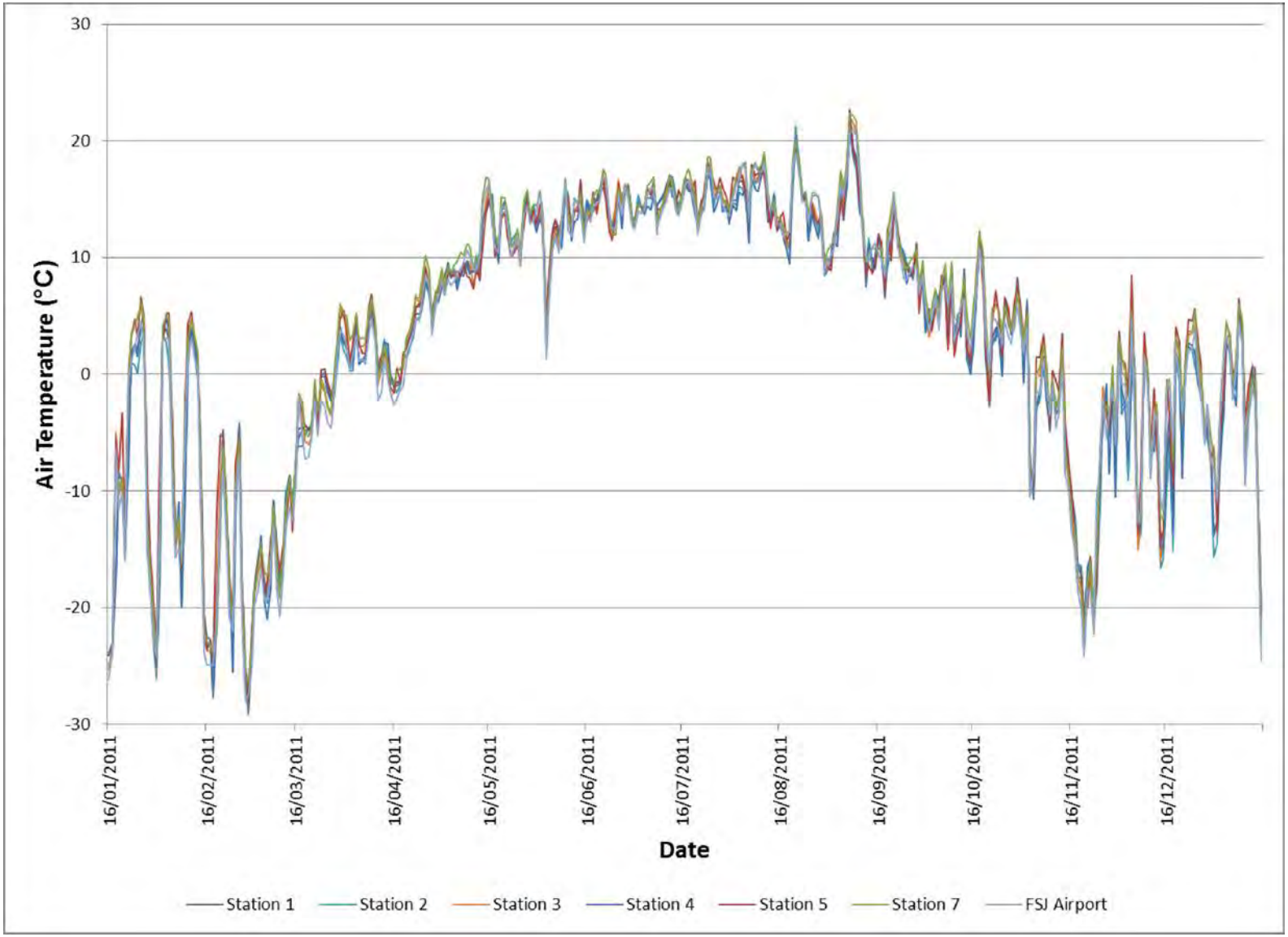

SITE C CLEAN ENERGY PROJECT

RWDI BC hydro

Figure 3.2.1
Mean daily temperatures at climate stations and Fort St. John Airport

DATE	Dec. 3, 2012		R 0

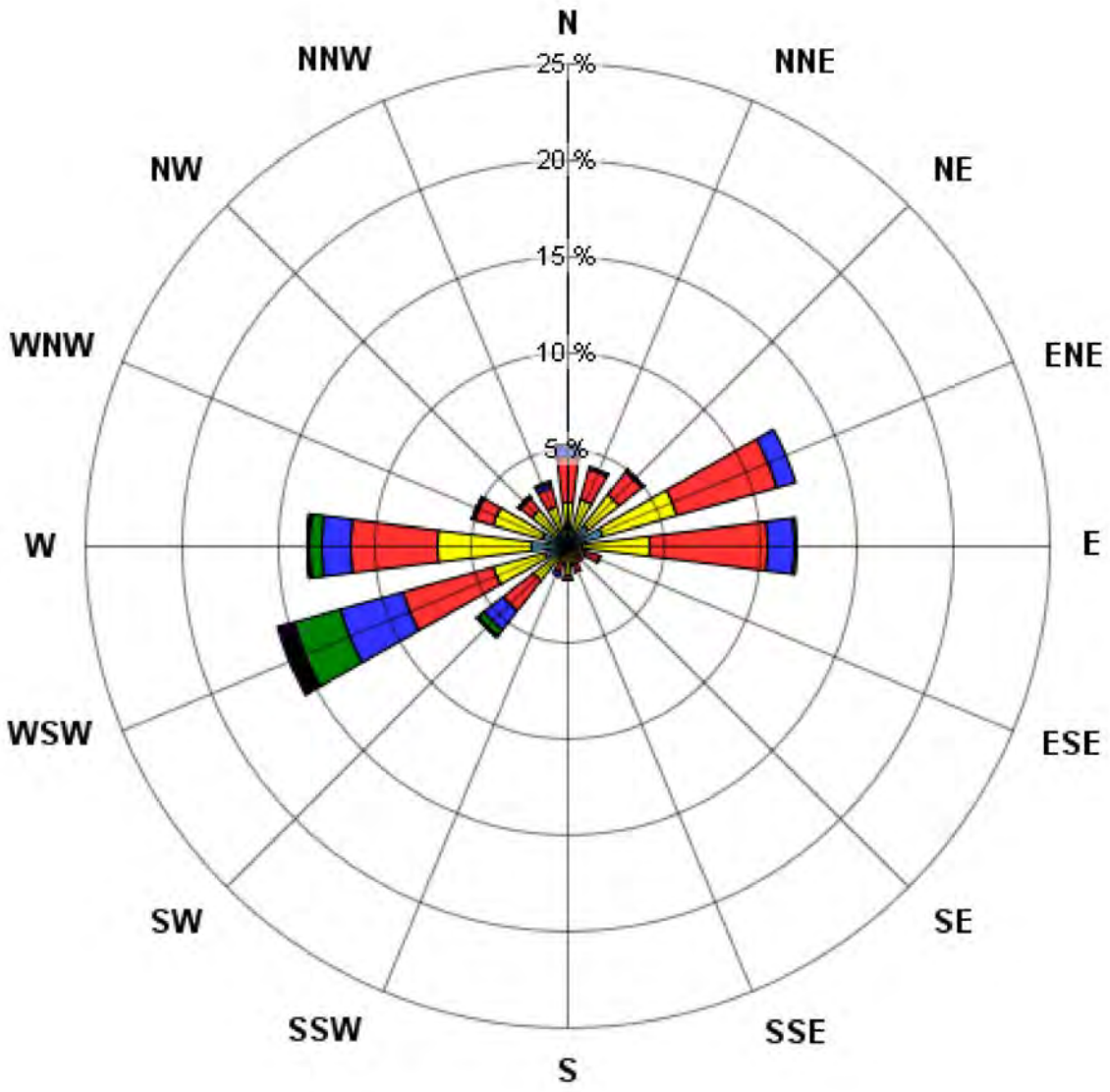

Calms: 6.79%

Windrose for Station 1 during first year of operation

Wind Speed (m/s)

- > 10.0
- > 8.0 - 10.0
- > 6.0 - 8.0
- > 4.0 - 6.0
- > 2.0 - 4.0
- > 1.0 - 2.0
- > 0.5 - 1.0

SITE C CLEAN ENERGY PROJECT

RWDI BC hydro

Figure 3.2.2
Windrose for Station 1
during first year of operation

DATE	Dec. 3, 2012		R 0

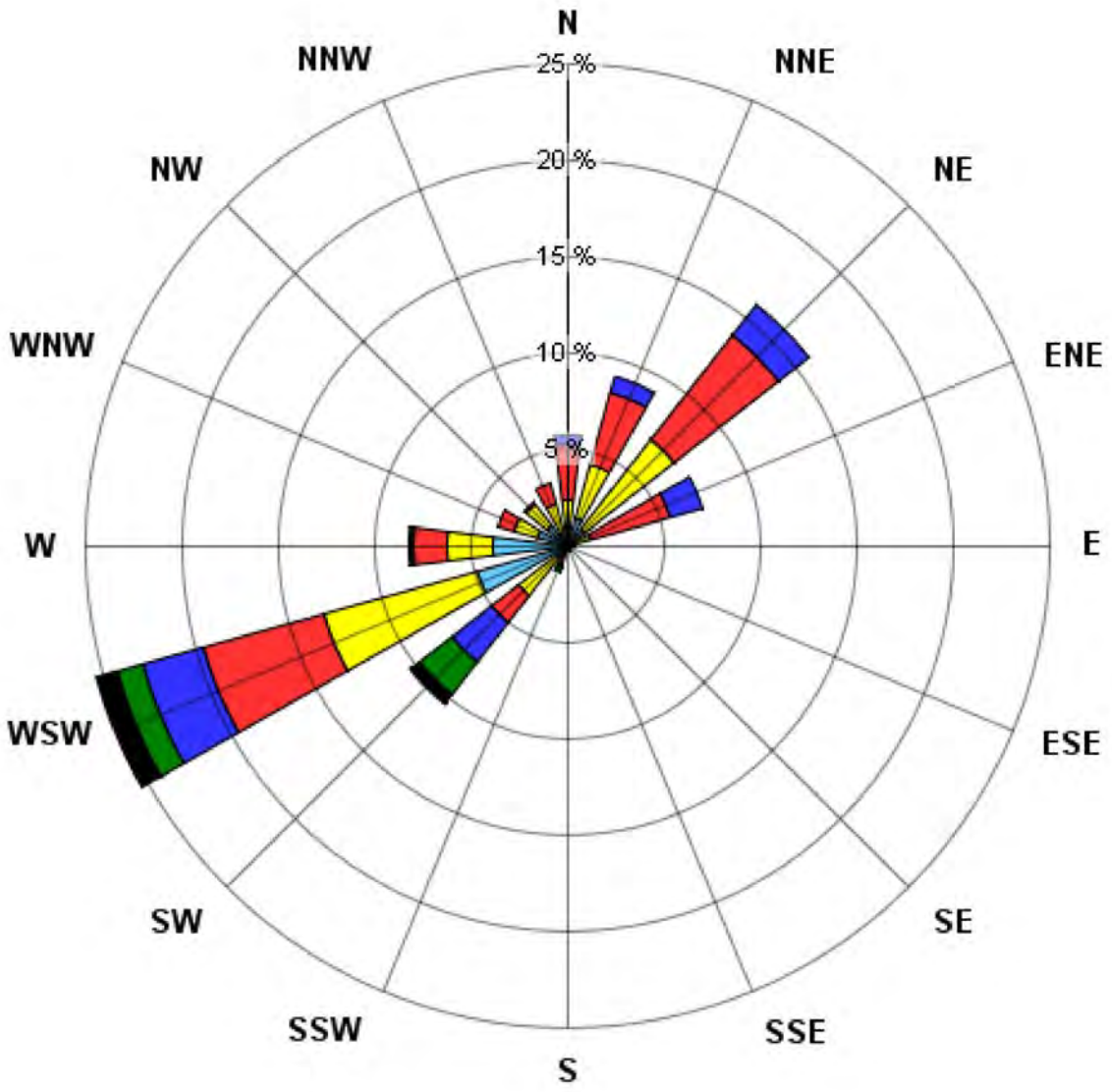

Calms: 5.52%

Windrose for Station 2 during first year of operation

Wind Speed (m/s)

- > 10.0
- > 8.0 - 10.0
- > 6.0 - 8.0
- > 4.0 - 6.0
- > 2.0 - 4.0
- > 1.0 - 2.0
- > 0.5 - 1.0

SITE C CLEAN ENERGY PROJECT

RWDI BC hydro

Figure 3.2.3
Wind rose for Station 2
during first year of operation

DATE	Dec. 3, 2012		R 0

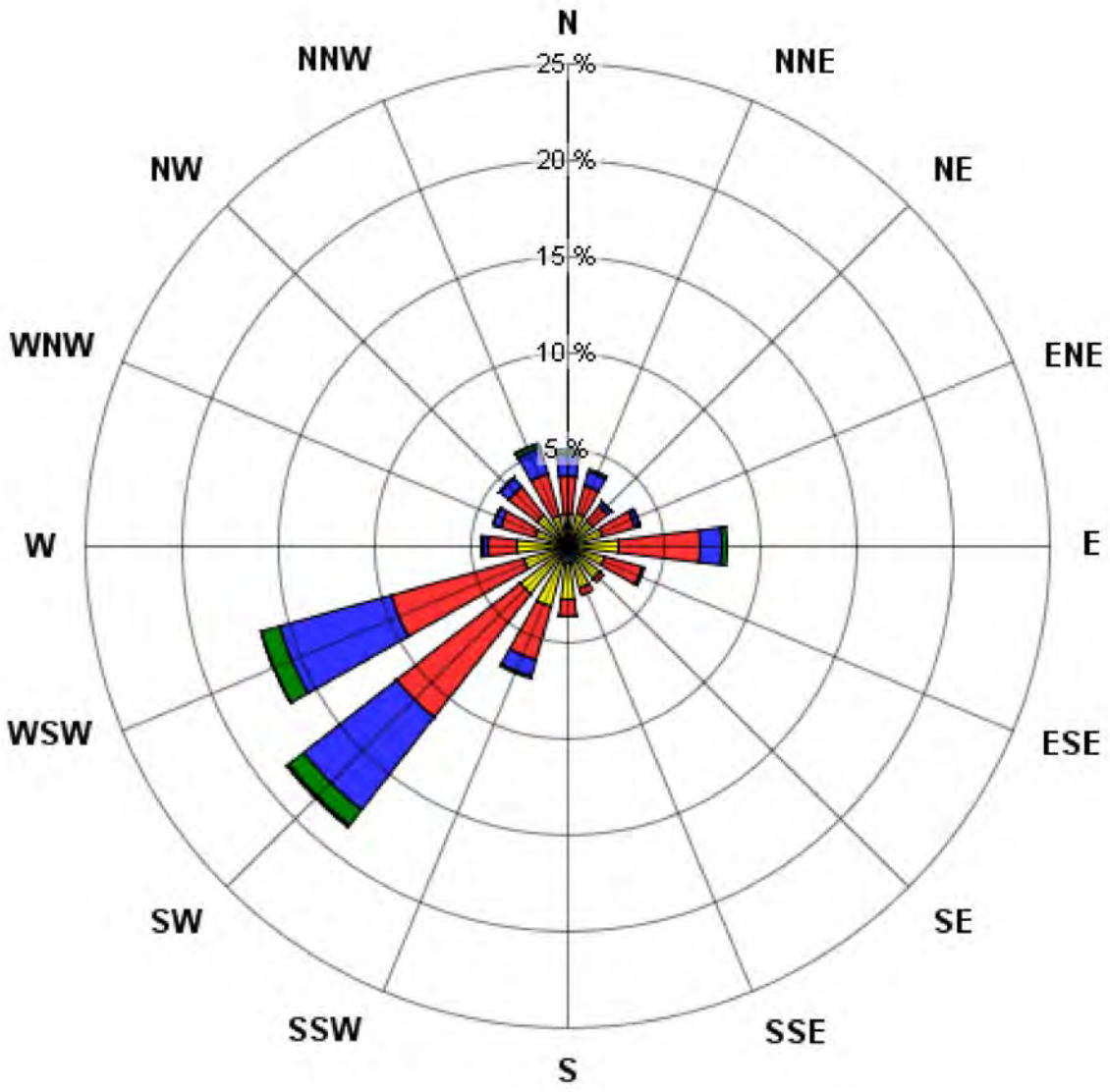

Calms: 2.36%

Windrose for Station 3 during first year of operation

Wind Speed (m/s)

- > 10.0
- > 8.0 - 10.0
- > 6.0 - 8.0
- > 4.0 - 6.0
- > 2.0 - 4.0
- > 1.0 - 2.0
- > 0.5 - 1.0

SITE C CLEAN ENERGY PROJECT

RWDI BC hydro

Figure 3.2.4
Wind rose for Station 3
during first year of operation

DATE	Dec. 3, 2012		R 0

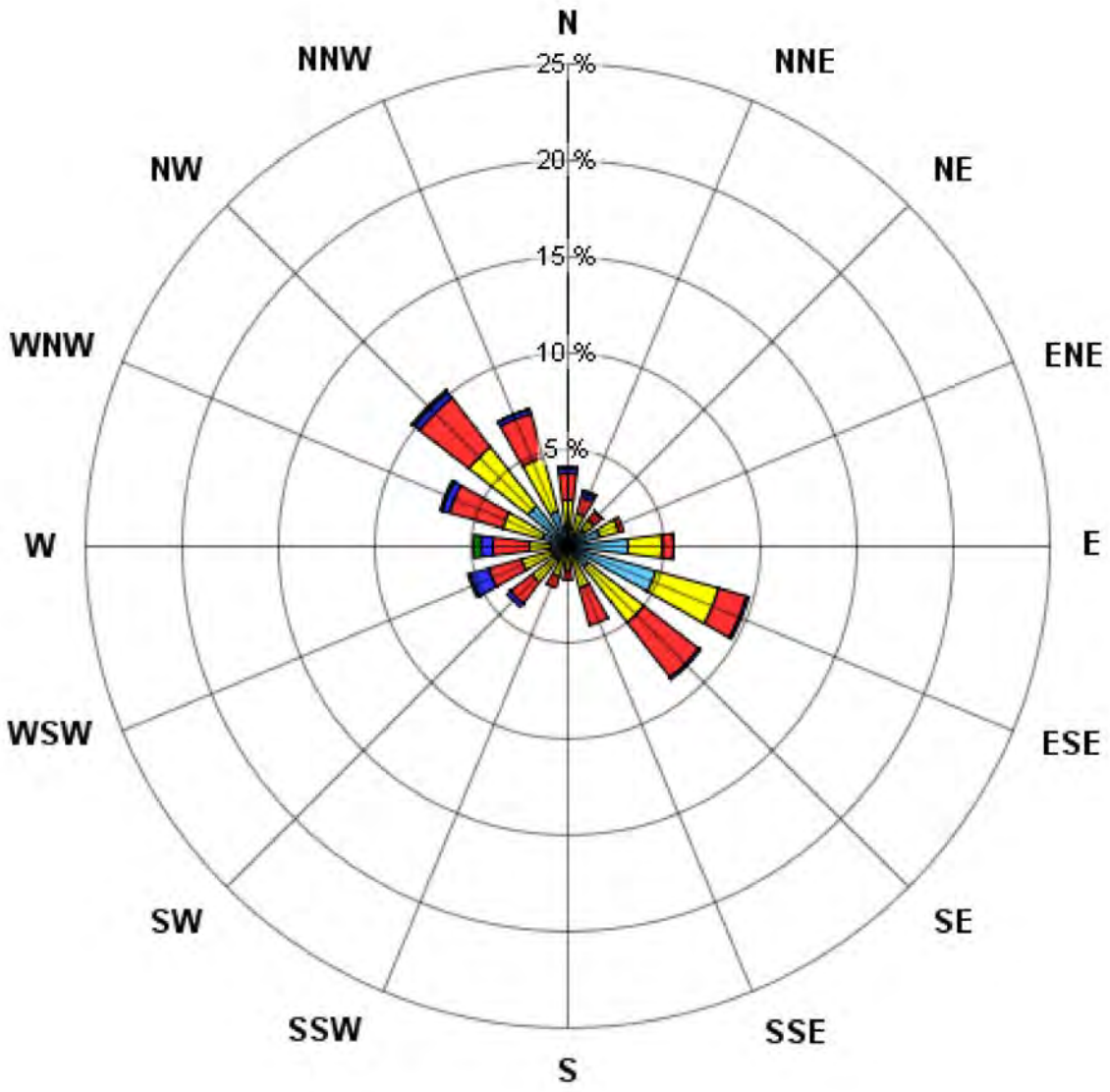

Calms: 16.85%

Windrose for Station 4 during first year of operation

Wind Speed (m/s)

- > 10.0
- > 8.0 - 10.0
- > 6.0 - 8.0
- > 4.0 - 6.0
- > 2.0 - 4.0
- > 1.0 - 2.0
- > 0.5 - 1.0

SITE C CLEAN ENERGY PROJECT

RWDI BC hydro

Figure 3.2.5
Wind rose for Station 4
during first year of operation

DATE	Dec. 3, 2012		R 0

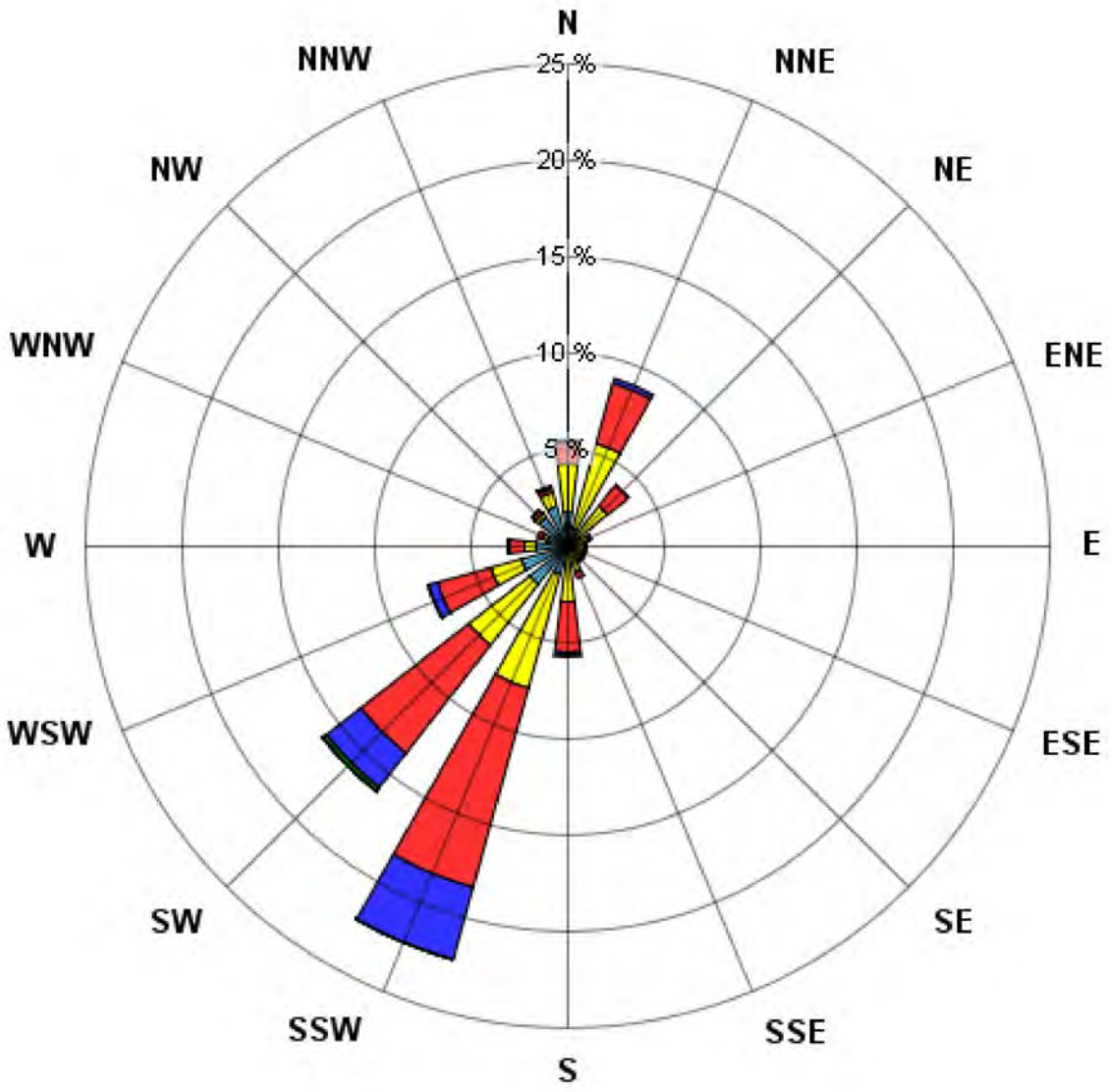

Calms: 13.62%

Windrose for Station 5 during first year of operation

Wind Speed (m/s)

- > 10.0
- > 8.0 - 10.0
- > 6.0 - 8.0
- > 4.0 - 6.0
- > 2.0 - 4.0
- > 1.0 - 2.0
- > 0.5 - 1.0

SITE C CLEAN ENERGY PROJECT

RWDI BC hydro

Figure 3.2.6
Wind rose for Station 5
during first year of operation

DATE	Dec. 3, 2012		R 0

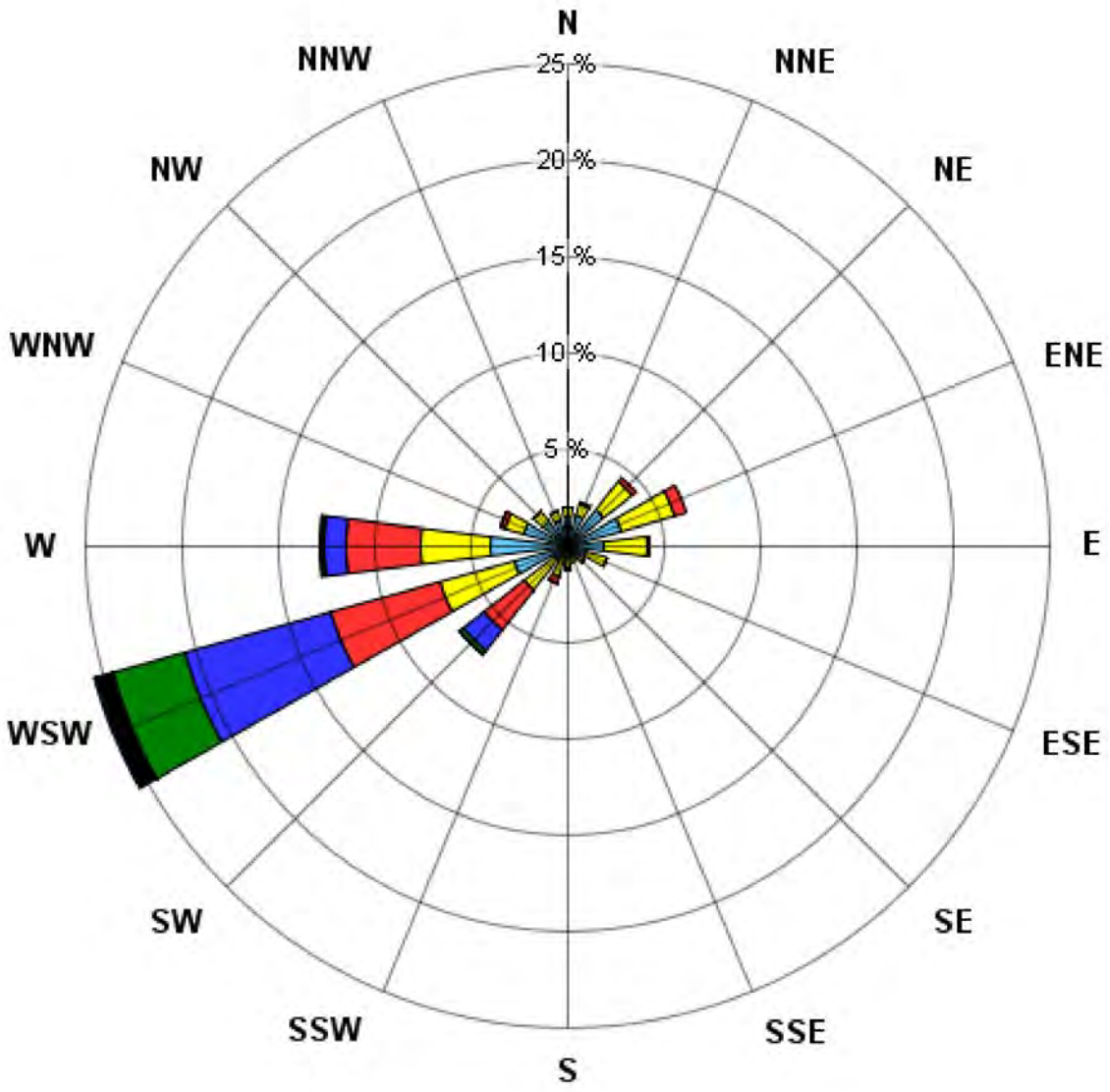

Calms: 19.78%

Windrose for Station 6 during first year of operation

Wind Speed (m/s)

- > 10.0
- > 8.0 - 10.0
- > 6.0 - 8.0
- > 4.0 - 6.0
- > 2.0 - 4.0
- > 1.0 - 2.0
- > 0.5 - 1.0

SITE C CLEAN ENERGY PROJECT

RWDI BC hydro

Figure 3.2.7
Wind rose for Station 6
during first year of operation

DATE	Dec. 3, 2012		R 0

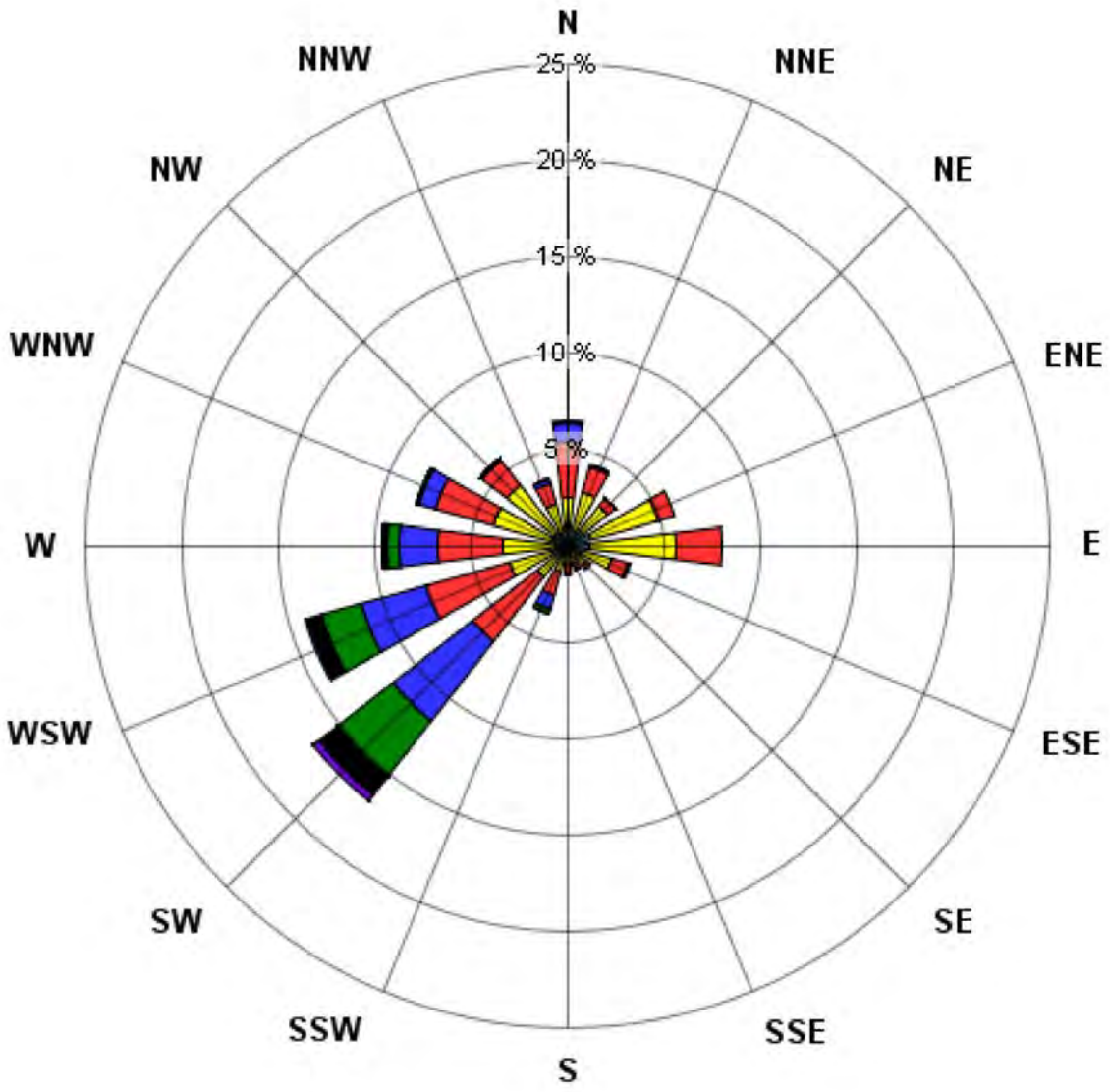

Calms: 2.99%

Windrose for Station 7 during first year of operation

Wind Speed (m/s)

- > 10.0
- > 8.0 - 10.0
- > 6.0 - 8.0
- > 4.0 - 6.0
- > 2.0 - 4.0
- > 1.0 - 2.0
- > 0.5 - 1.0

SITE C CLEAN ENERGY PROJECT

RWDI BC hydro

Figure 3.2.8
Wind rose for Station 7
during first year of operation

DATE	Dec. 3, 2012		R 0

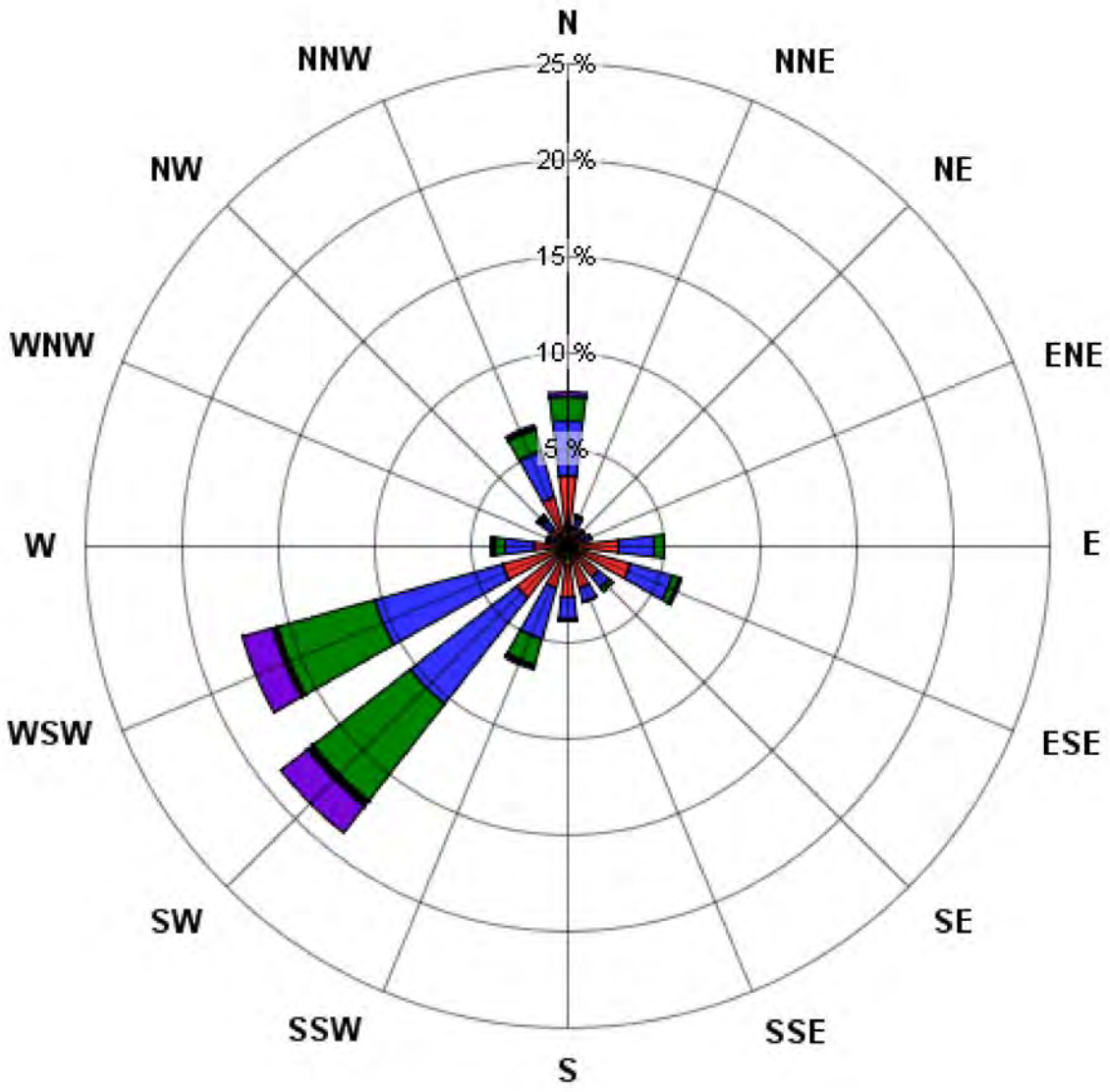

Calms: 10.46%

Windrose for Fort St. John during first year of operation

Wind Speed (m/s)

- > 10.0
- > 8.0 - 10.0
- > 6.0 - 8.0
- > 4.0 - 6.0
- > 2.0 - 4.0
- > 1.0 - 2.0
- > 0.5 - 1.0

SITE C CLEAN ENERGY PROJECT

RWDI BC hydro

Figure 3.2.9
Wind rose for Fort St. John Airport during first year of operation

DATE	Dec. 3, 2012		R 0

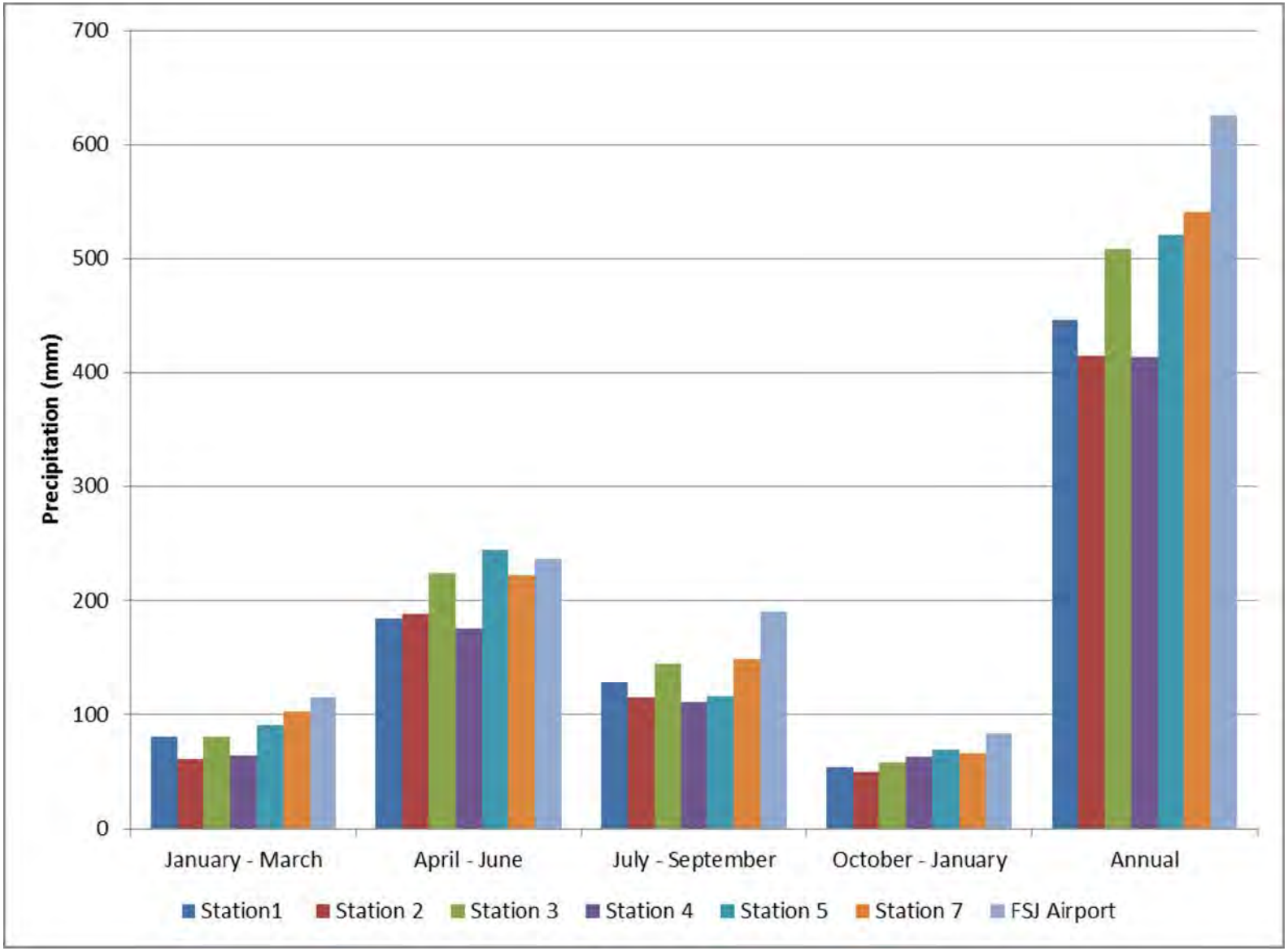

Seasonal and annual precipitation totals at climate stations and Fort St. John

SITE C CLEAN ENERGY PROJECT		RWDI BC hydro	**Figure 3.2.10 Seasonal and annual precipitation totals at climate stations and Fort St. John Airport**
DATE	Dec. 3, 2012		R 0

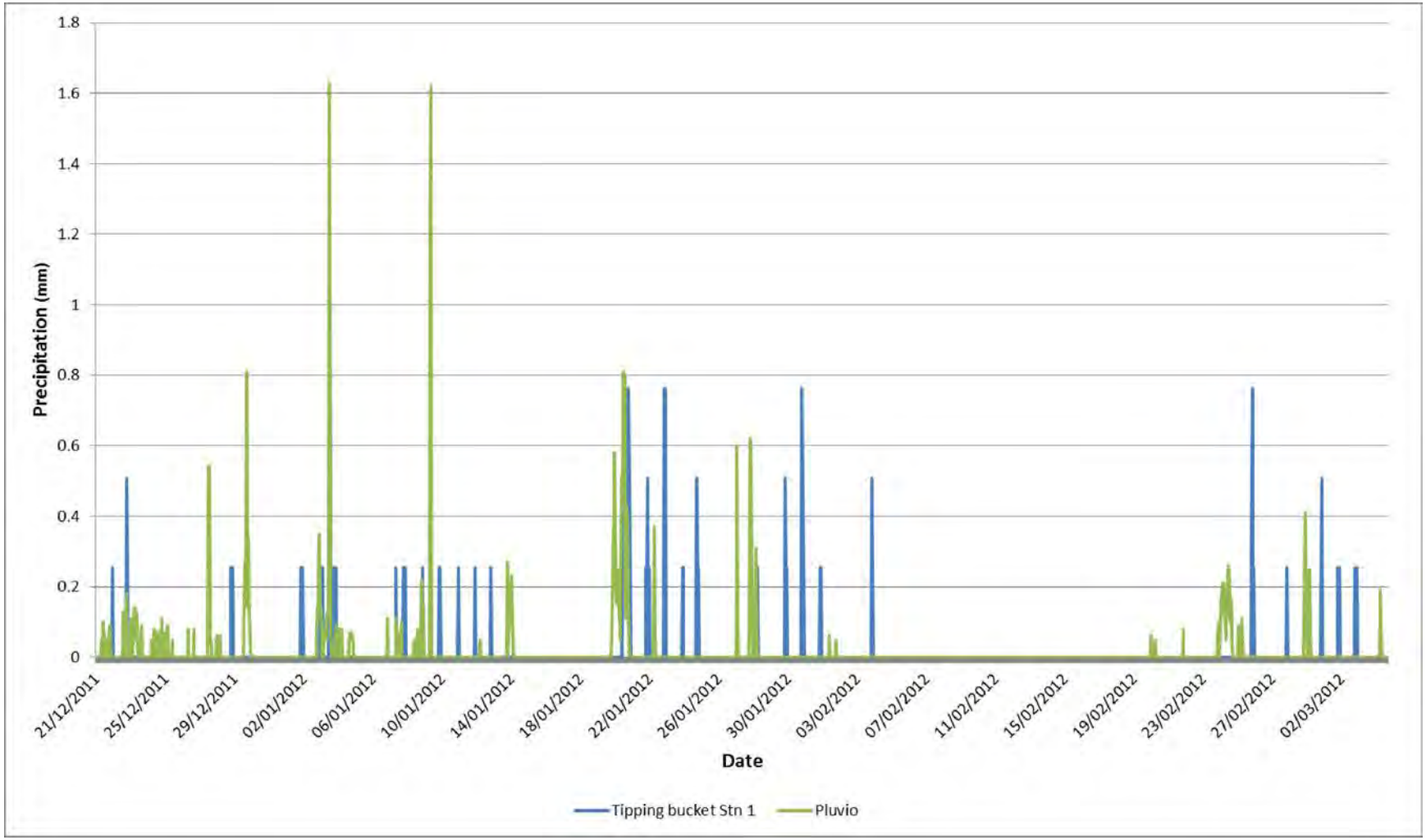

Hourly precipitation measured by two different gauges at Station 1

SITE C CLEAN ENERGY PROJECT		RWDI BC hydro	**Figure 3.2.11** **Hourly precipitation measured by two different gauges at Station 1**
DATE	Dec. 3, 2012		R 0

4.0 WEATHER RESEARCH AND FORECASTING MODEL EVALUATION

The purpose of this section is to evaluate the applicability of the WRF model predictions by comparing model output with real observations at Fort St. John Airport and the BC Hydro Site C climate network stations. In addition, a statistical evaluation of the representativeness of the October 2004 through September 2005 model period was performed.

For a rigorous model evaluation one requires field observations for the same period for which the model was run. For the October 2004 through September 2005 model period used for the study, the only observational data available are for Fort St. John Airport. This does not allow for a rigorous model evaluation that would be specifically applicable to locations closest to the proposed Site C reservoir.

However, observational data suitable for a rigorous model evaluation are available from the Site C climate stations for the FYO over the twelve-month period from January 16, 2011 through January 15, 2012. Therefore, the WRF model was run for this 12-month period using the Baseline configuration to allow a direct evaluation of how well the WRF model reproduces local meteorology closer to areas in the direct vicinity of the proposed Site C reservoir, as represented by the Site C climate network.

If the model is found to perform well for the FYO period, then by extension there is confidence that it would also be performing well during the October 2004 through September 2005 model period.

Observations from six of the Site C climate stations were available over the twelve-month period from January 16, 2011 through January 15, 2012 for comparison with WRF model output. Station 6 at Farrell Creek was not included in the model evaluation because it measures only wind speed and direction (see Table 2.1.1). Data from the six Site C stations were supplemented with data from Fort St. John Airport for the same period. The additional WRF model run for the same FYO period was evaluated against these observations. Additionally, meteorological observations for the baseline period from October 2004 through September 2005 and climate normals were collected from Fort St. John Airport. The Baseline WRF model run for this period was evaluated against Fort St. John Airport data only.

The WRF model was run with three nested grids (Section 2.3). For the model evaluation, the results of the run with the highest resolution (one kilometre) were extracted for the grid points nearest to Fort St. John Airport and the six field stations, respectively. Because of the high grid resolution and relatively flat terrain surrounding the airport, no horizontal or vertical interpolations between grid points were performed for model output at Fort St. John Airport. By comparison, the field stations are located in much steeper terrain, and elevation corrections were applied by using the WRF-modelled lapse rate (temperature change with elevation).

At Fort St. John Airport, the model evaluation was based on temperature (average, minimum, maximum), precipitation (total, rainfall, snowfall) and wind (speed, directions, and frequencies) as well as a general comparison to climate normals at this location. At the field stations, additional meteorological parameters were available for model evaluation from January 16,

2011 through January 15, 2012 but no climate normals, which would require thirty years of data. At these locations, the evaluation focuses on the WRF model's ability to capture site-specific meteorological conditions.

For each model parameter of interest discussed in the sub-sections below, the model is evaluated first in terms of performance for the baseline period from October 2004 through September 2005 compared to data from Fort St. John Airport only. It is then further evaluated for the additional FYO WRF model run using data from Fort St. John Airport and the Site C climate stations.

4.1 TEMPERATURE

In the model evaluation examining temperatures, meteorological observations are compared to climate normals to evaluate the baseline period's representativeness and to model predictions to evaluate model performance.

4.1.1 Representativeness of the Baseline Period at Fort St. John Airport

Monthly averages of observed daily mean temperatures at Fort St. John Airport are compared to the model predictions and climate normals in Figure 4.1.1. Temperatures in the cooler seasons from October 2004 through May 2005, with the exception of January, were above the climate normals, while in the summer months from June to August 2005 they were below. Averaged over the entire baseline period, the observations were 1.08 degrees Celsius above the climate normals.

Monthly averages of observed daily maximum and minimum temperatures at Fort St. John Airport are shown in Figure 4.1.2 and Figure 4.1.3. For daily maximum temperatures, deviations from the 1971 through 2000 climate normals were similar to daily mean temperatures. Daily minimum temperatures show similar positive deviations from climate normals during the cooler seasons, while in the summer months the observations were close to the climate normals. Averaged over October 2004 through September 2005, the anomalies from the climate normals were 0.98 degrees Celsius for maximum and 0.86 degrees Celsius for minimum daily temperatures.

Appendix B provides a detailed statistical analysis of the representativeness of the baseline period. When minimum and maximum temperatures are combined into one data set and compared with the climate normals, the mean of the baseline period is equal to the climate average with high probability. Therefore, the mean is unbiased. Furthermore, the standard deviation is lower for the study period than the climate normals, implying that temperatures during the baseline period were closer to the climate averages than a random year from the 1971 through 2000 climate normals. Overall, it can be concluded that the baseline period is representative of average monthly temperatures over the climate normals period.

Physically, this conclusion is reasonable. Fort St. John has a climate that is predominantly continental subarctic (e.g., Edmonton) but there are occasional maritime (e.g., Vancouver) influences. Inter-annual variability is higher than in a maritime climate, in particular in the winter.

Over the 1971 through 2000 climate normals, standard deviations for monthly means of daily minimum and maximum temperatures vary roughly between 1 degree Celsius to 6 degrees Celsius dependent on the month. Therefore, annual average anomalies on the order of about 1 degree Celsius for temperatures during the October 2004 through September 2005 baseline period are small.

4.1.2 Model Skill at Fort St. John Airport Relative to the Climatologic Mean

For a weather forecast model to have predictive skill, it needs to make better predictions than the climatologic mean. This means that the model has to do a better job at a specific location than a long term average taken from a monitoring station. For example, at one of the Site C climate network locations, the WRF model has to provide a better estimate of station measurements than one would get by just taking the climate normals from Fort St. John Airport. In the context of this model evaluation, the WRF model output would have to capture at least some of the monthly anomalies from the climate normals discussed in the previous section. Obviously, that is a demanding requirement when the baseline period is close to the climatologic mean.

One basic measure for the WRF model outperforming the climatologic mean is that the model predicts the sign, or direction, of the anomalies correctly.

Figure 4.1.1 through Figure 4.1.3 confirm that the WRF model produces warm anomalies for the colder season months and cold anomalies for the summer months. Over the entire baseline period, the model can be said to outperform the climatologic mean if the model's differences from the observations are smaller than the climate normal differences from the observations. An appropriate measure is the root mean square error (RMSE), which is the square root of the average of squared differences (Table 4.1.1). The smaller RMSE for the WRF model output confirms that the model outperforms the climatologic mean as a predictor of monthly mean temperatures. The Reduction-of-Error (RE) Score in the last column in Table 4.1.1 is often used in climate research to quantify a model's predictive skill. The RE scores in Table 4.1.1 are close to 1 indicating that the model predicts temperatures better than the climatologic mean. Values near 0 would indicate that model and mean are about equally strong predictors, while negative values would indicate that predictions from the model are worse than the climatologic mean.

Table 4.1.1 WRF model prediction skill for temperatures at Fort St. John Airport

	RMSE of Climate	RMSE of WRF Model	RE
Mean	2.81	**1.20**	0.82
Maximum	2.83	**1.61**	0.68
Minimum	2.92	**1.36**	0.78

NOTES:

Bold numbers highlight greater prediction skills.

[b] Root Mean Square Error (RMSE); smaller values represent higher skill.

[c] Reduction-of-Error score (RE); values close to one represent higher WRF model skill, values close to zero represent similar skills, and negative values represent higher Fort St. John Airport skill.

[a] Root mean square errors of climate normals from baseline observations from October 2004 through September 2005 at Fort St. John Airport for monthly averages of daily mean, maximum, and minimum temperatures. Smaller values represent higher skill.

[b] Root mean square errors of WRF model output from baseline observations from October 2004 through September 2005 at Fort St. John Airport for monthly averages of daily mean, maximum, and minimum temperatures. Smaller values represent higher skill.
[c] Reduction-of-error score of WRF model against climate normals, respectively. Values close to one represent higher WRF model skill, values close to zero represent similar skills, and negative values represent higher Fort St. John Airport skill.

4.1.3 Modelling of Extremes

Extremely high or low temperature can have influence on people's health, agricultural yield, etc. Being rare by definition, extreme events are difficult to characterize statistically. Furthermore, they are often very localized and caused by unusual environmental conditions that are insufficiently captured in numerical models. Therefore, numerical models often tend to underestimate the strength and frequency of extreme events.

The WRF model predictions of extreme minimum and maximum monthly temperatures are compared to observations at Fort St. John Airport in Figure 4.1.4 and Figure 4.1.5. As expected, model predictions of extreme maximum temperatures are too low in all calendar months, while predictions of extreme minima are too high in all months but July and September.

The results in Figure 4.1.4 and Figure 4.1.5 indicate that the frequency distributions of temperatures are narrower for model output than observations. This is a common characteristic, and requires an approach to correct the model's inability to predict the strength of extremes for other periods than October 2004 through September 2005, and in particular for future model runs. One approach is to match the temperature cut-offs of extreme percentiles in the tails of the frequency distributions of model output and observations (e.g., Reuten, et al. 2012). As these cut-off temperatures change for different model years, the associated temperatures in the observational frequency distribution can be determined.

Prediction of extreme events was not the main focus of the microclimate study. Since the model is driven by observed large-scale meteorology, the Future Case with the Project model case would not spawn any additional storm that did not occur in the inputs given to the model. Therefore the model, over a single year, cannot predict any change in the *frequency* of extreme events. However, the model can provide an estimate of changes that might occur for a *specific* event that was captured by the inputs given to the model. Such changes would be evident in parameters such as the maximum wind speed predicted by the model. However, in general the occurrence of extreme wind speed events is driven by large scale synoptic atmospheric conditions. It is expected that influence of the proposed Site C reservoir would be limited to the Technical Study Area. Thus is would not have any influence on synoptic weather patterns and would not change the frequency of occurrence of extreme wind events.

4.1.4 Model Time Series Comparisons at Fort St. John Airport

Time series of modelled and observed daily average temperatures at Fort St. John Airport are shown in Figure 4.1.6. Generally, model predictions are in good agreement with observed temperatures. The tendency of the model to under predict extreme high and over predict extreme low temperatures, as discussed in the previous section, is also apparent in the time series.

A plot of predicted and observed hourly temperatures is shown in Figure 4.1.7 for the first week in December 2004. This particular week was chosen to evaluate the model performance when hourly temperature variations are dominated by large-scale weather systems rather than local diurnal cycles. The diurnal temperature cycle in Figure 4.1.7 is very weak. Instead, the weekly time series is dominated by a 30 degrees Celsius temperature drop between December 3 and 5, which was most likely caused by an inflow of cold Arctic air due to a change in synoptic weather patterns. The temperature drop is qualitatively well captured by the model, although the absolute temperature decrease is under predicted and the drop is predicted to occur roughly eight hours later. Similarly to very high and low daily temperatures of Figure 4.1.6, the model under predicts the unusually warm temperatures on the first two days and over predicts the very cold temperatures on the last three days.

Hourly temperature time series in the summer are dominated by diurnal temperature variations. An example is shown in Figure 4.1.8 for the first week of June. The observed daily temperature range was about 5-10 degrees Celsius which is well captured by the WRF model. Some of the range between daily high and low temperatures is reduced by the model, in particular in the middle of the week. This might be related to over or under predicted precipitation and the associated incorrect prediction of soil moisture. This is a particular problem with the sporadic and local convective precipitation in the summer, which is very difficult to predict accurately, and is discussed in the next section.

4.1.5 Model Skill at the Field Stations Relative to Fort St. John Airport

The main intention of modelling an extra year and comparing with the field stations is to evaluate the model's ability to capture spatial variability. As such, the WRF model should therefore model local temperatures better than Fort St. John Airport temperatures can represent local temperatures. This goal is hampered by a number of factors.

In the relatively flat terrain of the Technical Study Area, temperatures do not vary much over the length scale of the Technical Study Area (tens of kilometres). Therefore, observations at Fort St. John Airport are likely going to be a good representation of temperatures at the field stations, in particular for those that are located more closely to Fort St. John Airport (see, for example, the close visual agreement between observations at the field stations and Fort St. John Airport in Figure 3.2.1). The WRF model's ability to correct for elevation differences and local thermal processes is less powerful in this geography. Furthermore, the Technical Study Area experiences extreme changes in temperatures over very short periods, up to ten degrees in one hour. These rapid changes occur typically within about two hours over the entire Technical Study Area so that temperature changes at Fort St. John Airport track those at the field stations reasonably well. The WRF simulations represent the associated weather systems over a large domain, and therefore the arrival of a weather system might be out by several hours. Finally, local variations and surface characteristics under extreme conditions are often not fully captured by numerical models so that there is a tendency for the WRF model to underestimate the absolute value of extremely high or low temperatures.

For the prediction-skill evaluation, six stations had data available in the FYO from January 16, 2011 through January 15, 2012. Table 4.1.2 presents summary statistics for monthly averages of daily mean, maximum, and minimum temperatures of WRF model grid-cell averages at the station locations. For comparison, the same statistics were calculated for the corresponding observations at Fort St. John Airport.

Table 4.1.2 WRF model prediction skill for temperatures at the field stations

	Mean Bias[a]		RMSE[b]		
Station	**WRF[d]**	**Fort St. John Airport[e]**	**WRF**	**Fort St. John Airport**	**RE[c]**
Mean Temperature					
Station 1 - Attachie Flat Upper Terrace	**0.18**	0.31	1.07	**0.75**	-1.03
Station 2 – Attachie Flat Lower Terrace	-0.26	**0.12**	1.09	**0.85**	-0.64
Station 3 – Attachie Plateau	0.79	**0.43**	1.03	**0.54**	-2.67
Station 4 – Bear Flat	**0.1**	0.36	1.02	**0.79**	-0.68
Station 5 – Hudson's Hope	**0.81**	0.87	1.26	**0.98**	-0.66
Station 7 – Site C Dam	1.19	**1.05**	1.07	**0.42**	-5.57
Maximum Temperature					
Station 1 - Attachie Flat Upper Terrace	**1.45**	1.55	0.93	**0.7**	-0.8
Station 2 – Attachie Flat Lower Terrace	**1.54**	1.93	0.97	**0.74**	-0.69
Station 3 – Attachie Plateau	1.48	**0.98**	1.14	**0.56**	-3.2
Station 4 – Bear Flat	**1.54**	1.65	1	**0.73**	-0.88
Station 5 – Hudson's Hope	**2.13**	2.31	1.26	**0.84**	-1.24
Station 7 – Site C Dam	1.68	**1.49**	1.13	**0.55**	-3.31
Minimum Temperature					
Station 1 - Attachie Flat Upper Terrace	-1.22	**-0.85**	1.71	**1.19**	-1.07
Station 2 – Attachie Flat Lower Terrace	-2.29	**-1.65**	1.66	**1.27**	-0.7
Station 3 – Attachie Plateau	**-0.44**	-0.48	1.62	**0.73**	-3.96
Station 4 – Bear Flat	-1.45	**-0.87**	1.56	**1.15**	-0.85
Station 5 – Hudson's Hope	-1.57	**-1.23**	1.61	**1.42**	-0.28
Station 7 – Site C Dam	**0.81**	0.86	1.18	**0.59**	-2.99

NOTES:
The three sections display statistics for daily mean, maximum, and minimum temperatures from January 16, 2011 until January 15, 2012. Bold numbers highlight greater skills between the WRF model and Fort St. John Airport. All statistics are based on monthly averages of station observations and WRF model output.
[a] Values closer to zero represent higher skill.
[b] Root Mean Square Error (RMSE); smaller values represent higher skill.
[c] Reduction-of-Error score (RE); values close to one represent higher WRF model skill, values close to zero represent similar skills, and negative values represent higher Fort St. John Airport skill.
[d] Weather Research and Forecasting (WRF) model output.
[e] Fort St. John Airport station observations.

Mean biases of the WRF model and Fort St. John Airport from field observations are mostly positive for mean temperatures. Therefore, averaged over the entire year, observed temperatures at the field stations were higher than observed at Fort St. John Airport and predicted by the WRF model. For Fort St. John Airport, this result is expected, because the

airport is located at an elevation between 50 and 260 meters higher than the field locations. To explain the WRF model's underestimation, it is instructive to investigate mean biases for maximum and minimum temperatures. Positive mean biases of maximum temperatures imply that the WRF model underestimates particularly warm temperatures, as expected for a numerical model. Negative mean biases of minimum temperatures imply that the WRF model predicts higher temperatures, effectively failing to fully represent particularly cold days. Notice that the signs of mean biases also apply to Fort St. John Airport statistics. The reason may be that Fort St. John Airport lacks the thermal amplification in the valley locations of the field stations. These two changes partially cancel in the mean temperatures both for Fort St. John Airport and the WRF model, but an overall underestimation of mean temperatures remains (with the exception of station 2).

Consistently negative reduction-of-error scores in Table 4.1.2 show that observations at Fort St. John Airport have greater predictive skill of monthly temperatures at the field locations than WRF model output. However, the root mean square errors of the WRF model are lower than typical values from numerical modelling results at coarser resolutions in this region (for example Reuten, et al. 2011).

Figure 4.1.9 through Figure 4.1.11 show the monthly breakdown of the WRF model and Fort St. John Airport differences from the station observations. Outputs from the WRF model and Fort St. John Airport observations show mostly similar seasonality of biases suggesting that there are local influences at the field locations that are not fully captured by the WRF model or Fort St. John Airport.

In Figure 4.1.9, a roughly 2 degrees Celsius overestimation of field observations by the WRF model, but not by Fort St. John Airport, is seen in the month of November. A look at the time series (not shown) reveals a temperature drop of about 20 degrees Celsius that lasted for about ten days before temperatures recovered to seasonal average temperatures in November 2011. The model captured the temperature drop qualitatively but underestimated the full temperature drop by several degrees. Probably the local influence of variation in snow cover was not fully captured by the WRF model, because snow cover would have come from the coarse scale North American Regional Reanalysis fields used as input to the model. The domain average snow cover should have been well estimated by the NARR.

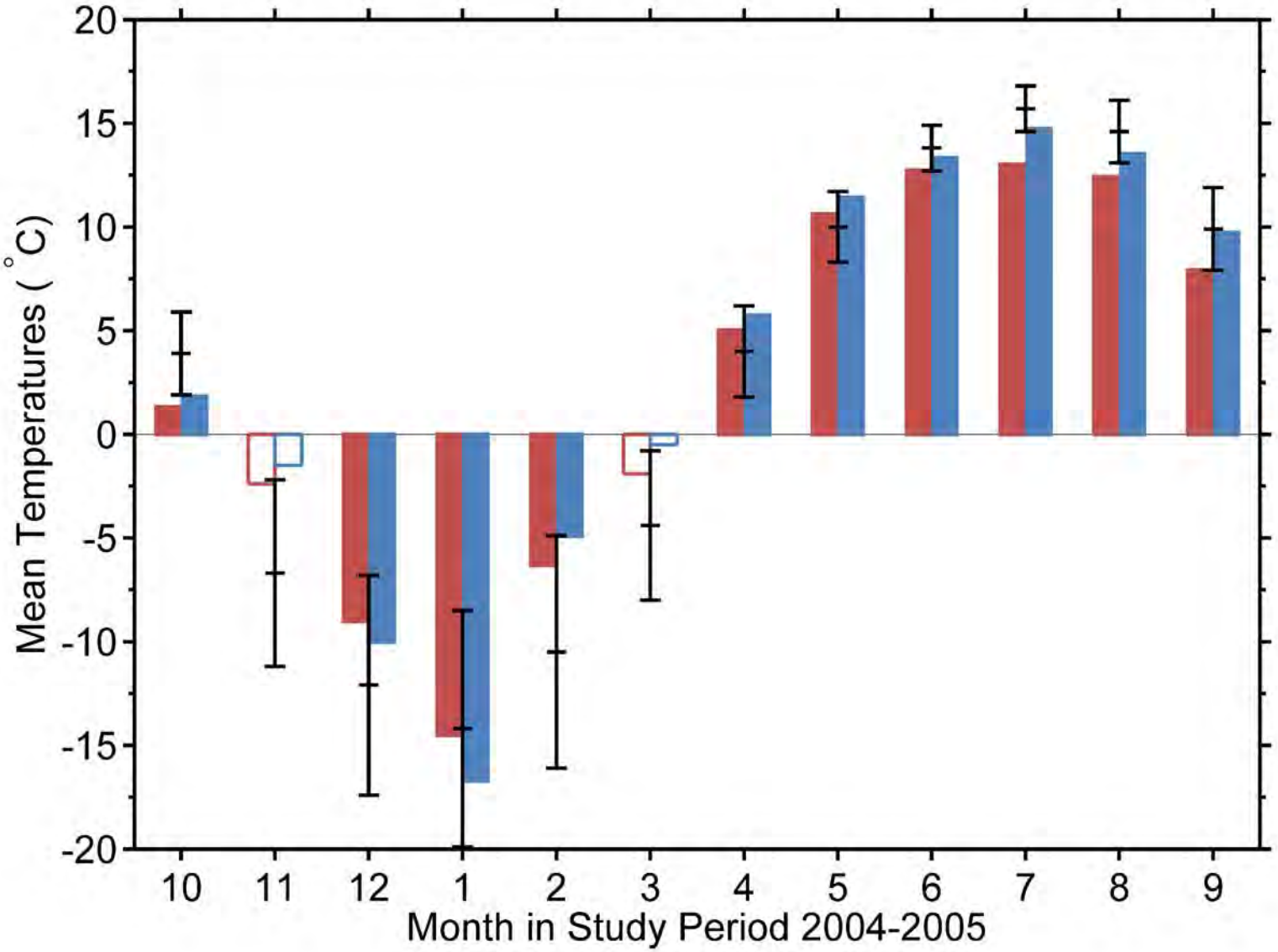

Observed (blue) and predicted (red) monthly averages of daily mean temperatures at Fort St. John Airport for October 2004 to September 2005. Error bars show 1971-2000 averages (climate normals) and their standard deviations. Open bars indicate months in which the observations were outside of the standard deviation of the climate normals.

SITE C CLEAN ENERGY PROJECT		RWDI BC hydro	**Figure 4.1.1 Observed, predicted, and climate-normal mean temperatures at Fort St. John Airport**
DATE	Dec. 3, 2012		R 0

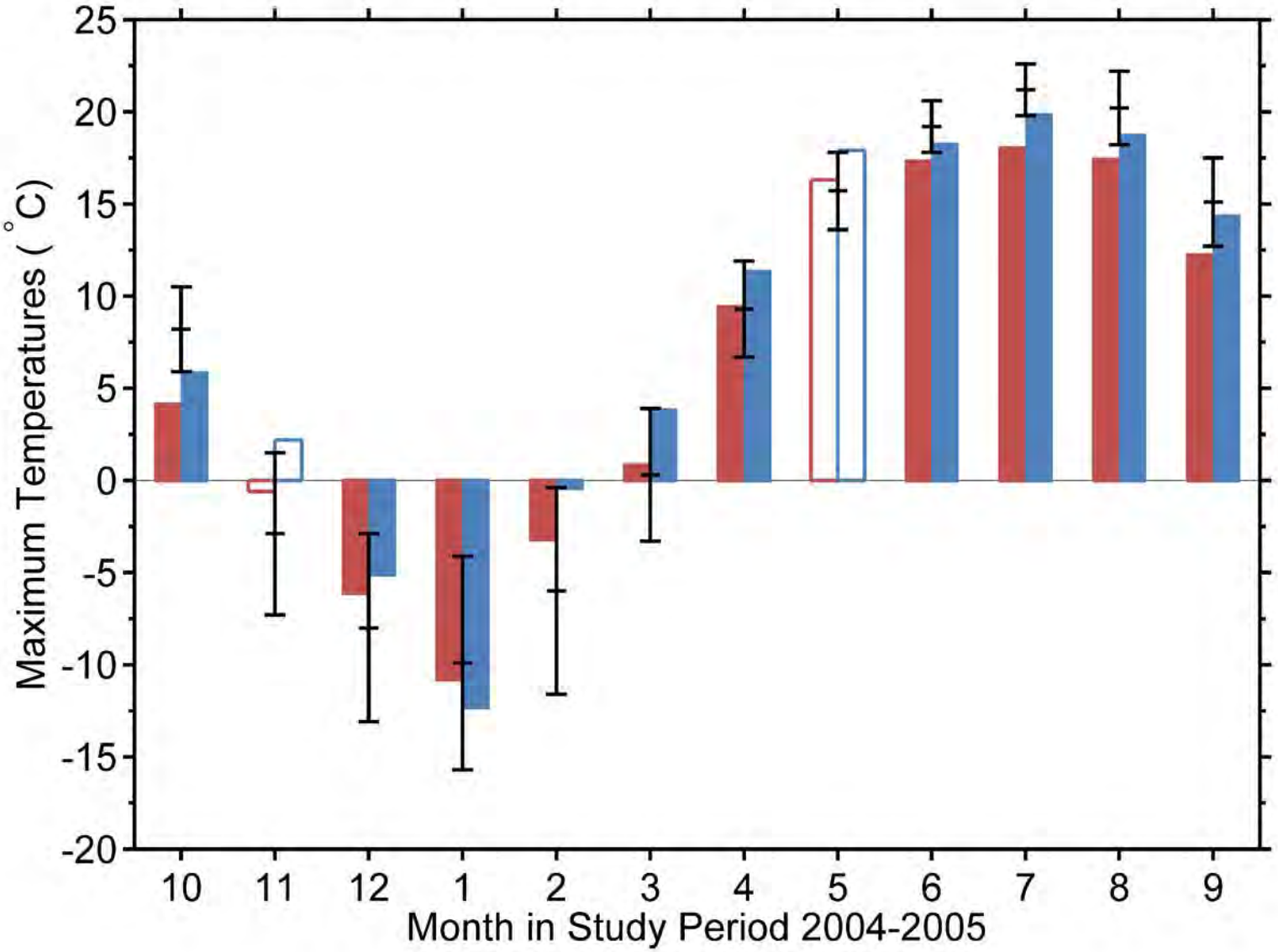

Observed (blue) and predicted (red) monthly averages of daily maximum temperatures at Fort St. John Airport for October 2004 to September 2005. Error bars show 1971-2000 averages (climate normals) and their standard deviations. Open bars indicate months in which the observations were outside of the standard deviation of the climate normals.

SITE C CLEAN ENERGY PROJECT		RWDI BC hydro	**Figure 4.1.2 Observed, predicted, and climate-normal maximum temperatures at Fort St. John Airport**
DATE	Dec. 3, 2012		R 0

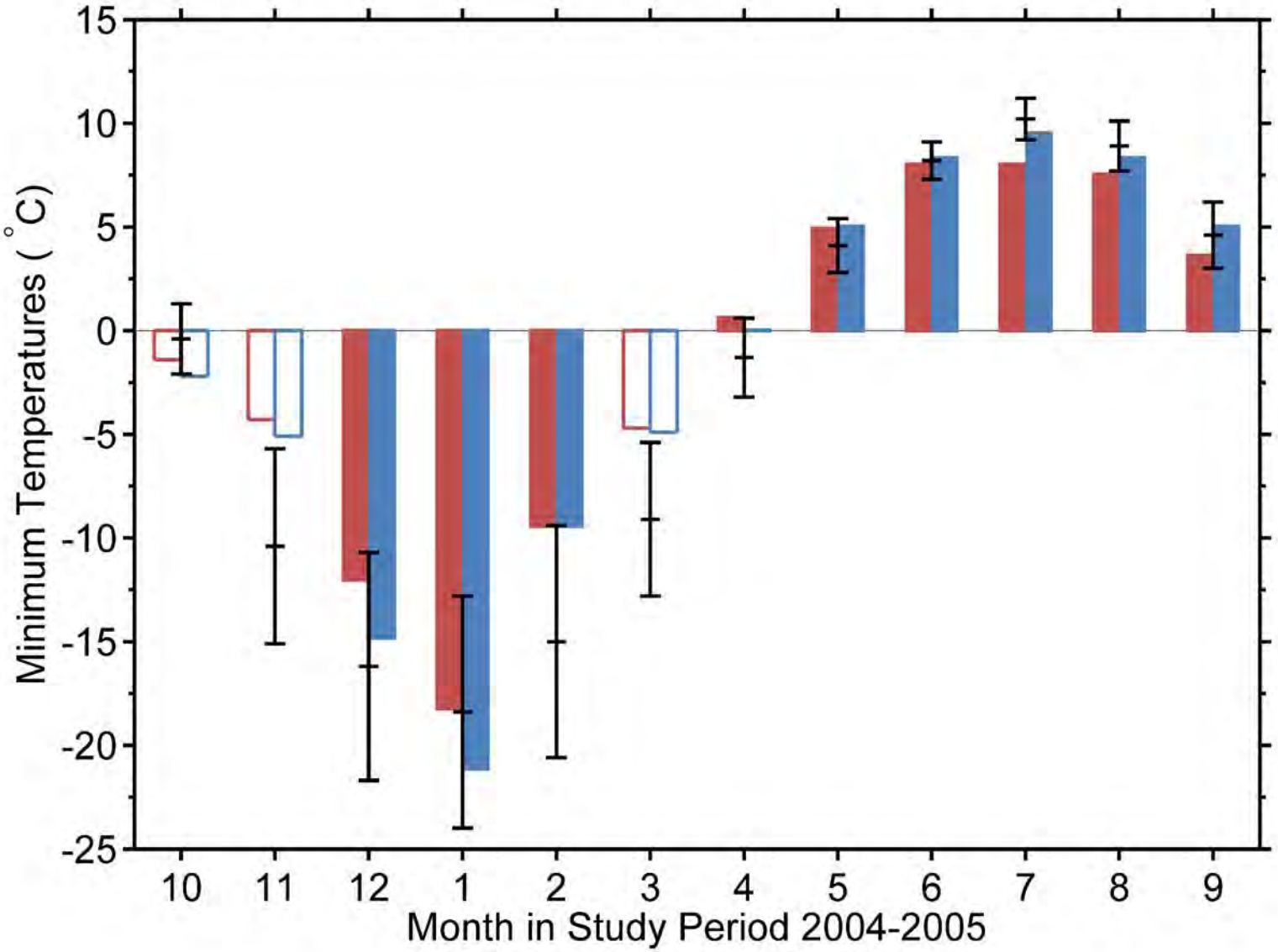

Observed (blue) and predicted (red) monthly averages of daily minimum temperatures at Fort St. John Airport for October 2004 to September 2005. Error bars show 1971-2000 averages (climate normals) and their standard deviations. Open bars indicate months in which the observations were outside of the standard deviation of the climate normals.

SITE C CLEAN ENERGY PROJECT

RWDI BC hydro

Figure 4.1.3
Observed, predicted, and climate-normal minimum temperatures at Fort St. John Airport

DATE	Dec. 3, 2012		R 0

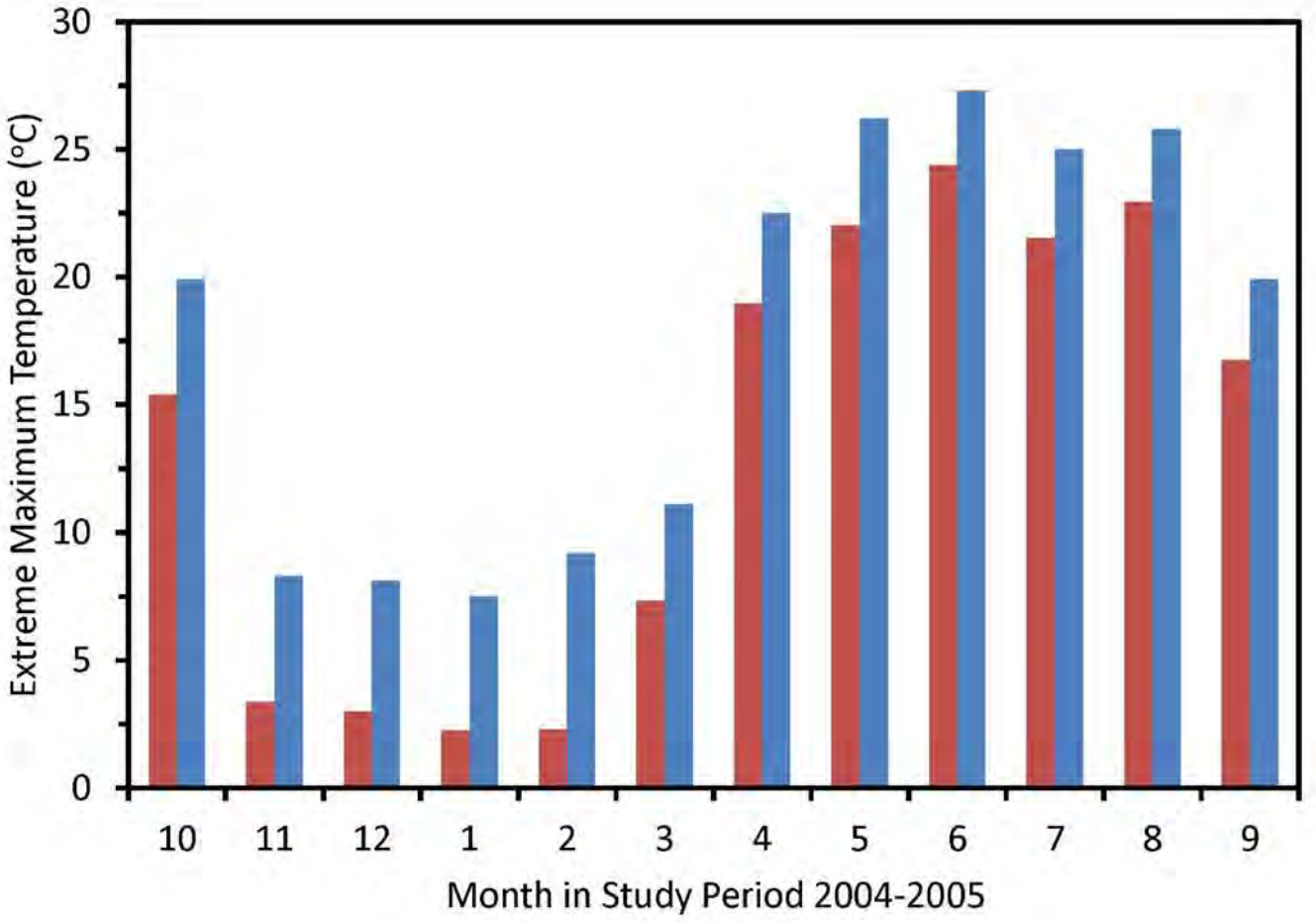

Observed (blue) and predicted (red) monthly extreme maximum temperatures at Fort St. John Airport for October 2004 to September 2005.

SITE C CLEAN ENERGY PROJECT

RWDI BC hydro

Figure 4.1.4
Observed and predicted extreme maximum temperatures at Fort St. John Airport

DATE	Dec. 3, 2012		R 0

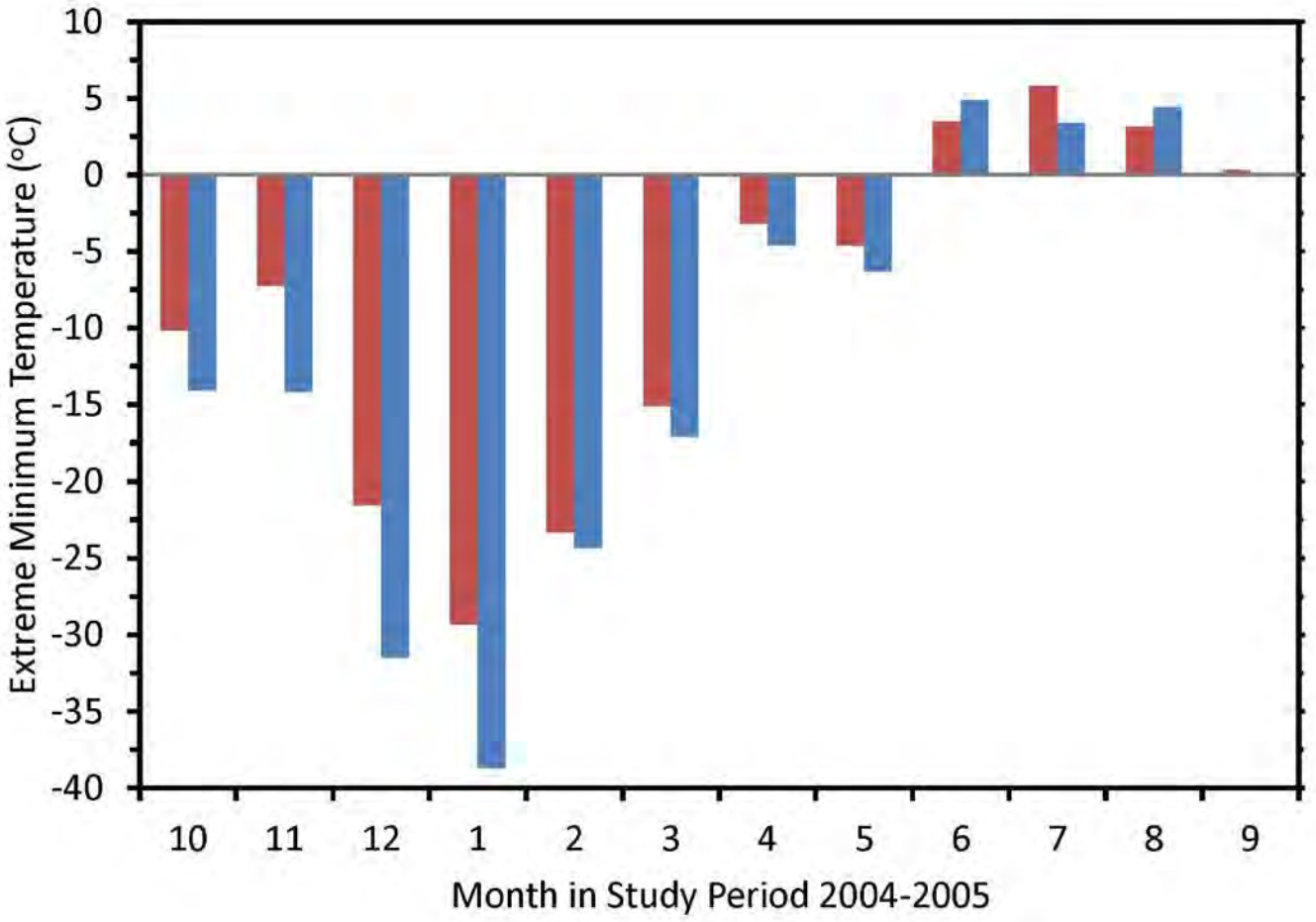

Observed (blue) and predicted (red) monthly extreme minimum temperatures at Fort St. John Airport for October 2004 to September 2005.

SITE C CLEAN ENERGY PROJECT

RWDI BC hydro

Figure 4.1.5
Observed and predicted extreme minimum temperatures at Fort St. John Airport

DATE	Dec. 3, 2012		R 0

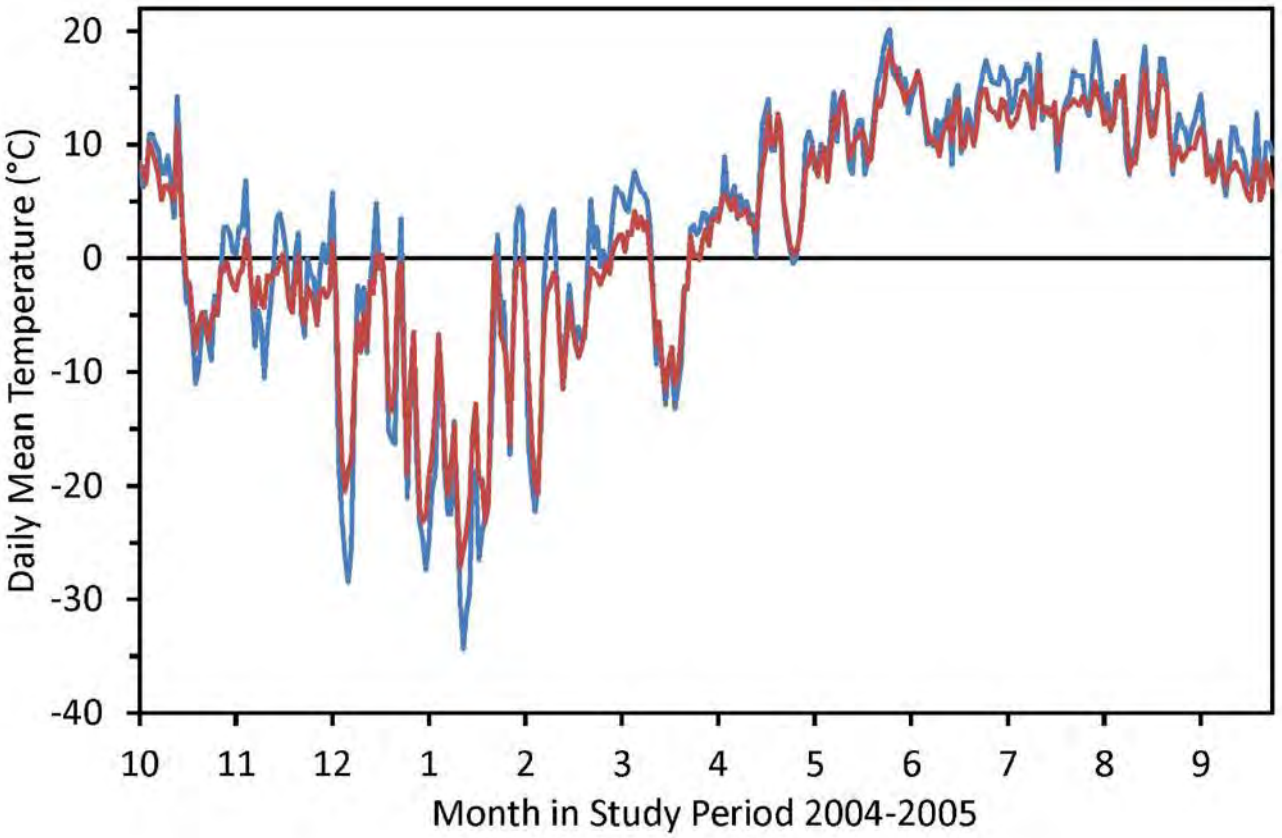

Observed (blue) and predicted (red) monthly extreme maximum temperatures at Fort St. John Airport for October 2004 to September 2005.

SITE C CLEAN ENERGY PROJECT		RWDI BC hydro	
		Figure 4.1.6 One year of observed and predicted daily mean temperatures at Fort St. John Airport	
DATE	Dec. 3, 2012		R 0

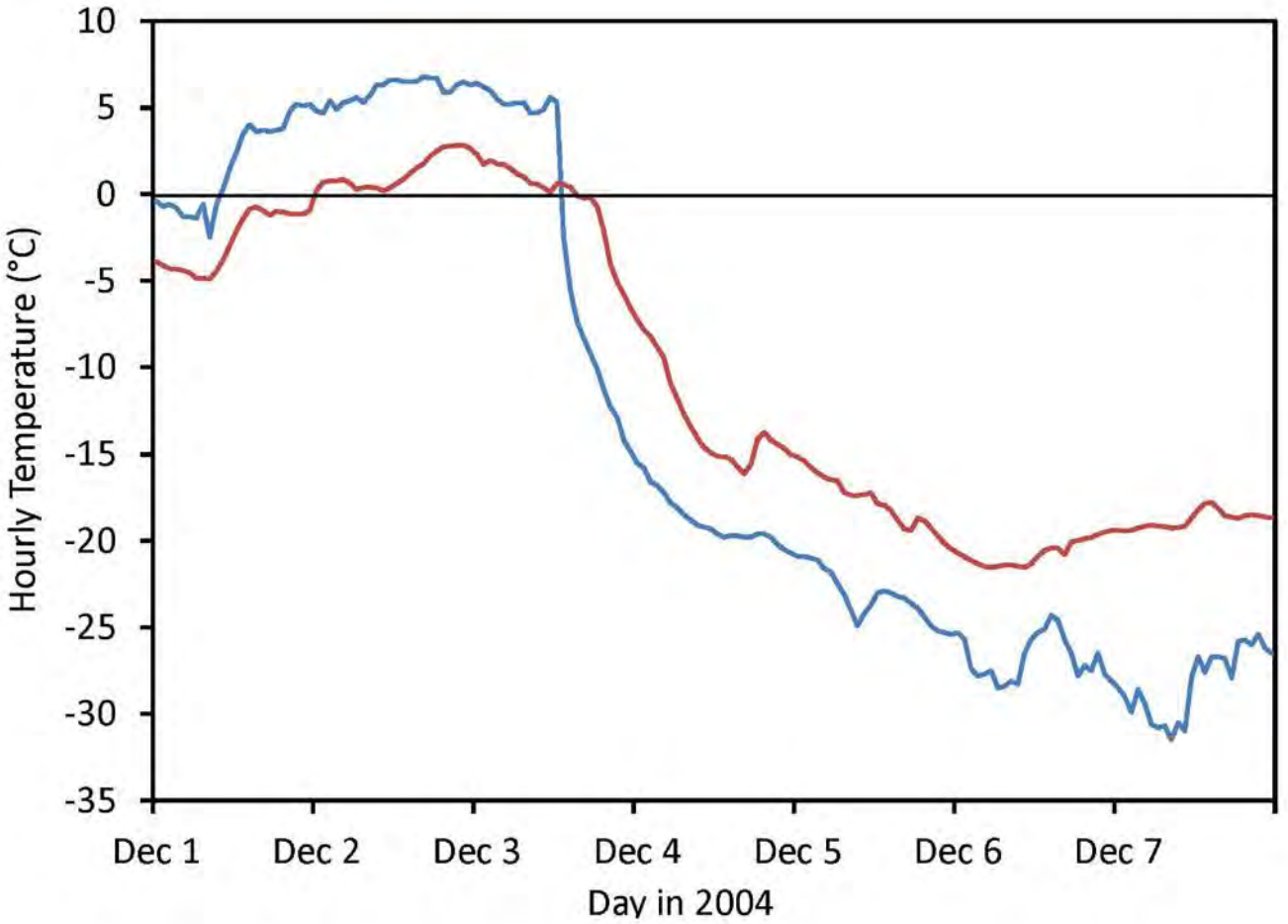

Observed (blue) and predicted (red) hourly temperatures at Fort St. John Airport for the week of December 1 to 7, 2004.

SITE C CLEAN ENERGY PROJECT

RWDI BC hydro

Figure 4.1.7
One winter week of observed and predicted hourly temperatures at Fort St. John Airport

DATE	Dec. 3, 2012		R 0

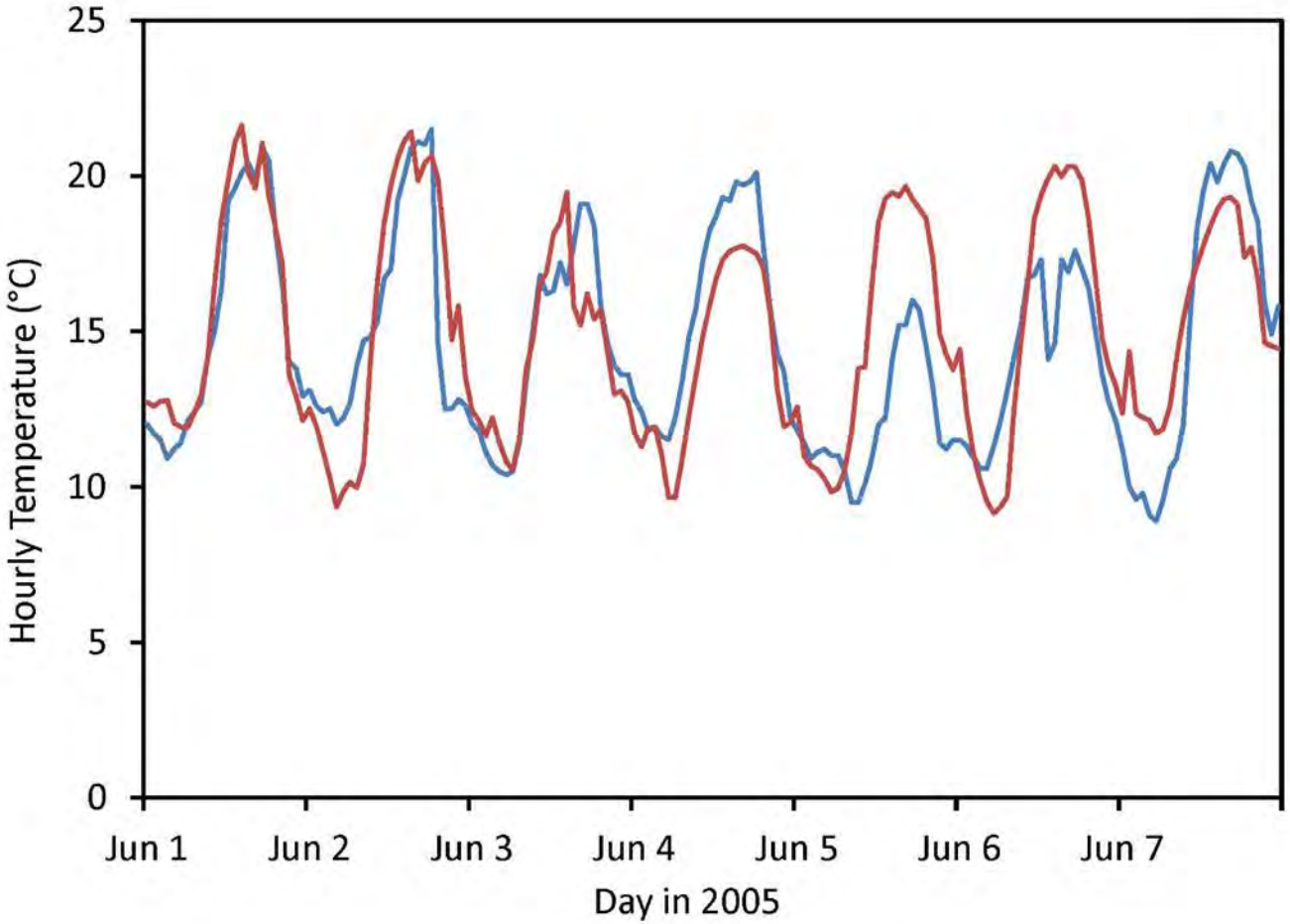

Observed (blue) and predicted (red) hourly temperatures at Fort St. John Airport for the week of June 1 to 7, 2005.

SITE C CLEAN ENERGY PROJECT

RWDI BC hydro

Figure 4.1.8
One summer week of observed and predicted hourly temperatures at Fort St. John Airport

DATE	Dec. 3, 2012		R 0

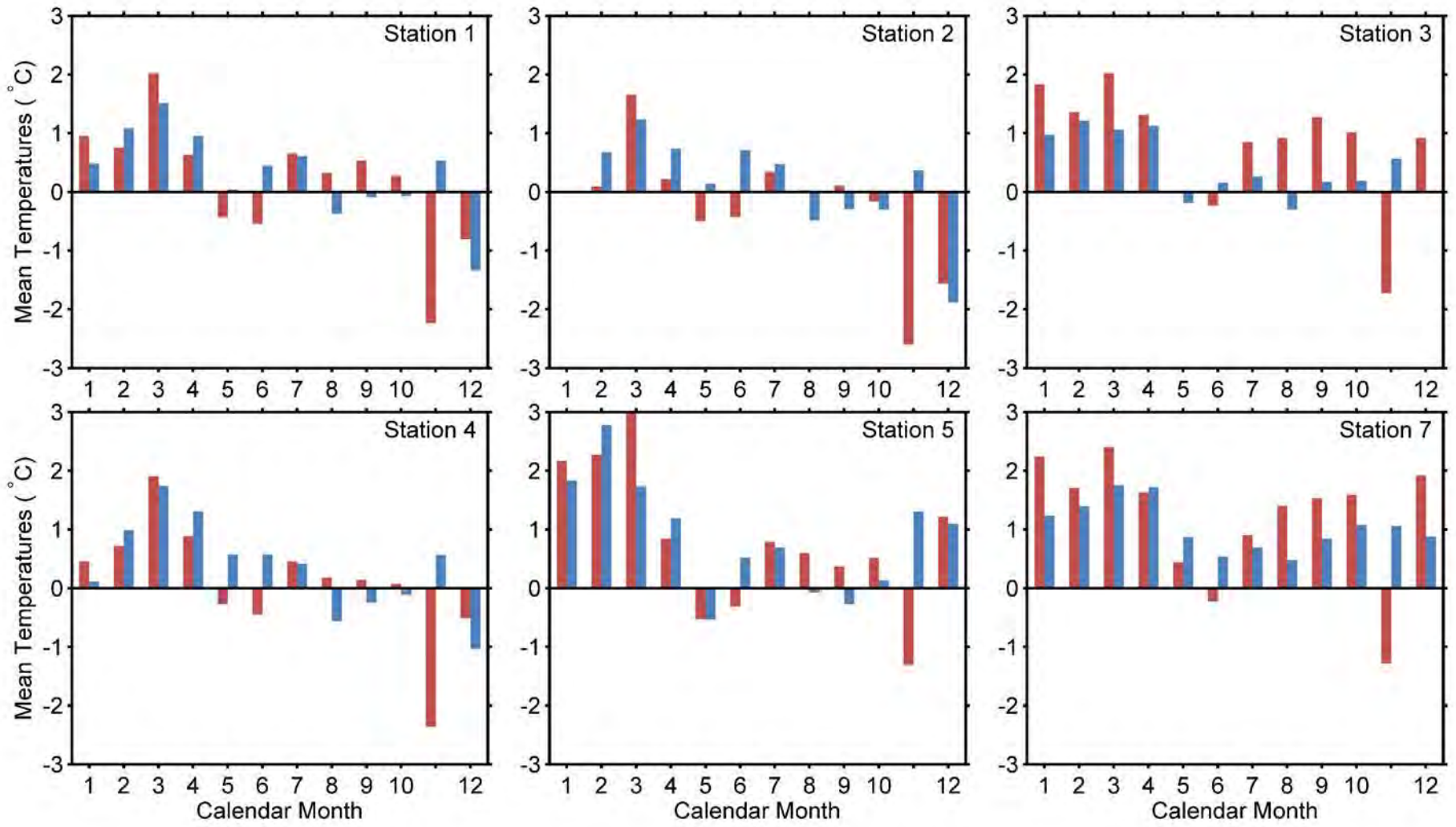

Differences of Weather Research and Forecasting (WRF) model prediction (red) and Fort St. John observations (blue) from local station observations of daily mean temperatures for January 16, 2011 to January 15, 2012 at six field station locations as labelled. WRF prediction is the grid center result for the cell encompassing the station location. Red background highlights times when WRF model outputs were better predictors than Fort St. John observations and vis versa for blue background.

SITE C CLEAN ENERGY PROJECT	RWDI BC hydro **Figure 4.1.9** **Weather Research and Forecasting model versus Fort St. John Airport predictions of mean temperature at field stations**
DATE: Dec. 3, 2012	R 0

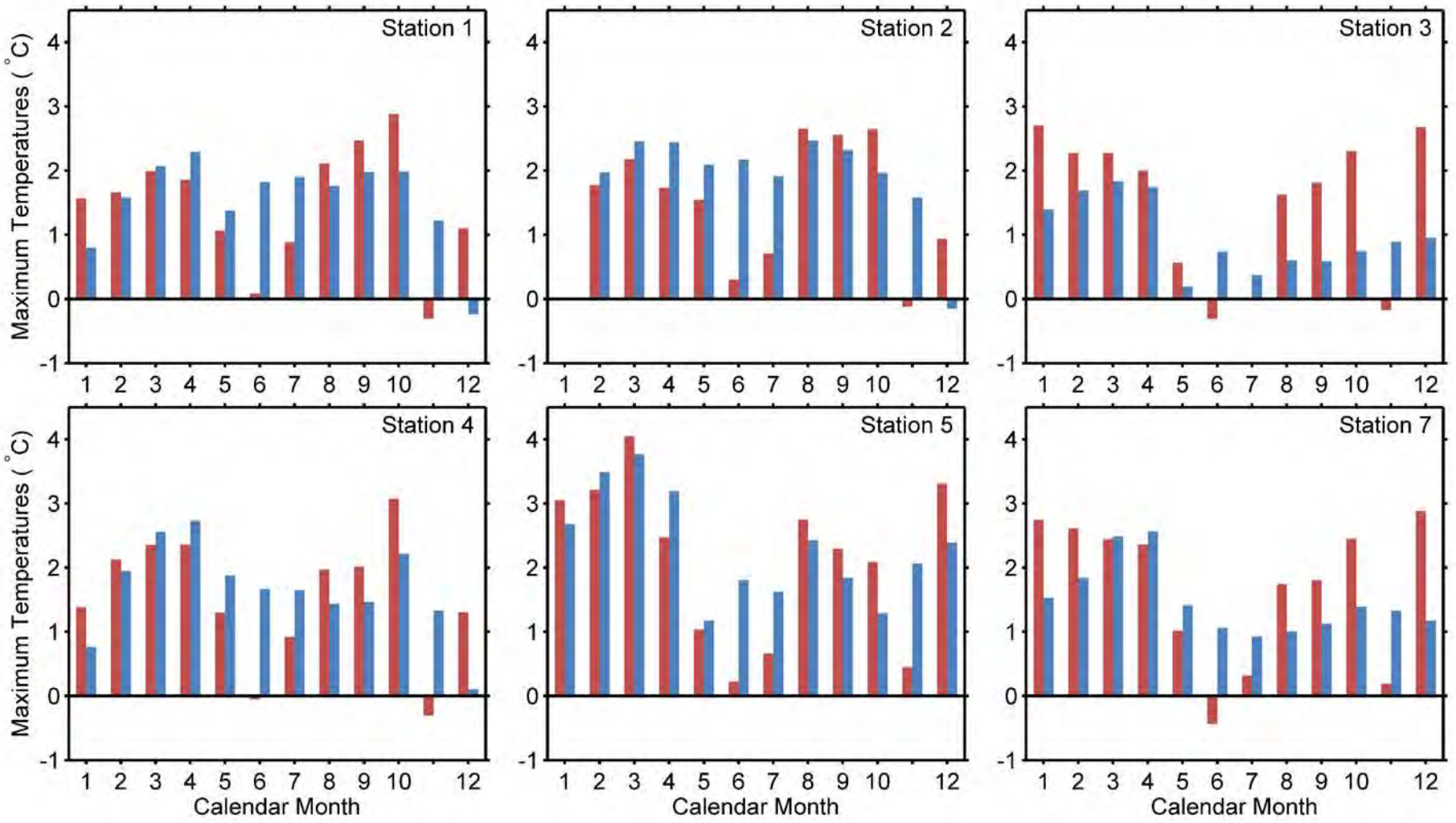

Differences of Weather Research and Forecasting (WRF) model prediction (red) and Fort St. John observations (blue) from local station observations of daily maximum temperatures for January 16, 2011 to January 15, 2012 at six field station locations as labelled. WRF prediction is the grid center result for the cell encompassing the station location. Red background highlights times when WRF model outputs were better predictors than Fort St. John observations and vice-versa for blue background.

SITE C CLEAN ENERGY PROJECT

RWDI BC hydro

Figure 4.1.10
Weather Research and Forecasting model versus Fort St John Airport predictions of maximum temperature at field stations

DATE	Dec. 3, 2012		R 0

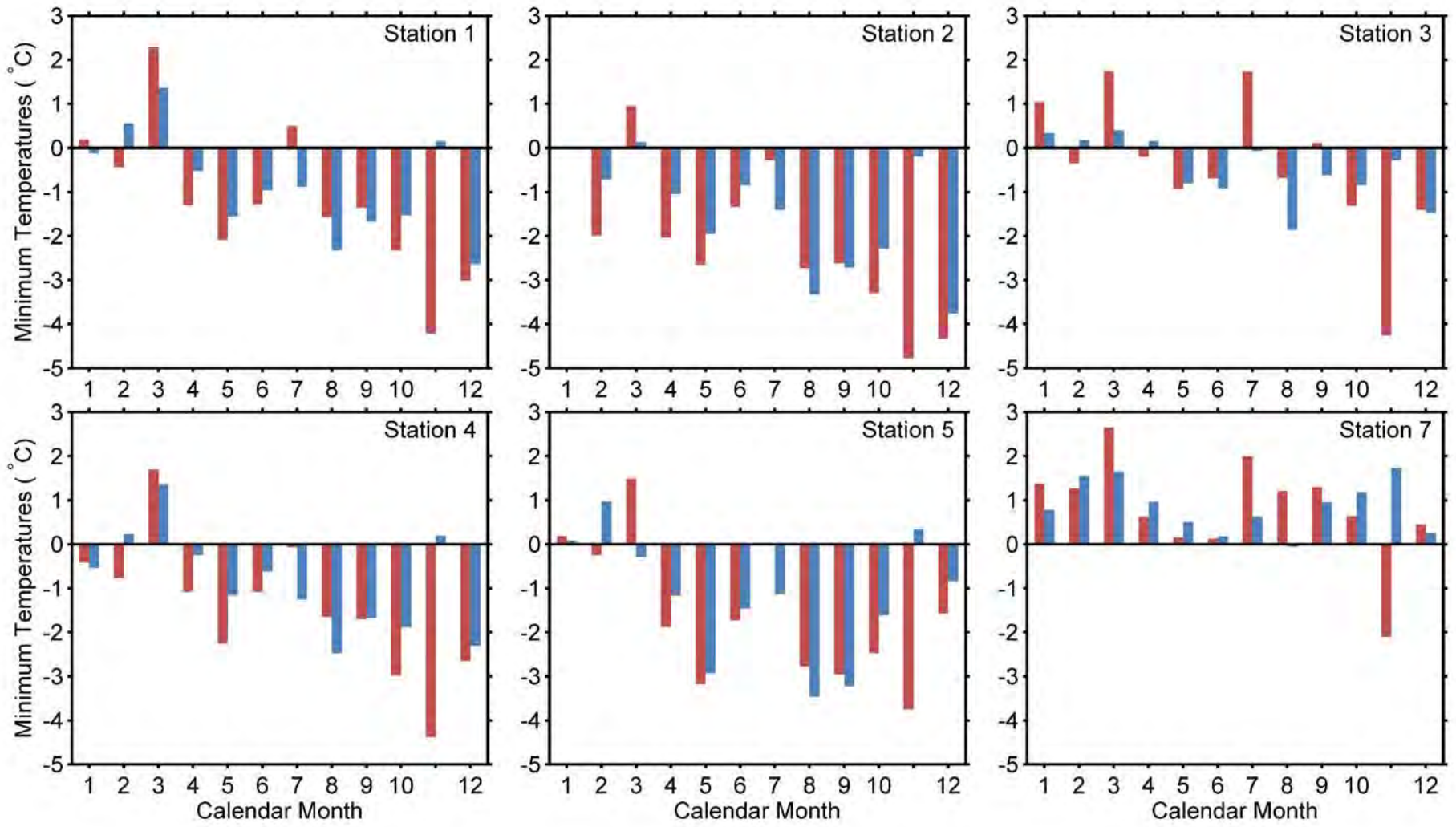

Differences of Weather Research and Forecasting (WRF) prediction (red) and Fort St. John observations (blue) from local station observations of daily minimum temperatures for January 16, 2011 to January 15, 2012 at six field station locations as labelled. WRF prediction is the grid center result for the cell encompassing the station location. Red background highlights times when WRF model outputs were better predictors than Fort St. John observations and vis versa for blue background.

SITE C CLEAN ENERGY PROJECT

RWDI BC hydro

Figure 4.1.11
Weather Research and Forecasting model versus Fort St. John Airport predictions of minimum temperature at field stations

DATE	Dec. 3, 2012		R 0

4.2 PRECIPITATION

Similarly to temperatures, the goals of the model evaluation using precipitation are the evaluations of the period's representativeness and of the model's ability to predict observations at Fort St. John Airport.

Generally, predictions of precipitation are less reliable than predictions of temperature. Reasons include greater temporal and spatial variability, greater measurement uncertainties, and dependence on more environmental parameters. Furthermore, observations are point measurements, while model predictions are grid-cell averages. Finally, frequency distributions of precipitation tend to be better approximated by log-normal than normal distributions. For these reasons, it is common to evaluate model performance for predicting precipitation based on the ratio between predictions and observations rather than the difference.

4.2.1 Representativeness of the Baseline Period at Fort St. John Airport

A thorough analysis of the representativeness of the baseline period for rain and snow is presented in Appendix B. Individually, rain, snow, and total precipitation show high probabilities for representativeness of the climate normals. For rain and snow data combined, the representativeness is statistically highly significant. Therefore, the 1971 through-2000 climate normals are a very good estimate of the October 2004 through September 2005 baseline period, and the WRF model output is unlikely to outperform the climatologic mean. Evidence for this is provided by the statistics that are summarized in Table 4.2.1 and further explained below. Because precipitation is always positive and its distributions are highly skewed, it is customary to calculate statistics that are based on ratios. The corresponding equivalent to mean bias and root mean square error are the geometric mean bias and the geometric variance, respectively. For the latter statistics, values closer to one are indicative of better agreement.

Table 4.2.1 WRF model prediction skill for precipitation at Fort St. John Airport

Parameter	MG[a]		VG[b]		Difference		RE Score[c]
	WRF	Climate Normals	WRF	Climate Normals	WRF	Climate Normals	
Total Precipitation	1.28	**1.06**	1.31	**1.26**	-16%	**-11%**	0.28
Rain	**0.97**	1.20	7105	**1.61**	**-13%**	-15%	-0.56
Snow	N/A	N/A -	N/A	N/A	-24%	**-1%**	-0.29

NOTES:
Statistics of WRF model output and climate normals relative to observations of precipitation, rain, and snow at Fort St. John Airport for October 2004 through September 2005. Bold numbers highlight greater skills. Abbreviations given in List of Acronyms
[a] Values closer to one represent greater skill.
[b] Smaller values represent greater skill.
[c] Values close to one represent higher WRF model skill, values close to zero represent similar skills, and negative values represent higher climate-normals skill.
[c] Reduction-of-Error score (RE); values close to one represent higher WRF model skill, values close to zero represent similar skills, and negative values represent higher Fort St. John Airport skill.
[d] Weather Research and Forecasting (WRF) model output.

Figure 4.2.1 shows model output, station observations, and climate normals of total monthly precipitation for October 2004 through September 2005. All three show a very strong seasonality of wet summers and drier cooler seasons. The baseline ratios between observations and climate normals vary from 0.35 (May) to 1.50 (March), with a geometric variance of 1.26 and an annual mean ratio ('geometric mean bias') of 1.06 (Table 4.2.1).

Figure 4.2.2 and Figure 4.2.3 show precipitation separated into rain and snow, respectively. Because winters in Fort St. John Airport are cold, there is a very strong seasonal cycle of rain (most rain occurs in the summer, very little in the winter; Figure 4.2.2) and snow (most snow occurs in the winter, very little in the summer; Figure 4.2.3). This seasonality is apparent in the climate normals and observations and is well captured by the model.

For rain, the ratios between observations and climate normals vary between 0.39 (May) and 2.86 (March), with a geometric variance of 1.61 and a geometric mean bias of 1.20 (Table 4.2.1). For snow, these statistics cannot be calculated since the ratio is not defined in months without any snow.

Ratios between observations and climate normals give each month equal weight, which is a desired feature for purposes of evaluating representativeness across all seasons. The standardization in the analysis in Appendix B also weights all calendar months equally. In contrast, cumulative annual quantities, which are of interest for some applications, are dominated by the months with the largest values. Table 4.2.1 shows that the climate normals are lower than the observed annual totals for the baseline period by 11% (total precipitation), 15% (rain), and 1% (snow).

Table 4.2.1 includes the same statistics discussed above for WRF model output, which are be discussed next. Together, the statistics suggest that the baseline period was wetter than the 1971 through 2000 climate normals, but close enough to consider the October 2004 through September 2005 period representative of average climate in Fort St. John Airport.

4.2.2 Model Skill at Fort St. John Airport Relative to the Climatologic Mean

It is difficult to determine qualitatively from Figure 4.2.1 through Figure 4.2.3 if the WRF model output captures at least some of the monthly precipitation anomalies from the climate normals. For total precipitation, Table 4.2.1 shows that the geometric variance is further from one for WRF model output (1.31) than for climate normals (1.26). In particular, the geometric mean bias of 1.28 for the WRF model is substantially further from one than for climate normals (1.06). Note that geometric variance becomes a highly sensitive statistic for values close to zero. The modelled rain fall of 5.81 millimetres in January is 29 times the observed value of 0.20 millimetres, which causes the extremely large geometric variance for the WRF model output in Table 4.2.1.

Because of the sensitivity of ratios to very small value, it is helpful to also consider differences, which give less weight to smaller values. In addition, they are also valid for snow. The under prediction of total precipitation (16%), rain (13%), and snow (24%) by the model are worse than the climatologic means (11%, 15%, and 1%). The RE scores in Table 4.2.1 show only very

weak improvement of WRF model predictions over the climatologic mean for total precipitation (0.28); for rain (-0.56) and snow (-0.29), model predictions are worse than the climatologic mean.

In terms of these statistics, the WRF model does not produce better predictions of precipitation than the climate normals. This is mostly attributable to a relatively representative choice of baseline period. The baseline period was chosen to minimize the precipitation difference with the climate normals. Therefore, it cannot be expected that WRF model predictions of precipitation are closer to the observations during the baseline period than the climate normals. In addition, numerical models usually have difficulties in predicting precipitation at point locations. Given these limitations, the WRF model performed as well as could be expected, and differences seen in model results should be representative of changes in microclimate with the Peace River Valley. Precipitation is commonly better reproduced during cold than warm months when it is often convectively driven. Convective precipitation is more localized, and the total condensation of water vapour is difficult to predict. Extremely heavy precipitation is often associated with convection, which usually shows spatial maxima over sub-grid scale areas while the model predicts grid-cell average precipitation, only. Because of these challenges, predictions of extreme precipitation events are not considered.

4.2.3 Model Time Series Comparisons at Fort St. John Airport

The time series of total daily precipitation during the week of June 21 to 27 (Figure 4.2.4) exemplifies the difficulty of predicting individual convective events. On June 22 and 23, the model predicted rain when no precipitation was observed at Fort St. John Airport. On the other hand, the model fails to predict the large rainfall event on June 26. The under prediction of about 30 mm of precipitation on June 26 is greater than the under prediction of total monthly precipitation in June (less than 10 millimetres; Figure 4.2.1). If several individual convective precipitation events happened in June within the model grid cell, it is likely that the Fort St. John Airport station collected a statistically representative sample of the average over all precipitation events in this grid cell in June. As spatio-temporal averages, the model predictions in the summer are good.

Figure 4.2.5 shows total daily precipitation for the winter week of December 1 to 7. The model predictions agree well with the observations. Over the course of the week, there is a slight under prediction of total precipitation. The model predicts the precipitation to begin and end later than observed, but that temporal mismatch could be related to the sampling period, which was from midnight to midnight for the model output but may be a different time of day for the observations.

4.2.4 Model Skill at the Field Stations Relative to Fort St. John Airport

Similar to temperatures in section 4.1.5, the main intention of modelling an extra year and comparing precipitation with field stations is to evaluate the model's ability to capture spatial variability. The challenges for the WRF model to provide predictions with high skill are different for precipitation than temperature.

Precipitation tends to vary spatially more than temperatures, because precipitation is dependent on land-cover and topography and upwind moisture accumulation and losses. Therefore, observations at Fort St. John Airport are likely going to have less predictive skill for precipitation than for temperature observations at the field locations. However, numerical modelling of precipitation is more challenging than temperature, and the WRF model may not be fully capable of accounting for sub-grid scale processes, topography, local land cover, and larger-scale moisture transport and change. Highly localized convective precipitation in the summer is particularly challenging as demonstrated in the previous section. Therefore, both Fort St. John Airport's and the WRF model's predictive skills can be expected to be lower for precipitation than for temperatures. Additional uncertainties can be expected from the instrument issues at the field locations (section 3.2.3).

For the prediction-skill evaluation, six stations had data available in the FYO from January 16, 2011 through January 15, 2012. Table 4.2.2 presents the same summary statistics as Table 4.1.2 above, but for monthly totals of all forms of precipitation. For the WRF model, these are grid-cell averages at the station locations. For comparison, the same statistics were calculated for the corresponding observations at Fort St. John Airport.

Table 4.2.2 WRF model prediction skill for precipitation at the field stations

Parameter	MG[a]		VG[b]		Diff[c]		RE Score[d]
	WRF	Fort St. John Airport	WRF	Fort St. John Airport	WRF	Fort St. John Airport	
Station 1 – Attachie Flat Upper Terrace	2.55	**0.57**	2.09	**1.22**	**47.98**	-177.79	-2.56
Station 2 – Attachie Flat Lower Terrace	**1.21**	0.49	1.84	**1.46**	**-2.31**	-219.33	-1.46
Station 3 – Attachie Plateau	1.57	**0.93**	1.45	**1.27**	**48.75**	-116.49	-4.46
Station 4 – Bear Flat	2.04	**1.01**	4.03	**1.72**	**54.77**	-147.3	-1.53
Station 5 – Hudson's Hope	2.39	**1.64**	**1.37**	1.66	**103.92**	-104.67	0.12
Station 7 – Site C Dam	2.96	**0.94**	3.01	**1.32**	167.3	**-84.33**	-7.76

NOTES:
Statistics for monthly total precipitation from January 16, 2011 until January 15, 2012. Numbers in bold highlight greater skills.
[a] Values closer to one represent greater skill.
[b] Smaller values represent greater skill.
[c] Difference is for annual total in mm water equivalent.
[d] Values close to one represent higher WRF model skill, values close to zero represent similar skills, and negative values represent higher climate-normals skill.
[c] Reduction-of-Error score (RE); values close to one represent higher WRF model skill, values close to zero represent similar skills, and negative values represent higher Fort St. John Airport skill.
[d] Weather Research and Forecasting (WRF) model output.
[e] Fort St. John Airport station observations.

Geometric mean biases for Fort St. John Airport observations are closer to one than for the WRF model predictions with the exception of station 2. Overall, relative to total monthly precipitation, Fort St. John Airport observations are less biased than the WRF model predictions. Also, geometric variances are closer to one for Fort St. John Airport than for the WRF model, indicating less uncertainty in predicting station observations from Fort St. John Airport observations than from WRF model output (with the exception of station 5).

The Fort St. John Airport absolute annual differences from the station observations are greater than the absolute differences of WRF from the station observations. That seems to contradict Fort St. John Airport's geometric mean bias being closer to one. However, Figure 4.2.6 explains the apparent contradiction: greatest absolute discrepancies occur during the rainiest months of the year (June and July, not shown). Observations at Fort St. John Airport show monthly totals of roughly 150 millimetres, while observations at the field locations are roughly 50 millimetres lower. This overestimation by Fort St. John Airport in the rainy summer months adds to overestimations in other months but changes the ratios less. The overall overestimation by Fort St. John Airport might be related to undercatch of precipitation at the field locations (section 3.2.3). By contrast, the WRF model underestimates summer precipitation observations at the field locations in June and July, but the WRF model tends to overestimate in the other months. This reduces the difference from field observations for total annual precipitation, but does not improve the geometric mean bias, which is based on monthly ratios. The WRF model's underestimation in June and July is consistent with Figure 4.2.2 and the baseline analysis in section 4.2.1. Note also from Figure 4.2.2 that in the FYO, June and July precipitation amounts were more than one standard deviation above the climate normals. Both months were therefore particularly wet, which may decrease the WRF model's predictive skill.

Overall, the reduction-of-error scores indicate greater skill for Fort St. John Airport than the WRF model, except at station 5. The reduction-of-error score is based on root mean square errors (see footnote d in Table 4.2.2), but basing it on geometric variance does not change the conclusion. These results agree with a potential undercatch at the field locations and the WRF model's difficulties in accounting for convective precipitation in June and July. The deviation of the WRF model predictions from true precipitation cannot be evaluated, because the observational errors are unknown. It is likely that the WRF model has the same difficulties in accurately predicting local precipitation events in the summer than any numerical model would be expected to have. A key point to remember, however, is that the WRF model is used to model differences in precipitation between Baseline Case and Future Case. Any biases in WRF model predictions apply to both cases and cancel when the difference is calculated. As for any other numerical model, it can be expected that the WRF model is able to reasonably predict changes in average precipitation between Baseline Case and Future Case.

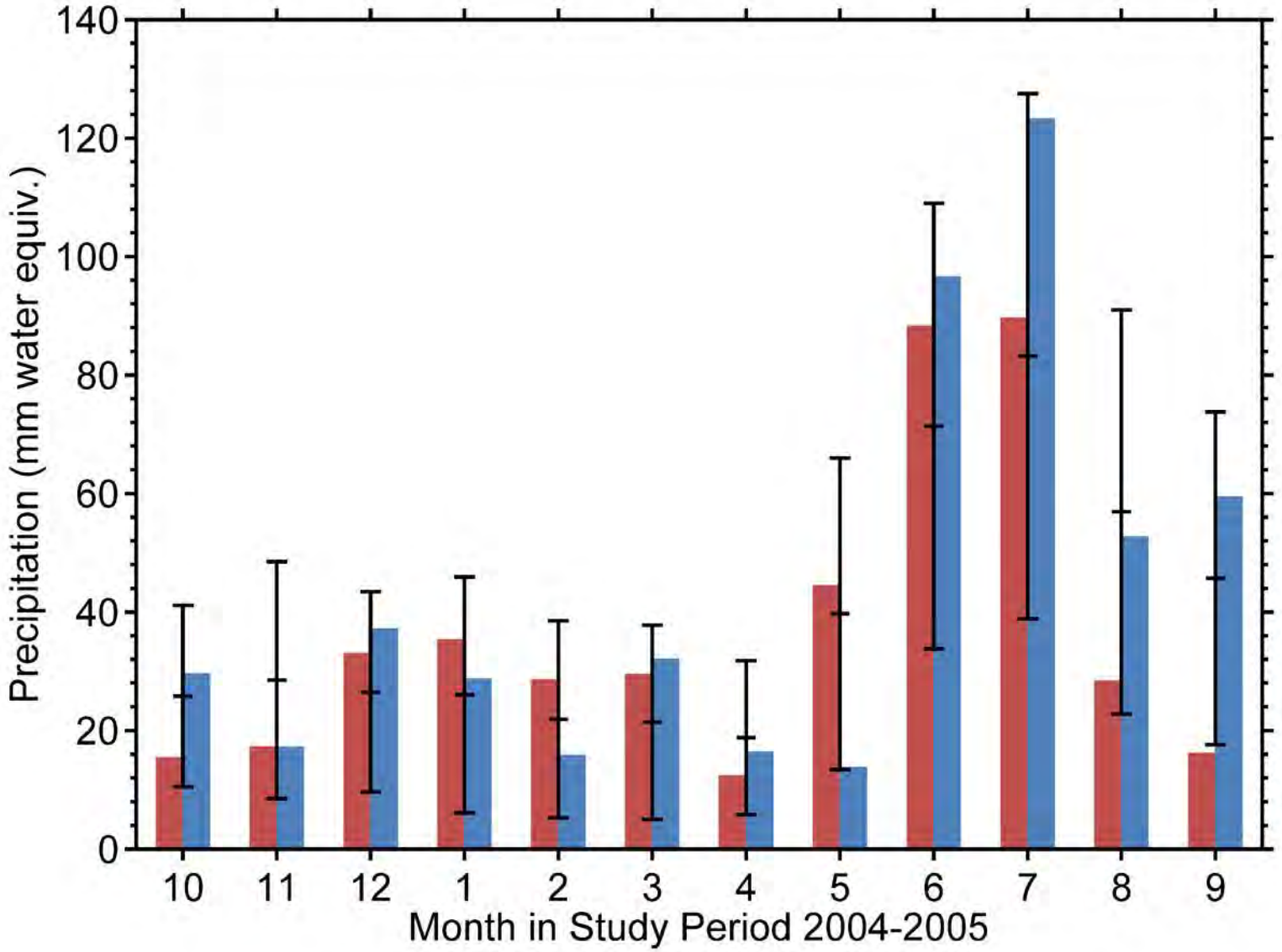

Observed (blue) and predicted (red) monthly total precipitation at Fort St. John Airport for October 2004 to September 2005. Error bars show 1971-2000 averages (climate normals) and their standard deviations.

SITE C CLEAN ENERGY PROJECT

RWDI BC hydro

Figure 4.2.1
Observed, predicted, and climate-normal precipitation at Fort St. John Airport

DATE	Dec. 3, 2012		R 0

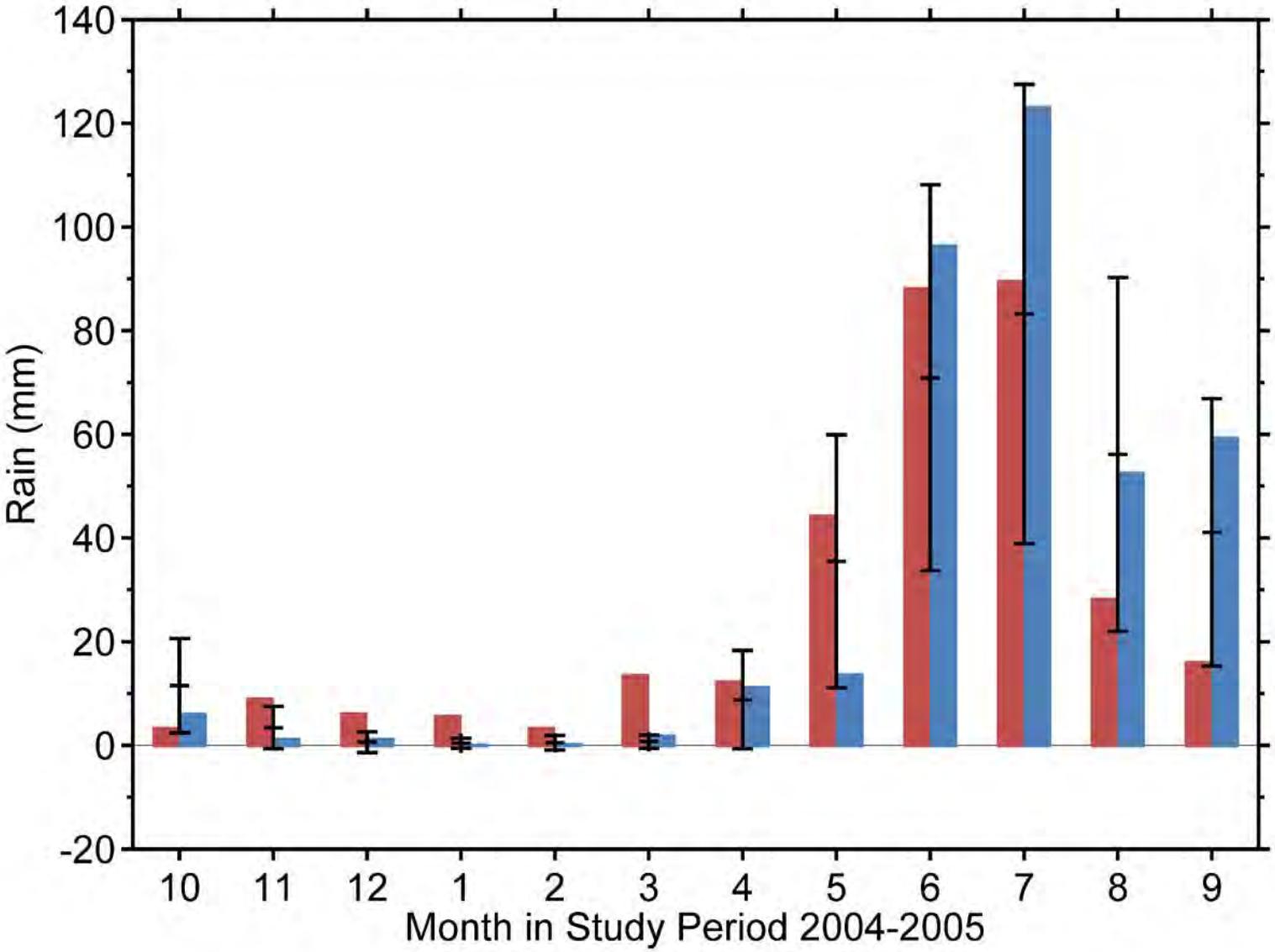

Observed (blue) and predicted (red) monthly total rainfall at Fort St. John Airport for October 2004 to September 2005. Error bars show 1971-2000 averages (climate normals) and their standard deviations.

SITE C CLEAN ENERGY PROJECT	RWDI BC hydro
	Figure 4.2.2 **Observed, predicted, and climate-normal rainfall at Fort St. John Airport**
DATE: Dec. 3, 2012	R 0

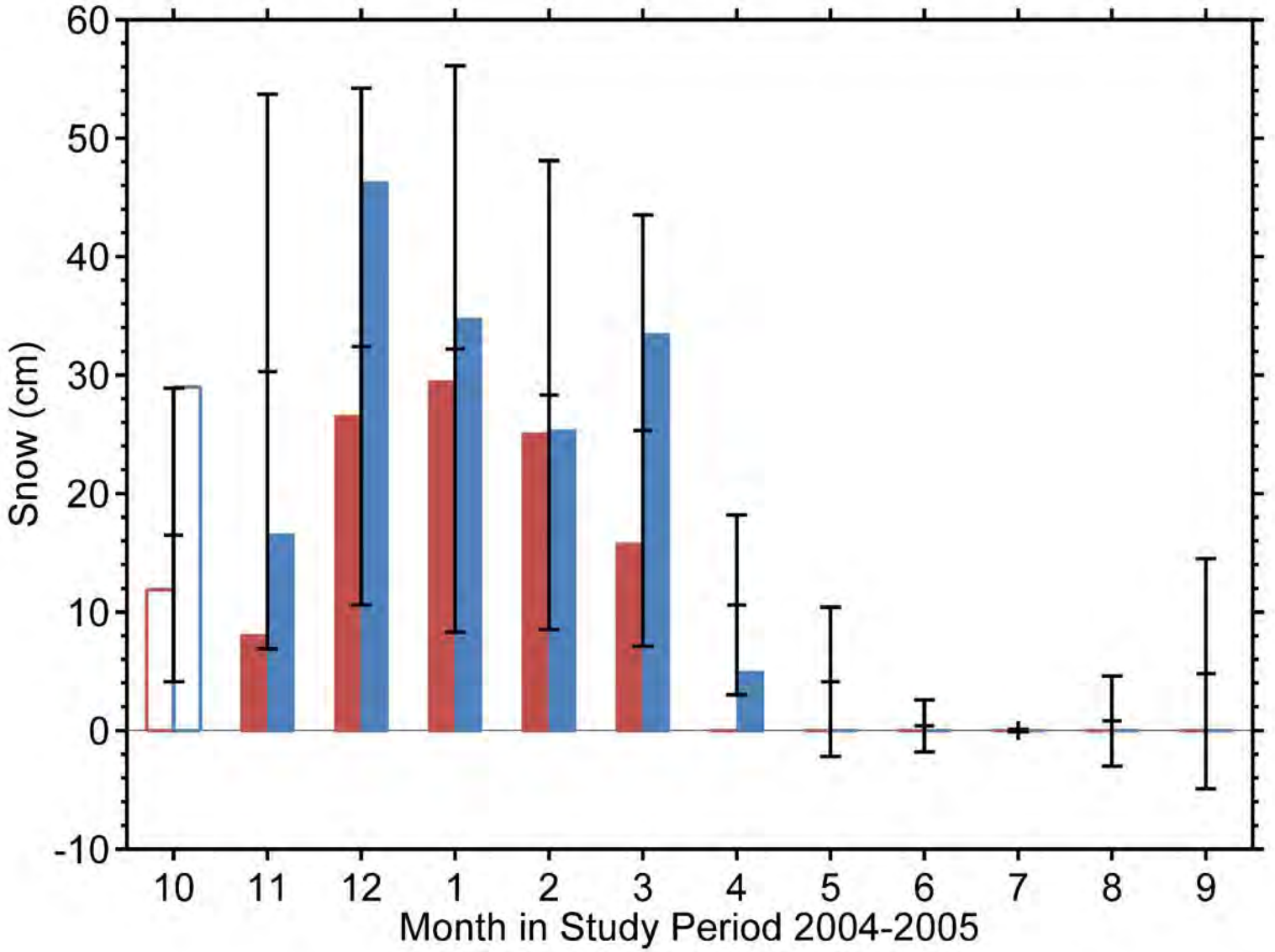

Observed (blue) and predicted (red) monthly total snowfall at Fort St. John Airport for October 2004 to September 2005. Error bars show 1971-2000 averages (climate normals) and their standard deviations. Open bars indicate months in which the observations were outside of the standard deviation of the climate normals.

SITE C CLEAN ENERGY PROJECT

RWDI BC hydro

Figure 4.2.3
Observed, predicted, and climate-normal snowfall at Fort St. John Airport

DATE	Dec. 3, 2012		R 0

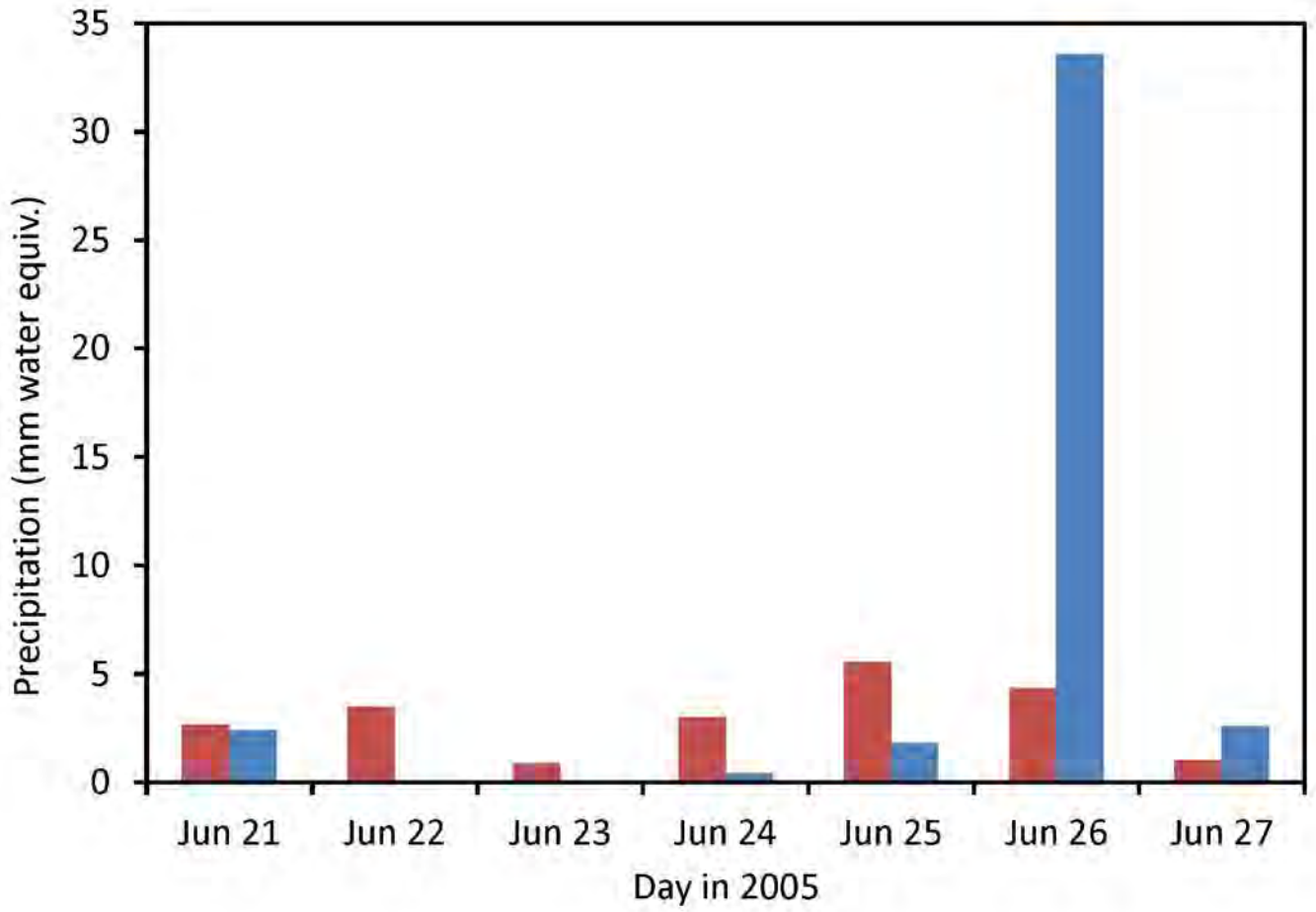

Observed (blue) and predicted (red) daily total precipitation at Fort St. John during the summer week of June 21 to 27, 2005.

SITE C CLEAN ENERGY PROJECT

RWDI BC hydro

Figure 4.2.4
One summer week of observed and predicted daily precipitation at Fort St. John Airport

DATE	Dec. 3, 2012		R 0

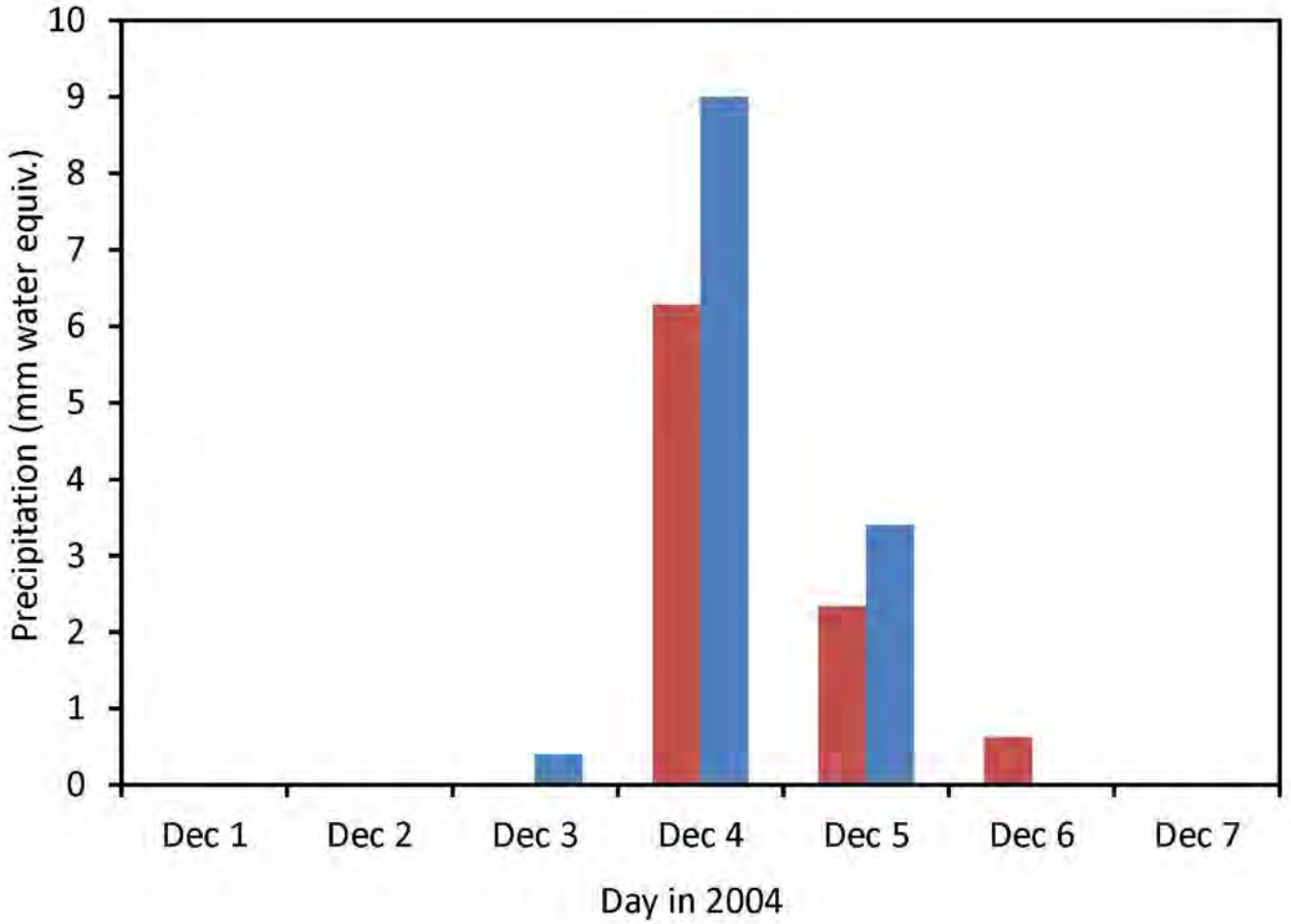

Observed (blue) and predicted (red) total precipitation for Fort St. John during the winter week of December 1 to 7, 2004.

SITE C CLEAN ENERGY PROJECT

RWDI BC hydro

Figure 4.2.5
One winter week of observed and predicted daily precipitation at Fort St. John Airport

DATE	Dec. 3, 2012		R 0

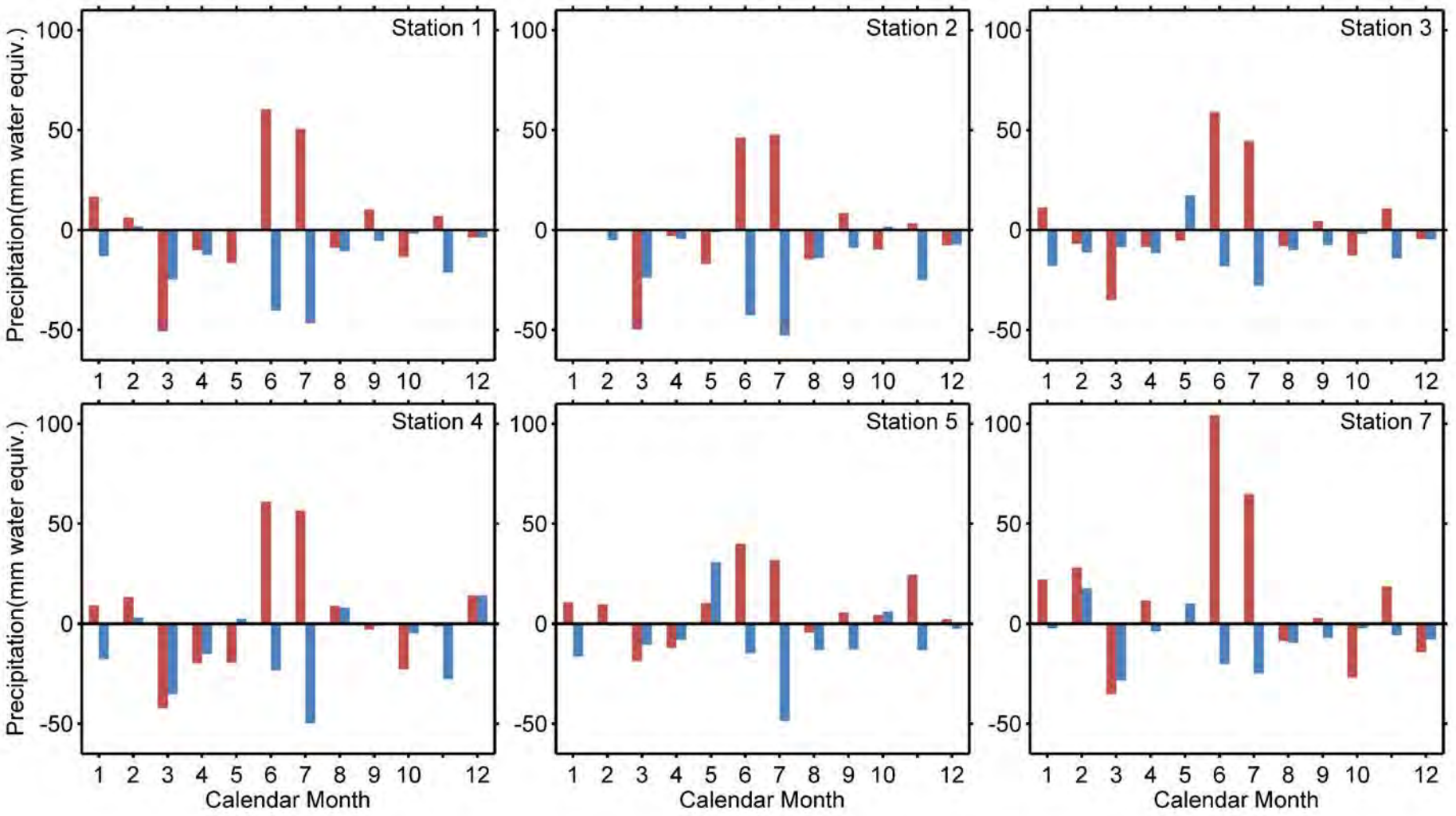

Differences of Weather Research and Forecasting (WRF) model prediction (red) and Fort St. John observations (blue) from local station observations of monthly total precipitation for the first year of observations at six field-station locations as labelled. WRF prediction is the grid-center average for the cell encompassing the station location. January data are averages over January 16-31, 2011 and January 1-15, 2012.

SITE C CLEAN ENERGY PROJECT		RWDI BC hydro	**Figure 4.2.6 Weather Research and Forecasting model versus Fort St. John Airport predictions of precipitation at field stations**
DATE	Dec. 3, 2012		R 0

4.3 WIND

Model predicted winds are hourly and grid-cell averages, while observations are measured for a few minutes once an hour at a point location. Winds can vary strongly over the course of an hour and depend on small scale features below model resolution. Furthermore, small scale thermally driven flows are difficult to model, particularly at night. Finally, wind speed and direction strongly depend on height above ground and local surface characteristics, which are often difficult to model correctly. All these challenges combined can lead to uncertainties in wind speed and direction of roughly one metre per second and 10°, respectively. The binning of wind speeds in ranges and wind directions in sectors, which is typically done for model-observation comparisons, tends to amplify differences and uncertainties.

4.3.1 Comparisons of Model Output with Observations at Fort St. John Airport

Wind roses are graphical depictions in radial charts for showing wind direction and wind speed frequencies where the lengths of the radii represent wind direction frequency. The wind roses of Fort St. John Airport hourly wind observations and model predictions are presented in Figure 4.3.1 for the period of October 2004 through September 2005. Predicted and observed wind directions do not agree well by individual 22.5° sectors. However, when two or three adjacent sectors are combined into a general coarse wind direction, model and observations agree well. Most frequently, winds at Fort St. John Airport were observed from a south-westerly direction (37%), which the model predicted to occur in 42% of all hours. Winds were observed to blow from the east to southeast about 19% of the time, while they were predicted to blow from these three sectors 15% of all hours. The third most frequent wind direction was from the north-northwest and north, observed about 16% and predicted 14% of the time. These three general directions account for 71-72% of all observed and predicted winds.

Of particular interest are calms (wind speeds up to one metres per second) and strong wind events above 10 metres per second. More calms were observed (4.3%) than predicted (2.5%). The model agrees with observations that strong winds occurred only from south-westerly directions and north-northwesterly to northerly directions, although the model seems to under predict the frequency of high wind speeds.

To investigate this further, it is easier to compare wind speeds in a frequency plot (Figure 4.3.2). Note that the vertical scales in the panels are different. The top row shows frequencies for the same wind speed classes as the wind roses in Figure 4.3.1. Since the coarse resolution and particular choice of wind class boundaries can distort the comparison, the bottom row shows the same data presented with finer wind speed class resolution.

The frequency distributions of the model outputs are very similar for coarsely and finely binned wind classes and follow the commonly observed Weibull shape. By contrast, station observations have flatter frequency distributions in the centre of the wind ranges. The more finely binned wind speed classes in the bottom row of Figure 4.3.2 show variability between adjacent wind ranges that are probably artifacts of the conversion of the observed wind speeds

from integers of kilometres per hour to metres per second. Given this caveat, the main conclusion that can be drawn from Figure 4.3.2 is that the model tends to under predict the frequency of calms and weak winds of less than 2.0 metres per second. Considering both binning resolutions, there is no indication that the model under predicts high wind-speed events.

These biases would be present in both the Baseline and Future Case with the Project model runs and would thus cancel. Difference between the runs should still be representative of influence resulting from the formation of the proposed Site C reservoir.

4.3.2 Comparisons of Model Output with Observations at the Field Stations

Meteorological stations at airports are often well sited because of few local obstructions. Wind measurements at such open sites tend to be more representative of larger-scale wind flows on the scale of tens of kilometres than measurements at sites with local obstructions from buildings, vegetation, or topography. The field stations were intentionally sited to represent local conditions. The comparison of winds modelled in WRF with winds observed at the field stations therefore provides a good indication of the WRF model‘s ability to capture local flow structures at scales smaller than ten kilometres.

Figure 4.3.3 shows normalized frequencies of wind-speed ranges for the WRF model predictions and observations at the field locations and for Fort St. John Airport observations of hourly winds over the course of the FYO. Observations at Fort St. John Airport are consistently higher than at any of the field stations, probably caused by Fort St. John Airport‘s higher elevation and open exposure. The highest frequency bin is for wind speeds from 4.0 to less than 6.0 metres per second, while all field stations recorded most frequent wind speeds in wind speed bins up to 4.0 metres per second. In four percent of all hours, wind speeds at Fort St. John Airport exceeded 10 metres per second, while winds above this value rarely occurred at the field sites. The WRF model agrees with both characteristics of station observations. Furthermore, it tends to represent some of the spatial differences between the field locations, for example the lower wind speeds at Station Four.

In conclusion, the WRF model output appears to predict wind speeds at the field locations more skillfully than Fort St. John Airport observations.

Observed

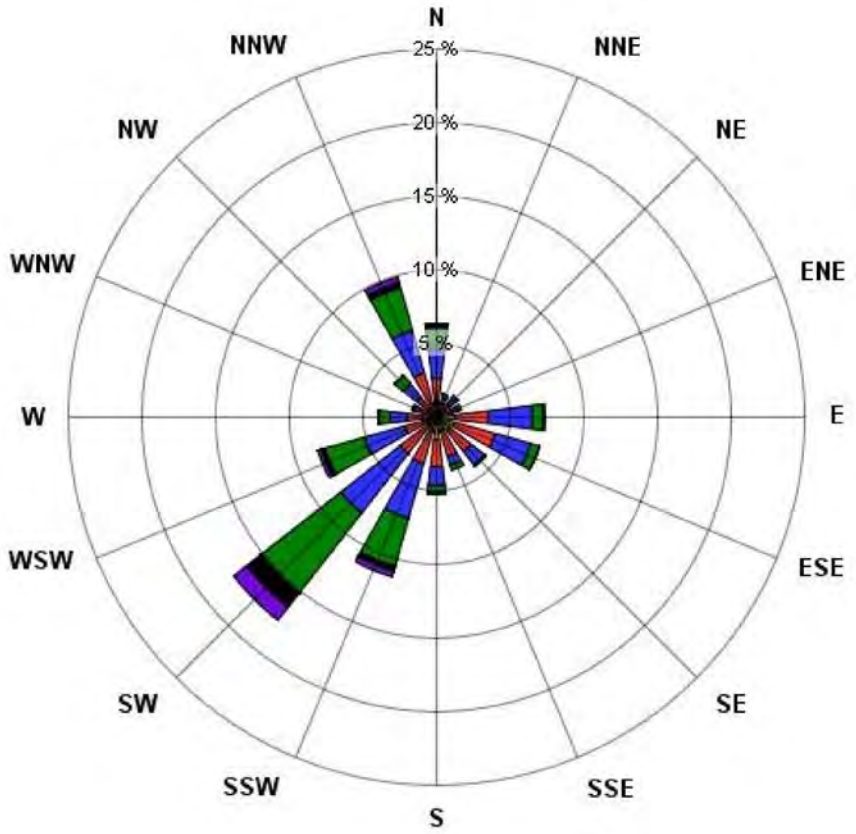

Calms: 4.19%

Predicted

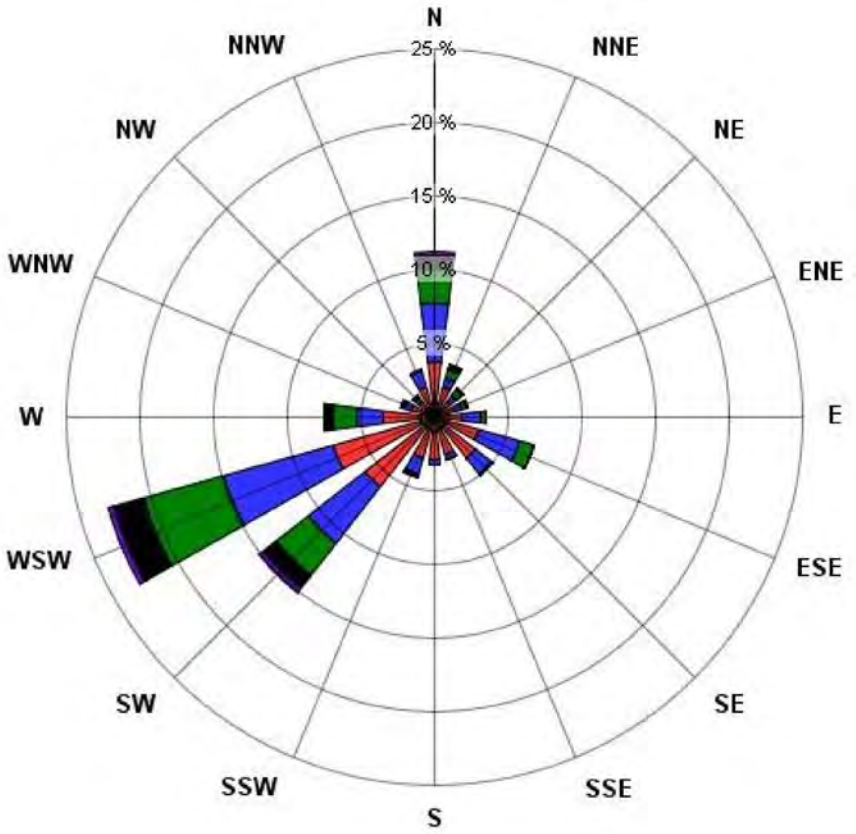

Calms: 0.58%

Observed and Weather Research and Forecasting (WRF) model predicted wind roses for Fort St. John Airport for October 2004 to September 2005. The direction represents the origin of the wind (where it is blowing from).

Wind Speed (m/s)

- > 10.0
- > 8.0 - 10.0
- > 6.0 - 8.0
- > 4.0 - 6.0
- > 2.0 - 4.0
- > 1.0 - 2.0
- > 0.5 - 1.0

SITE C CLEAN ENERGY PROJECT

RWDI BC hydro

Figure 4.3.1
Observed and predicted wind roses at Fort St. John Airport

DATE	Dec. 3, 2012		R 0

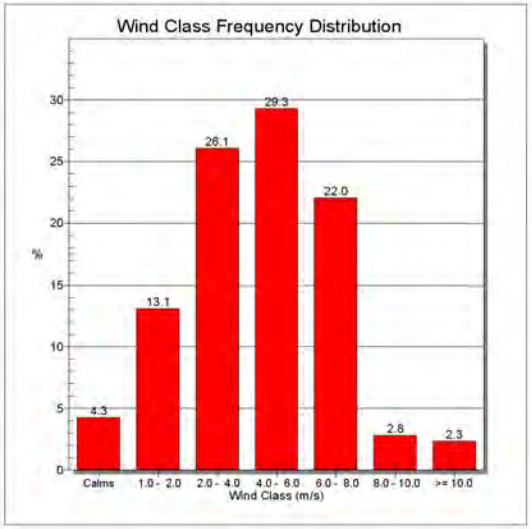

Observed coarse

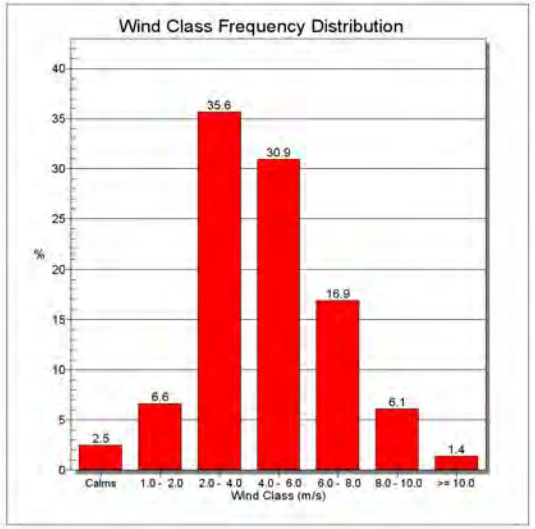

Predicted coarse

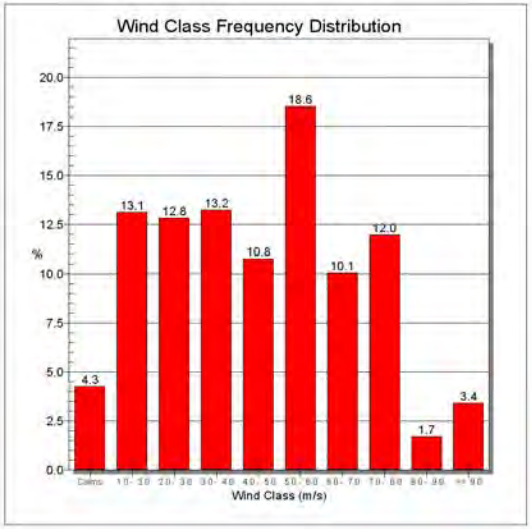

Observed fine

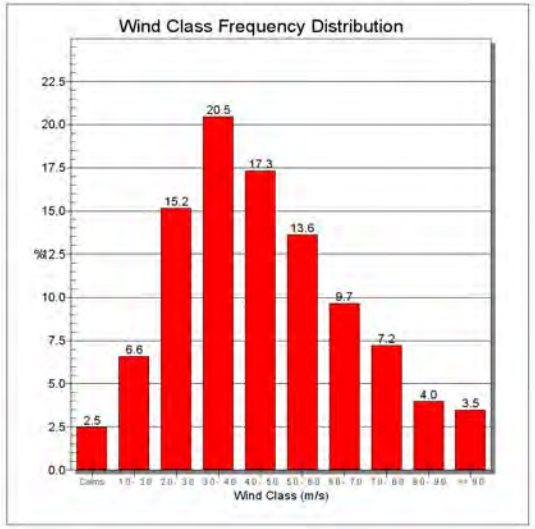

Predicted fine

Fort St. John observed (left) and Weather Research and Forecasting (WRF) model predicted (right) hourly wind-speed distributions for Fort St. John Airport for October 2004 to September 2005. Wind classes in top row match with wind roses in Figure 4.3.1; bottom row shows wind classes of finer resolution. Note the differences in vertical scale.

SITE C CLEAN ENERGY PROJECT

RWDI BC hydro

Figure 4.3.2
Observed and predicted wind-speed frequencies at Fort St. John Airport

DATE	Dec. 3, 2012		R 0

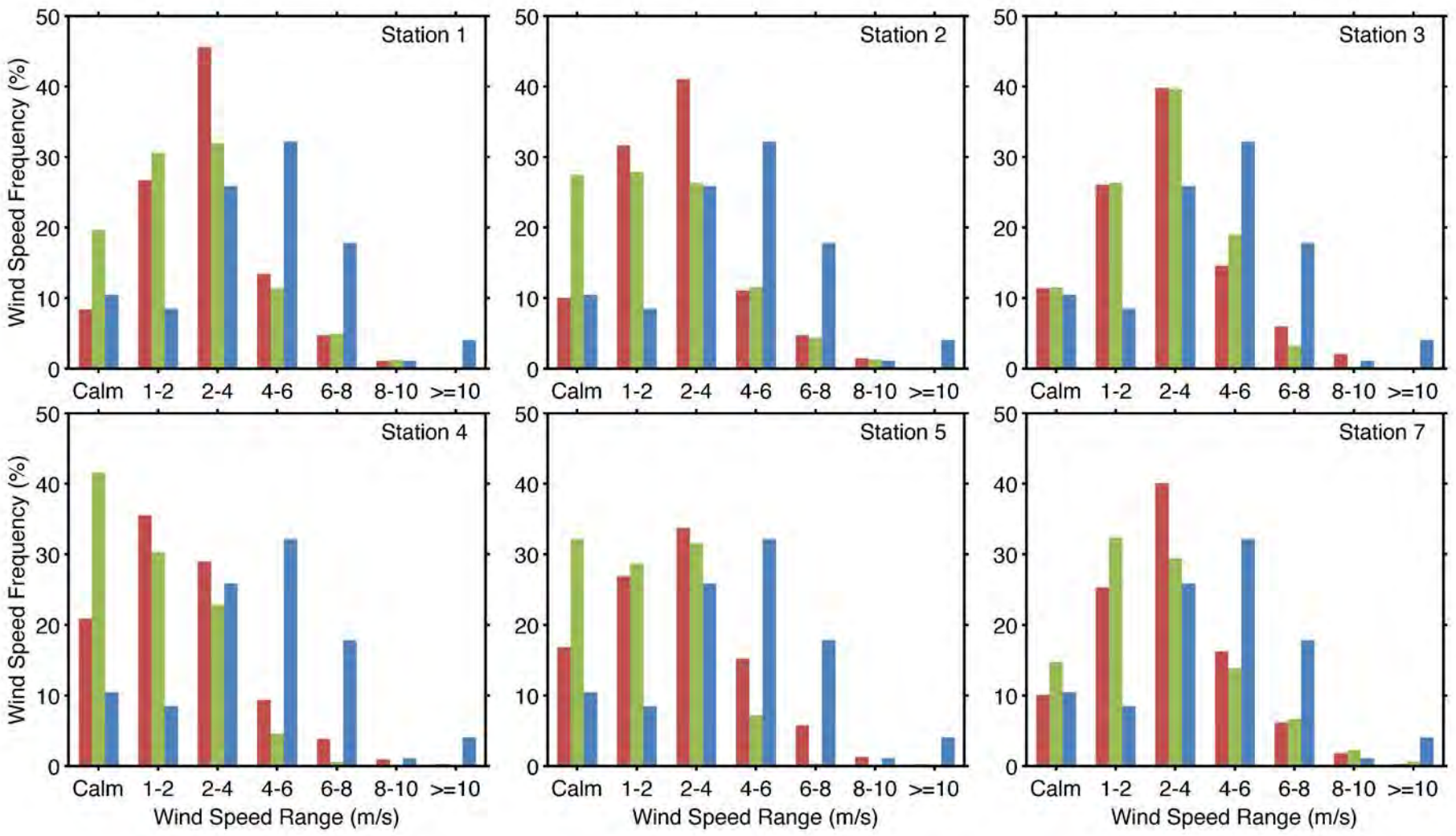

Weather Research and Forecasting (WRF) model prediction (red) and local station observations (green) at the six field station locations (as labelled) and Fort St. John observations (blue) of hourly wind-speed distributions for January 16, 2011 to January 15, 2012. WRF prediction is the grid center result (destaggered and interpolated from the cell faces) for the cell encompassing the station location. Note the differences in vertical scale.

SITE C CLEAN ENERGY PROJECT		RWDI BC hydro	**Figure 4.3.3 Observed and predicted wind-speed frequencies at field stations**
DATE	Dec. 3, 2012		R 0

4.4 CONCLUSIONS

Station observations of temperatures at Fort St. John Airport during the baseline period from October 2004 through September 2005 were 1.08 degrees Celsius warmer than the climate normals from 1971 through 2000. The seasonal break-up of temperatures during the baseline period shows warmer temperatures during the cooler seasons and lower temperatures during the summer than climate normals. Considering the high inter annual variability, the October 2004 through September 2005 baseline period can be considered representative of normal temperatures in Fort St. John Airport.

Various statistics demonstrate that temperatures modelled with the WRF model are better predictors for observed temperatures at Fort St. John Airport than climate normals. The model predicts temperature anomalies from climate normals well, with the exception of extreme temperatures. Model predictions of extreme maximum temperatures are too low in all calendar months, while predictions of extreme minima are too high in all months but July and September.

Time series of modelled and observed daily average temperature at Fort St. John Airport agree well. The model is able to predict the onset of a strong temperature drop in the winter with some caveats: it under predicts warm temperatures prior to the temperature drop and over predicts cold temperatures afterwards, and the drop is predicted roughly eight hours too late. For a typical summer week, the model captures the strong diurnal temperature cycle reasonably well. Discrepancies could be related to over or under predicted precipitation and the associated incorrect prediction of soil moisture.

The baseline period was wetter than the 1971 through 2000 climate normals but close enough to consider the October 2004 through September 2005 period representative of average climate in Fort St. John Airport. Because of this representativeness and the general difficulties of models to predict precipitation at point locations, the WRF model is not able to predict precipitation better than the climate normals. However, biases between model predictions and observations are expected to be the same for Baseline Case and Future Case and therefore do not diminish the model‘s ability to predict the difference between the two periods.

The predictive skill of the model for one summer month‘s total precipitation was shown to be skewed by a single-day precipitation event. Model predictions of monthly totals in the summer and daily and monthly totals in the winter agree well with observations.

Predicted and observed wind directions agree well after combining adjacent 22.5° wind sectors into common coarse wind directions. The model predicts correctly that strong winds occurred only from south-westerly directions and north-northwesterly to northerly directions. The model tends to under predict the frequency of calms and weak winds of less than 2.0 metres per second. The wind-speed frequency distribution of the model output appears to follow a more natural and typical shape than the observations, which may be an artifact of coarse observations and unit conversions. Overall model and observation agree well enough that changes in predicted model results should be indicative of changes that would be observed at

Fort St. John Airport, and by extension, model results should also be indicative of changes in winds that would occur within the Peace River Valley.

The FYO at six field stations along the proposed reservoir provide an opportunity to test the WRF model's ability to capture spatial variability within the Technical Study Area. With respect to wind-speed distributions, the WRF model is capable of capturing differences between field stations and clearly outperforms observations at Fort St. John Airport as predictors. On the other hand, given the relatively flat terrain and therefore homogeneous temperature distribution in the Technical Study Area, Fort St. John Airport observations of temperatures have greater predictive skills for the corresponding temperature observations at station locations than WRF model output. The WRF model simulation was weak in capturing unusually high and low temperatures and in the timing of rapid temperature changes. However, the WRF model's overall predictive skill at one kilometre resolution appears greater than typical numerical modelling skills at coarser resolutions. Predictive skills for total monthly precipitation from Fort St. John Airport observations and WRF model output are lower than one would expect for the flat topography and homogeneous land cover. This may be attributable to instrument issues at the field stations, specifically undercatch. In addition, the WRF model seems to fail to fully capture convective precipitation, which dominates the rainy June-July period. It should also be noted that there is sub grid scale variation in relief and land cover within the valley that is not fully captured by the inputs to the WRF model.

In conclusion, the WRF model performs as would typically be expected from a meso-scale model at one kilometre grid resolution: it cannot capture sub grid scale (less than 1 kilometer) variations, but represents average variation on the same scale as the model resolution (1 kilometre and greater); it predicts observed temperatures well; it predicts winds, daily winter precipitation, and monthly summer precipitation reasonably well; it has difficulties in predicting daily summer precipitation. The latter difficulties are not expected to reduce the model's ability to predict differences between Baseline Case and Future Case with the Project because the error would be present in both cases so differences due solely to the proposed reservoir should still be discernible in the model results.

5.0 ESTIMATED PROJECT MICROCLIMATE INFLUENCES

In this section, modelled microclimate changes associated with the proposed reservoir are quantified and their statistical significance determined. These changes ignore the influence of global climate change on the Technical Study Area. However, a brief comparison of the modelled microclimate changes with changes due to global climate changes are drawn in a later subsection (6.1).

Winds that move across the proposed reservoir would carry the water-surface characteristics that are distinct from adjacent land surfaces (e.g., higher relative humidity and lower daily maximum temperature) horizontally over the land. At the same time, turbulence transports these characteristics vertically upward forming an internal boundary layer that grows deeper with longer downwind distance over the water surface. Field observations and analytical models on

the growth of internal boundary layers show that several kilometres of horizontal distance are required to form an internal boundary layer with a depth on the order of hundreds of metres (e.g., Luhar, 1998). As the internal boundary layer meets the adjacent land surface, a new internal boundary layer begins to form and erode the previous layer from below and dilute the water-surface characteristics. Most of the time, the rougher land surface generates more turbulence and therefore grows the internal boundary layer faster than the water surface.

The future reservoir as represented in the model has a typical estimated width on the order of one kilometre. The associated internal boundary layer, under cross wind conditions, would typically be less than one hundred metres and therefore would be eroded after travelling less than one kilometre over land. Since the internal boundary layer formed over the land continues to grow from below and entrain air from above, the characteristics of the water surface would no longer be measurable after a few kilometres downwind distance over land. Measurable temperature changes would therefore be expected to be limited to a few kilometres from the reservoir. Precipitation changes might extend an additional few kilometres, because of delays due to the formation of precipitation and fallout time and due to horizontal advection of precipitation by large-scale winds. Under convective conditions, the reservoir is wide enough to modify local convective patterns right over the reservoir, but the horizontal extent of the convective cells is also limited to about the first two kilometres from the water. Given these general considerations, it is not expected that the formation of the reservoir would statistically significantly modify the microclimate in the Technical Study Area beyond a few kilometres from the reservoir.

Also it is important to note that the Attachie flat Lower Terrace location would be flooded by the filling of the Site C reservoir. Therefore, the changes in climate parameters at this location discussed below reflect a change from a land surface to a water surface.

5.1 TEMPERATURE

Differences in air temperature were predicted at several locations close to the reservoir. Daily air temperature, a measure of the average air temperature experienced in one day, was found to increase at locations adjacent to the reservoir and change less at locations farther away from the proposed reservoir. Locations where the largest change in annual average temperature was predicted were at Hudson‘s Hope, Farrell Creek, and Site C Dam. On an annual basis the average daily air temperature at each of these locations was predicted to increase by no more than 0.4 degrees Celsius. The least annual change was predicted at Fort St. John Airport and Attachie Flat Upper Terrace with no increase in temperature. The change in the annual average air temperature at all locations was found not to be statistically significant. The results of the model and significance test suggest that there would be no noticeable change in annual average air temperature at any of the extracted locations due to the construction of the proposed reservoir. This is in line with the expected short range of local microclimate changes.

Figure 5.1.1 (right) shows WRF-predicted changes of annual average temperatures due to the formation of the reservoir for the entire Technical Study Area. No changes of more than 1.0 Celsius degree are predicted.

A probabilistic analysis of the significance of changes in the annual average of daily average temperatures was performed (Figure 5.1.2). It was found that a statistically significant change is extremely unlikely at almost all locations in the Technical Study Area. Statistically significant changes are between likely and extremely likely only in a few grid cells over the proposed reservoir near station 3 and west of the proposed dam. The results of the model and significance test suggest that the formation of the reservoir would not cause a noticeable change in annual average temperature in the Technical Study Area with the exception of a few isolated small areas over the proposed reservoir.

When daily average temperatures are averaged over an entire year, the larger data sample size increases the statistical significance of predicted changes, but the averaging process potentially eliminates changes. Therefore, the analysis was broken down seasonally and into daily minimum and maximum temperatures.

The two left panels in Figure 5.1.1 show WRF-predicted changes in annual averages of daily maximum and minimum temperatures. As in the case of daily average temperatures, no changes exceeding 1.0 Celsius degree are predicted anywhere in the Technical Study Area beyond one or two kilometres from the modelled reservoir surface. However, daily maximum temperatures are predicted to decrease by several degrees along the land areas directly adjacent the proposed reservoir, with temperature decreases exceeding 6.0 degrees Celsius in some areas. Figure 5.1.2 shows that these changes are extremely likely to be statistically significant, while it is extremely unlikely outside of the reservoir valley that any statistically significant change would occur.

For the annual average of daily minimum temperatures, a spatially more varied response to the formation of the reservoir is predicted by the WRF model (lower left panel in Figure 5.1.1). Increases of more than 6.0 degrees Celsius are predicted adjacent the proposed reservoir south of Hudson‘s Hope. In the other areas near the reservoir temperature decreases are expected of up to about 4.0 degrees Celsius. These predicted changes are extremely likely statistically significant, while it is again extremely unlikely that statistically significant changes of daily minimum temperatures would occur farther from the proposed reservoir (Figure 5.1.2).

Because the annual averaging might reduce statistically significant temperature changes, predicted changes were further analyzed by season. The predicted difference in daily average air temperatures throughout the year at each location is shown in Figure 5.1.3. The most variation in change is predicted to occur at Attachie Flat Upper Terrace, Attachie Flat Lower Terrace, Bear Flat, and Site C Dam. Less variation is seen at Attachie Plateau, Hudson‘s Hope, and Farrell Creek with very little change predicted to occur away from the proposed reservoir at Fort St. John Airport. The general positive bias throughout the year is evident in the graphics with only a few periods where the change is predicted to be a decrease in daily average air temperature.

Predicted seasonal differences between the Baseline Case and Site C Case are shown in Table 5.1.1 as Future Case with the Project minus Baseline Case, or change from the Baseline Case. Seasonal daily average air temperatures were predicted to increase the most in the fall ranging

from a 0.1 to 2.0 degrees Celsius change at Attachie Flat Upper Terrace, Attachie Flat Lower Terrace and Site C Dam. Decreases in daily average air temperature were predicted during the spring at all locations except Fort St. John Airport, and Attachie Flat Plateau. The least seasonal change was predicted in summer and winter at all locations.

Table 5.1.1 Seasonal change in daily average temperature

Difference (Future Case with the Project – Baseline Case)	Spring	Summer	Fall	Winter	Year
Fort St. John Airport	0.0	0.0	0.1	0.0	0.0
Station 1 - Attachie Flat Upper Terrace	-1.1	0.1	2.0	-0.4	0.1
Station 2 - Attachie Flat Lower Terrace	-1.3	0.0	2.0	-0.6	0.0
Station 3 - Attachie Flat Plateau	0.0	0.1	0.4	0.1	0.1
Station 4 - Bear Flat	-1.2	0.2	1.9	-0.5	0.1
Station 5 - Hudson's Hope	-0.2	0.1	0.7	0.5	0.3
Station 6 - Farrell Creek	-0.1	0.1	0.6	0.2	0.2
Station 7 - Site C Dam	-0.9	0.5	2.0	-0.1	0.4

NOTES:
All values in degrees Celsius.
[e] Fort St. John Airport station observations.

The changes in the daily average temperature are dominated by the increase in daily minimum temperature, especially during the warm season. The changes in daily minimum and maximum air temperature are shown in Table 5.1.2 and Table 5.1.3. At Attachie Flat Lower Terrace the daily minimum air temperature was predicted to increase by 2.4 degrees Celsius in summer and 2.5 degrees Celsius in fall while the maximum daily temperature was predicted to decrease by 3.6 degrees Celsius in spring.

Table 5.1.2 Seasonal change in daily minimum temperature

Difference (Future Case with the Project – Baseline Case)	Spring	Summer	Fall	Winter	Year
Fort St. John Aiport	0.0	0.1	0.1	0.0	0.1
Station 1 - Attachie Flat Upper Terrace	1.2	2.4	2.4	-0.7	1.3
Station 2 - Attachie Flat Lower Terrace	1.2	2.4	2.5	-0.9	1.3
Station 3 - Attachie Flat Plateau	0.3	0.5	0.5	0.1	0.4
Station 4 - Bear Flat	1.1	2.6	2.2	-0.9	1.2
Station 5 - Hudson's Hope	0.1	0.6	0.8	0.6	0.5
Station 6 - Farrell Creek	0.1	0.4	0.6	0.3	0.4
Station 7 - Site C Dam	1.4	3.0	2.4	-0.4	1.6

NOTES:
All values in degrees Celsius.
[e] Fort St. John Airport station observations.

Table 5.1.3 Seasonal change in daily maximum temperature

Difference (Future Case with the Project – Baseline Case)	Spring	Summer	Fall	Winter	Year
Fort St. John Airport	0.0	0.0	0.1	0.0	0.0
Station 1 - Attachie Flat Upper Terrace	-3.3	-2.5	1.3	-0.2	-1.2
Station 2 - Attachie Flat Lower Terrace	-3.6	-2.7	1.2	-0.4	-1.4
Station 3 - Attachie Flat Plateau	-0.3	-0.3	0.2	0.1	-0.1
Station 4 - Bear Flat	-3.3	-2.4	1.2	-0.1	-1.1
Station 5 - Hudson's Hope	-0.4	-0.2	0.4	0.2	0.0
Station 6 - Farrell Creek	-0.3	-0.3	0.4	0.1	0.0
Station 7 - Site C Dam	-3.0	-2.2	1.4	0.1	-0.9

NOTES:
All values in degrees Celsius.
[e] Fort St. John Airport station observations.

Overall the daily minimum air temperature is predicted to increase at all locations with the greatest change predicted to occur in the spring and summer at Attachie Flat Upper Terrace, Attachie Flat Lower Terrace, Bear Flat, and Site C Dam by more than one degree Celsius. Conversely, the daily maximum air temperature is predicted to decrease in spring, summer, and winter and increase in fall.

A statistical significance test was performed on the seasonal change for each of the six locations of interest. Bear Flat was the only location where the change was found to be statistically significant, specifically only in the summer. The change predicted for other seasons (spring, fall and winter) were not found to be statistically significant.

To explore the spatial and seasonal characteristics of WRF-predicted temperature changes, Figure 5.1.4 displays monthly averages of daily mean temperatures for the months of October, January, April, and July. The likelihood of these changes to be statistically significant is shown in Figure 5.1.5. As in the annual case, no changes exceeding 1.0 degrees Celsius are predicted outside of the reservoir, where statistically significant changes are very unlikely. In October, temperature increases of up to 3.0 degrees Celsius are expected along the reservoir shores. There is not enough evidence, however, that these changes are statistically significant, with the exception of the area near the proposed reservoir southwest of Hudson‘s Hope and a few isolated areas in the most eastern part of the reservoir, where the changes are likely statistically significant. In January, statistically significant increases of up to about 5.0 degrees Celsius are predicted adjacent the proposed reservoir near and particularly south of Hudson‘s Hope. Predicted decreases of up to 2.0 degrees Celsius in the northeastern half of the proposed reservoir are unlikely statistically significant. April shows moderate decreases of up to 2.0 degrees Celsius adjacent most of the reservoir, but their statistical significance cannot be confirmed. July shows the least changes of up to 2.0 degrees Celsius only in the southwestern half of the proposed reservoir, but the statistical significance of these small changes over land is

likely to extremely likely along the whole length of the reservoir with the exception of the eastern most section.

The same analysis was repeated for monthly averages of daily maximum (Figure 5.1.6 and Figure 5.1.7) and minimum (Figure 5.1.8 and Figure 5.1.9) temperatures. For both parameters, outside of the proposed reservoir, predicted changes are less than 1.0 degrees Celsius, and it is unlikely or very unlikely that any statistically significant changes occur in the Technical Study Area outside of the proposed reservoir (Figure 5.1.7 and Figure 5.1.9). Monthly averages of daily maximum temperatures (Figure 5.1.6) are predicted to decrease over most of the reservoir by more than 6.0 degrees Celsius in April with extremely likely statistical significance (Figure 5.1.7). Decreases of up to 5.0 degrees Celsius in July are extremely likely statistically significant. For October, the spatial patterns are similar, but areas with 5.0 degrees Celsius decreases are smaller. These decreases, however, appear unlikely or very unlikely statistically significant. No changes exceeding 1.0 degrees Celsius are predicted anywhere in the Technical Study Area in January. Southwest of Hudson‘s Hope, small changes appear statistically significant while in the remaining areas near the proposed reservoir, changes are unlikely statistically significant.

Daily minimum temperatures (Figure 5.1.8) are predicted to increase by more than 6.0 degrees Celsius over most of the proposed reservoir in October. These increases are likely or very likely statistically significant (Figure 5.1.9). More moderate increases of up to 4.0 degrees Celsius over some parts of the reservoir are predicted for April and July. It is extremely likely that these results are statistically significant in July along most of the reservoir (Figure 5.1.9). However, near Hudson‘s Hope, the predicted changes are unlikely statistically significant. In April, the predicted changes are unlikely statistically significant along most of the reservoir. Only southwest of station 7 and northwest of station 3, the changes are likely to extremely likely statistically significant. In January, increases of more than 6.0 degrees Celsius are predicted adjacent the reservoir mostly south of Hudson‘s Hope and decreases of up to 4.0 degrees Celsius are predicted for the remaining area along the reservoir. Figure 5.1.9 shows that only the changes over land south of Hudson‘s Hope are very likely and extremely likely statistically significant, while the changes in the remaining areas along the reservoir are unlikely statistically significant.

Overall, these results are in line with the general consideration at the beginning of this section for impounding a reservoir of these dimensions. With a typical width of approximately one kilometre, the reservoir can only exert influence on microclimate right over the reservoir and within a horizontal distance of similar scale from the reservoir via local convective patterns and near-surface downwind transport of water-surface characteristics. With respect to temperatures, the main changes predicted are a lower daily temperature range and substantially warmer temperatures when air temperatures drop below 0 degrees Celsius before the water surface freezes over.

Extreme minimum and maximum air temperatures shown in Table 5.1.4 and Table 5.1.5 are the lowest and highest hourly air temperatures in each season, respectively. The extreme minimum air temperatures are shown to increase in spring and summer and mainly decrease in fall and

winter. Overall, the largest increase to the extreme minimum air temperature is predicted to occur in summer at the Proposed Site C Dam (5.4 degrees Celsius) and the largest decrease is predicted to occur in the winter at Bear Flat (-3.9 degrees Celsius). Overall, the change in the annual extreme minimum air temperature is less than the change predicted in the warm season given that the annual extreme minimum is controlled by the cold season where less change is predicted.

Table 5.1.4 Seasonal change in extreme minimum temperature

Difference (Future Case with the Project – Baseline Case)	Spring	Summer	Fall	Winter	Year
Fort St. John Airport	0.0	0.3	0.0	0.1	0.1
Station 1 - Attachie Flat Upper Terrace	2.2	3.3	-1.9	-2.1	-2.1
Station 2 - Attachie Flat Lower Terrace	2.8	3.3	-2.5	-2.3	-2.3
Station 3 - Attachie Flat Plateau	0.0	0.7	0.0	0.3	0.3
Station 4 - Bear Flat	2.8	4.4	-2.6	-3.9	-3.9
Station 5 - Hudson's Hope	0.3	0.5	0.4	0.8	0.8
Station 6 - Farrell Creek	0.0	0.7	0.1	1.6	1.6
Station 7 - Site C Dam	2.8	5.4	-0.9	-1.7	-1.7

NOTES:
All values in degrees Celsius.
[e] Fort St. John Airport station observations.

Table 5.1.5 Seasonal change in extreme maximum temperature

Difference (Future Case with the Project – Baseline Case)	Spring	Summer	Fall	Winter	Year
Fort St. John Airport	0.0	-0.1	-0.1	0.0	0.0
Station 1 - Attachie Flat Upper Terrace	-5.9	-4.8	-3.8	0.3	-5.9
Station 2 - Attachie Flat Lower Terrace	-6.0	-5.2	-3.9	0.0	-6.0
Station 3 - Attachie Flat Plateau	-0.8	-0.6	-0.2	0.1	-0.8
Station 4 - Bear Flat	-5.7	-4.5	-3.9	0.4	-5.7
Station 5 - Hudson's Hope	-1.3	-1.4	-0.2	-0.1	-1.3
Station 6 - Farrell Creek	-1.0	-1.3	-0.2	0.0	-1.0
Station 7 - Site C Dam	-4.9	-4.5	-3.9	0.7	-4.9

NOTES:
All values in degrees Celsius.
[e] Fort St. John Airport station observations.

The extreme maximum air temperatures are shown to mainly decrease with the greatest change predicted to occur in spring and summer. The greatest change during the spring and summer is predicted to occur at Attachie Flat Lower Terrace (-6.0 degrees Celsius and -5.2 degrees Celsius, respectively.). Little to no change is predicted at Fort St. John Airport, and Attachie Flat Plateau.

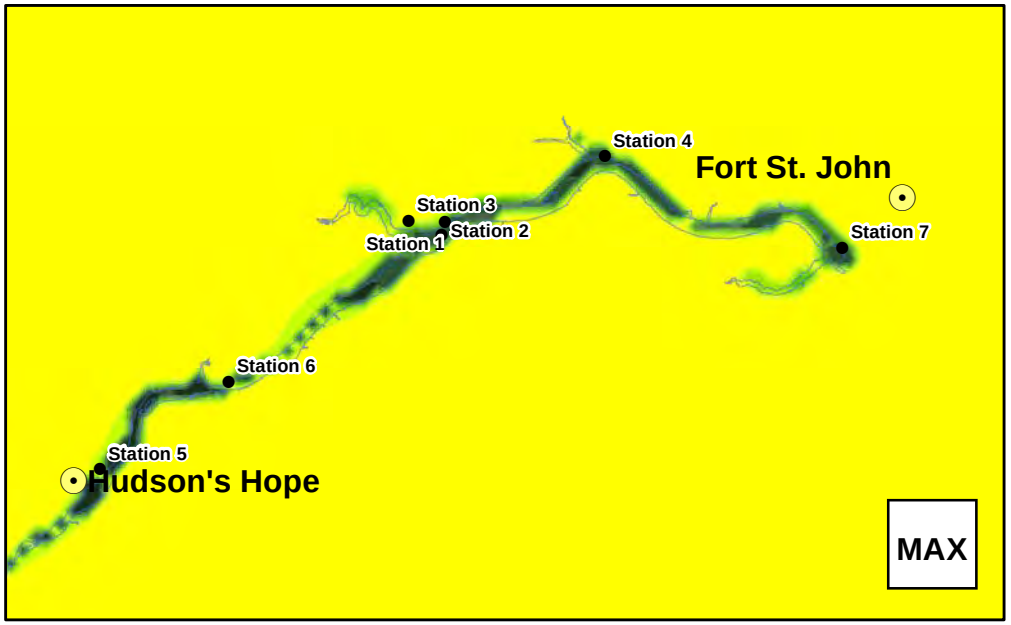

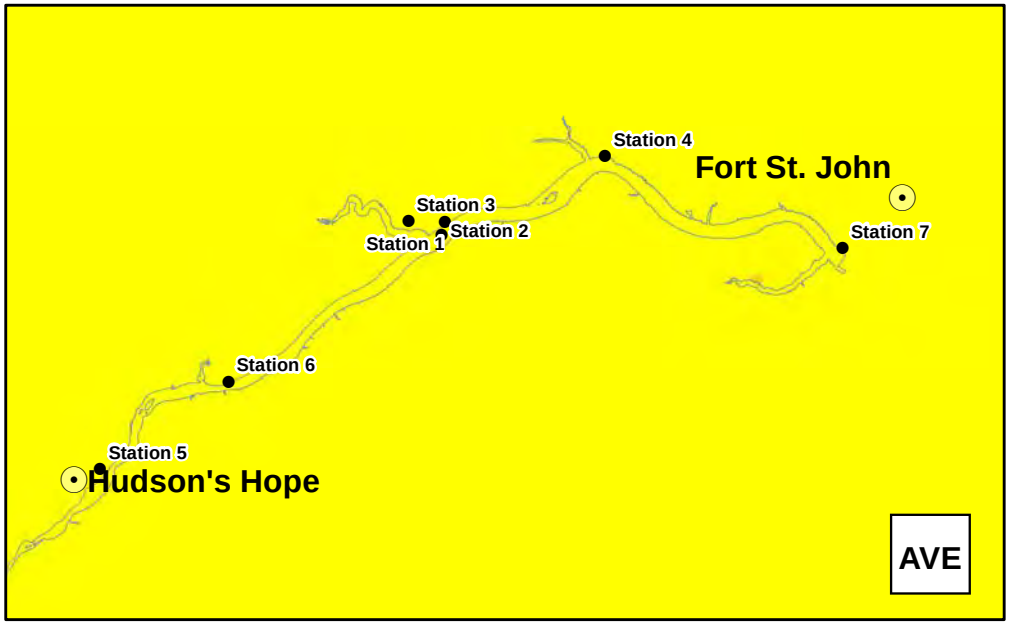

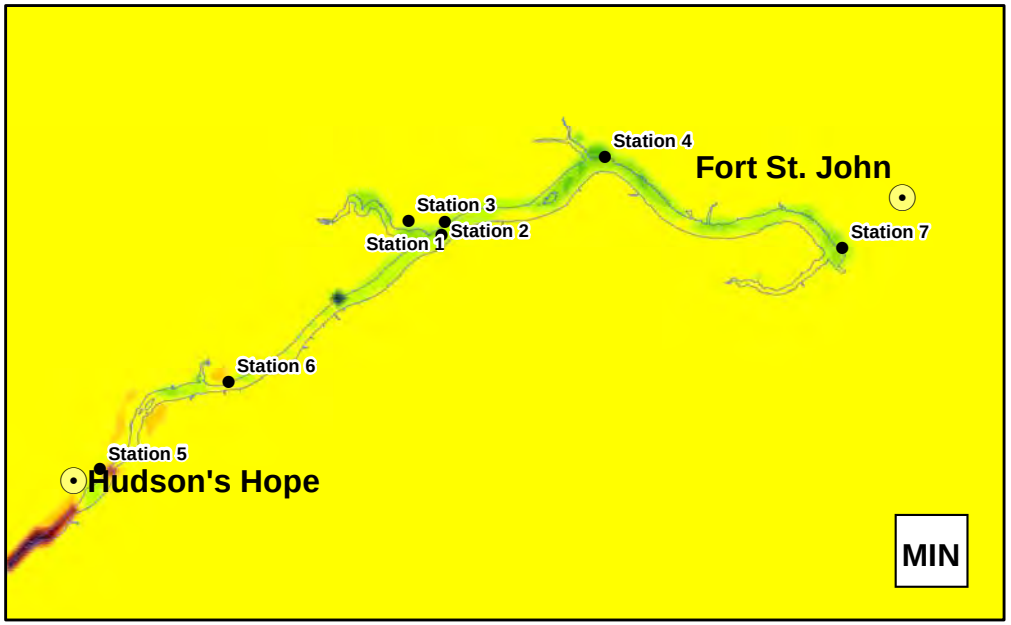

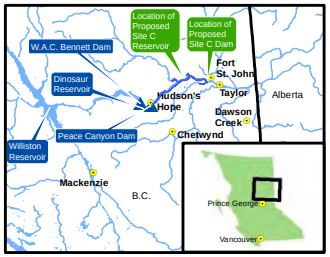

Weather Research and Forecasting (WRF) model-predicted changes in annual averages of daily average (Ave), maximum (Max), and minimum (Min) temperatures after formation of the reservoir as labelled.

Legend

- BC Hydro - Site C Stations
- City / District Municipality
- Proposed Reservoir

Temperature Change (in °C)

> 6
5 to 6
4 to 5
3 to 4
2 to 3
1 to 2
-1 to 1
-2 to -1
-3 to -2
-4 to -3
-5 to -4
-6 to -5
< -6

N

1:600,000

0 20 km

Map Notes:
1. Datum/Projection: NAD83/UTM Zone 10N
2. Proposed Reservoir Area (461.8 m maximum normal elevation) from Digital Elevation Models (DEM) generated from LiDAR data acquired July/August 2006.

SITE C CLEAN ENERGY PROJECT

RWDI BC hydro

Figure 5.1.1
Predicted changes in temperatures - annual

DATE	Dec. 3, 2012	1016-C14-A5503	R 0

© BC Hydro 2012 - all rights reserved. This map is for information purposes only and accuracy is not guaranteed.

Construction of the Site C Clean Energy Project is subject to required regulatory approvals including environmental certification

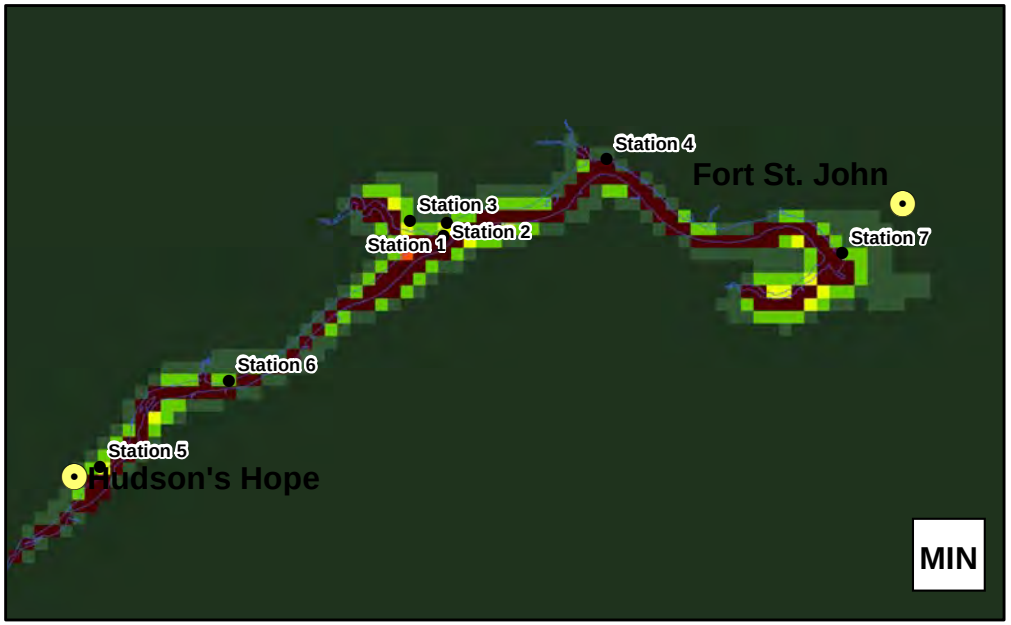

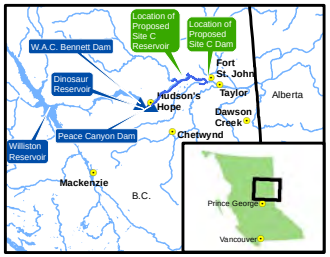

Likelihoods of statistically significant changes in annual averages of daily average (Ave), maximum (Max), and minimum (Min) temperatures after formation of the reservoir as labelled. Likelihoods are based on a Bayesian probability calculation, and the terminology follows the definition in IPCC WG (2007).

Legend

- BC Hydro - Site C Stations
- City / District Municipality
- Proposed Reservoir

Likelihood of Change

- extremely likely
- very likely
- likely
- about as likely as not
- unlikely
- very unlikely
- extremely unlikely

N

1:600,000

0 20 km

Map Notes:
1. Datum/Projection: Customized Lambert Conformal Conic.
2. Proposed Reservoir Area (461.8 m maximum normal elevation) from Digital Elevation Models (DEM) generated from LiDAR data acquired July/August 2006.

SITE C CLEAN ENERGY PROJECT

RWDI BC hydro

Figure 5.1.2
Likelihoods of statistically significant changes in temperatures - annual

DATE	Dec. 3, 2012	1016-C14-A5504	R 0

© BC Hydro 2012 - all rights reserved. This map is for information purposes only and accuracy is not guaranteed.

Construction of the Site C Clean Energy Project is subject to required regulatory approvals including environmental certification

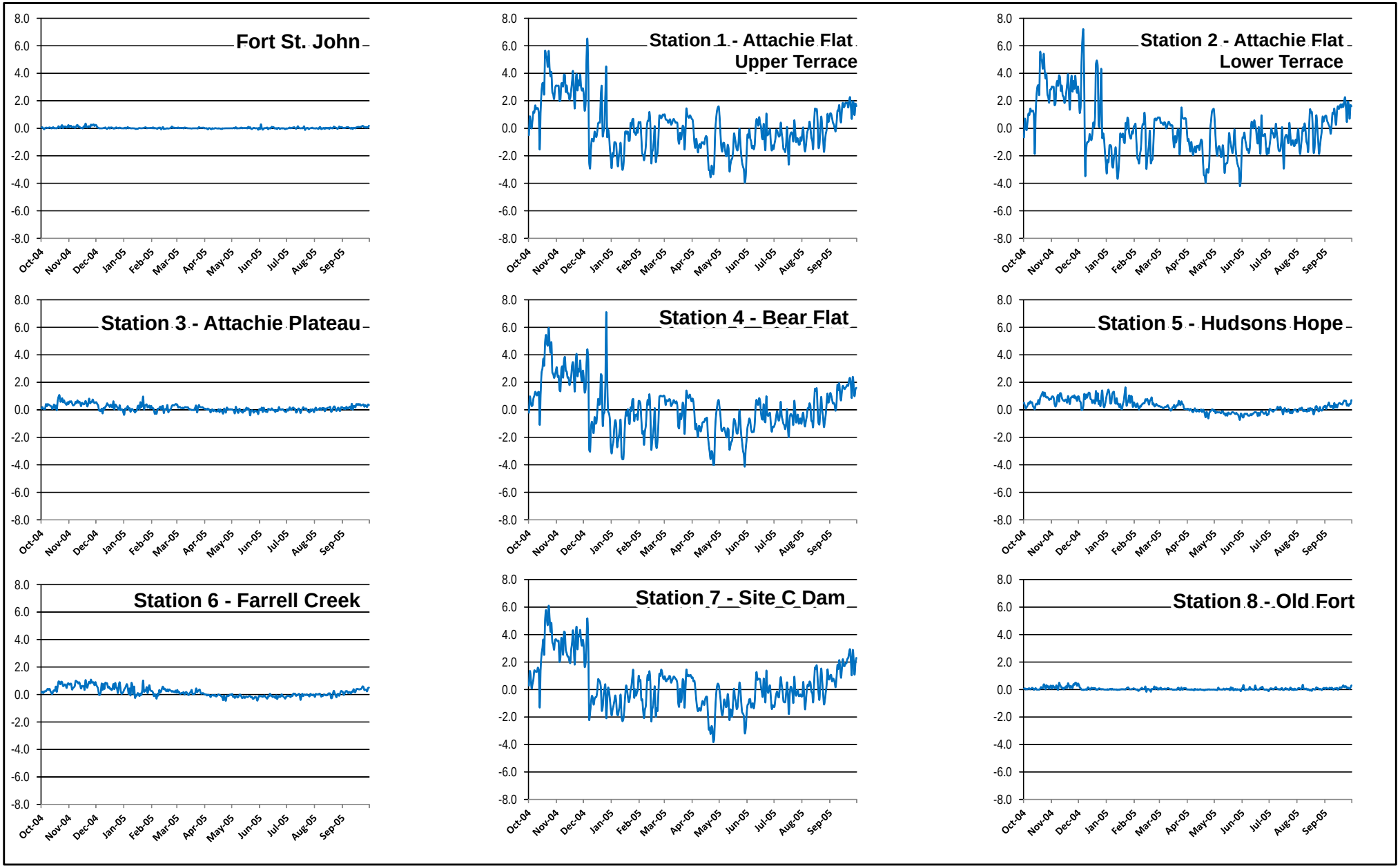

Predicted difference in daily average temperature (degrees Celsius) content at each location from October 2004 to September 2005 (Future Case with Project minus Baseline Case)

SITE C CLEAN ENERGY PROJECT

RWDI BC hydro

Figure 5.1.3
Change in daily average temperature

DATE	Dec. 3, 2012		R 0

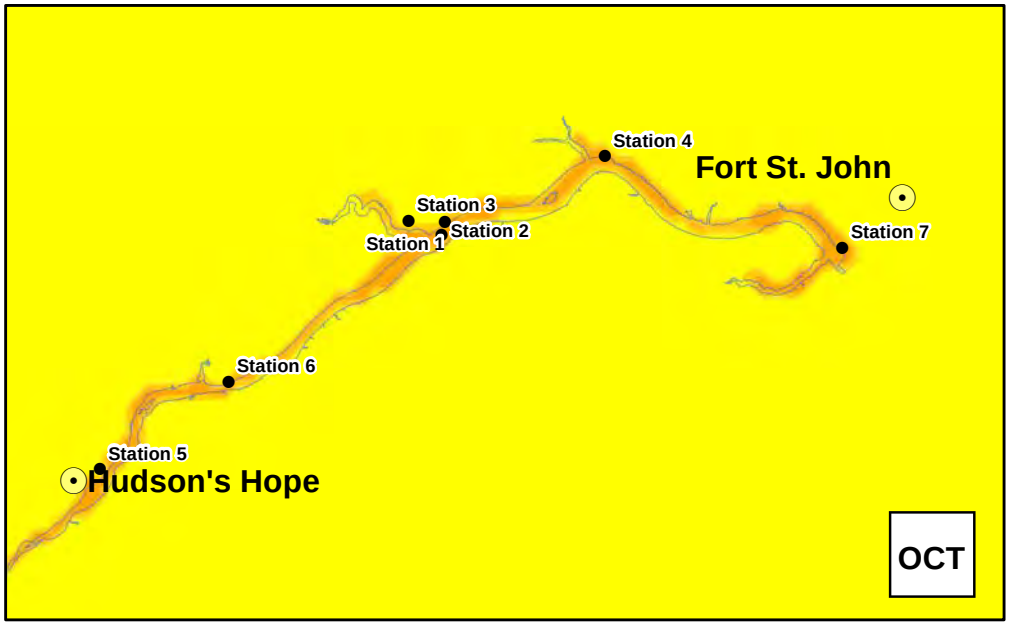

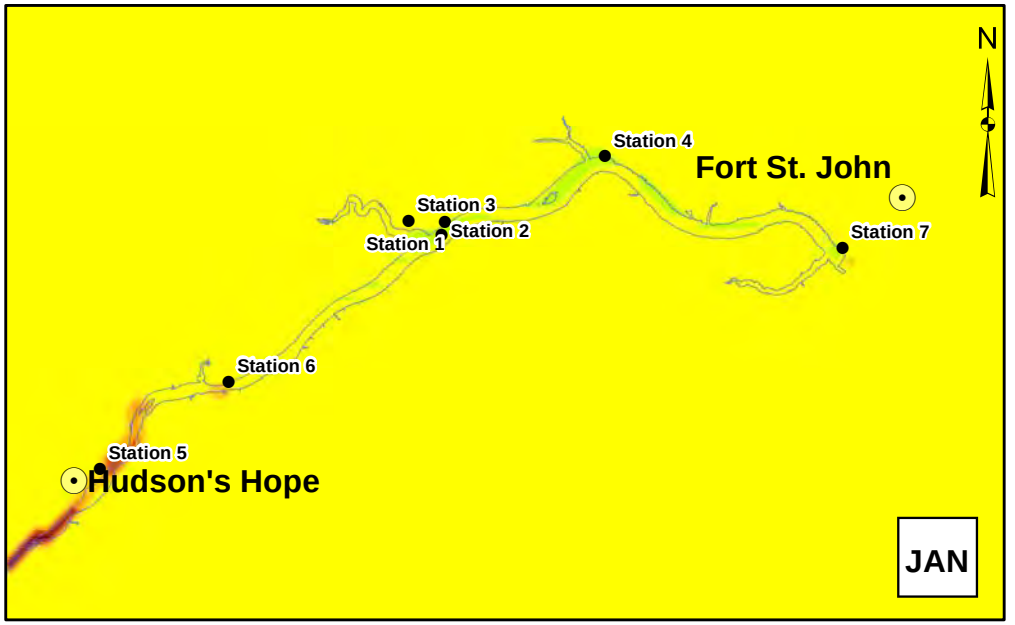

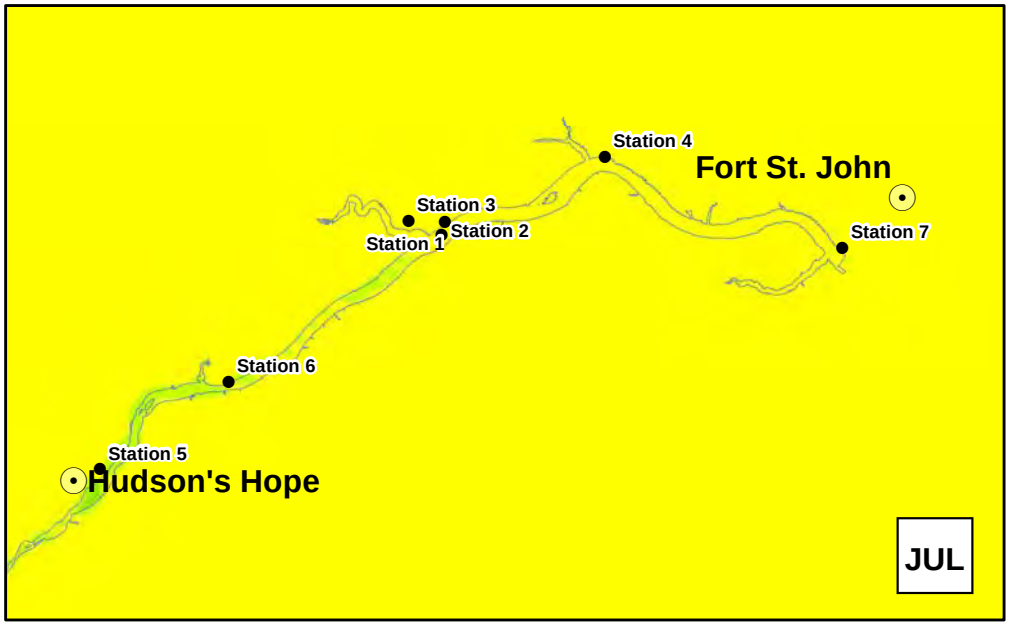

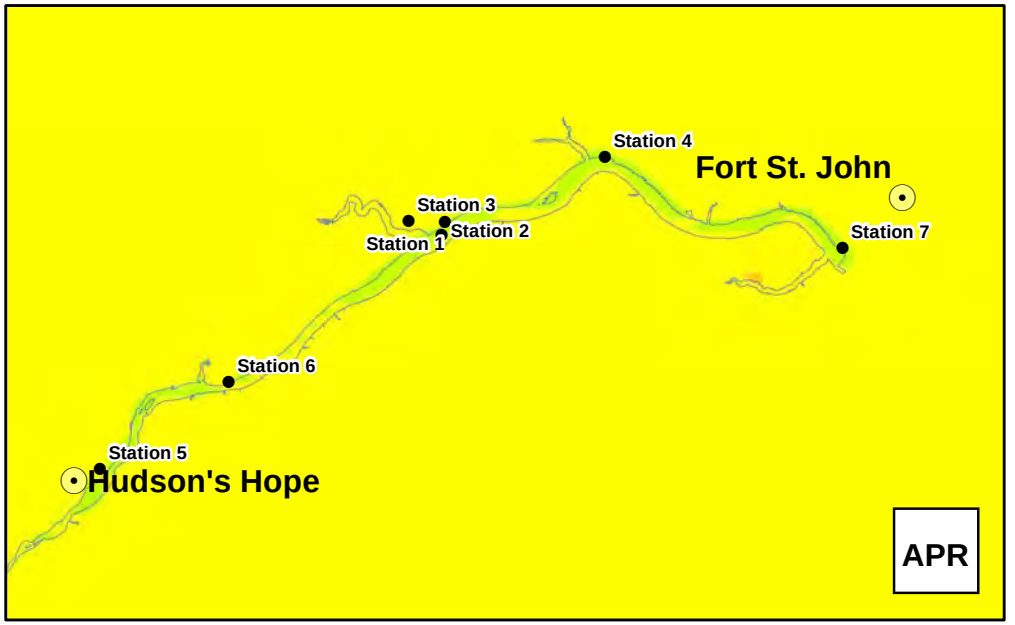

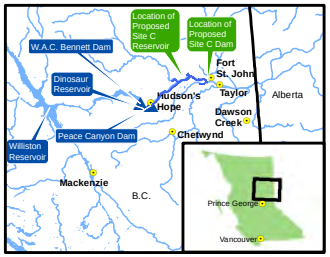

Weather Research and Forecasting (WRF) model-predicted changes in monthly averages of daily mean temperatures after formation of the reservoir (positive are increases) for four calendar months as labelled clockwise from top left: October, January, April, and July.

Map Notes:
1. Datum/Projection: NAD83/UTM Zone 10N
2. Proposed Reservoir Area (461.8 m maximum normal elevation) from Digital Elevation Models (DEM) generated from LiDAR data acquired July/August 2006.

Legend

- BC Hydro - Site C Stations
- City/District Municipality
- Proposed Reservoir

Temperature Change (in °C)

> 6
5 to 6
4 to 5
3 to 4
2 to 3
1 to 2
-1 to 1
-2 to -1
-3 to -2
-4 to -3
-5 to -4
-6 to -5
< -6

1:600,000

0 20 km

SITE C CLEAN ENERGY PROJECT

RWDI BC hydro

Figure 5.1.4
Predicted changes in mean temperatures - monthly

DATE	Dec. 3, 2012	1016-C14-A5505	R 0

© BC Hydro 2012 - all rights reserved. This map is for information purposes only and accuracy is not guaranteed.

Construction of the Site C Clean Energy Project is subject to required regulatory approvals including environmental certification

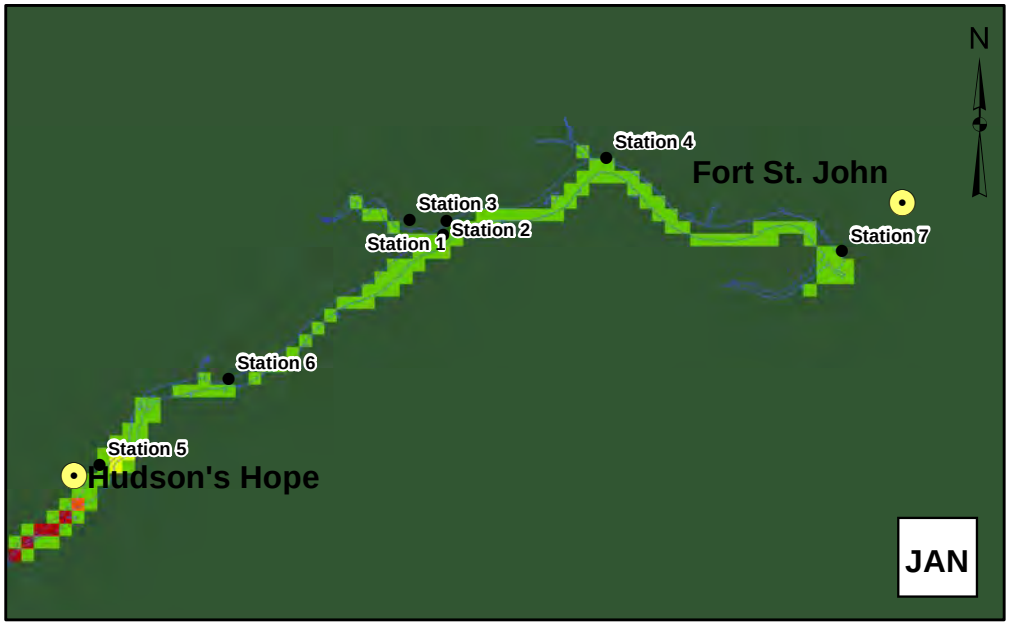

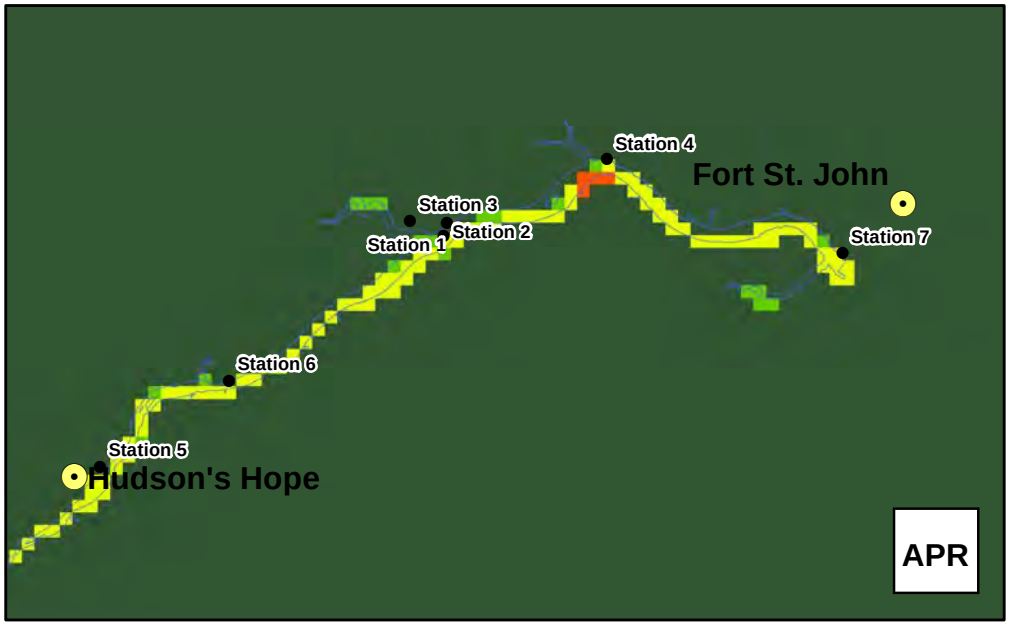

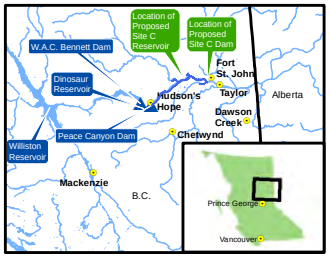

Likelihoods of statistically significant changes in daily mean temperatures after formation of the reservoir for four calendar months as labelled clockwise from top left: October, January, April, and July. Likelihoods are based on a Bayesian probability calculation, and the terminology follows the definition in IPCC WG (2007).

Map Notes:
1. Datum/Projection: Customized Lambert Conformal Conic.
2. Proposed Reservoir Area (461.8 m maximum normal elevation) from Digital Elevation Models (DEM) generated from LiDAR data acquired July/August 2006.

Legend

- BC Hydro - Site C Stations
- City / District Municipality
- Proposed Reservoir

Likelihood of Change

- extremely likely
- very likely
- likely
- about as likely as not
- unlikely
- very unlikely
- extremely unlikely

1:600,000

0 20 km

SITE C CLEAN ENERGY PROJECT

RWDI BC hydro

Figure 5.1.5
Likelihoods of statistically significant changes in mean temperatures - monthly

DATE	Dec. 3, 2012	1016-C14-A5506	R 0

© BC Hydro 2012 - all rights reserved. This map is for information purposes only and accuracy is not guaranteed.

Construction of the Site C Clean Energy Project is subject to required regulatory approvals including environmental certification

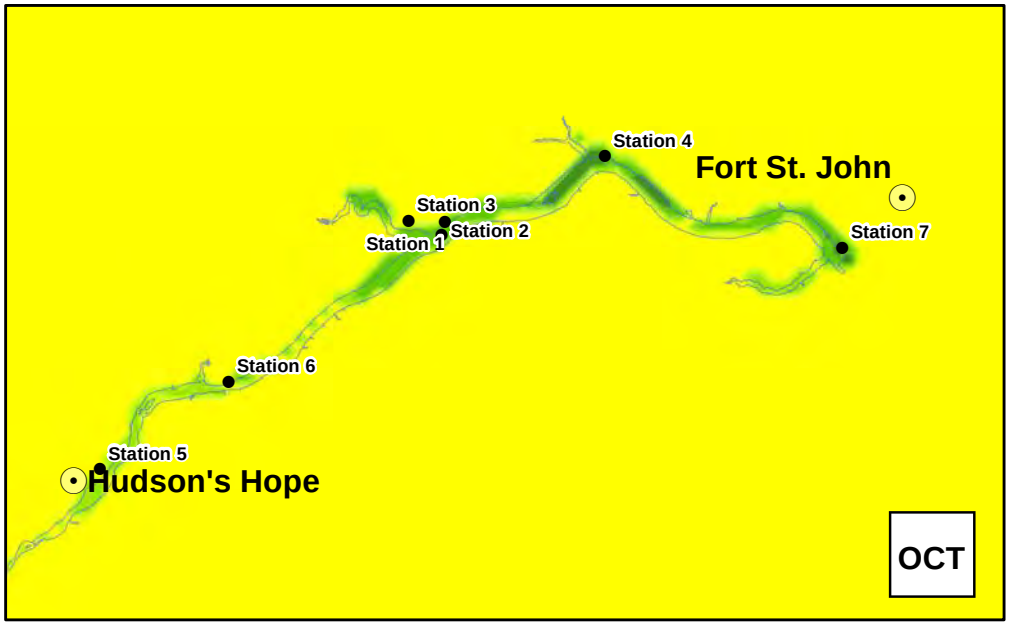

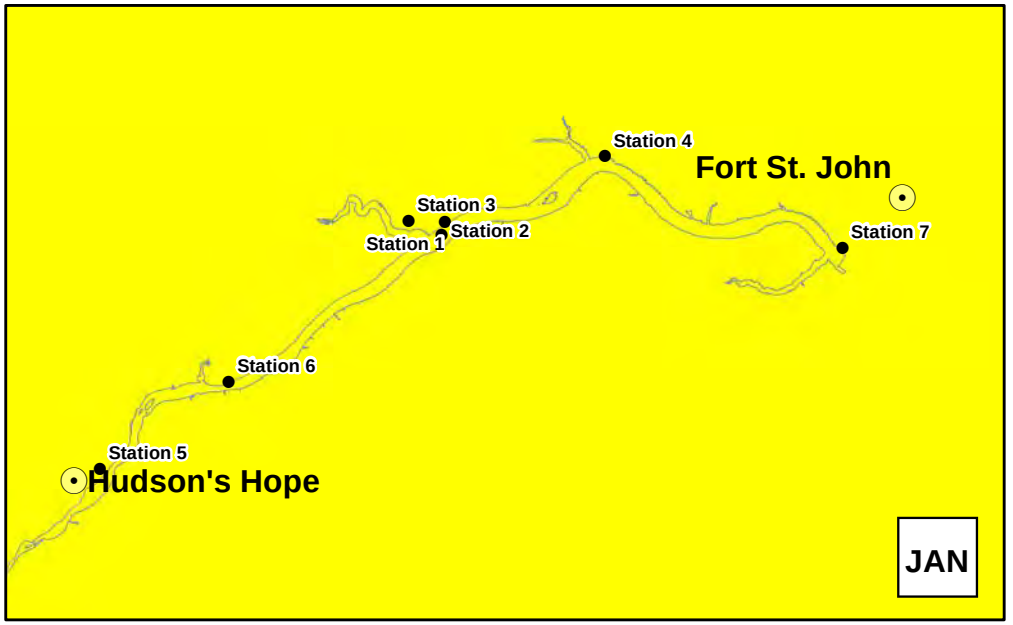

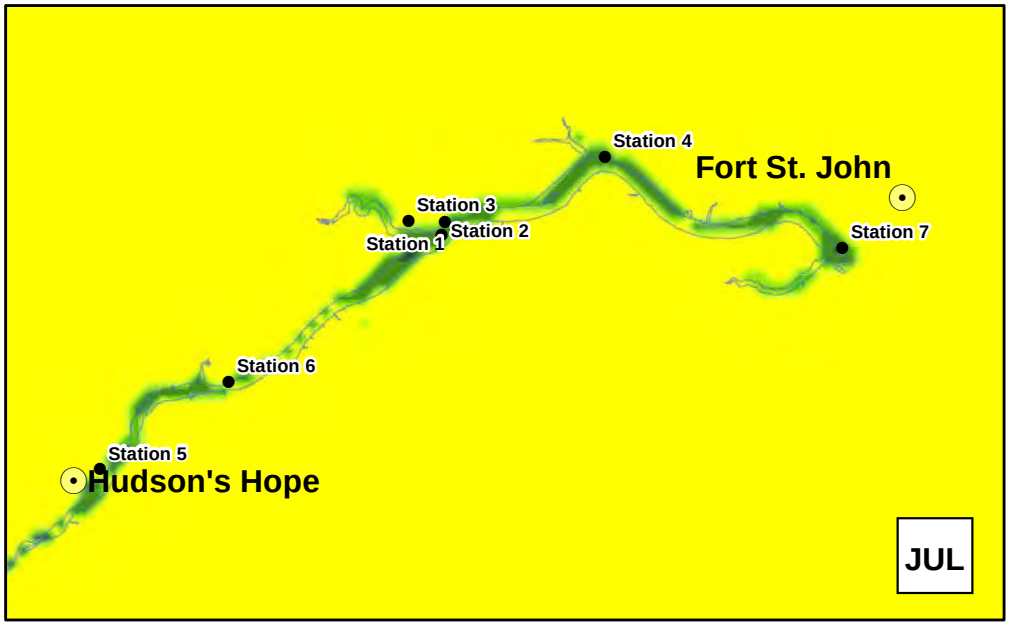

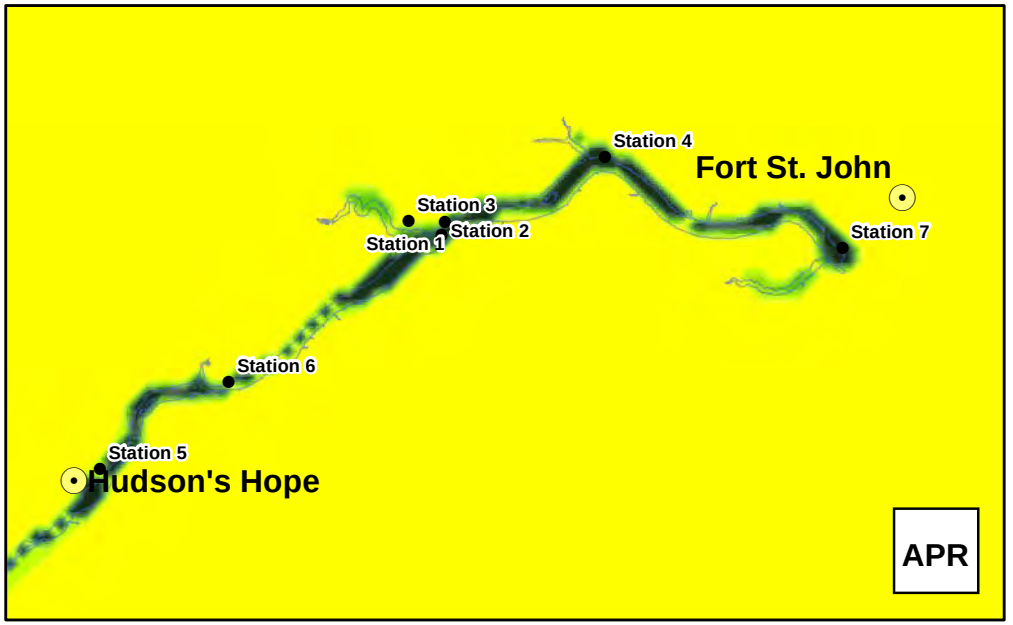

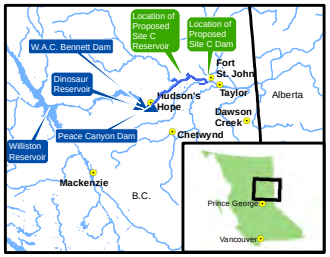

Weather Research and Forecasting (WRF) model-predicted changes in monthly averages of daily maximum temperatures after formation of the reservoir (positive are increases) for four calendar months as labelled clockwise from top left: October, January, April, and July.

Map Notes:
1. Datum/Projection: NAD83/UTM Zone 10N
2. Proposed Reservoir Area (461.8 m maximum normal elevation) from Digital Elevation Models (DEM) generated from LiDAR data acquired July/August 2006.

Legend

- BC Hydro - Site C Stations
- City / District Municipality
- Proposed Reservoir

Temperature Change (in °C)

> 6
5 to 6
4 to 5
3 to 4
2 to 3
1 to 2
-1 to 1
-2 to -1
-3 to -2
-4 to -3
-5 to -4
-6 to -5
< -6

N

1:600,000

0 20 km

SITE C CLEAN ENERGY PROJECT

RWDI BC hydro

Figure 5.1.6
Predicted changes in maximum temperatures - monthly

DATE	Dec. 3, 2012	1016-C14-A5507	R 0

© BC Hydro 2012 - all rights reserved. This map is for information purposes only and accuracy is not guaranteed.

Construction of the Site C Clean Energy Project is subject to required regulatory approvals including environmental certification

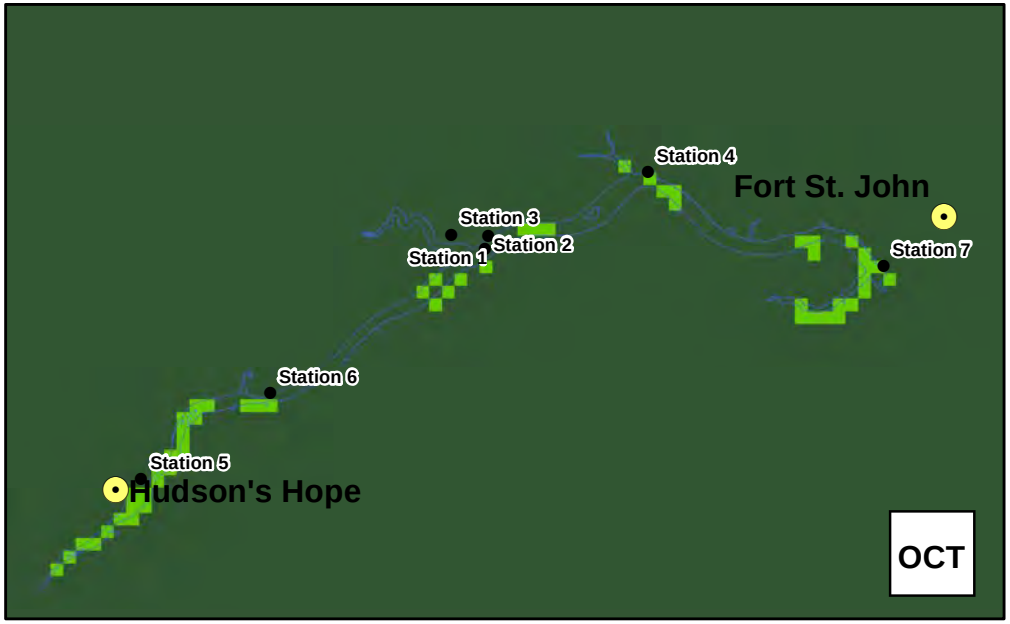

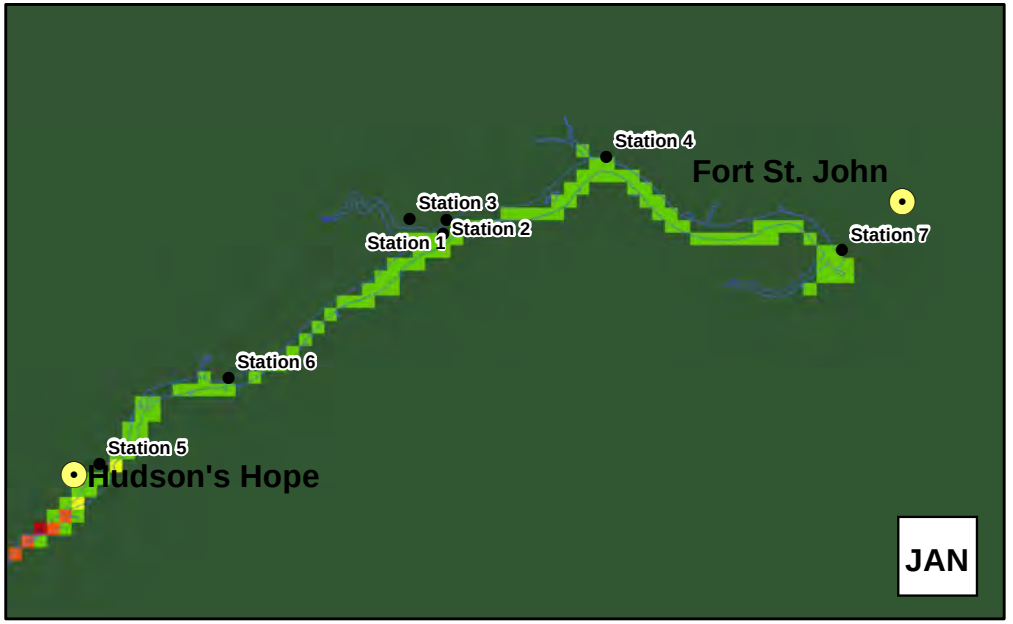

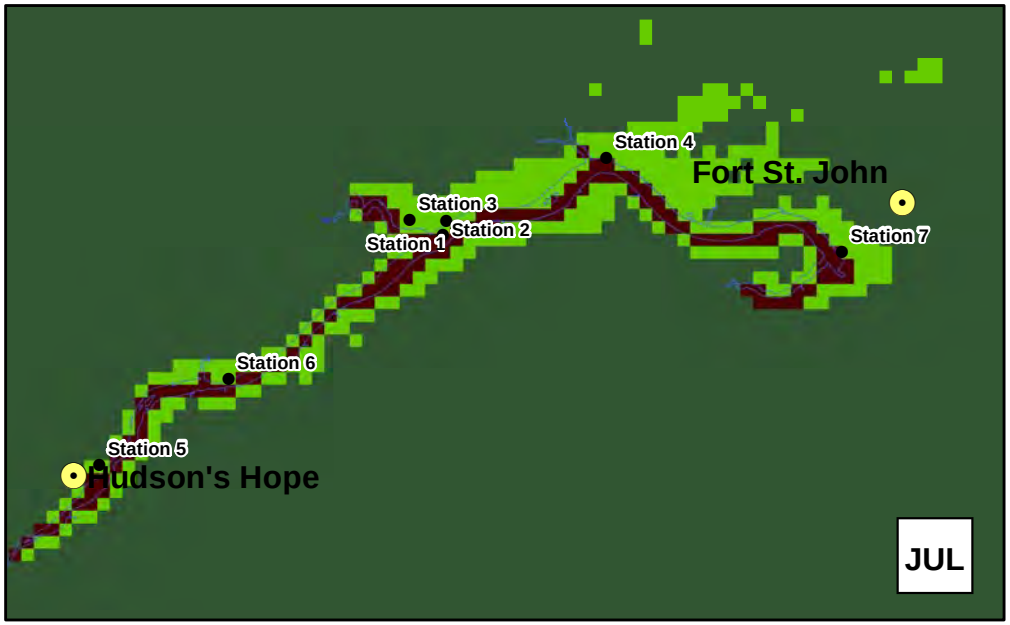

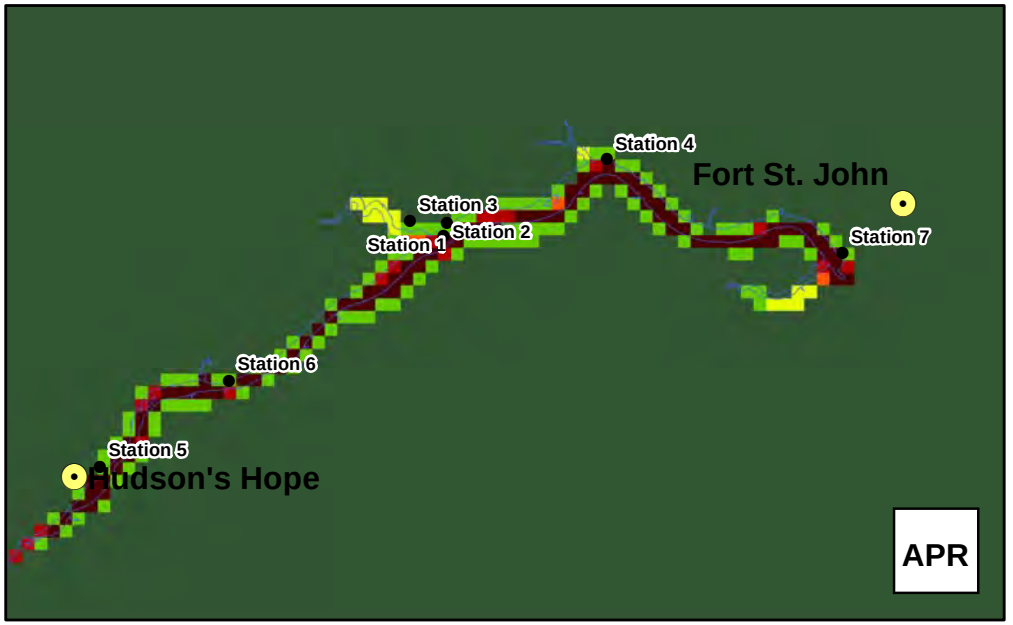

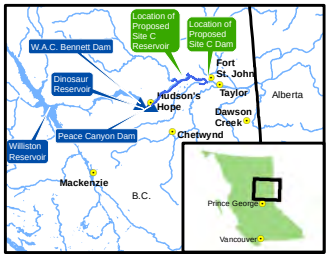

Likelihoods of statistically significant changes in daily maximum temperatures after formation of the reservoir for four calendar months as labelled clockwise from top left: October, January, April, and July. Likelihoods are based on a Bayesian probability calculation, and the terminology follows the definition in IPCC WG (2007).

Map Notes:
1. Datum/Projection: Customized Lambert Conformal Conic.
2. Proposed Reservoir Area (461.8 m maximum normal elevation) from Digital Elevation Models (DEM) generated from LiDAR data acquired July/August 2006.

Legend

- BC Hydro - Site C Stations
- City / District Municipality
- Proposed Reservoir

Likelihood of Change

- extremely likely
- very likely
- likely
- about as likely as not
- unlikely
- very unlikely
- extremely unlikely

N

1:600,000

0 20 km

SITE C CLEAN ENERGY PROJECT

RWDI BC hydro

Figure 5.1.7
Likelihoods of statistically significant changes in maximum temperatures - monthly

DATE	Dec. 3, 2012	1016-C14-A5508	R 0

© BC Hydro 2012 - all rights reserved. This map is for information purposes only and accuracy is not guaranteed.

Construction of the Site C Clean Energy Project is subject to required regulatory approvals including environmental certification

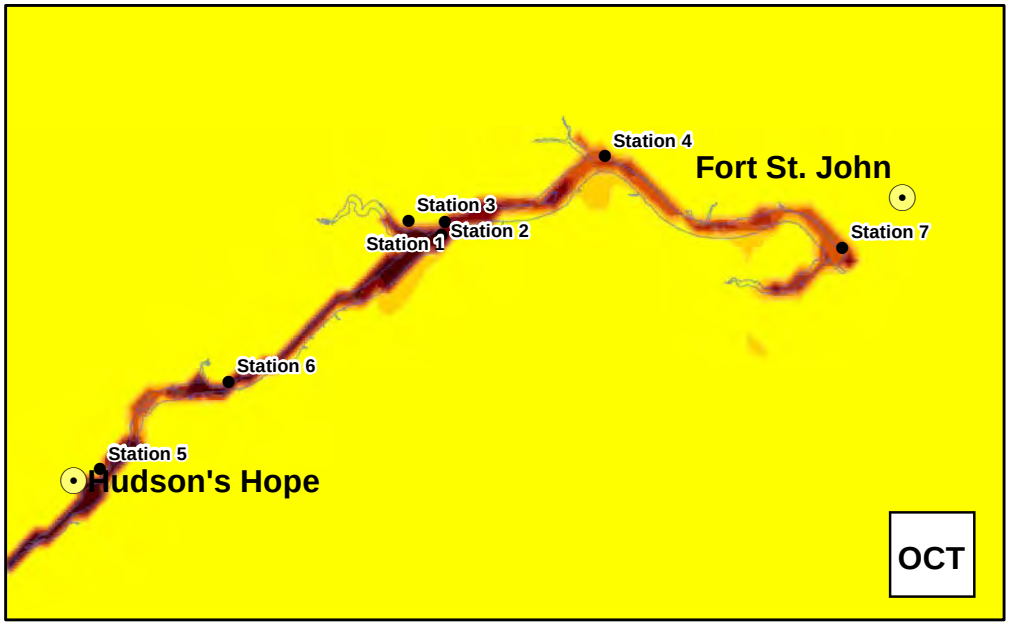

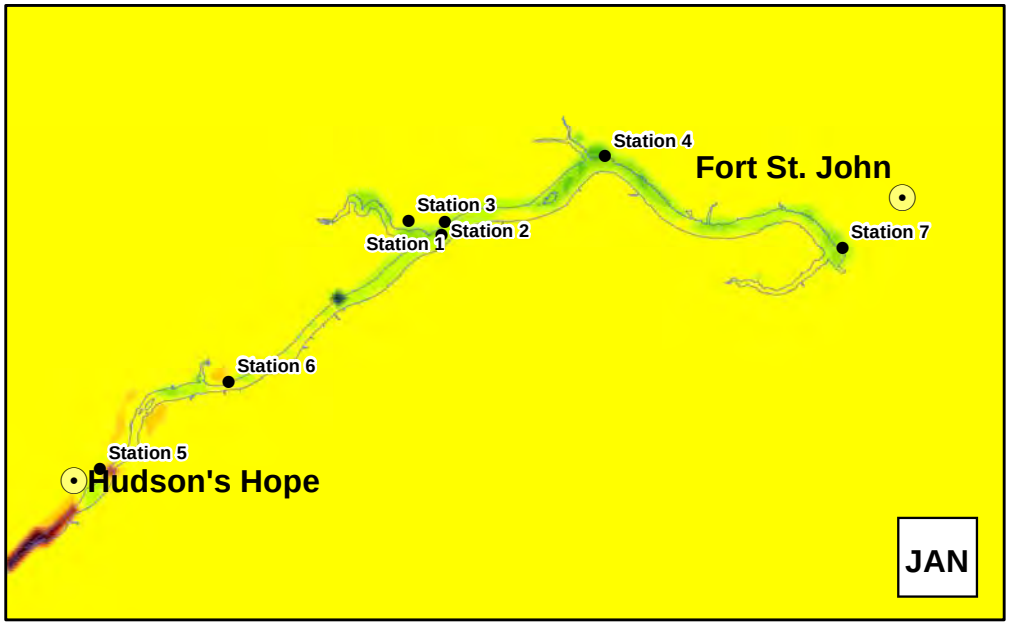

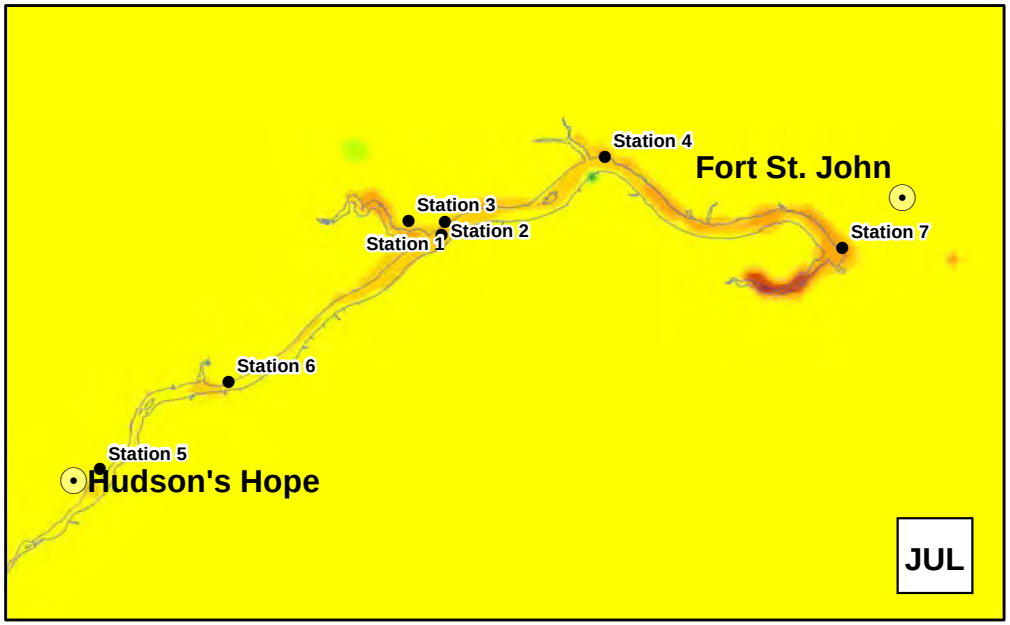

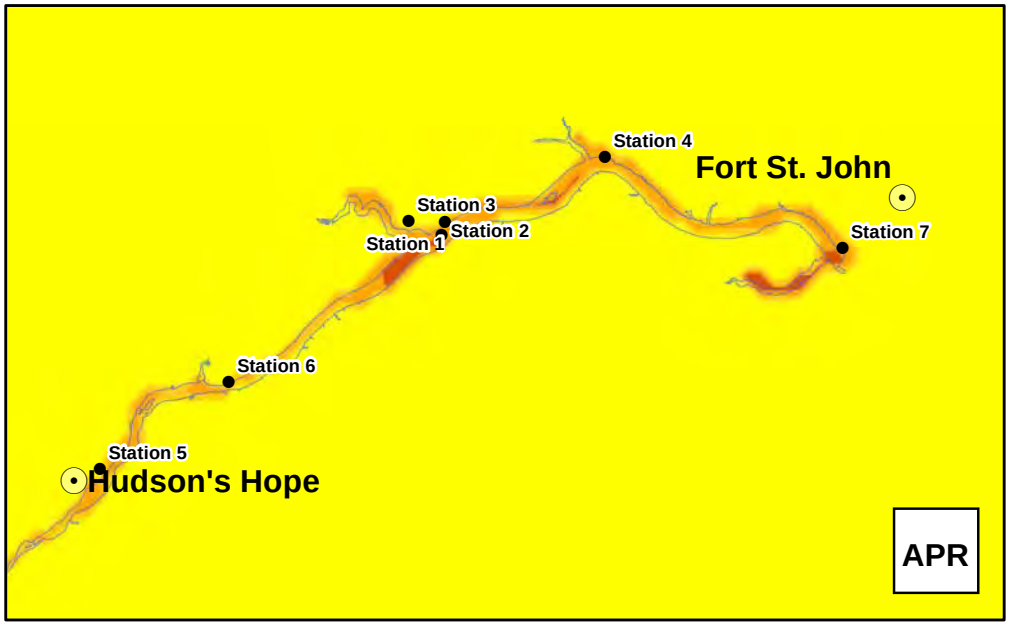

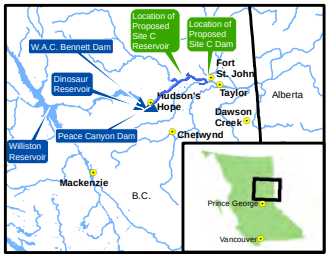

Weather Research and Forecasting (WRF)model-predicted changes in monthly averages of daily minimum temperatures after formation of the reservoir (positive are increases) for four calendar months as labelled clockwise from top left: October, January, April, and July.

Map Notes:
1. Datum/Projection: NAD83/UTM Zone 10N
2. Proposed Reservoir Area (461.8 m maximum normal elevation) from Digital Elevation Models (DEM) generated from LiDAR data acquired July/August 2006.

© BC Hydro 2012 - all rights reserved. This map is for information purposes only and accuracy is not guaranteed.

Legend

- BC Hydro - Site C Stations
- City / District Municipality
- Proposed Reservoir

Temperature Change (in °C)

- > 6
- 5 to 6
- 4 to 5
- 3 to 4
- 2 to 3
- 1 to 2
- -1 to 1
- -2 to -1
- -3 to -2
- -4 to -3
- -5 to -4
- -6 to -5
- < -6

N

1:600,000

0 20 km

SITE C CLEAN ENERGY PROJECT

RWDI BC hydro

Figure 5.1.8
Predicted changes in minimum temperatures - monthly

DATE	Dec. 3, 2012	1016-C14-A5509	R 0

Construction of the Site C Clean Energy Project is subject to required regulatory approvals including environmental certification

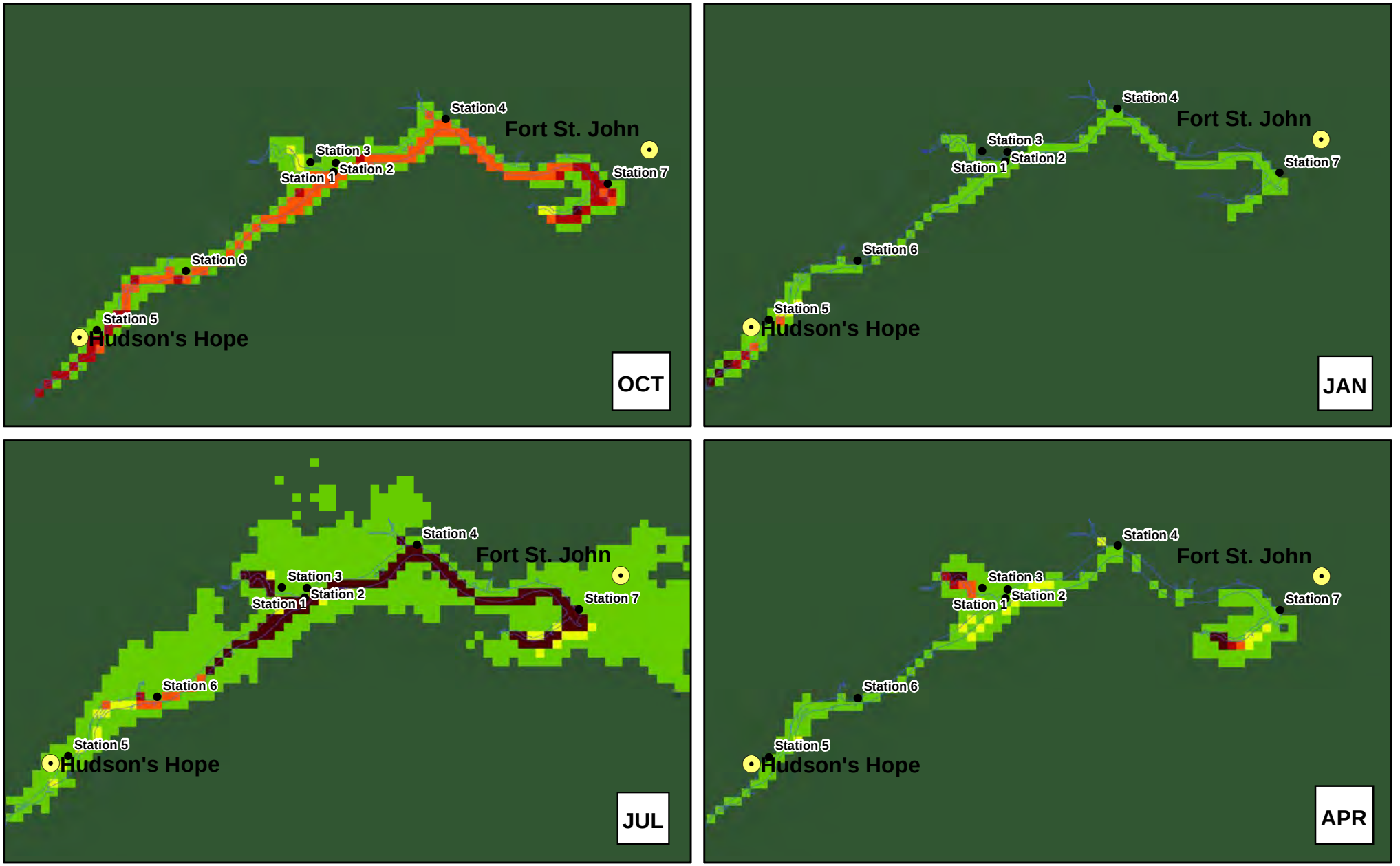

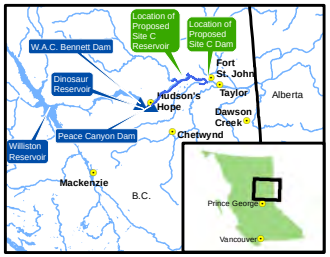

Likelihoods of statistically significant changes in daily minimum temperatures after formation of the reservoir for four calendar months as labelled clockwise from top left: October, January, April, and July. Likelihoods are based on a Bayesian probability calculation, and the terminology follows the definition in IPCC WG (2007).

Legend

- BC Hydro - Site C Stations
- City / District Municipality
- Proposed Reservoir

Likelihood of Change

- extremely likely
- very likely
- likely
- about as likely as not
- unlikely
- very unlikely
- extremely unlikely

N

1:600,000

0 20 km

Map Notes:
1. Datum/Projection: Customized Lambert Conformal Conic.
2. Proposed Reservoir Area (461.8 m maximum normal elevation) from Digital Elevation Models (DEM) generated from LiDAR data acquired July/August 2006.

SITE C CLEAN ENERGY PROJECT

RWDI BC hydro

Figure 5.1.9
Likelihoods of statistically significant changes in minimum temperatures - monthly

DATE	Dec. 3, 2012	1016-C14-A5510	R 0

© BC Hydro 2012 - all rights reserved. This map is for information purposes only and accuracy is not guaranteed.

Construction of the Site C Clean Energy Project is subject to required regulatory approvals including environmental certification

5.2 PRECIPITATION

As pointed out in Section 5.0, precipitation changes caused by the formation of the reservoir might reach further from the reservoir than temperature changes but are still expected to be limited to a downwind distance of a few kilometres.

The change in monthly precipitation was found not to be statistically significant at any of the climate stations or Fort St. John Airport. Table 5.2.1 shows the seasonal change in total precipitation at each location. Overall, little to no change is predicted to occur in the fall and winter. This is expected as precipitation patterns are dominated by synoptic conditions during the cold season and less by local terrain or surface characteristics. In the warm season, precipitation is predicted to decrease at most of the locations, however confidence in these results is reduced since the WRF model is known to have less skill in predicting precipitation in the warm season, as discussed in Section 6.2.

Farrell Creek appears to change the most with a decrease in total annual precipitation of 18 millimetres. Attachie Flat Upper Terrace, Attachie Flat Lower Terrace, and the Proposed Site C Dam site are predicted to have a decrease of greater than ten millimetres of total annual precipitation. All other locations are predicted to have a change less than ten millimetres of total precipitation on an annual basis. As shown in Table 3.2.1, measured precipitation at the stations locations ranges from around 400 to 600 millimetres per year.

Table 5.2.1 Seasonal change in total precipitation

Difference (Future Case with the Project – Baseline Case)	Spring	Summer	Fall	Winter	Year
Fort St. John Airport	2.7	-10.5	-0.2	0.3	-7.7
Station 1 - Attachie Flat Upper Terrace	-12.2	-0.1	-2.8	-0.5	-15.6
Station 2 - Attachie Flat Lower Terrace	-3.6	-2.2	-3.2	-2.6	-11.6
Station 3 - Attachie Flat Plateau	-7.0	0.9	-1.4	2.4	-5.1
Station 4 - Bear Flat	-19.3	13.0	-1.8	2.0	-6.2
Station 5 - Hudson's Hope	1.4	3.3	-1.7	0.2	3.2
Station 6 - Farrell Creek	-10.4	-6.3	-1.1	-0.2	-18.0
Station 7 - Site C Dam	-5.0	-8.4	-0.4	2.5	-11.3

NOTES:
All values in millimetre water equivalent.
[e] Fort St. John Airport station observations.

A full spatial view over the entire Technical Study Area of the WRF-predicted changes in monthly total precipitation is shown in Figure 5.2.1 for October, January, April, and July. It is unlikely to extremely unlikely that the changes seen for all spatial precipitation figures in this section are statistically significant anywhere within the Technical Study Area. Therefore, no likelihood figures are shown. This does not imply that the changes are unlikely to happen but

that the predicted changes are statistically indistinguishable from the large inter annual and intra-annual variability of precipitation.

The apparently random pattern for July is indicative of the local convective character of precipitation in the Technical Study Area in the summer. April shows similar spatial patterns but much weaker changes. A different spatial pattern arises in October. Increased precipitation is predicted south and southeast of the proposed reservoir, which is downwind of cold northerly winds. This might suggest that these cold air masses pick up moisture over the reservoir which then preferentially precipitates a few kilometres downwind of the reservoir. Precipitation increases of more than 6 millimetres appear in localized areas over the reservoir in January.

To understand these patterns better, a breakdown of total precipitation into snow and all other forms of precipitation (mostly rain) is shown in Figure 5.2.2 and Figure 5.2.3. The spatial patterns of precipitation changes in April and July are entirely driven by rainfall, while those in October and January are entirely driven by snowfall. A large proportion of precipitation in October is rain, but changes are mostly associated with snowfall changes. That supports the hypothesis that the increased snowfall to the south and southeast of the proposed reservoir is a lake influenced process of northerly cold air picking up moisture over the water surface which then precipitates as snow downwind.

Total annual precipitation (Figure 5.2.4) emphasizes the spatial patterns discussed above. Total annual precipitation is dominated by the random convective rainfall patterns. Only snowfall shows a pattern of increases (of more than 30 millimetres in some areas) south and southeast of the proposed reservoir and a decrease of similar magnitude over the reservoir.

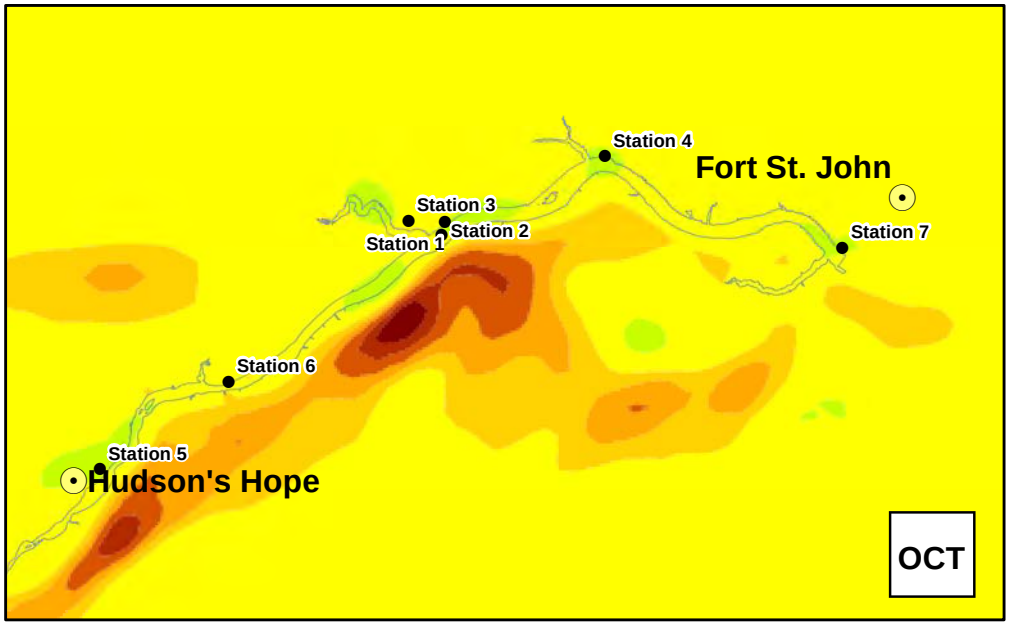

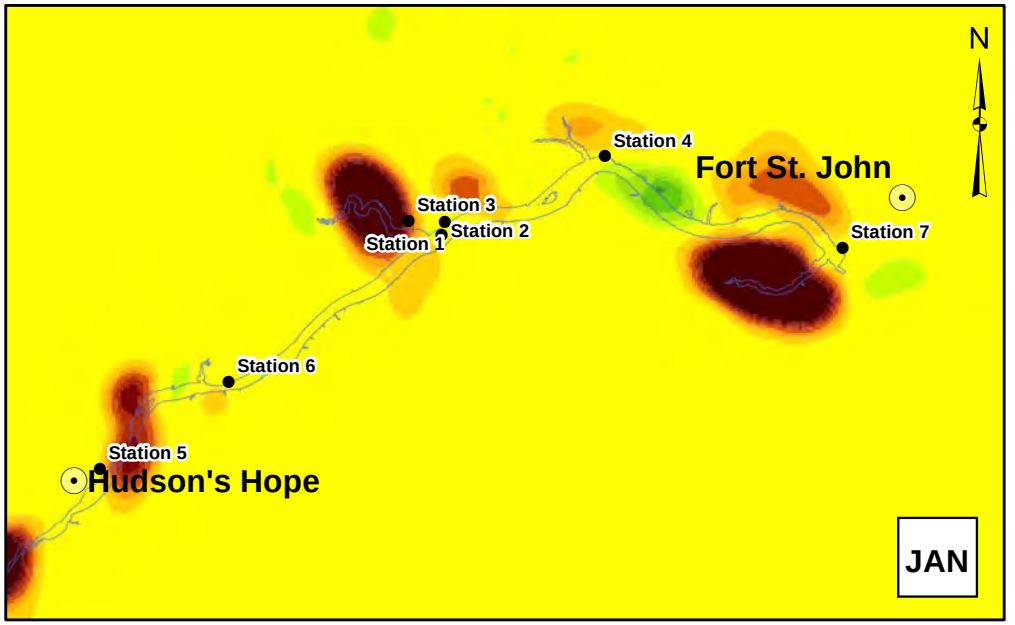

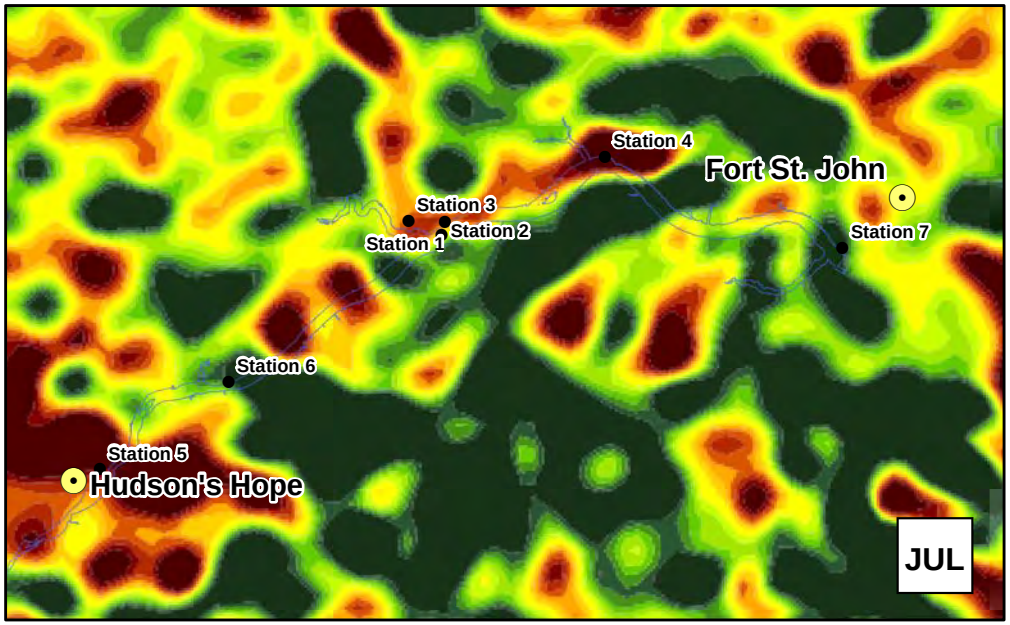

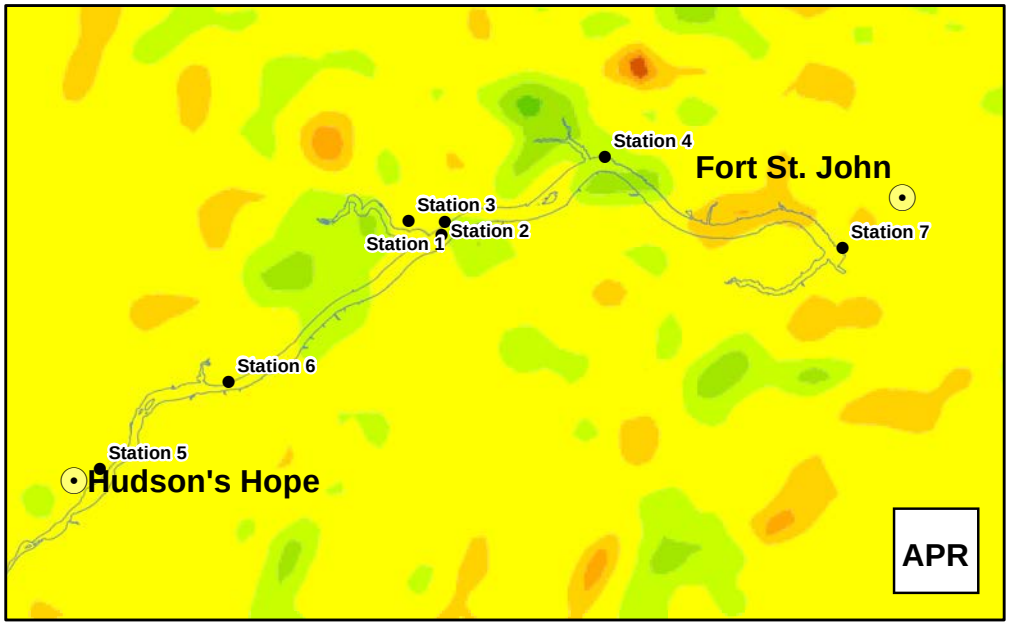

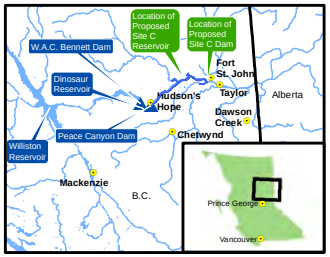

Weather Research and Forecasting (WRF) model-predicted changes in total monthly precipitation after formation of the reservoir (positive are increases) for four calendar months as labelled clockwise from top left: October, January, April, and July.

Legend

- BC Hydro - Site C Stations
- City / District Municipality
- Proposed Reservoir

Precipitation Change (in mm)

- > 6
- 5 to 6
- 4 to 5
- 3 to 4
- 2 to 3
- 1 to 2
- -1 to 1
- -2 to -1
- -3 to -2
- -4 to -3
- -5 to -4
- -6 to -5
- < -6

1:600,000

0 20 km

Map Notes:
1. Datum/Projection: NAD83/UTM Zone 10N
2. Proposed Reservoir Area (461.8 m maximum normal elevation) from Digital Elevation Models (DEM) generated from LiDAR data acquired July/August 2006.

SITE C CLEAN ENERGY PROJECT

RWDI BC hydro

Figure 5.2.1
Predicted changes in precipitation - monthly

DATE	Dec. 3, 2012	1016-C14-A5511	R 0

© BC Hydro 2012 - all rights reserved. This map is for information purposes only and accuracy is not guaranteed.

Construction of the Site C Clean Energy Project is subject to required regulatory approvals including environmental certification

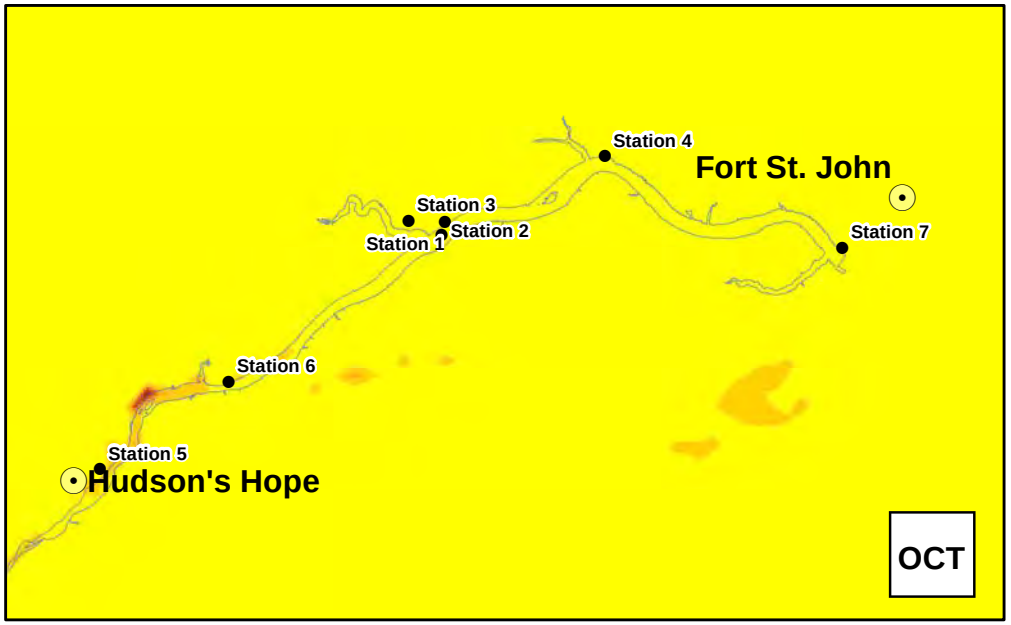

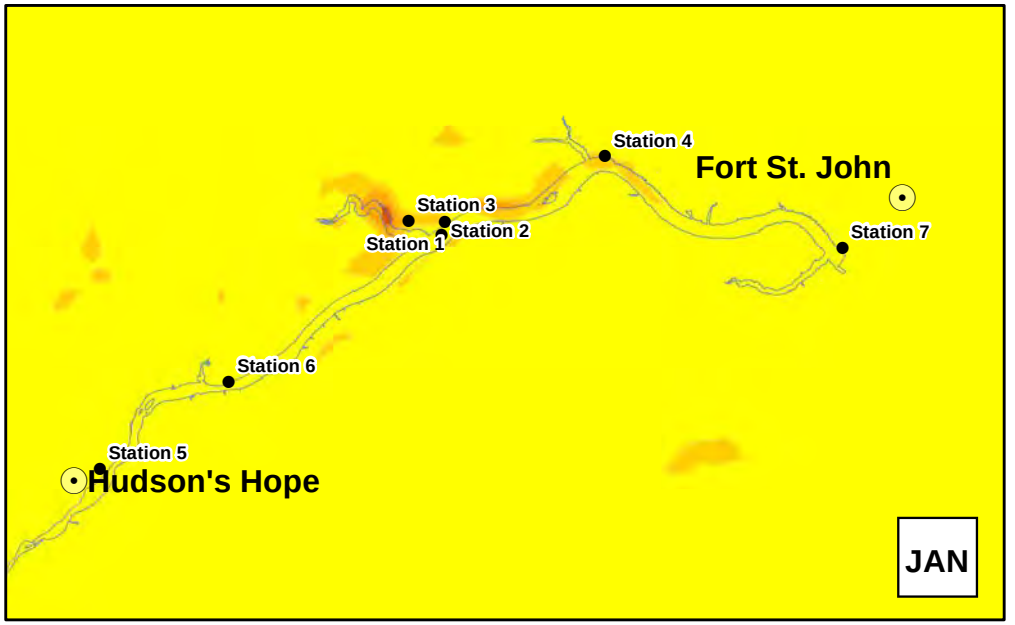

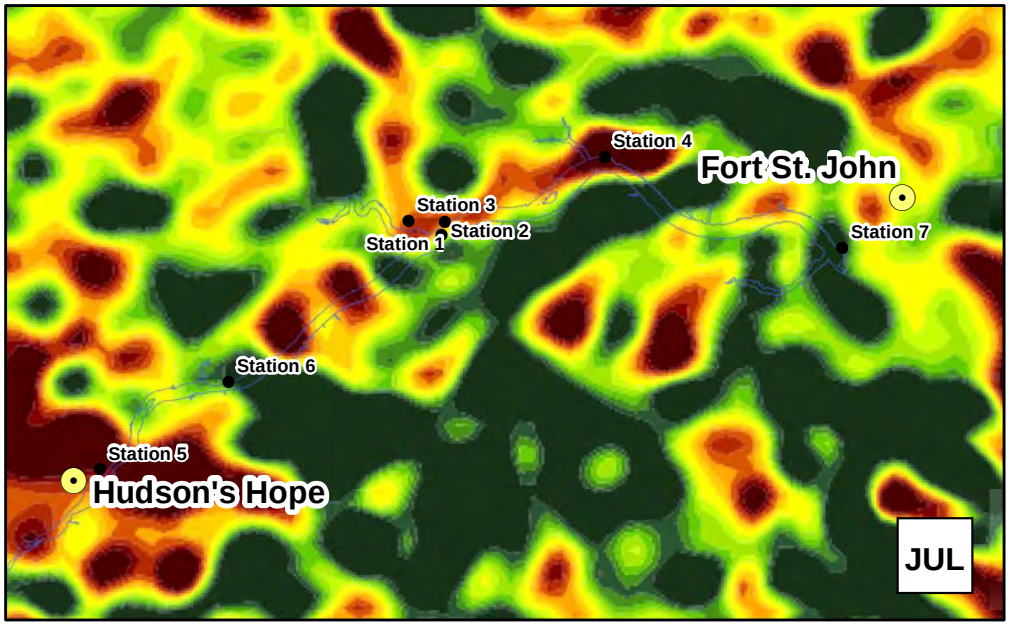

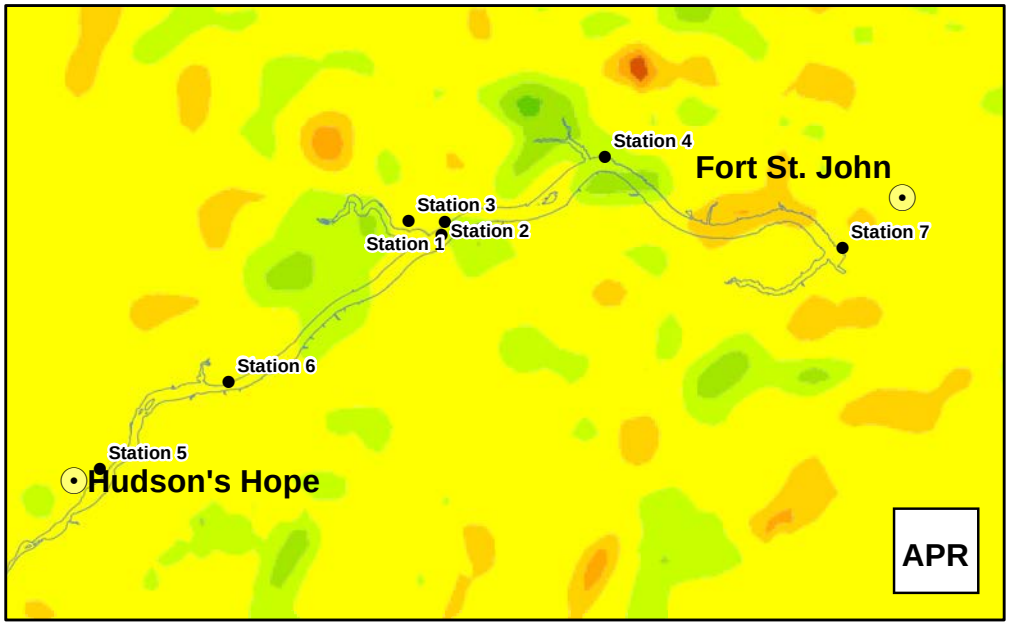

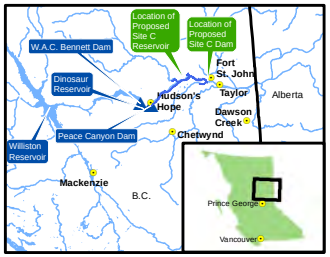

Weather Research and Forecasting (WRF) model-predicted changes in total monthly rainfall after formation of the reservoir (positive are increases) for four calendar months as labelled clockwise from top left: October, January, April, and July.

Map Notes:
1. Datum/Projection: NAD83/UTM Zone 10N
2. Proposed Reservoir Area (461.8 m maximum normal elevation) from Digital Elevation Models (DEM) generated from LiDAR data acquired July/August 2006.

© BC Hydro 2012 - all rights reserved. This map is for information purposes only and accuracy is not guaranteed.

Legend

- BC Hydro - Site C Stations
- City / District Municipality
- Proposed Reservoir

Rainfall Change (in mm)

> 6
5 to 6
4 to 5
3 to 4
2 to 3
1 to 2
-1 to 1
-2 to -1
-3 to -2
-4 to -3
-5 to -4
-6 to -5
< -6

N

1:600,000

0 20 km

SITE C CLEAN ENERGY PROJECT

RWDI BC hydro

Figure 5.2.2
Predicted changes in rainfall - monthly

DATE	Dec. 3, 2012	1016-C14-A5512	R 0

Construction of the Site C Clean Energy Project is subject to required regulatory approvals including environmental certification

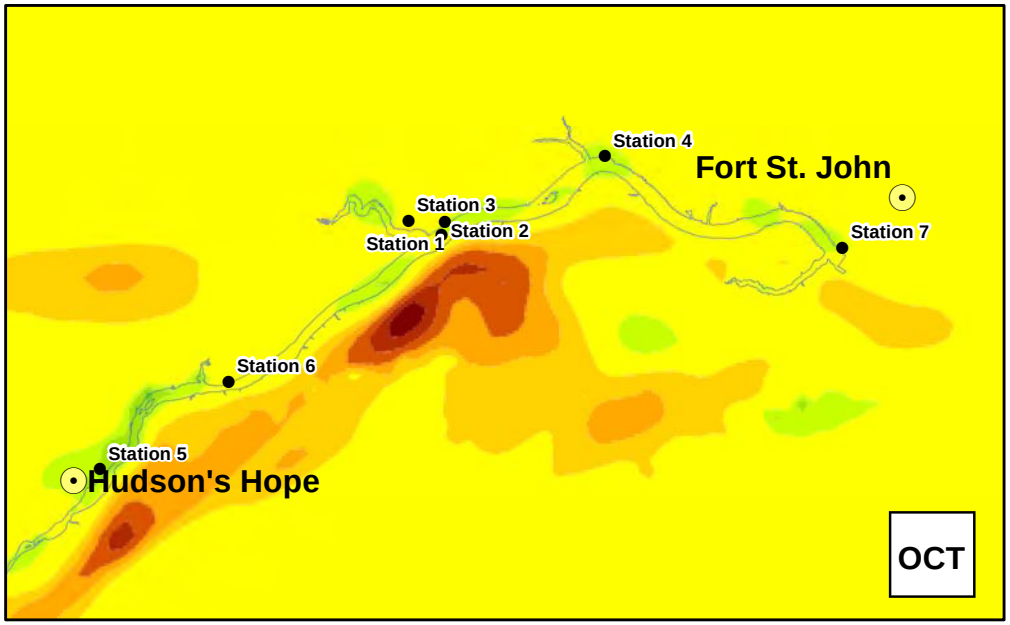

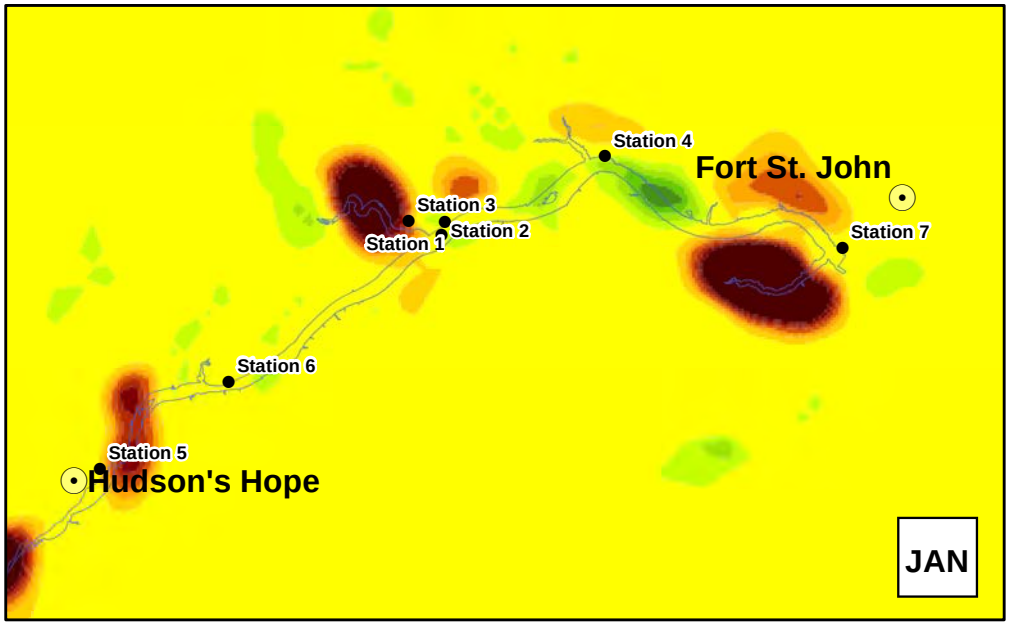

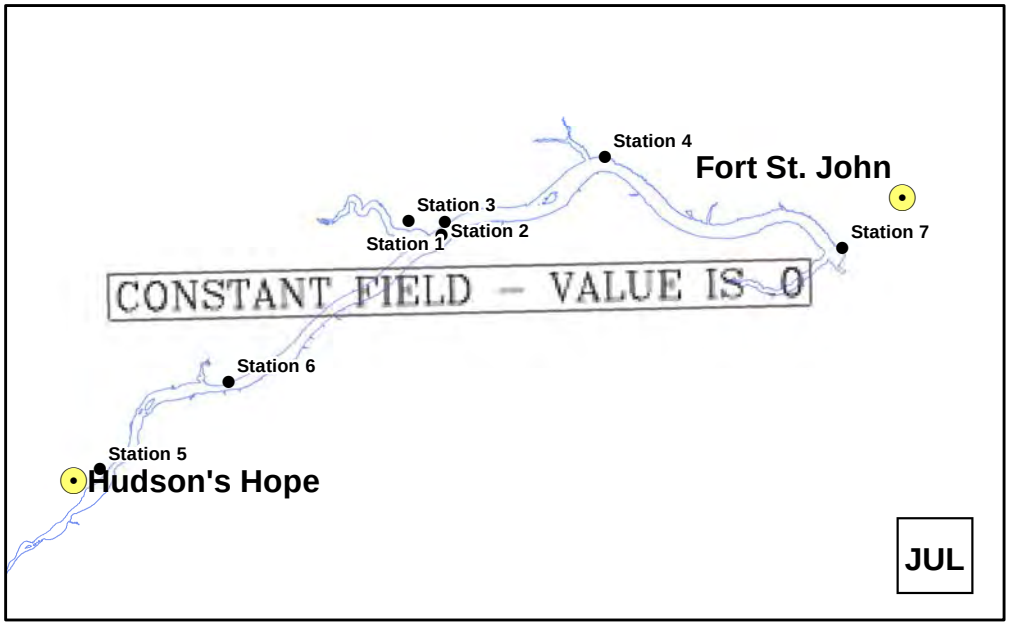

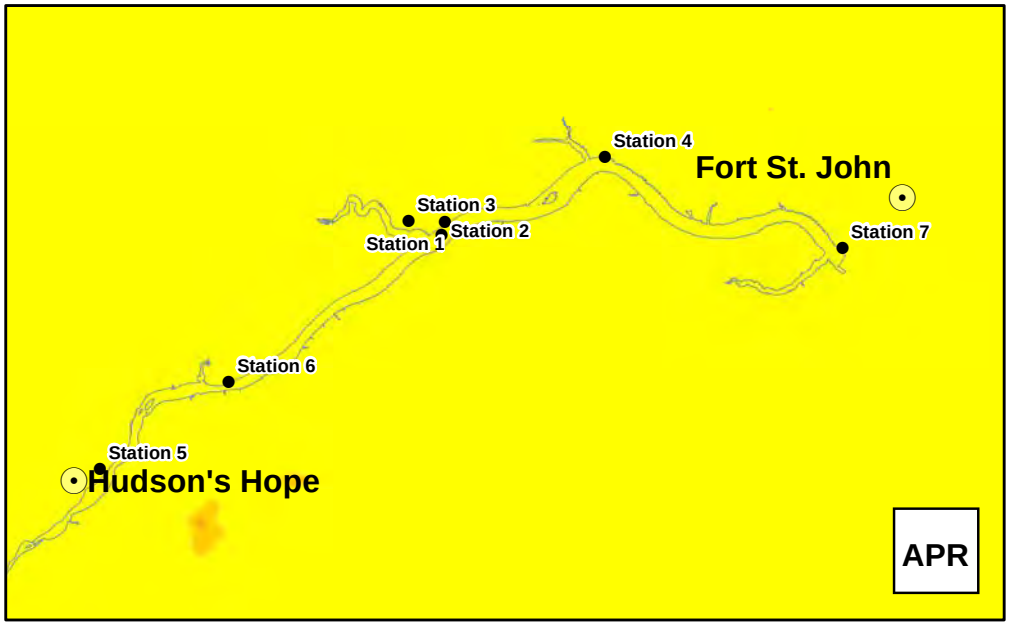

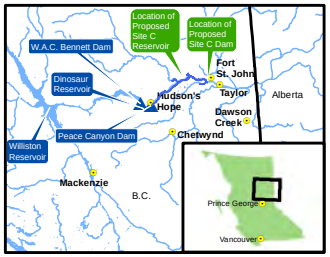

Weather Research and Forecasting (WRF) model-predicted changes in total monthly snow- and icefall after impoundment of the reservoir (positive are increases) for four calendar months as labelled clockwise from top left: October, January, April, and July.

Legend

- BC Hydro - Site C Stations
- City / District Municipality
- Proposed Reservoir

Snowfall Change (in mm water equivalent)

- > 6
- 5 to 6
- 4 to 5
- 3 to 4
- 2 to 3
- 1 to 2
- -1 to 1
- -2 to -1
- -3 to -2
- -4 to -3
- -5 to -4
- -6 to -5
- < -6

N

1:600,000

0 20 km

Map Notes:
1. Datum/Projection: NAD83/UTM Zone 10N
2. Proposed Reservoir Area (461.8 m maximum normal elevation) from Digital Elevation Models (DEM) generated from LiDAR data acquired July/August 2006.

© BC Hydro 2012 - all rights reserved. This map is for information purposes only and accuracy is not guaranteed.

RWDI BC hydro

SITE C CLEAN ENERGY PROJECT

Figure 5.2.3
Predicted changes in snowfall - monthly

DATE	Dec. 3, 2012	1016-C14-A5513	R 0

Construction of the Site C Clean Energy Project is subject to required regulatory approvals including environmental certification

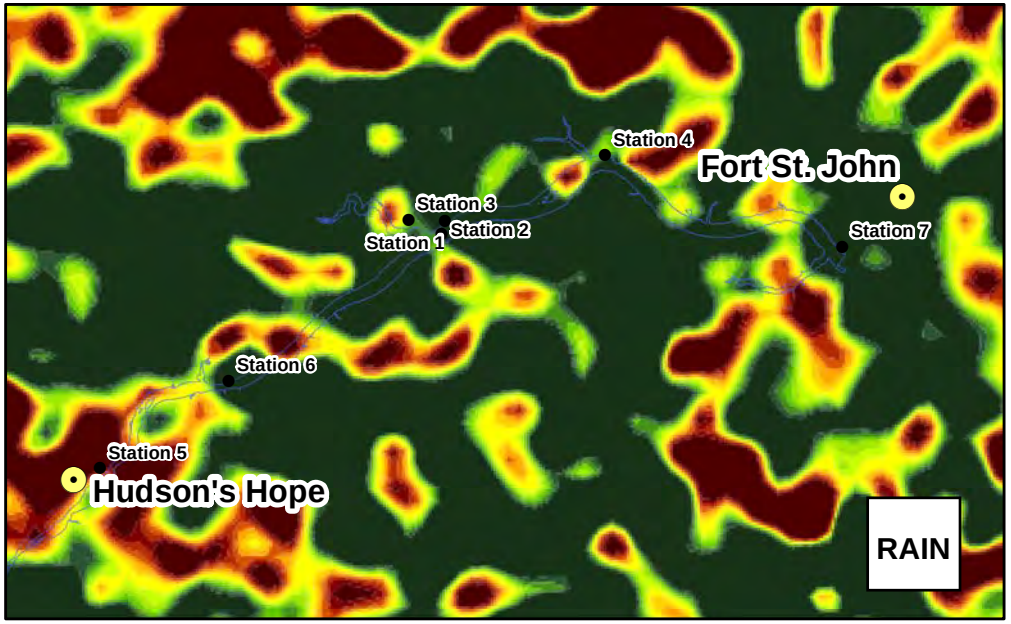

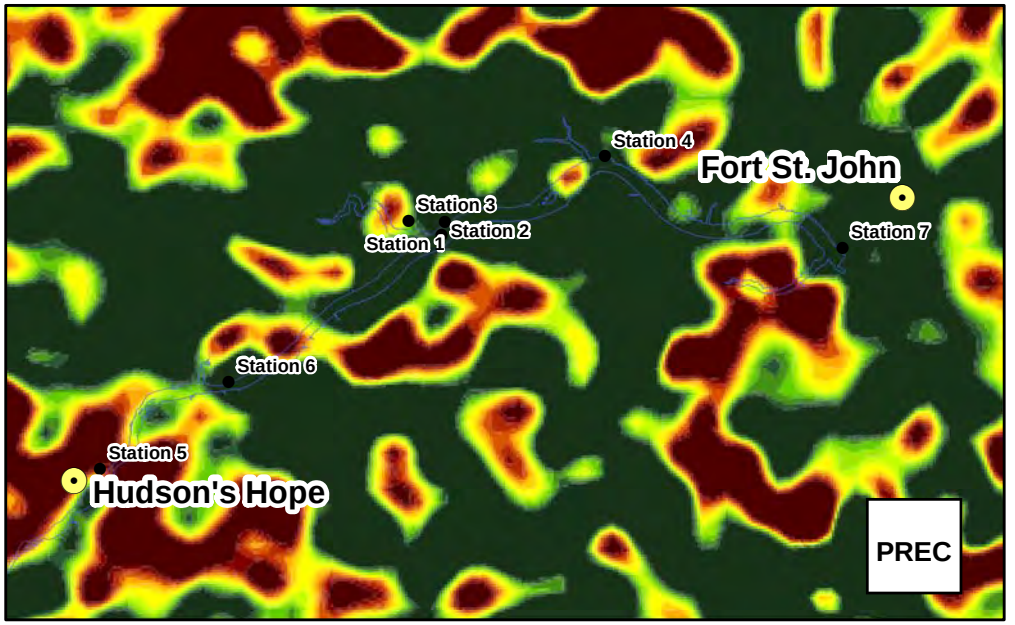

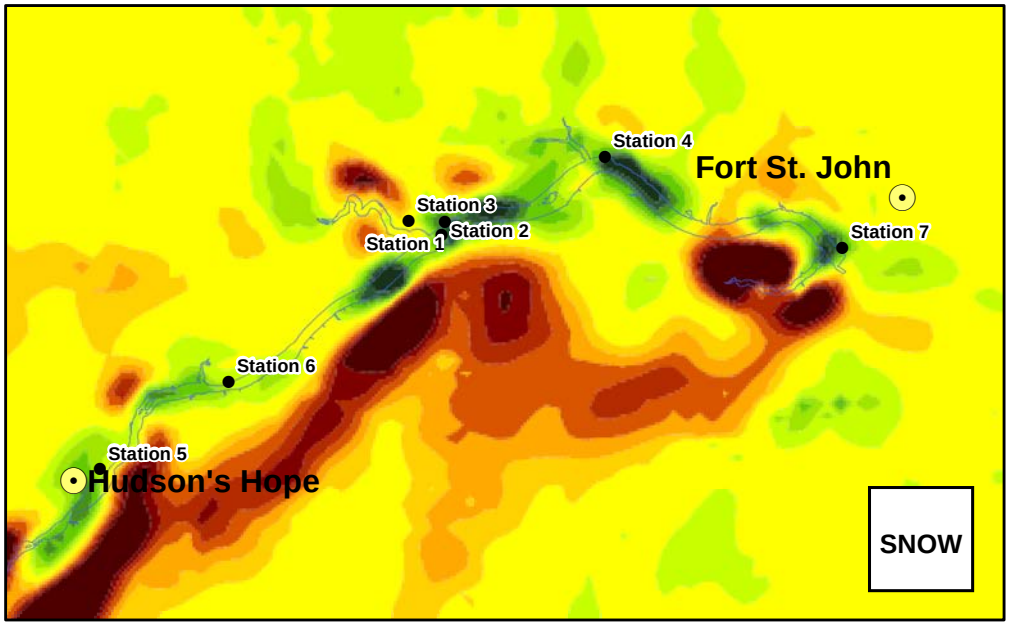

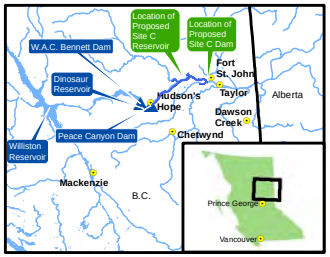

Weather Research and Forecasting (WRF) model-predicted changes in total annual precipitation (Prec), rainfall only (Rain), and snow- and icefall only (Snow) after formation of the reservoir (positive are increases).

Map Notes:
1. Datum/Projection: NAD83/UTM Zone 10N
2. Proposed Reservoir Area (461.8 m maximum normal elevation) from Digital Elevation Models (DEM) generated from LiDAR data acquired July/August 2006.

Legend

- BC Hydro - Site C Stations
- City / District Municipality
- Proposed Reservoir

Change (in mm water equivalent)

- > 30
- 25 to 30
- 20 to 25
- 15 to 20
- 10 to 15
- 5 to 10
- -5 to 5
- -10 to -5
- -15 to -10
- -20 to -15
- -25 to -20
- -30 to -25
- < -30

N

1:600,000

0 20 km

SITE C CLEAN ENERGY PROJECT

RWDI BC hydro

Figure 5.2.4
Predicted changes in precipitation - annual

DATE	Dec. 3, 2012	1016-C14-A5514	R 1

© BC Hydro 2012 - all rights reserved. This map is for information purposes only and accuracy is not guaranteed.

Construction of the Site C Clean Energy Project is subject to required regulatory approvals including environmental certification

5.3 WIND

Overall, winds were predicted to increase in speed at all climate station locations with the exception of the locations outside of the proposed Site C reservoir valley (i.e., Attachie Flat Plateau and Taylor). The increase in wind speeds can be attributed to the smoother surface roughness of the reservoir and larger fetch distance compared with a typical river valley. Simply put, winds have fewer impediments when travelling across the reservoir and thus wind speeds would tend to be higher at locations adjacent to the reservoir. The largest changes to wind speed were predicted to occur during the warm season (spring and summer) when large scale weather patterns in the region tend to be associated with clearer skies and lower overall wind speeds. Lower wind speeds from large scale conditions mean that local topographically driven wind systems are more dominant. That is, if winds from synoptic scale highs and lows are not strongly developed, then changes in wind speed caused by the change from the rougher valley bottom to the smoother water surface would be more noticeable.

Conversely, during winter, prevailing weather systems tend to show higher wind speeds that dominate over any local terrain induced wind systems. In addition, for any periods where synoptic scale wintertime winds are light, the reduced solar input from the low wintertime solar angle would not heat the ground surface sufficiently to allow any local scale wind systems to develop. As a result of both of these processes, any changes in wind speed due to the changes in surface roughness are minimized for the winter months.

Season change in wind speed is presented in Table 5.3.1. For each time period the seasonal Attachie Flat Lower Terrace was predicted to experience the greatest change with an increase in the seasonal average of 4.3 kilometres per hour in the fall and 2.5 kilometres per hour for the annual average. Hudson‘s Hope was predicted to have annual increase of 2.4 kilometres per hour while Fort St. John Airport, Attachie Flat Plateau, and Bear Flat were predicted to increase by no more than 1.0 kilometre per hour. The annual average wind speed was not predicted to change at Fort St. John Airport. For most stations this represents a change of approximately 10%. The biggest changes are seen in winter and correspond to prevailing wind direction aligning with the future water surface, resulting in a longer and smoother upwind fetch. A general increase in wind speeds as what one would expect from the reduced roughness and larger fetch that results from the creation of the reservoir surface. The increase in wind speeds over water would also mean higher wind speeds for land areas immediately adjacent to the water surface.

Table 5.3.1 Seasonal change in wind speed

Difference (Future Case with the Project – Baseline Case)	Spring	Summer	Fall	Winter	Year
Fort St. John Airport	0.0 (13.9)	0.0 (15.6)	0.1 (19.0)	0.0 (17.0)	0.0 (16.3)
Station 1 - Attachie Flat Upper Terrace	0.6 (10.4)	1.2 (11.0)	2.8 (10.3)	1.5 (9.1)	1.5 (10.2)
Station 2 - Attachie Flat Lower Terrace	1.2 (9.8)	2.1 (10.7)	4.3 (9.7)	2.4 (8.5)	2.5 (9.7)
Station 3 - Attachie Flat Plateau	0.7 (11.2)	0.8 (10.8)	1.7 (10.7)	0.7 (9.7)	1.0 (10.6)
Station 4 - Bear Flat	-0.3 (9.9)	0.0 (8.5)	1.2 (9.0)	0.7 (8.6)	0.4 (9.0)
Station 5 - Hudson's Hope	1.0 (9.3)	1.9 (10.9)	3.7 (10.7)	2.8 (9.2)	2.4 (10.0)
Station 6 - Farrell Creek	0.5 (8.8)	1.3 (10.3)	2.9 (9.3)	1.4 (8.1)	1.6 (9.1)
Station 7 - Site C Dam	-0.3 (10.9)	0.1 (11.0)	1.7 (11.8)	1.4 (10.8)	0.7 (11.1)

NOTES:
All values in kilometres per hour. Baseline average wind speed for same period is shown in parentheses.
[e] Fort St. John Airport station observations.

The change in maximum hourly wind speed was predicted and reported in Table 5.3.2. The maximum hourly wind speeds reported for each season is the highest hourly wind speed predicted in that season. Hudson‘s Hope was predicted to experience the greatest change with an increase of 3.4 kilometres per hour in spring and summer, 7.5 kilometres per hour in the fall, and 8.7 kilometres per hour in winter. On an annual basis little to no change was predicted for Fort St. John Airport, Bear Flat and the proposed Site C Dam site. Similar to the average results, there is generalized increase that would be expected from the reduction in surface roughness and the greatest changes seem to occur during periods when the prevailing winds align with the orientation of the lake. However, during some seasons, there are stations that show a decrease in maximum wind speed. In these cases it is possible that the reduced depth of the valley from filling the reservoir causes less channelling of winds and that this influence is greater than the expected increase from reduced roughness. Statistical significance tests were not performed for maximum hourly wind speed as the sample size of the time series was too small to facilitate an appropriate test.

Table 5.3.2 Seasonal change in maximum hourly wind speed

Difference (Future Case with the Project – Baseline Case)	Spring	Summer	Fall	Winter	Year
Fort St. John Airport	-0.7 (43.3)	-0.2 (44.7)	0.4 (44.7)	0.4 (43.0)	0.4 (44.7)
Station 1 - Attachie Flat Upper Terrace	5.5 (38.0)	1.0 (39.0)	4.4 (42.8)	5.8 (35.6)	4.4 (42.8)
Station 2 - Attachie Flat Lower Terrace	2.6 (39.2)	4.7 (38.1)	6.9 (42.7)	6.3 (39.0)	6.9 (42.7)
Station 3 - Attachie Flat Plateau	1.2 (37.8)	1.7 (41.3)	4.9 (51.1)	4.4 (43.8)	4.9 (51.1)
Station 4 - Bear Flat	-5.0 (41.4)	-2.4 (37.6)	1.3 (49.6)	-1.0 (41.2)	1.3 (49.6)
Station 5 - Hudson's Hope	3.4 (35.3)	3.4 (46.2)	7.5 (53.7)	8.7 (55.5)	8.7 (55.5)
Station 6 - Farrell Creek	3.6 (35.6)	-0.6 (42.5)	5.2 (47.7)	5.5 (42.3)	5.2 (47.7)
Station 7 - Site C Dam	2.6 (38.9)	-2.1 (37.4)	1.0 (52.4)	3.6 (42.4)	1.0 (52.4)

NOTES:
All values in kilometres per hour. Baseline maximum wind speed for same period is shown in parentheses.
[e] Fort St. John Airport station observations.

Differences in wind speed and direction frequencies are apparent as a result of the addition of the proposed reservoir, however the dominant winds predicted remain similar at each location. At Fort St. John Airport (shown in Figure 5.3.1) winds are primarily from the west-southwest direction, followed by winds from the southwest and north. Winds from the west-southwest direction were predicted to reduce in the Future Case with the Project. The percentage of weak winds from WSW seems to decrease a bit while the percentage of strong winds increases. The Fort St. John Airport location is greater than 10 kilometres from the reservoir, and given how winds respond to local terrain influences it is likely that the change is statistically insignificant. The model is likely responding to the change in channelling of wind from the change in valley elevation from the future reservoir surface. The west-southwest direction corresponds roughly to the tributary valley at the east end of the reservoir. As the valley is currently a little deeper than it would be in the future, it might have some channelling effect under neutral conditions for winds that slightly deviate from the WSW. With that channelling gone after reservoir formation, adjacent wind directions should become a little more frequent. On the other hand, for winds blowing from the WSW, the smoother upwind landscape after reservoir formation might increase the speed of stronger winds at Fort St. John Airport.

The dominant wind direction at Attachie Upper Terrace is from the west, followed by west-southwest and east-northeast (Figure 5.3.2). In the Future Case with the Project, the dominant wind directions are from the west-southwest, southwest, and west. Changes in wind speed and direction frequencies as a result of the proposed Site C reservoir can be attributed to the change in surface roughness and terrain characteristics due to the formation of the reservoir. Winds at Attachie Lower Terrace are from the west-southwest and southwest in both the Baseline Case and Future Case with the Project (Figure 5.3.3). Calm winds of less than one metre per second increased by 1.39% with the formation of the reservoir.

Little to no change is apparent outside of the reservoir valley at Attachie Flat Plateau (Figure 5.3.4). This is expected as the location is not adjacent to the reservoir and on a plateau above the river valley.

Changes in wind speed and wind direction at Bear Flat and Hudson‘s Hope are small as a result of the proposed reservoir (shown in Figure 5.3.5 and Figure 5.3.6, respectively). Dominant wind directions are not expected to change; however wind speeds are expected to increase with the formation of the reservoir.

Winds from the west-southwest are predicted to increase at Farrell Creek (Figure 5.3.7); winds from the west-southwest may increase by approximately three percent. At Site C Dam the dominant wind direction predicted is from the northwest for the Baseline Case and from the east for the Future Case with the Project (Figure 5.3.8). Winds from the east and west increased from the Baseline Case to the Future Case with the Project. There is also a predicted decrease in northwesterly and northeasterly winds.

Over the entire Technical Study Area (Figure 5.3.9), wind speed changes range from small decelerations to small accelerations on the order of a few tenths of metres per second along the proposed reservoir in April and July to substantial increases of up to 1 metre per second along sections of the proposed reservoir in October and January. Figure 5.3.10 shows that the changes are unlikely statistically significant over all four months and the entire Technical Study Area, with the exception of some small areas in January and October. After averaging over the entire year, however, predicted wind speed increases of about 0.1 to 0.2 metres per second along the reservoir (Figure 5.3.11) are extremely likely statistically significant (Figure 5.3.12).

Observed

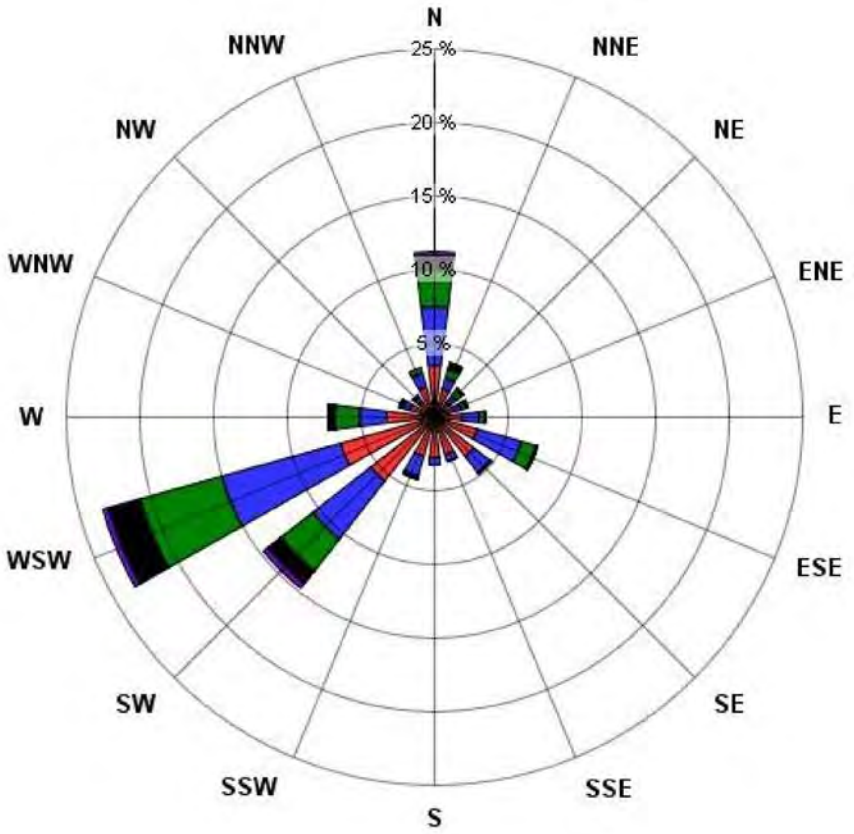

Calms: 0.47%

Predicted

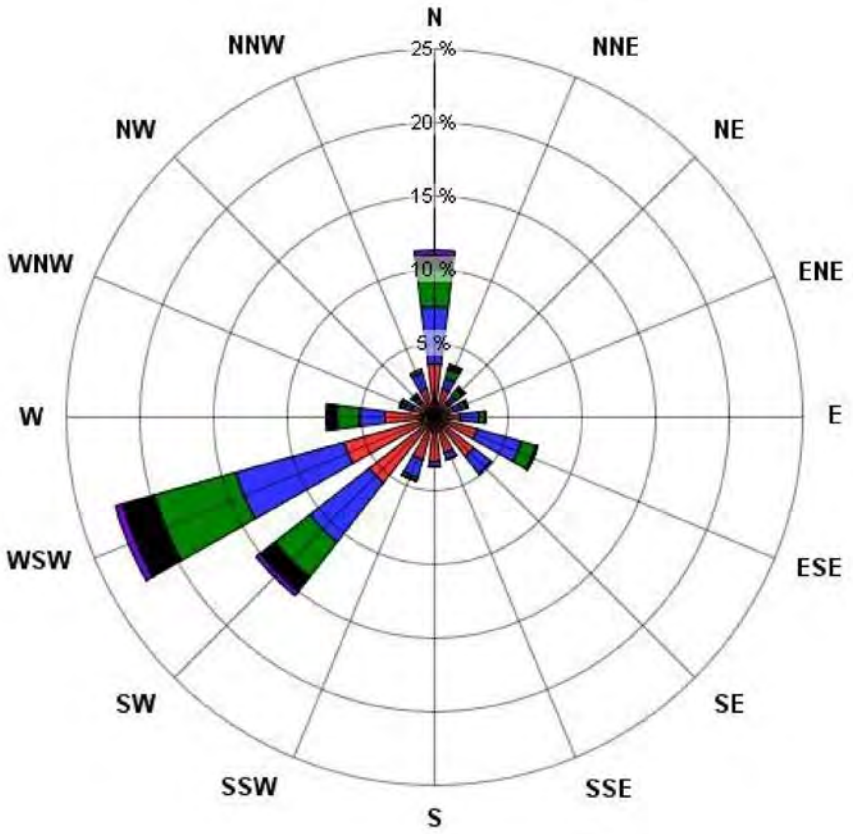

Calms: 0.47%

Wind Speed (m/s)

- > 10.0
- > 8.0 - 10.0
- > 6.0 - 8.0
- > 4.0 - 6.0
- > 2.0 - 4.0
- > 1.0 - 2.0
- > 0.5 - 1.0

SITE C CLEAN ENERGY PROJECT

RWDI BC hydro

Figure 5.3.1
Wind rose of Baseline Case and Future Case with the Project at Fort St. John Airport

DATE	Dec. 3, 2012		R 0

Observed

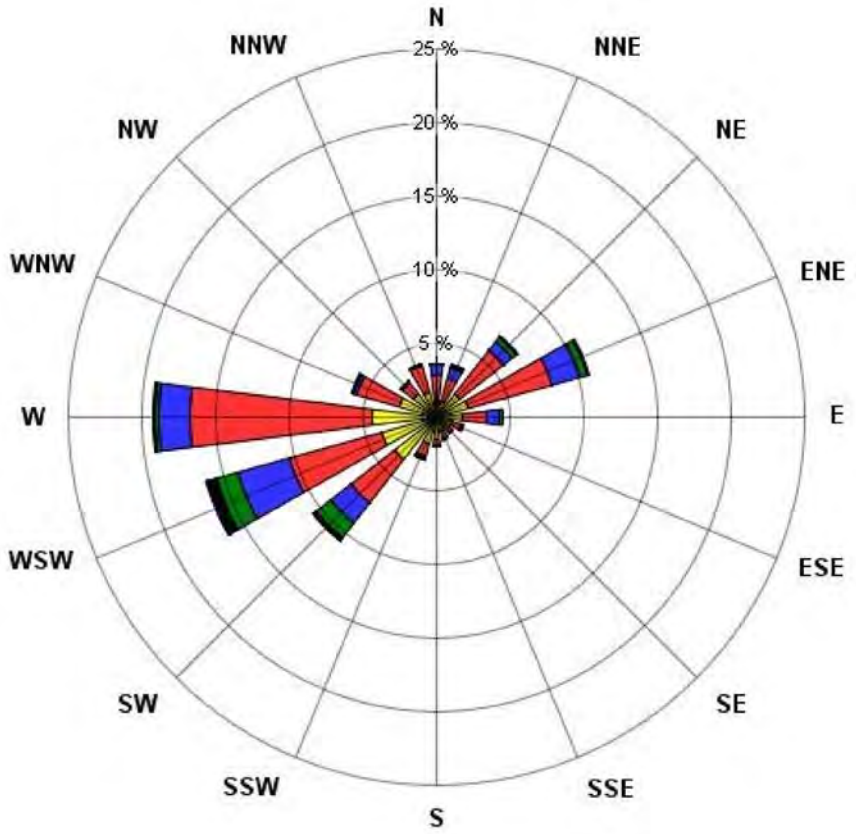

Calms: 1.76%

Predicted

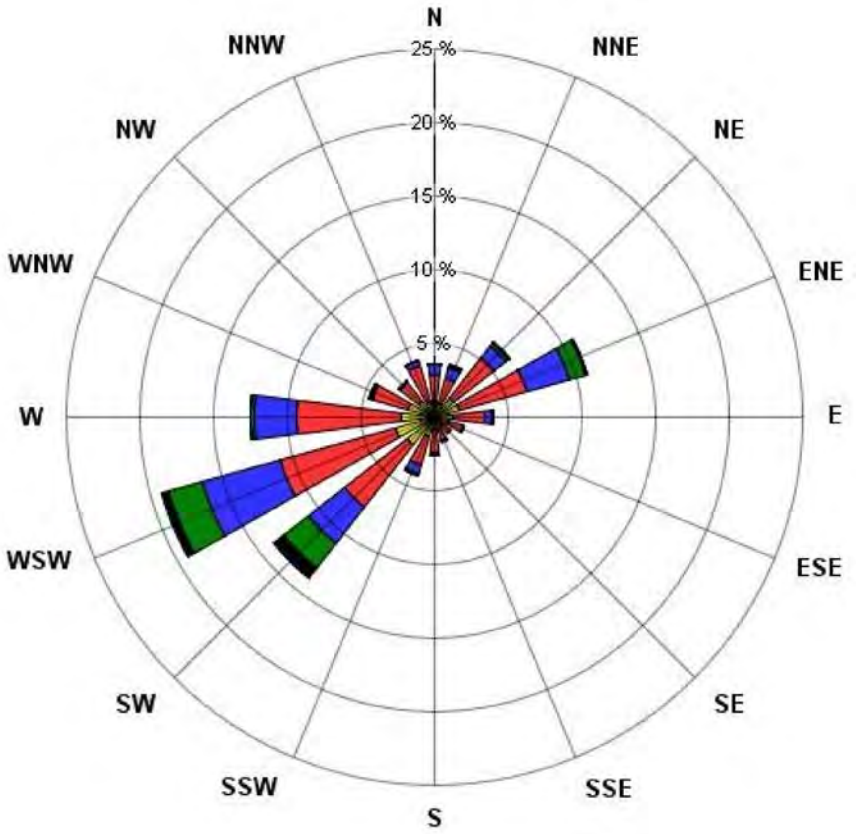

Calms: 1.89%

Wind Speed (m/s)

- > 10.0
- > 8.0 - 10.0
- > 6.0 - 8.0
- > 4.0 - 6.0
- > 2.0 - 4.0
- > 1.0 - 2.0
- > 0.5 - 1.0

SITE C CLEAN ENERGY PROJECT

RWDI BC hydro

Figure 5.3.2
Wind rose of Baseline Case and Future Case with the Project at Station 1 – Attachie Flat Upper Terrace

DATE	Dec. 3, 2012		R 0

Observed

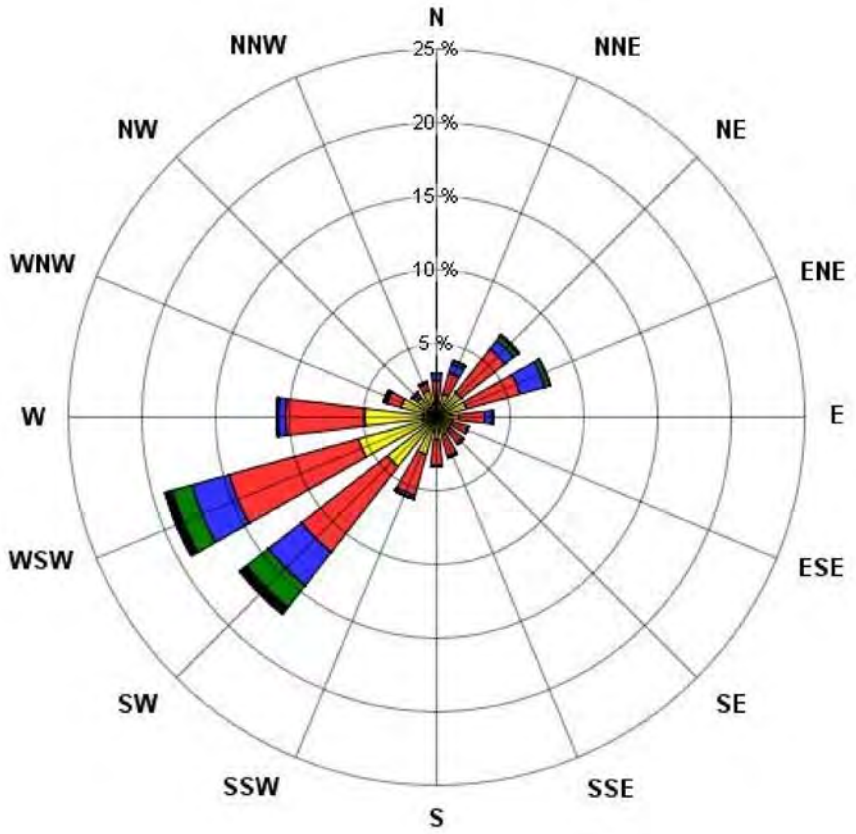

Calms: 1.91%

Predicted

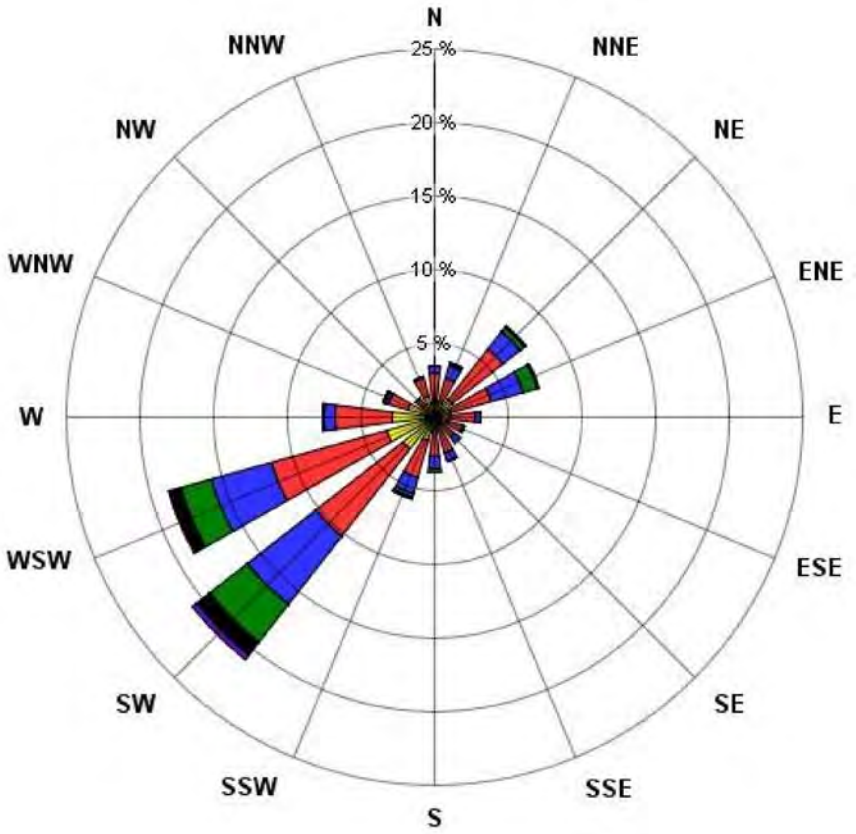

Calms: 1.89%

Wind Speed (m/s)

- > 10.0
- > 8.0 - 10.0
- > 6.0 - 8.0
- > 4.0 - 6.0
- > 2.0 - 4.0
- > 1.0 - 2.0
- > 0.5 - 1.0

SITE C CLEAN ENERGY PROJECT

RWDI BC hydro

Figure 5.3.3
Wind rose of Baseline Case and Future Case with the Project at Station 2 – Attachie Flat Lower Terrace

DATE	Dec. 3, 2012		R 0

Observed

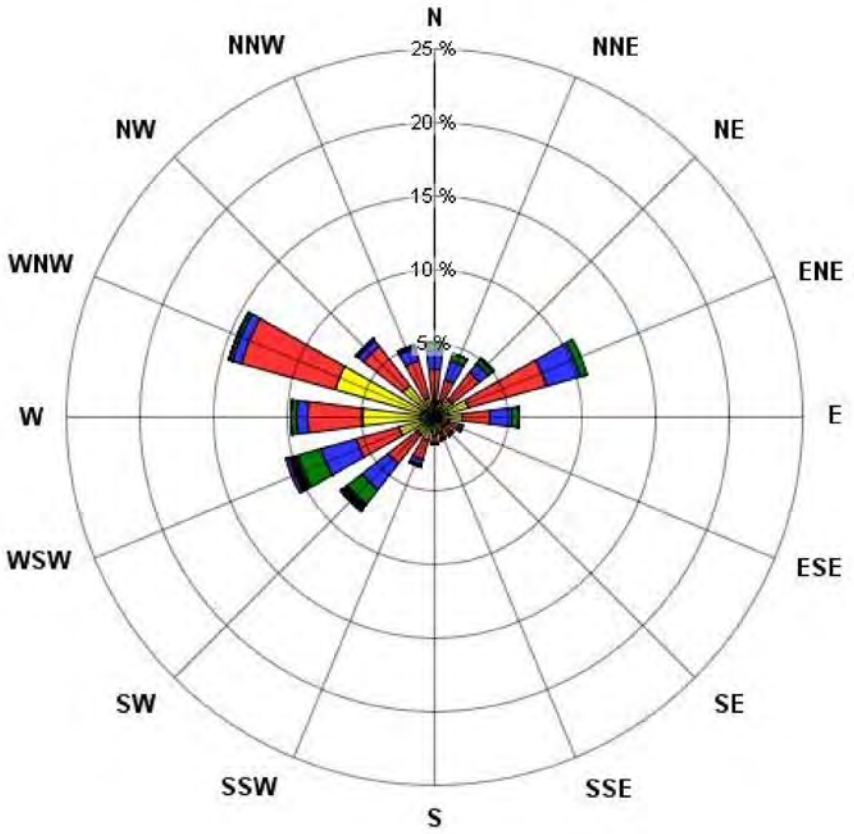

Calms: 3.29%

Predicted

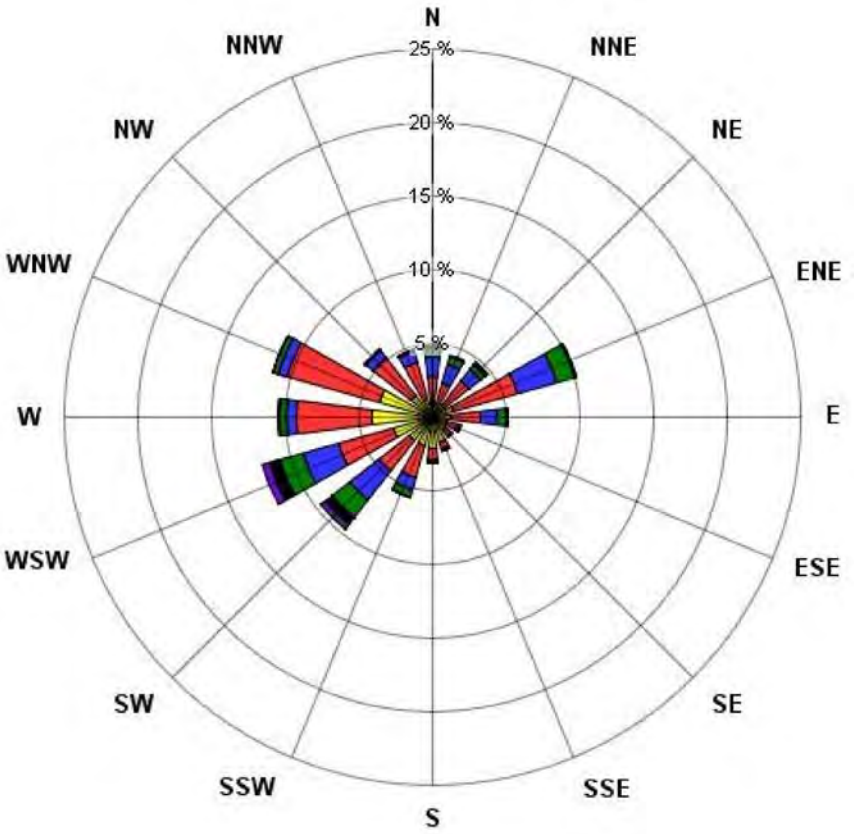

Calms: 1.85%

Wind Speed (m/s)

- > 10.0
- > 8.0 - 10.0
- > 6.0 - 8.0
- > 4.0 - 6.0
- > 2.0 - 4.0
- > 1.0 - 2.0
- > 0.5 - 1.0

SITE C CLEAN ENERGY PROJECT

RWDI BC hydro

Figure 5.3.4
Wind rose of Baseline Case and Future Case with the Project at Station 3 – Attachie Plateau

DATE	Dec. 3, 2012		R 0

Observed

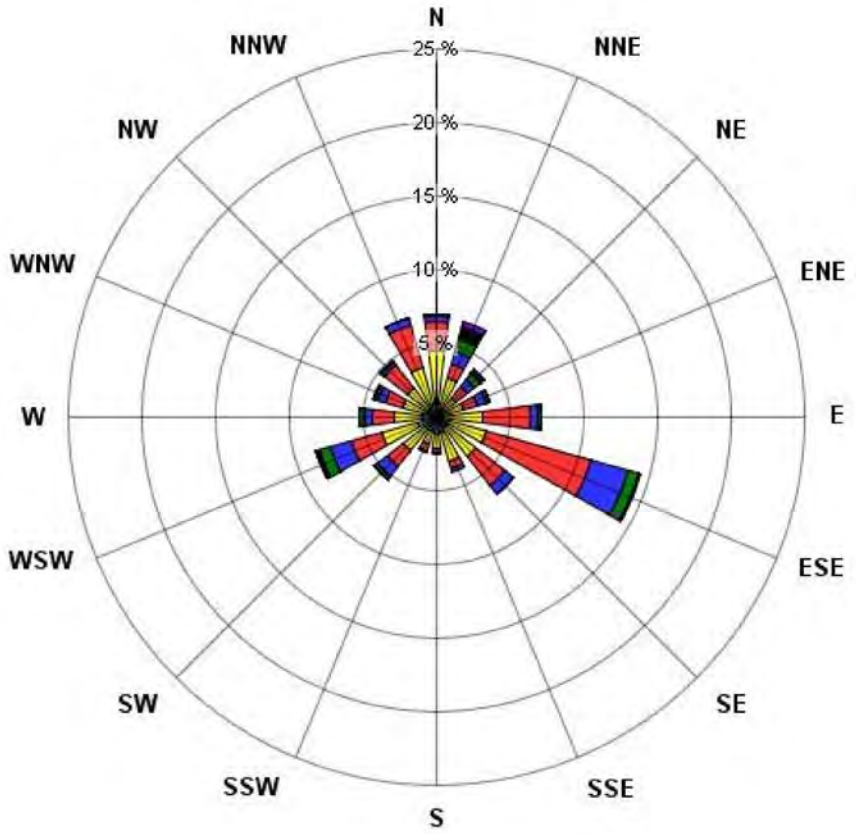

Calms: 5.87%

Predicted

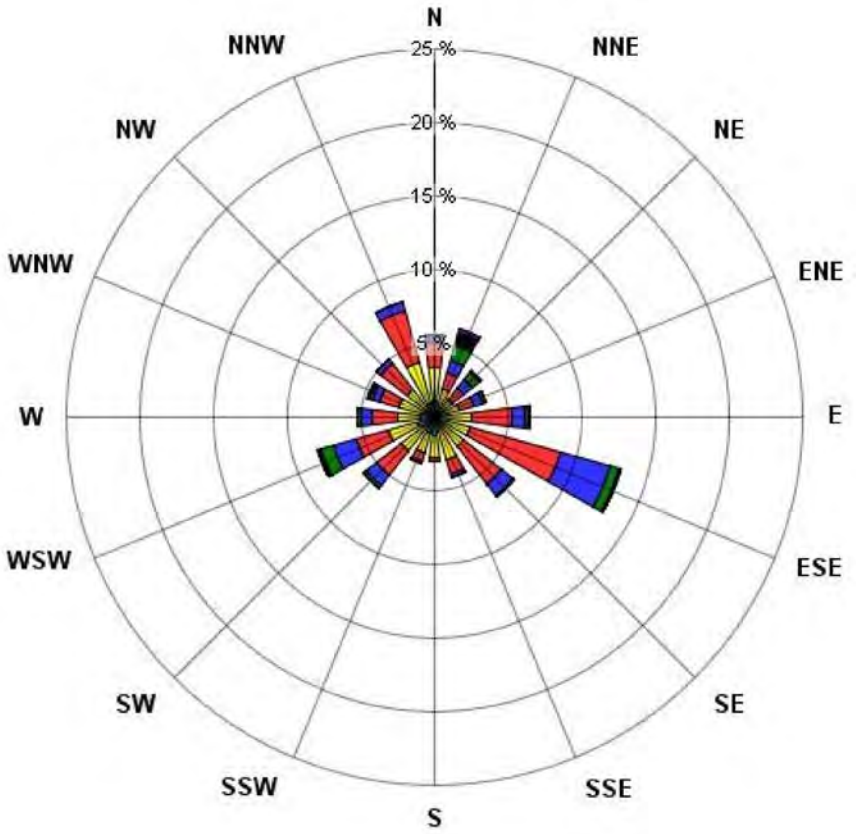

Calms: 5.87%

Wind Speed (m/s)

- > 10.0
- > 8.0 - 10.0
- > 6.0 - 8.0
- > 4.0 - 6.0
- > 2.0 - 4.0
- > 1.0 - 2.0
- > 0.5 - 1.0

SITE C CLEAN ENERGY PROJECT

RWDI BC hydro

Figure 5.3.5
Wind rose of Baseline Case and Future Case with the Project at Station 4 – Bear Flat

DATE	Dec. 3, 2012		R 0

Observed

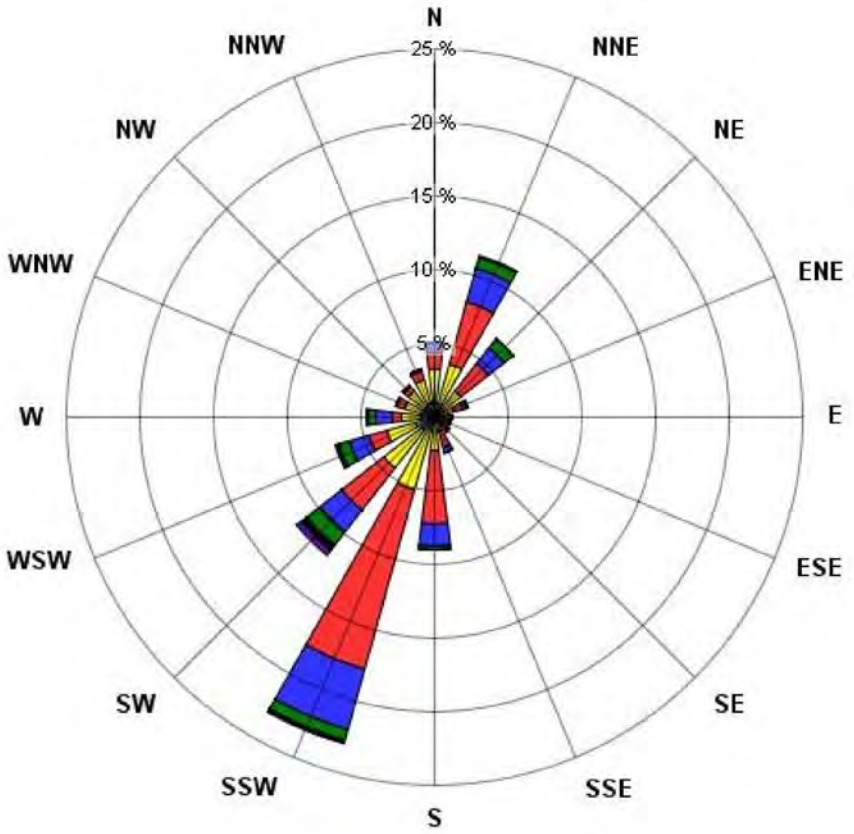

Calms: 4.05%

Predicted

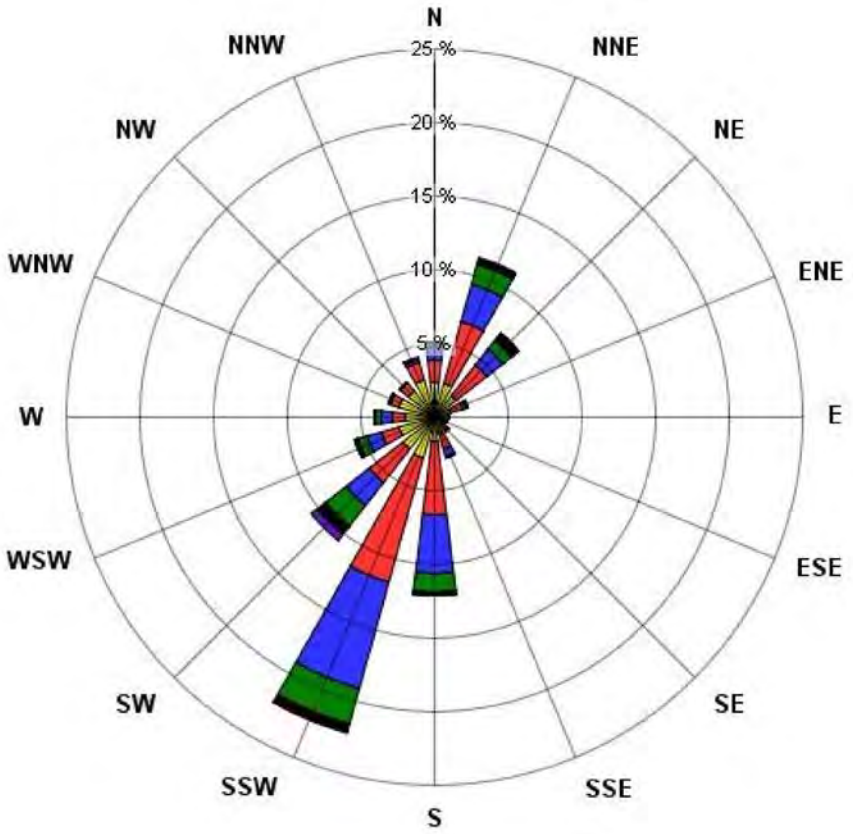

Calms: 2.47%

Wind Speed (m/s)

- > 10.0
- > 8.0 - 10.0
- > 6.0 - 8.0
- > 4.0 - 6.0
- > 2.0 - 4.0
- > 1.0 - 2.0
- > 0.5 - 1.0

SITE C CLEAN ENERGY PROJECT

RWDI BC hydro

Figure 5.3.6
Wind rose of Baseline Case and Future Case with the Project at Station 5 – Hudson's Hope

DATE	Dec. 3, 2012		R 0

Observed

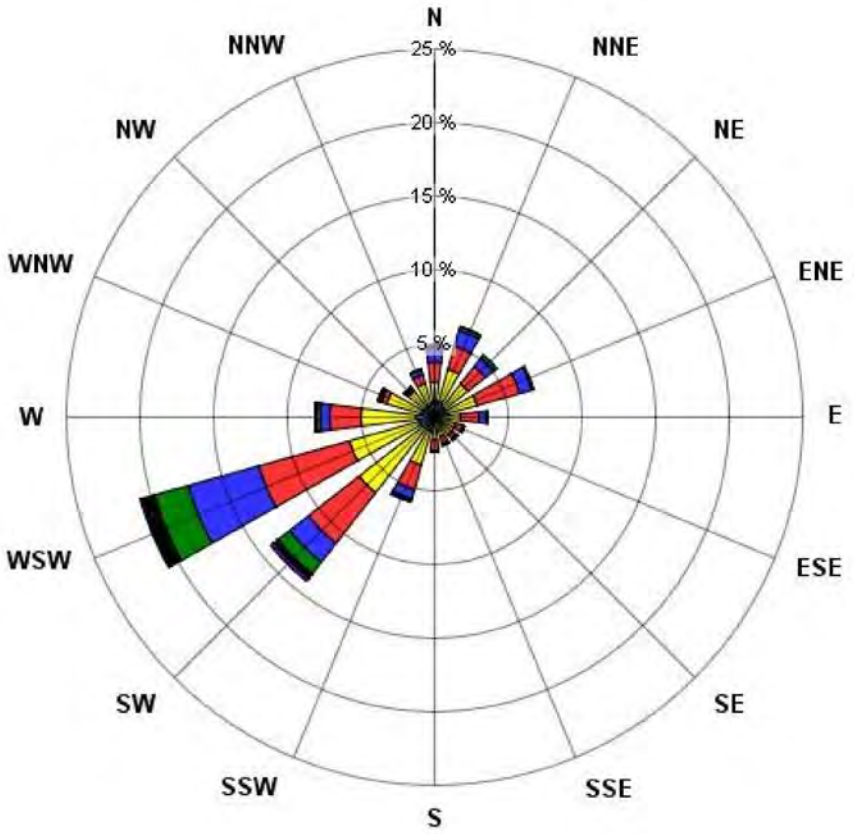

Calms: 5.16%

Predicted

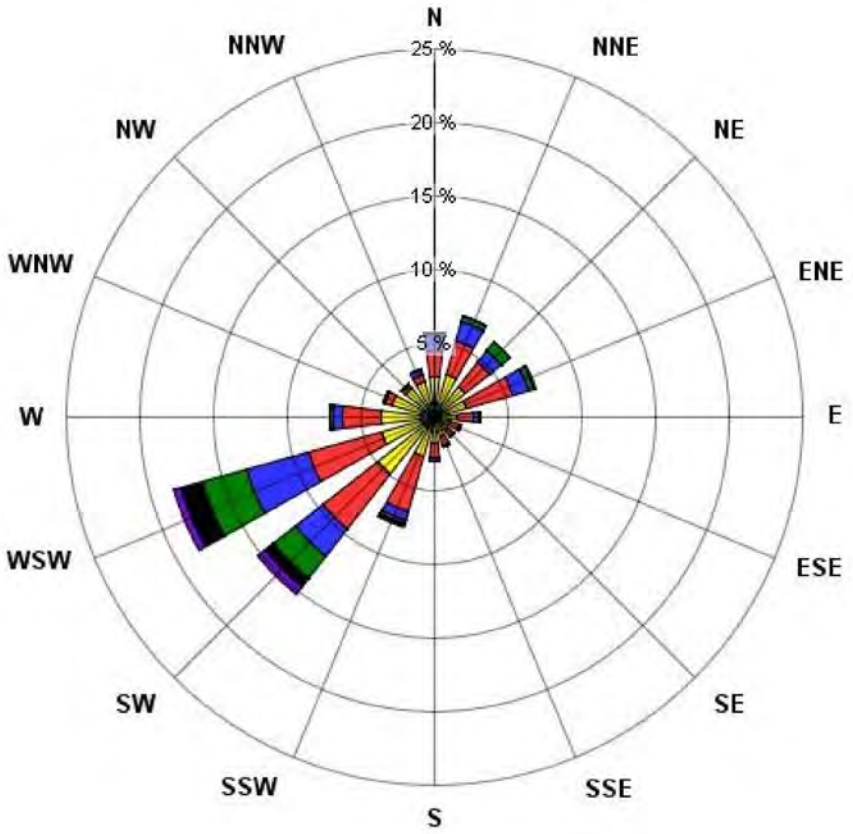

Calms: 3.33%

Wind Speed (m/s)

- > 10.0
- > 8.0 - 10.0
- > 6.0 - 8.0
- > 4.0 - 6.0
- > 2.0 - 4.0
- > 1.0 - 2.0
- > 0.5 - 1.0

SITE C CLEAN ENERGY PROJECT

RWDI BC hydro

Figure 5.3.7
Wind rose of Baseline Case and Future Case with the Project at Station 6 – Farrell Creek

DATE	Dec. 3, 2012		R 0

Observed

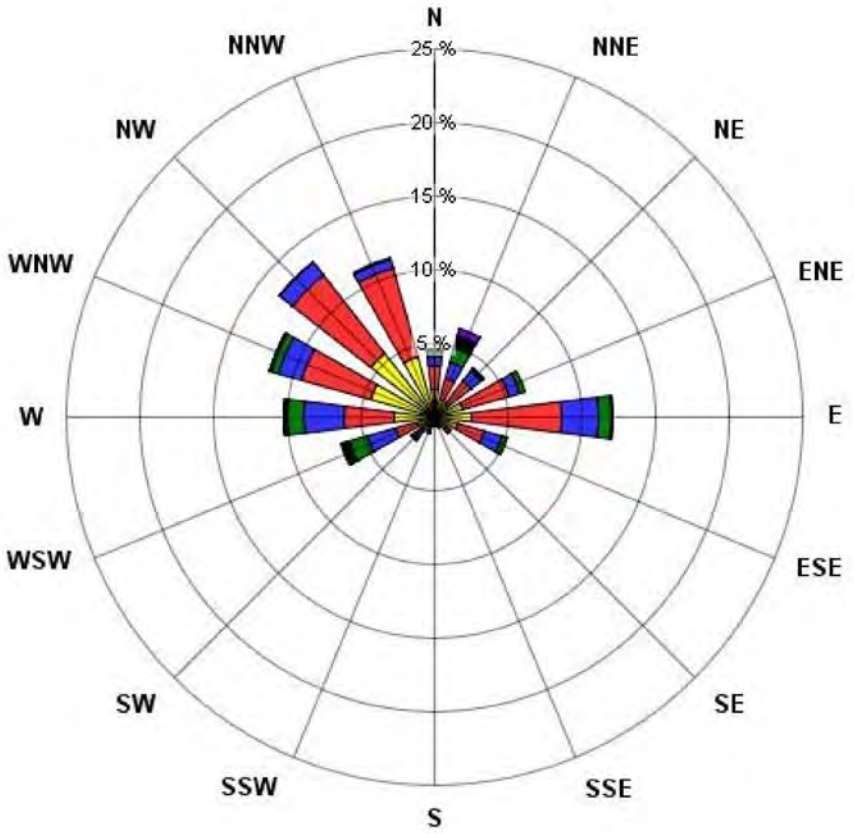

Calms: 2.21%

Predicted

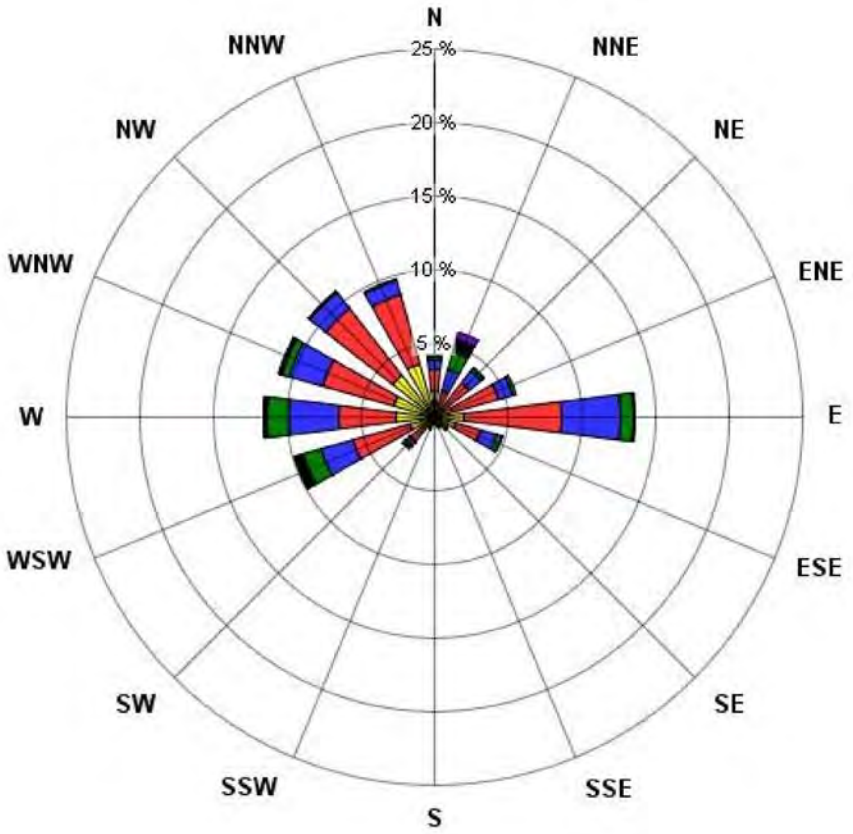

Calms: 2.35%

Wind Speed (m/s)

- > 10.0
- > 8.0 - 10.0
- > 6.0 - 8.0
- > 4.0 - 6.0
- > 2.0 - 4.0
- > 1.0 - 2.0
- > 0.5 - 1.0

SITE C CLEAN ENERGY PROJECT

RWDI BC hydro

Figure 5.3.8
Wind rose of Baseline Case and Future Case with the Project at Station 7 – Site C Dam

DATE	Dec. 3, 2012		R 0

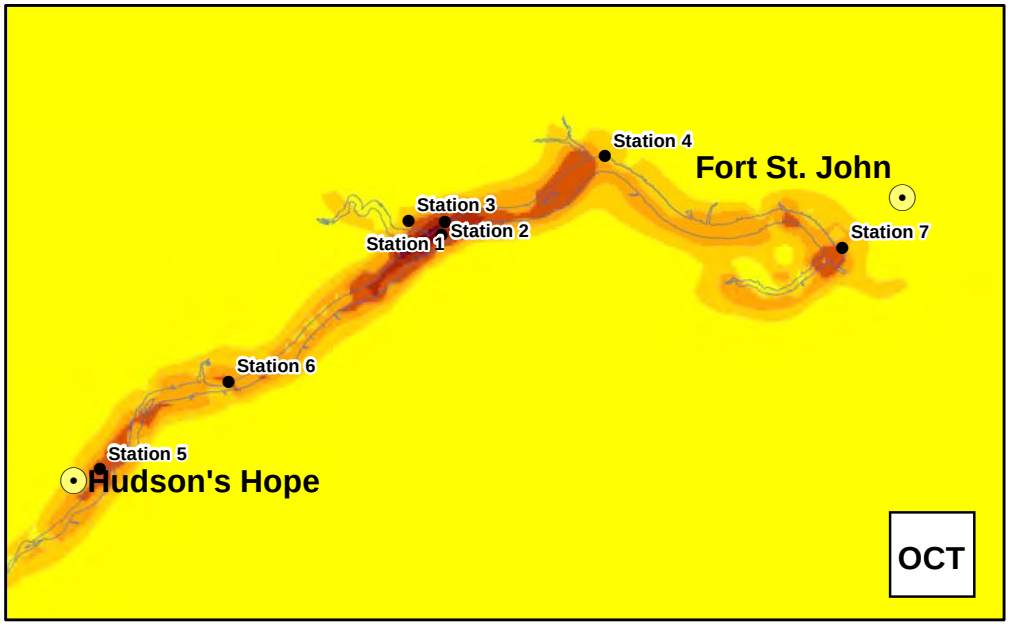

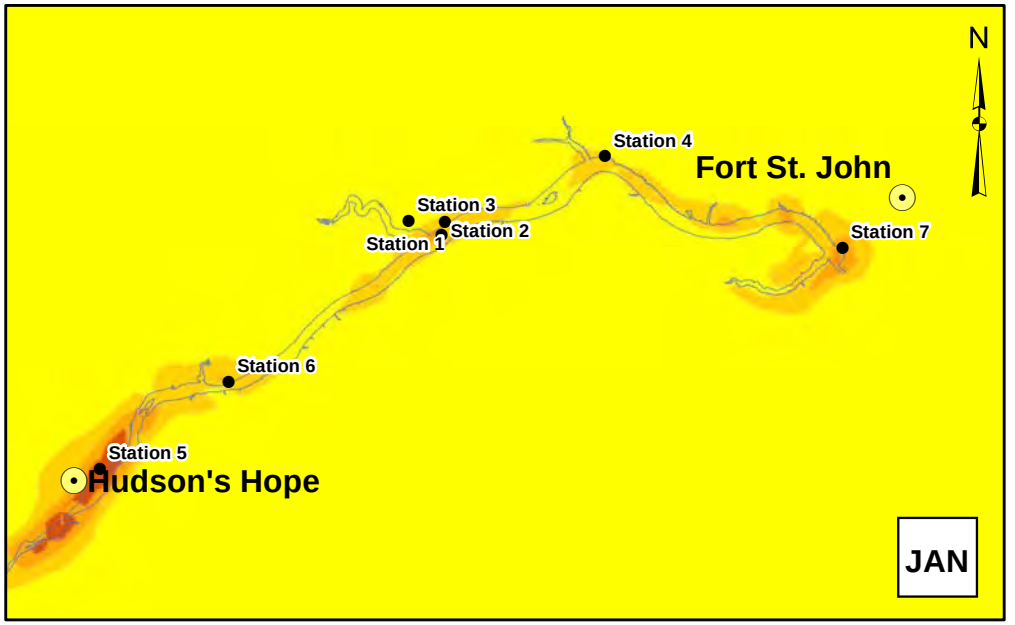

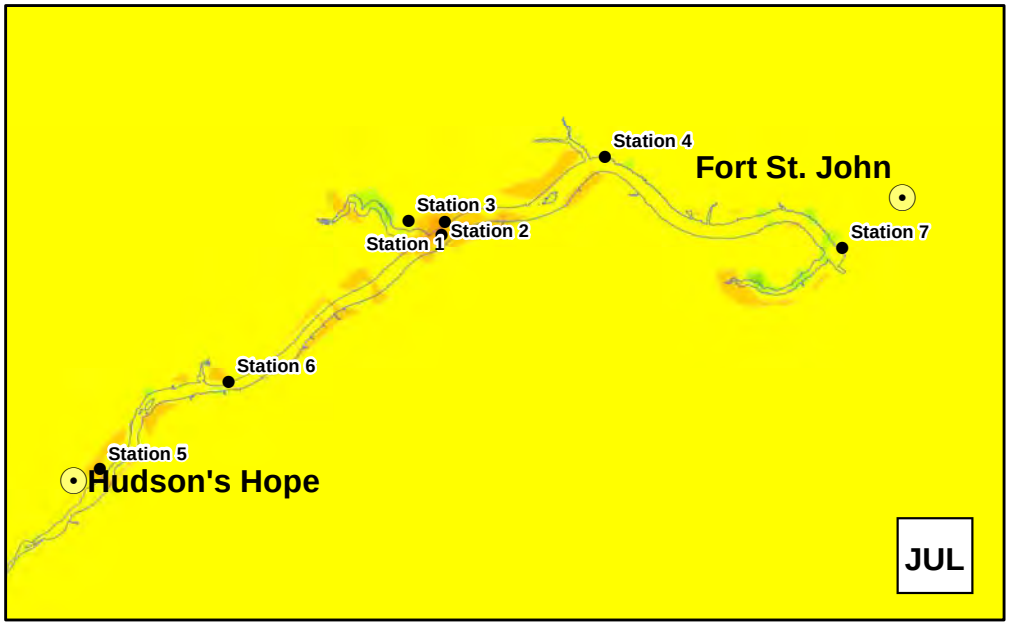

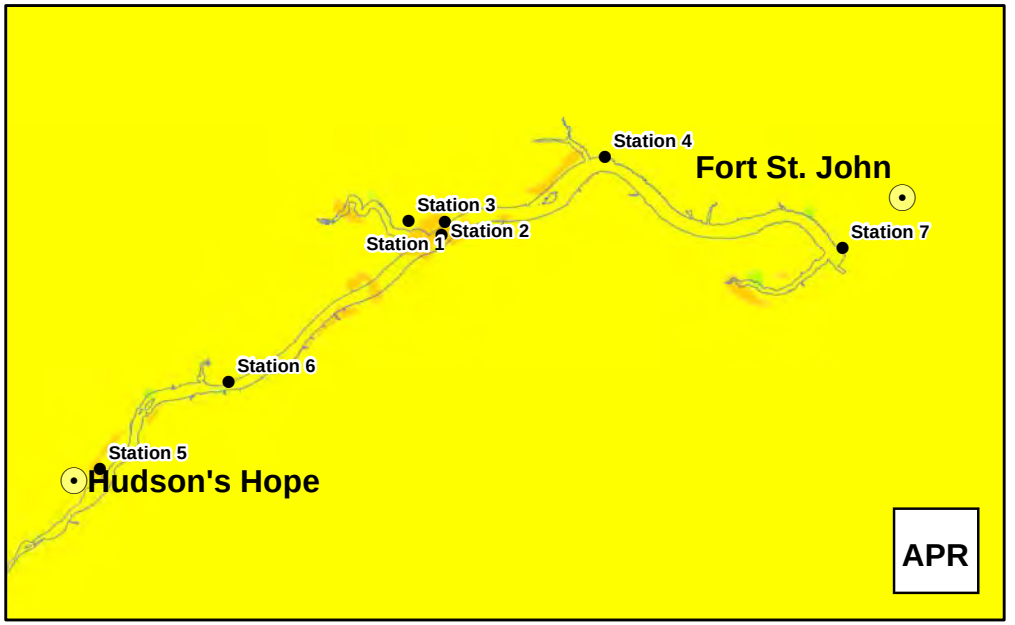

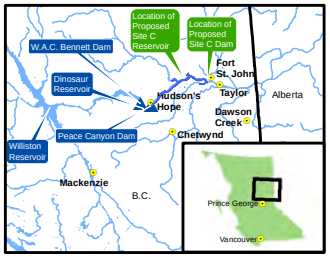

Weather Research and Forecasting (WRF) model-predicted changes in average monthly wind speeds after formation of the reservoir (positive are increases) for four calendar months as labelled clockwise from top left: October, January, April, and July.

Map Notes:
1. Datum/Projection: NAD83/UTM Zone 10N
2. Proposed Reservoir Area (461.8 m maximum normal elevation) from Digital Elevation Models (DEM) generated from LiDAR data acquired July/August 2006.

Legend

- BC Hydro - Site C Stations
- City / District Municipality
- Proposed Reservoir

Speed Change (in m/s)

- > 1.2
- 1.0 to 1.2
- 0.8 to 1.0
- 0.6 to 0.8
- 0.4 to 0.6
- 0.2 to 0.4
- -0.2 to 0.2
- -0.4 to -0.2
- -0.6 to -0.4
- -0.8 to -0.6
- -1.0 to -0.8
- -1.2 to -1.0
- < -1.2

1:600,000

0 20 km

RWDI BC hydro

SITE C CLEAN ENERGY PROJECT

Figure 5.3.9
Predicted changes in wind speeds - monthly

DATE	Dec. 3, 2012	1016-C14-A5515	R 0

© BC Hydro 2012 - all rights reserved. This map is for information purposes only and accuracy is not guaranteed.

Construction of the Site C Clean Energy Project is subject to required regulatory approvals including environmental certification

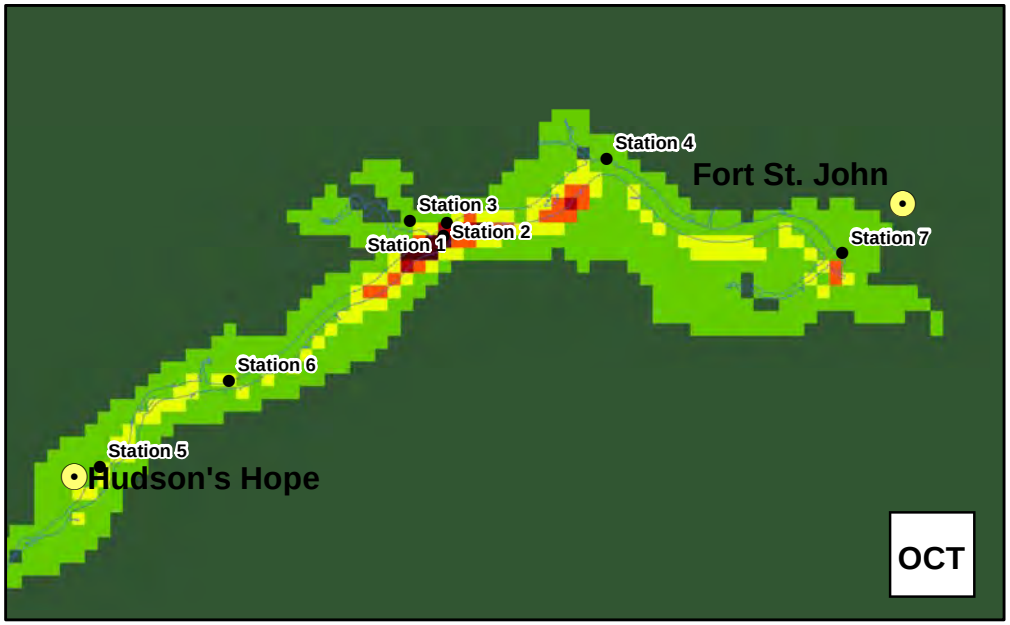

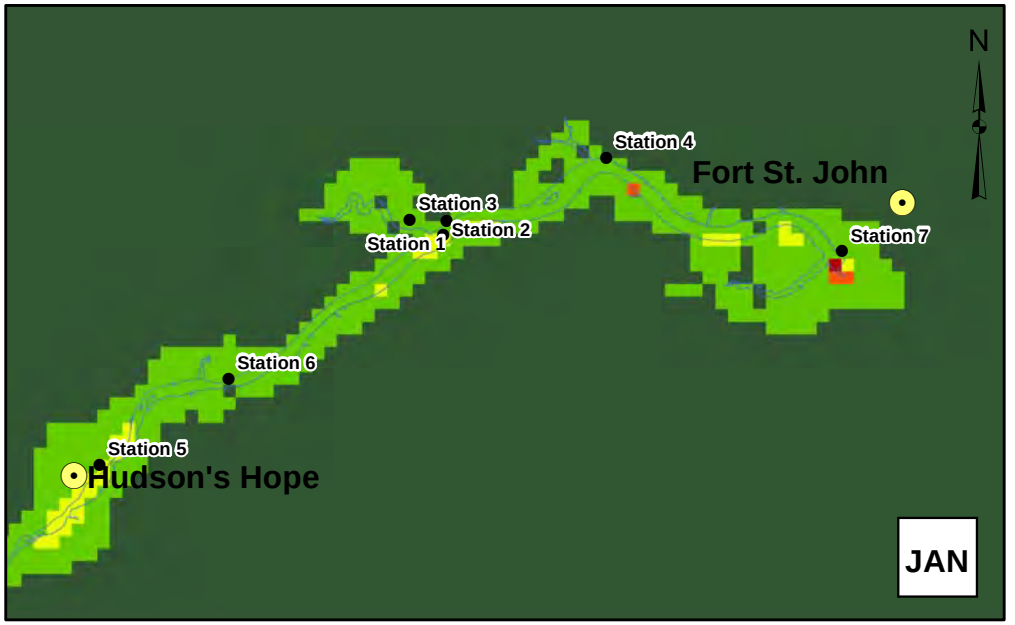

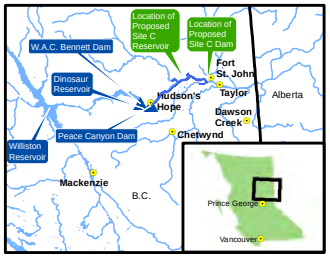

Likelihoods of statistically significant changes in daily mean wind speeds after formation of the reservoir for four calendar months as labelled clockwise from top left: October, January, April, and July. Likelihoods are based on a Bayesian probability calculation, and the terminology follows the definition in IPCC WG (2007).

Legend

- BC Hydro - Site C Stations
- City / District Municipality
- Proposed Reservoir

Likelihood of Change

- extremely likely
- very likely
- likely
- about as likely as not
- unlikely
- very unlikely
- extremely unlikely

1:600,000

0 20 km

Map Notes:
1. Datum/Projection: Customized Lambert Conformal Conic.
2. Proposed Reservoir Area (461.8 m maximum normal elevation) from Digital Elevation Models (DEM) generated from LiDAR data acquired July/August 2006.

SITE C CLEAN ENERGY PROJECT

RWDI BC hydro

Figure 5.3.10
Likelihoods of statistically significant changes in wind speeds - monthly

DATE	Dec. 3, 2012	1016-C14-A5516	R 0

© BC Hydro 2012 - all rights reserved. This map is for information purposes only and accuracy is not guaranteed.

Construction of the Site C Clean Energy Project is subject to required regulatory approvals including environmental certification

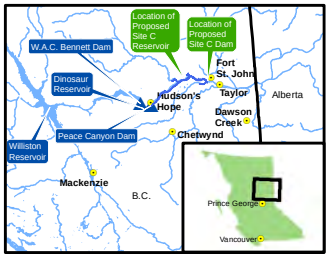

Weather Research and Forecasting (WRF) model-predicted changes in average annual wind speeds (positive are increases).

Map Notes:
1. Datum/Projection: NAD83/UTM Zone 10N
2. Proposed Reservoir Area (461.8 m maximum normal elevation) from Digital Elevation Models (DEM) generated from LiDAR data acquired July/August 2006.

Legend

- BC Hydro - Site C Stations
- City / District Municipality
- Proposed Reservoir

Speed Change (in m/s)

- > 0.30
- 0.25 to 0.30
- 0.20 to 0.25
- 0.15 to 0.20
- 0.10 to 0.15
- 0.05 to 0.10
- -0.05 to 0.05
- -0.10 to -0.05
- -0.15 to -0.10
- -0.20 to -0.15
- -0.25 to -0.20
- -0.30 to -0.25
- < -0.30

N

1:400,000

0 20 km

SITE C CLEAN ENERGY PROJECT

RWDI BC hydro

Figure 5.3.11
Predicted changes in wind speeds - annual

DATE	Dec. 3, 2012	1016-C14-A5517	R 0

© BC Hydro 2012 - all rights reserved. This map is for information purposes only and accuracy is not guaranteed.

Construction of the Site C Clean Energy Project is subject to required regulatory approvals including environmental certification

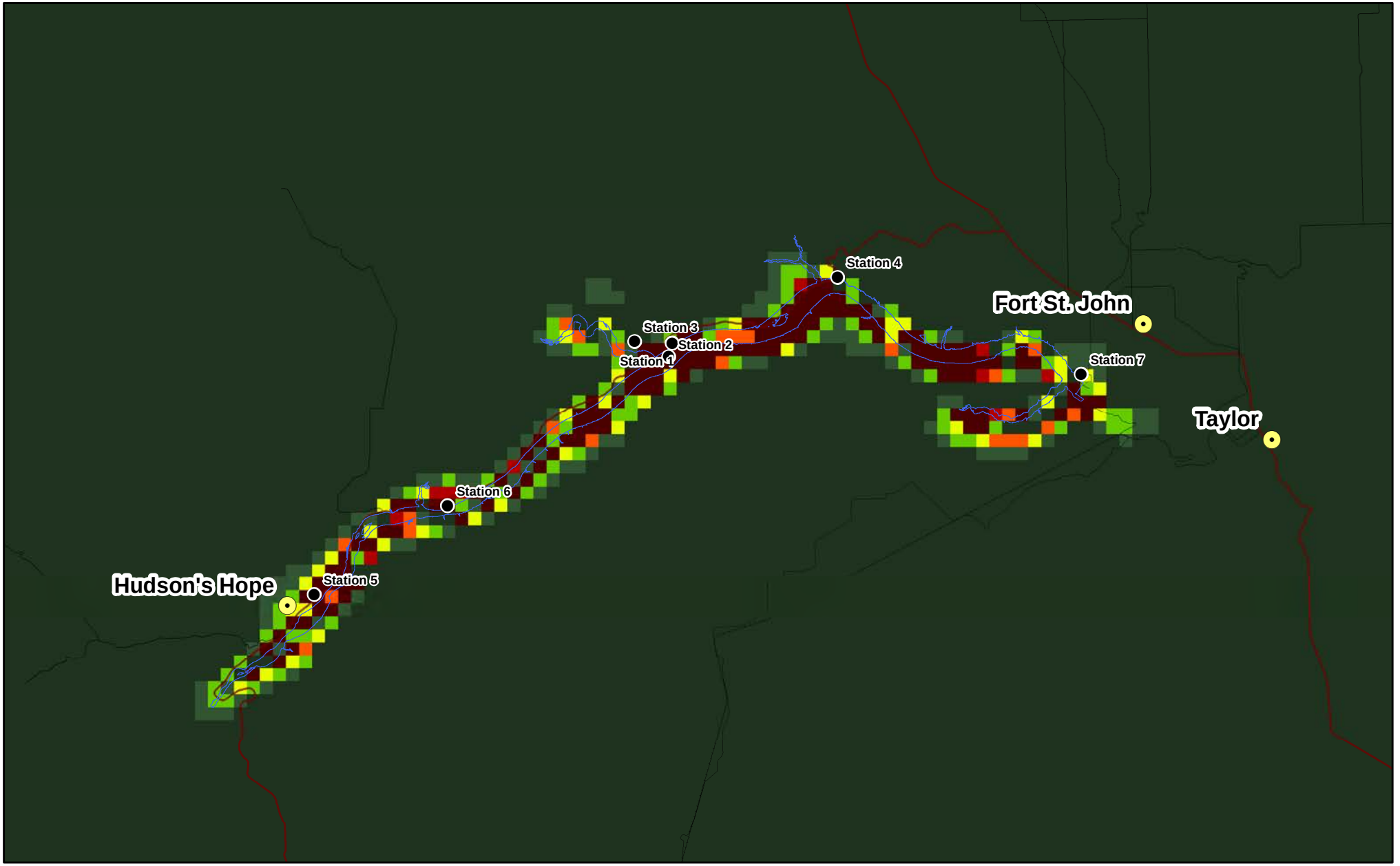

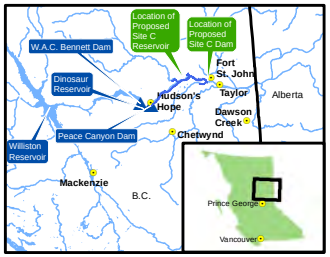

Likelihoods of statistically significant changes in annual averages of daily mean wind speeds after formation of the reservoir. Likelihoods are based on a Bayesian probability calculation, and the terminology follows the definition in IPCC WG (2007).

Legend

- BC Hydro - Site C Stations
- City / District Municipality
- Proposed Reservoir
- Existing Road
- Existing Highway
- Existing Railway

Likelihood of Change

- extremely likely
- very likely
- likely
- about as likely as not
- unlikely
- very unlikely
- extremely unlikely

N

1:400,000

0 20 km

Map Notes:
1. Datum/Projection: Customized Lambert Conformal Conic.
2. Proposed Reservoir Area (461.8 m maximum normal elevation) from Digital Elevation Models (DEM) generated from LiDAR data acquired July/August 2006.

SITE C CLEAN ENERGY PROJECT

RWDI BC hydro

Figure 5.3.12
Likelihoods of statistically significant changes in wind speeds - annual

DATE	Dec. 3, 2012	1016-C14-A5518	R 0

© BC Hydro 2012 - all rights reserved. This map is for information purposes only and accuracy is not guaranteed.

Construction of the Site C Clean Energy Project is subject to required regulatory approvals including environmental certification

5.4 MIXING RATIO

Mixing ratio is the mass of water vapour (in grams) divided by mass of dry air (in kilograms) in a given volume of (moist) air.

Atmospheric moisture was predicted to increase at all locations adjacent to the proposed Site C reservoir. This result was expected as moisture would be more readily available with the presence of the proposed Site C reservoir. Evaporation is expected to increase at the surface and increase atmospheric moisture near the reservoir.

The change in atmospheric moisture is given as the change in water vapour mixing ratio expressed as a ratio of water vapour mass (in grams) per kilogram of dry air at a given pressure. The ‗saturation water vapour mixing ratio' is the total amount of water vapour that can be mixed with dry air. It strongly depends on air temperature and varies between 1 and 20 grams of water vapour per kilogram of dry air over the temperatures range from -15 to 25 degrees Celsius. Typical mixing ratios in the Fort St. John Airport region are on the order less than 1.0 gram per kilogram dry air in winter and over 10 grams per kilogram dry air on a hot humid summer day. The predicted change in atmospheric moisture is given in Table 5.4.1 and reported by season and year.

Table 5.4.1 Seasonal change in water vapour mixing ratio

Difference (Future Case with the Project – Baseline Case)	Spring	Summer	Fall	Winter	Year
Fort St. John Airport	0.00	0.03	0.02	0.00	0.01
Station 1 - Attachie Flat Upper Terrace	0.41	0.86	0.81	0.03	0.53
Station 2 - Attachie Flat Lower Terrace	0.41	0.83	0.85	0.02	0.53
Station 3 - Attachie Flat Plateau	0.00	0.06	0.09	0.00	0.04
Station 4 - Bear Flat	0.38	0.90	0.79	0.02	0.52
Station 5 - Hudson's Hope	-0.02	0.03	0.12	0.04	0.04
Station 6 - Farrell Creek	0.00	0.03	0.10	0.02	0.04
Station 7 - Site C Dam	0.41	0.98	0.77	0.02	0.55

NOTES:

All values in grams of water vapour per kilogram of dry air.

[e] Fort St. John Airport station observations.

The greatest changes are predicted to occur in the summer at Bear Flat and Proposed Site C Dam where changes were found to be statistically significant. The largest change in humidity is predicted to occur in summer at proposed Site C Dam with an increase of 0.98 gram per kilogram dry air or about a 15% increase in atmospheric moisture. The dam site area is expected to experience the greatest increase in atmospheric moisture given the reservoir is the widest at its terminus and has the largest surface area of water available for evaporation.

Temperatures in the fall are lower than in the summer and therefore less water vapour can mix with the air. However, during the baseline period, precipitation in the fall was less than half of

summer precipitation. Therefore, the air was drier during the fall permitting similarly large amounts of water vapour to mix with the air as in the summer.

Little to no change is predicted to occur in the winter at all locations. Most of the reservoir is ice covered in the winter and therefore does not permit evaporation. The greatest increase in winter mixing ratio is predicted at Hudson‘s Hope which has the least ice cover. In the other seasons, changes are predicted at Attachie Flat Upper Terrace, Attachie Flat Lower Terrace, Bear Flat and Site C. As expected, at the locations that are not adjacent to the reservoir (Fort St. John Airport, Attachie Flat Plateau, Hudson‘s Hope and Farrell Creek) mixing ratios are not predicted to change.

The variation of change in daily water vapour mixing ratio throughout the year is shown in Figure 5.4.1. It is evident that Attachie Flat Upper Terrace, Attachie Flat Lower Terrace, Bear Flat and Site C show the most variation of change throughout the year. It can be seen that the change in humidity is mostly positive and that the largest change occurs during the warm summer and the dry fall. Large increases in humidity occur during the warm season when the certain energy balance components (i.e., incoming solar radiation and sensible and latent heat flux) are the highest and when air temperature is the highest. These conditions allow more water to be evaporated and allow the air to hold more water vapour, respectively. In the fall, incoming solar radiation and air temperatures are lower, but the air is drier and therefore capable of mixing similarly large amounts of water vapour as in the summer.

A full spatial view of the changes in mixing ratio is provided in Figure 5.4.2 and the associated likelihoods of the statistical significance of the changes are displayed in Figure 5.4.3. Increases of up to 1 gram per kilogram dry air (roughly 10% of the saturation water vapour mixing ratio) are predicted along the entire proposed reservoir in October (very likely and extremely likely statistically significant). This also corresponds to the period of greatest evaporation of the reservoir surface, as discussed in section 5.7. In other months, similar increases are predicted to occur at shorter sections along the reservoir. These changes all tend to be likely to extremely likely statistically significant. Decreases of up to 0.4 gram per kilogram dry air are predicted at the southwestern end of the reservoir near Hudson‘s Hope in July. The latter decreases were determined to be statistically insignificant.

After averaging over the entire year (Figure 5.4.4), the increase in water vapour mixing ratio is more smoothly distributed over the entire reservoir and less than 0.8 gram per kilogram dry air. The annual average increase is mostly dominated by summer and fall increases and is less than 10% of the total amount of water vapour that can be mixed with dry air. This spatially homogeneous increase of mixing ratio over the proposed reservoir is extremely likely statistically significant (Figure 5.4.5).

Mixing ratio at elevations above ground level was also examined as this may be of concern to some transportation activities. Figure 5.4.6, Figure 5.4.7 and Figure 5.4.8 show the changes in monthly average mixing ratio at three different heights above ground. The heights for which WRF model results are presented were provided by Transport Canada as being of importance to airport operations.

In terms of pressure, the heights examined correspond to approximately At 900 hPa. At this pressure and at 0 degrees Celsius, the saturated mixing ratio is 4.25 g/kg. This value provides a reference for the magnitude of the predicted changes. At all levels extracted, increases or decreases predicted by the WRF model are less than 0.04 g/kg, which is less than 1% of the saturated mixing ratio and at most a few percent of typical mixing ratios at these levels. Such difference would be unobservable in measurement and therefore should not represent any meaningful change in mixing ratio.

It is important to note that for some area and times in the plots the mixing ratios at these heights are actually decreased by the creation of the reservoir. As the changes are minimal some of these decreases are just random noise within the model calculation. However, it is feasible that the reservoir could result in lower mixing ratio at elevations above ground.

The vast majority of sources of atmospheric water vapour lie on the Earth's surface as this is where most evaporation occurs. As a result, mixing ratio is usually much higher in the boundary layer than in the free troposphere above. As noted previously, the future water surface would tend to be cooler than existing surface in summer and warmer than the existing surface in winter. In turn this means that the boundary layer over the future water surface would tend to be deeper in winter and shallower in summer, as the depth of the boundary is driven by surface heating. Therefore a given level above ground over the future reservoir may see more free tropospheric (drier air) influence in summer and more boundary layer (moister air) due to the lower average boundary layer resulting from the cooler surface underneath. If a given level above ground sees more influence of drier air masses due to a reduced boundary layer, then the reservoir may result in lower mixing ratios than exist now. Similarly, increases at levels above ground may be greatest when a warmer surface results in a deeper boundary layer.

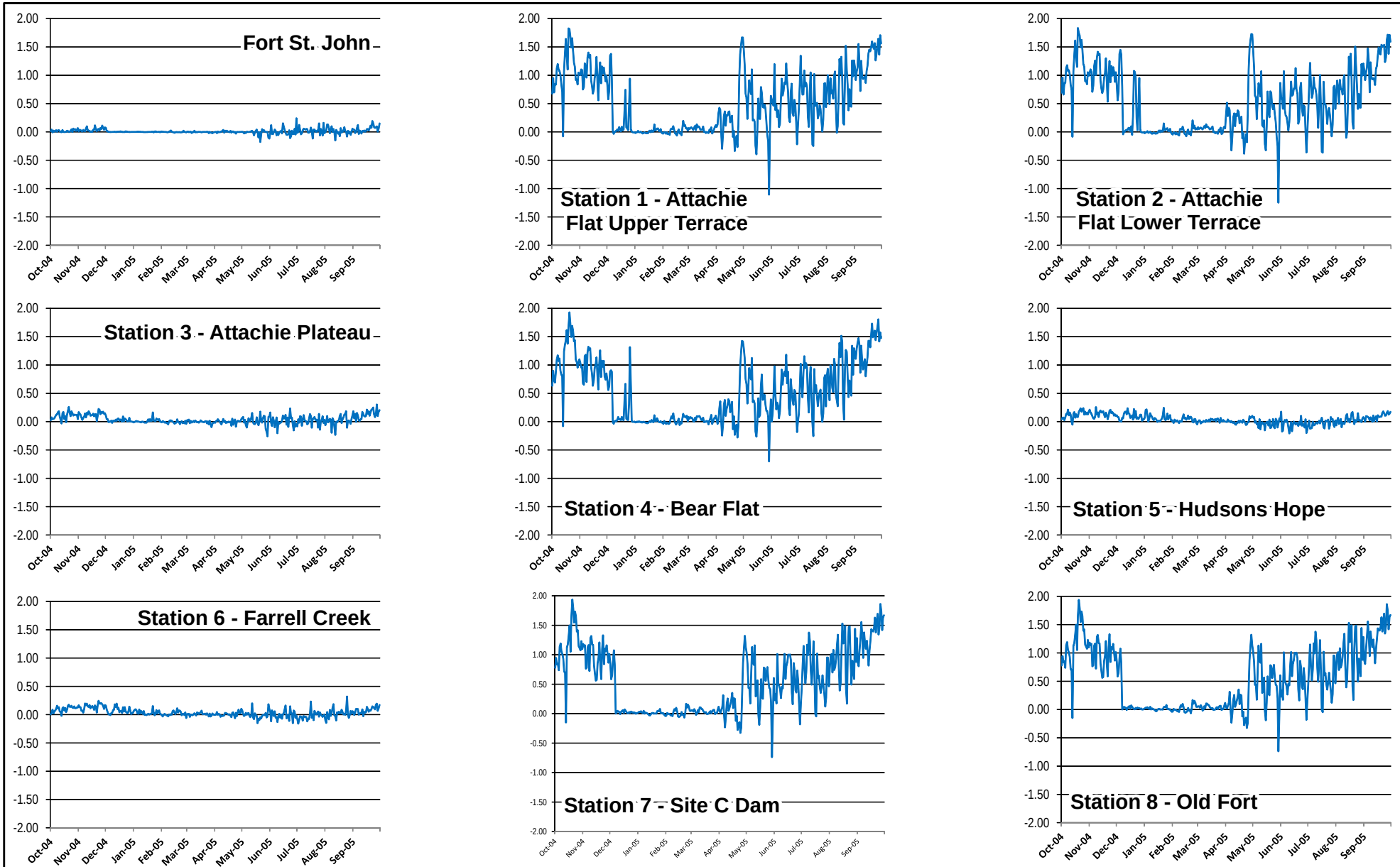

Predicted difference in daily average water vapour (g of water/ kg of air) content at each location from October 2004 to September 2005 (Future Case with Project minus Baseline Case)

SITE C CLEAN ENERGY PROJECT

RWDI BC hydro

Figure 5.4.1
Changes in daily average water vapour mixing ratio

DATE	Dec. 3, 2012		R 0

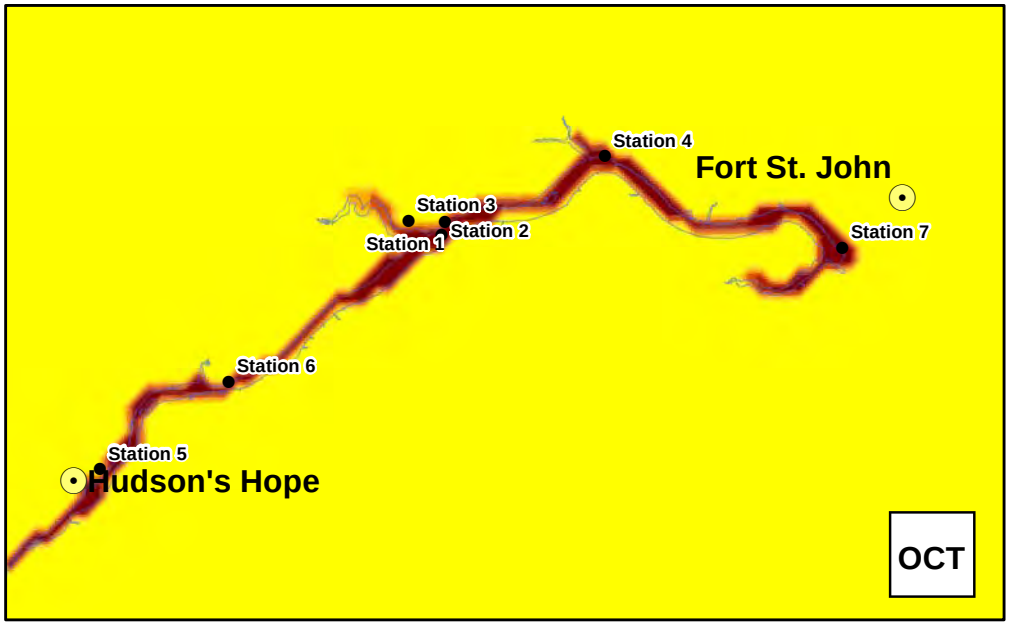

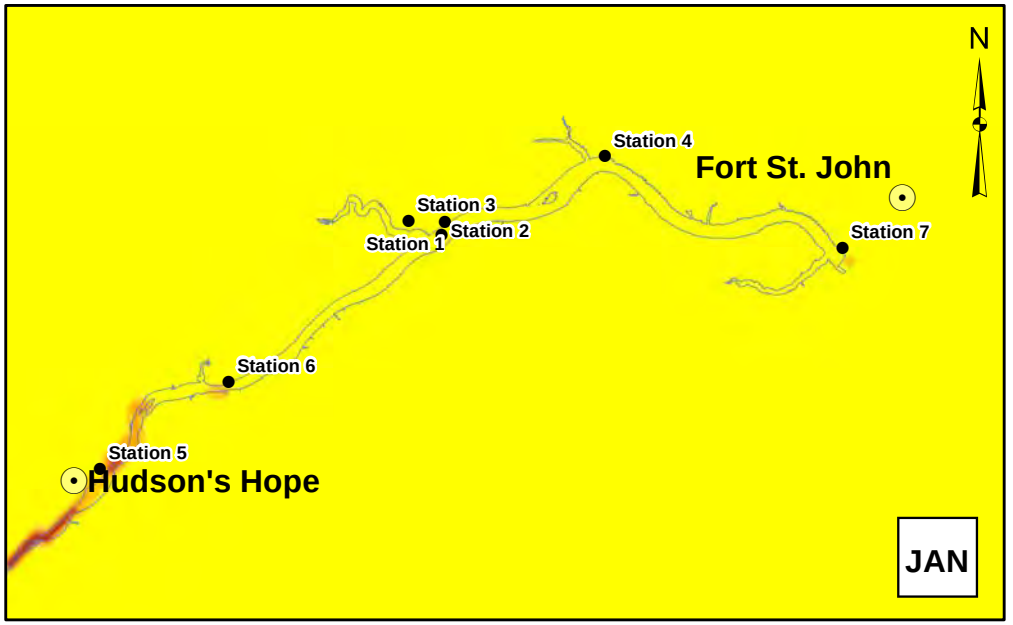

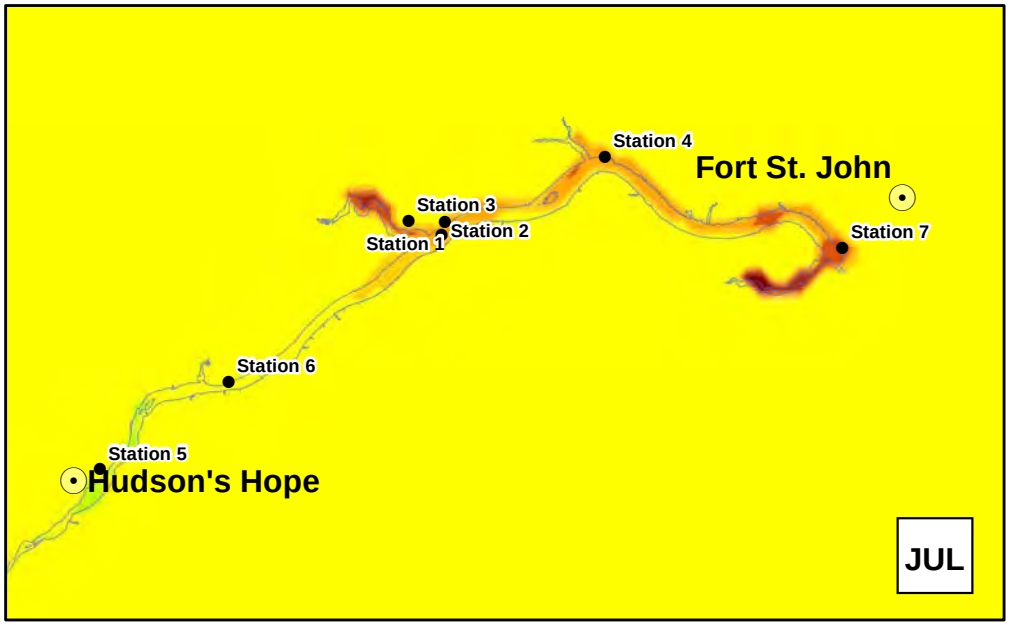

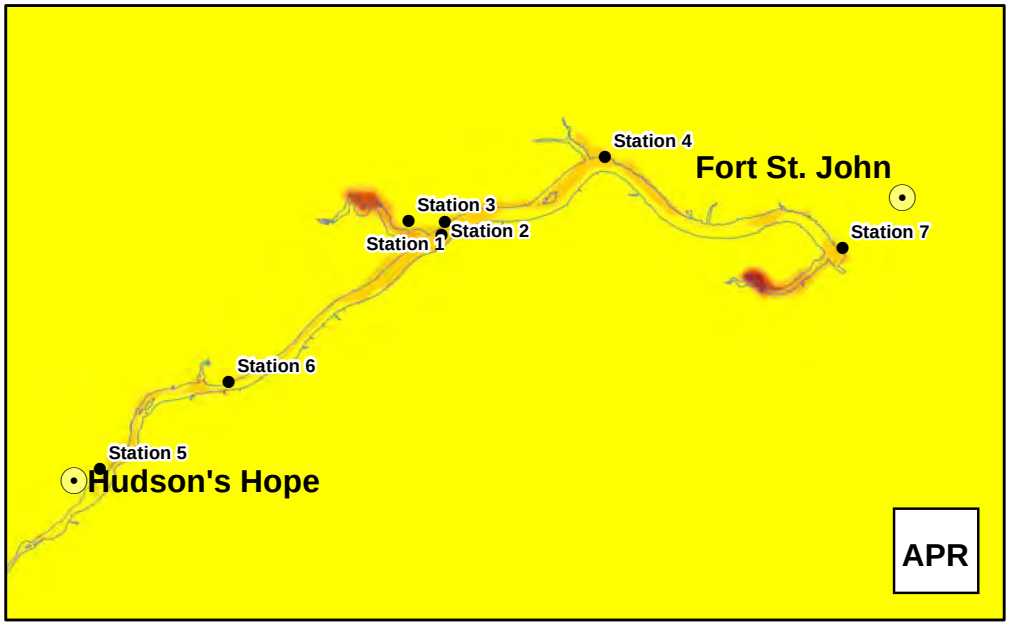

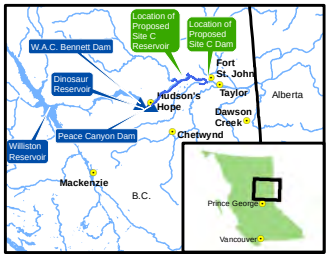

Weather Research and Forecasting (WRF) model-predicted changes in average monthly water vapour mixing ratio after formation of the reservoir (positive are increases) for four calendar months as labelled clockwise from top left: October, January, April, and July.

Map Notes:
1. Datum/Projection: NAD83/UTM Zone 10N
2. Proposed Reservoir Area (461.8 m maximum normal elevation) from Digital Elevation Models (DEM) generated from LiDAR data acquired July/August 2006.

Legend

- BC Hydro - Site C Stations
- City / District Municipality
- Proposed Reservoir

Mixing Ratio (in g/kg)

- > 1.2
- 1.0 to 1.2
- 0.8 to 1.0
- 0.6 to 0.8
- 0.4 to 0.6
- 0.2 to 0.4
- -0.2 to 0.2
- -0.4 to -0.2
- -0.6 to -0.4
- -0.8 to -0.6
- -1.0 to -0.8
- -1.2 to -1.0
- < -1.2

1:600,000

0 20 km

SITE C CLEAN ENERGY PROJECT

RWDI BC hydro

Figure 5.4.2
Predicted changes in mixing ratio - monthly

DATE	Dec. 3, 2012	1016-C14-A5519	R 0

© BC Hydro 2012 - all rights reserved. This map is for information purposes only and accuracy is not guaranteed.

Construction of the Site C Clean Energy Project is subject to required regulatory approvals including environmental certification

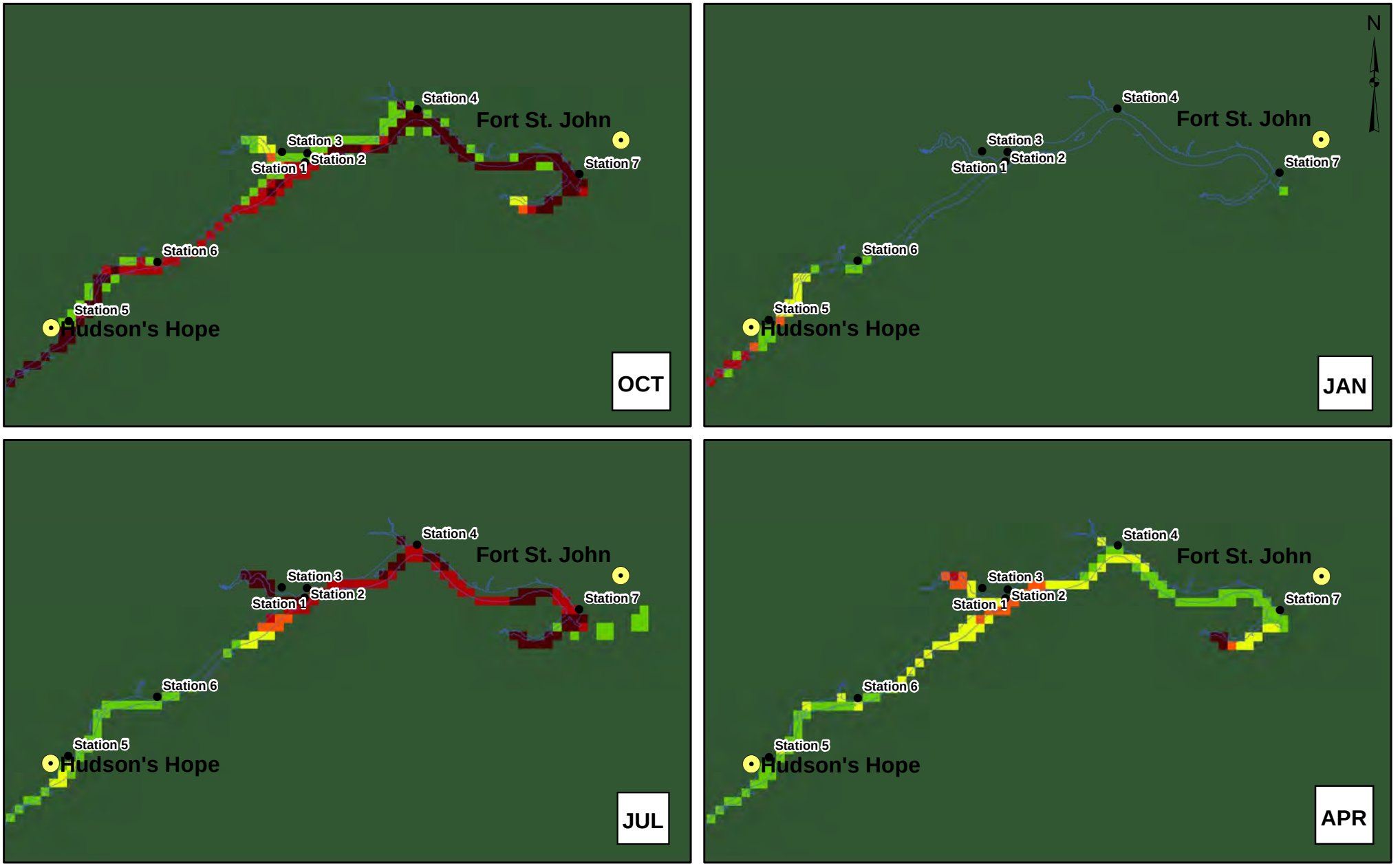

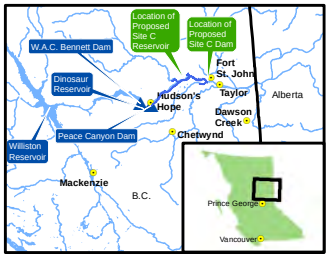

Likelihoods of statistically significant changes in daily mean water vapour mixing ratio after formation of the reservoir for four calendar months as labelled clockwise from top left: October, January, April, and July. Likelihoods are based on a Bayesian probability calculation, and the terminology follows the definition in IPCC WG (2007).

Legend

- BC Hydro - Site C Stations
- City / District Municipality
- Proposed Reservoir

Likelihood of Change

- extremely likely
- very likely
- likely
- about as likely as not
- unlikely
- very unlikely
- extremely unlikely

1:600,000

0 20 km

Map Notes:
1. Datum/Projection: Customized Lambert Conformal Conic.
2. Proposed Reservoir Area (461.8 m maximum normal elevation) from Digital Elevation Models (DEM) generated from LiDAR data acquired July/August 2006.

SITE C CLEAN ENERGY PROJECT

RWDI BC hydro

Figure 5.4.3
Likelihoods of statistically significant changes in mixing ratio - monthly

DATE	Dec. 3, 2012	1016-C14-A5520	R 0

© BC Hydro 2012 - all rights reserved. This map is for information purposes only and accuracy is not guaranteed.

Construction of the Site C Clean Energy Project is subject to required regulatory approvals including environmental certification

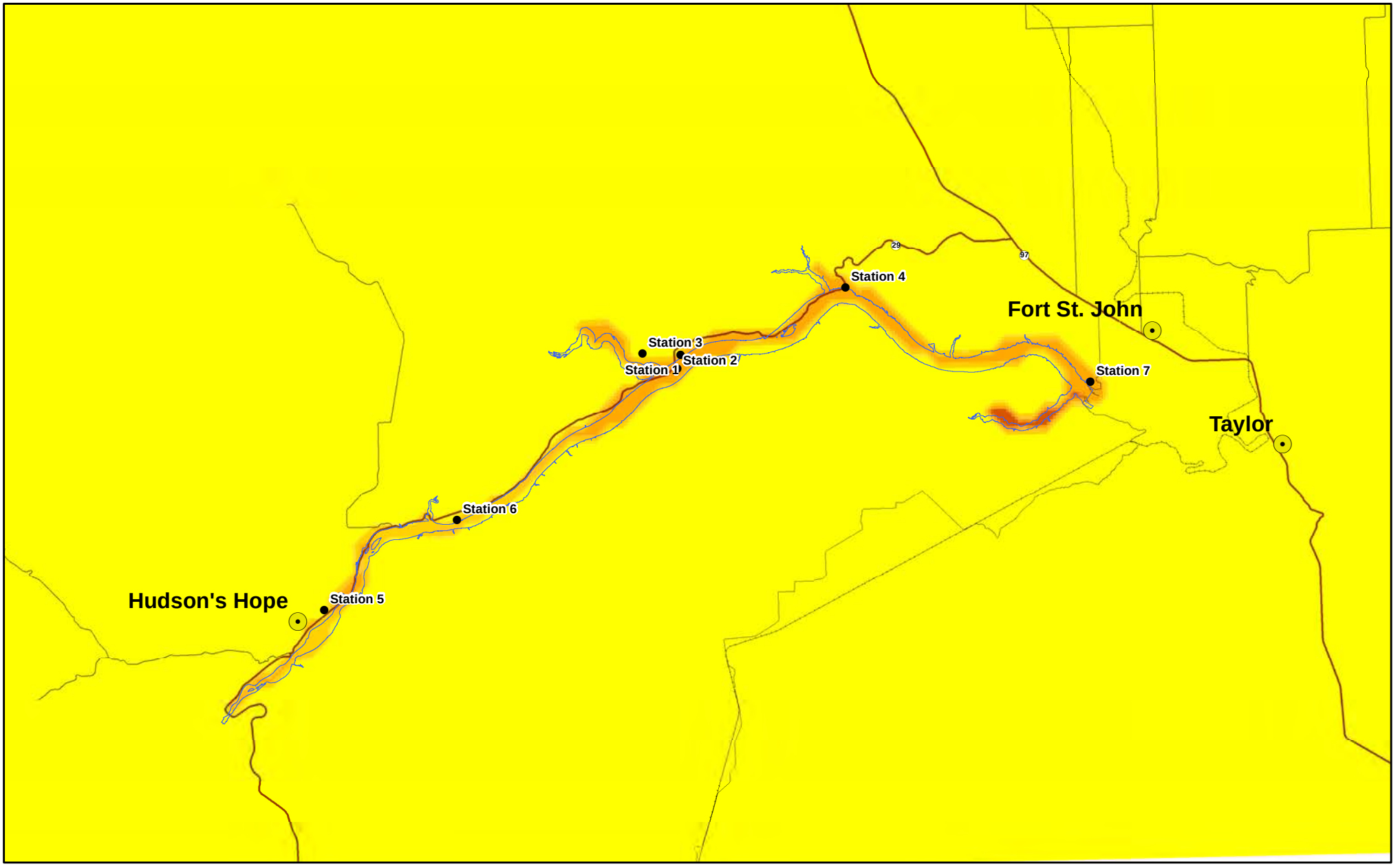

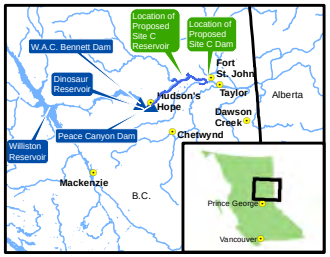

Weather Research and Forecasting (WRF)model-predicted changes in average annual water vapour mixing ratio after formation of the reservoir (positive are increases).

Map Notes:
1. Datum/Projection: NAD83/UTM Zone 10N
2. Proposed Reservoir Area (461.8 m maximum normal elevation) from Digital Elevation Models (DEM) generated from LiDAR data acquired July/August 2006.

Legend

- BC Hydro - Site C Stations
- City / District Municipality
- Proposed Reservoir

Mixing Ratio (in g/kg)

- > 1.2
- 1.0 to 1.2
- 0.8 to 1.0
- 0.6 to 0.8
- 0.4 to 0.6
- 0.2 to 0.4
- -0.2 to 0.2
- -0.4 to -0.2
- -0.6 to -0.4
- -0.8 to -0.6
- -1.0 to -0.8
- -1.2 to -1.0
- < -1.2

N

1:400,000

0 20 km

SITE C CLEAN ENERGY PROJECT

RWDI BC hydro

Figure 5.4.4
Predicted changes in mixing ratio - annual

DATE	Dec. 3, 2012	1016-C14-A5521	R 0

© BC Hydro 2012 - all rights reserved. This map is for information purposes only and accuracy is not guaranteed.

Construction of the Site C Clean Energy Project is subject to required regulatory approvals including environmental certification

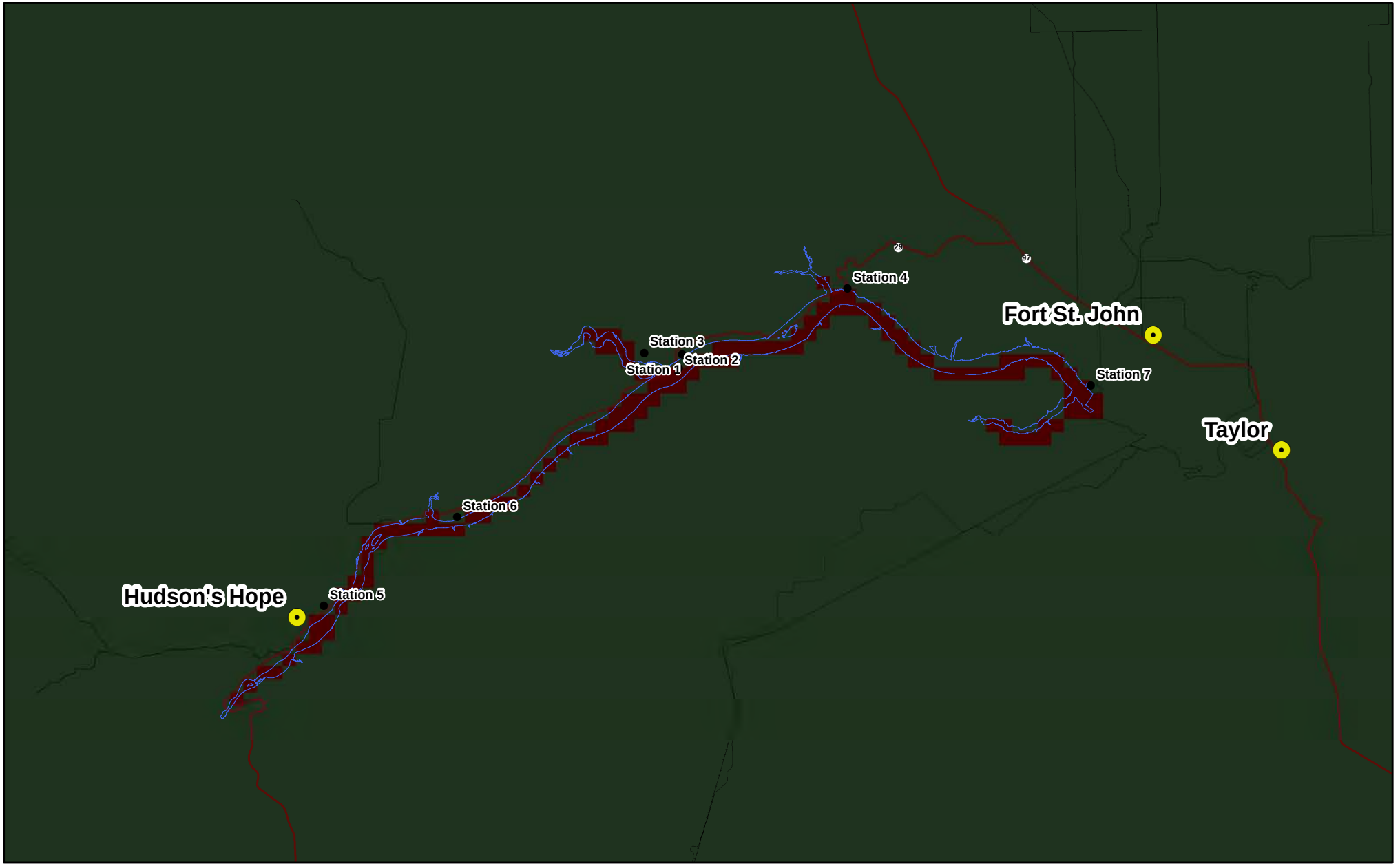

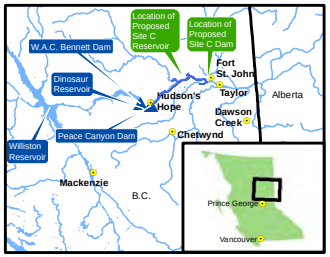

Likelihoods of statistically significant changes in annual averages of daily mean water vapour mixing ratio after formation of the reservoir. Likelihoods are based on a Bayesian probability calculation, and the terminology follows the definition in IPCC WG (2007).

Map Notes:
1. Datum/Projection: Customized Lambert Conformal Conic.
2. Proposed Reservoir Area (461.8 m maximum normal elevation) from Digital Elevation Models (DEM) generated from LiDAR data acquired July/August 2006.

Legend

- BC Hydro - Site C Stations
- City / District Municipality
- Proposed Reservoir
- Existing Road
- Existing Highway
- Existing Railway

Likelihood of Change

- extremely likely
- very likely
- likely
- about as likely as not
- unlikely
- very unlikely
- extremely unlikely

N

1:400,000

0 20 km

SITE C CLEAN ENERGY PROJECT

RWDI BC hydro

Figure 5.4.5
Likelihoods of statistically significant changes in mixing ratio - annual

DATE	Dec. 3, 2012	1016-C14-A5522	R 0

© BC Hydro 2012 - all rights reserved. This map is for information purposes only and accuracy is not guaranteed.

Construction of the Site C Clean Energy Project is subject to required regulatory approvals including environmental certification

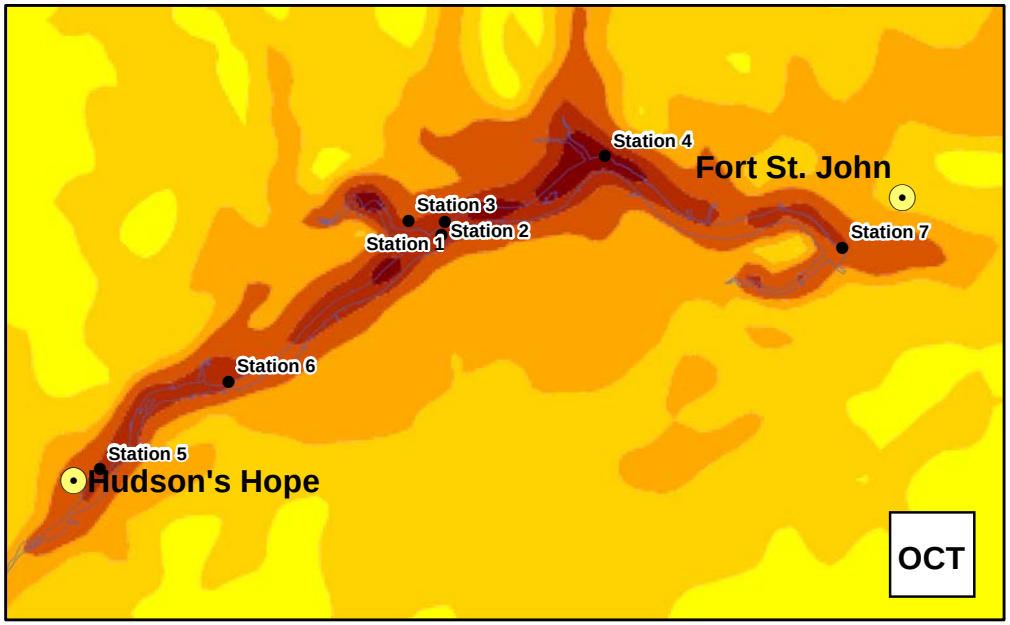

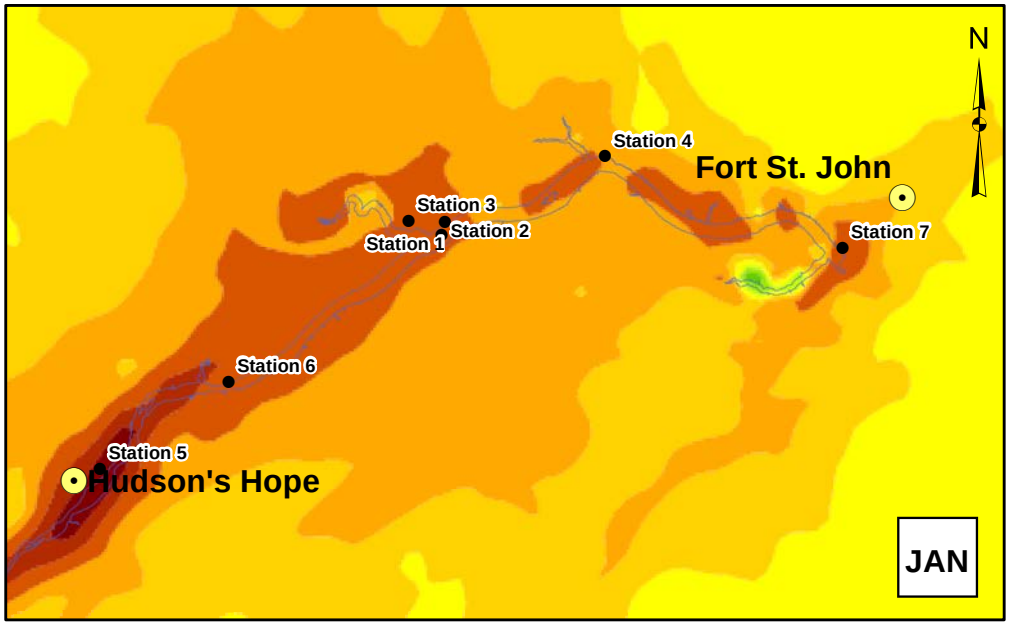

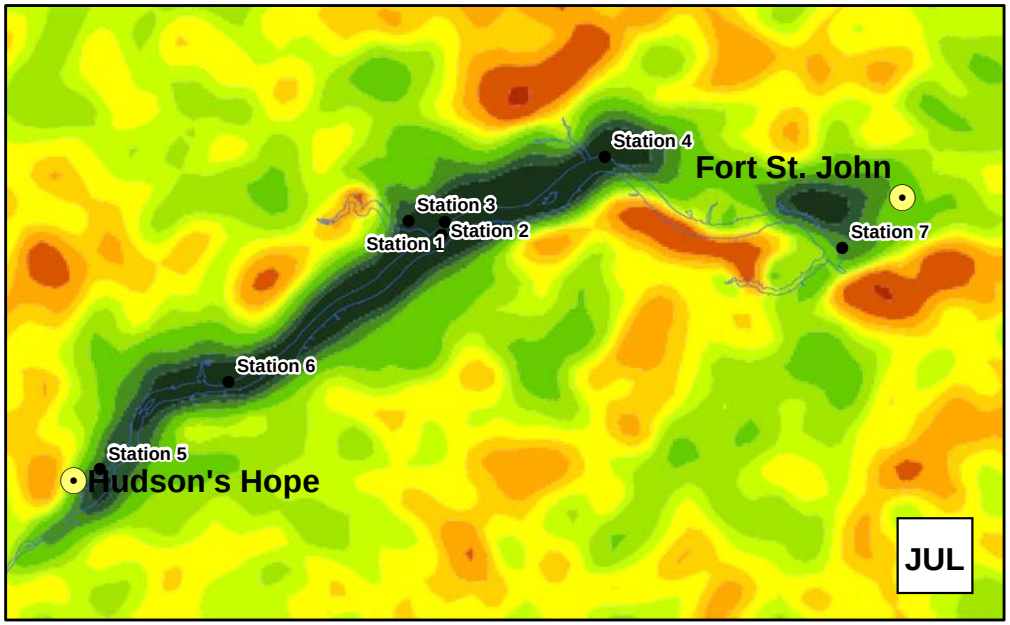

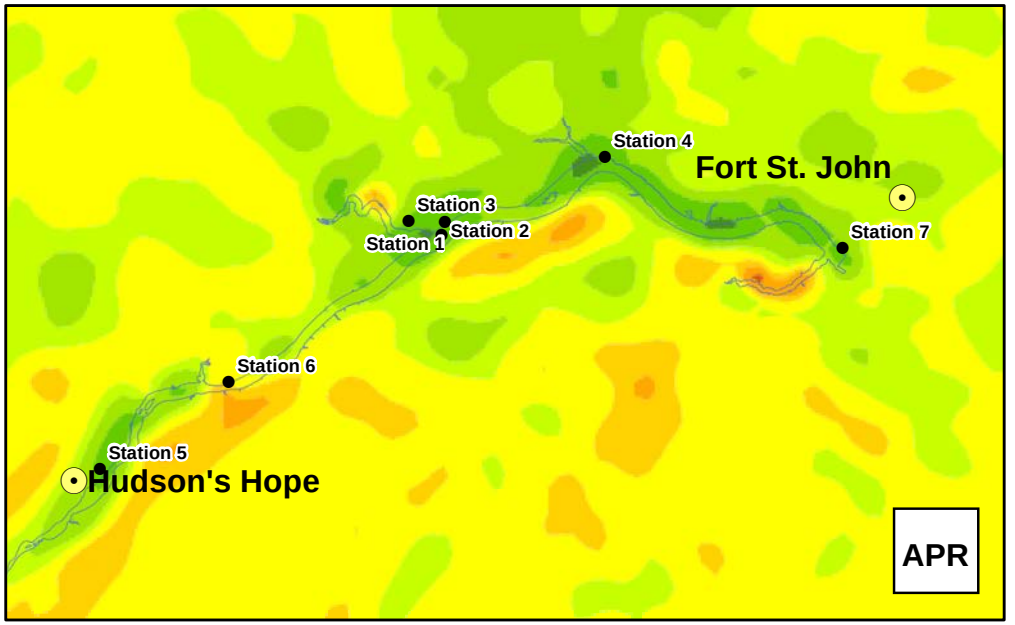

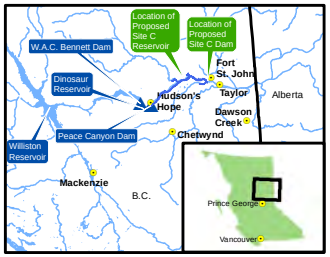

Weather Research and Forecasting (WRF) model-predicted changes in average monthly water vapour mixing ratio above ground level after formation of the reservoir (positive are increases) for four calendar months as labelled clockwise from top left: October, January, April, and July. Results are from WRF vertical grid level 5, corresponding to approximately 2640 feet above sea level.

Map Notes:
1. Datum/Projection: NAD83/UTM Zone 10N
2. Proposed Reservoir Area (461.8 m maximum normal elevation) from Digital Elevation Models (DEM) generated from LiDAR data acquired July/August 2006.

Legend

- BC Hydro - Site C Stations
- City / District Municipality
- Proposed Reservoir

Mixing Ratio Change (in g/kg)

- < -0.04
- -0.03 to -0.04
- -0.02 to -0.03
- -0.01 to -0.02
- -0.005 to -0.01
- -0.002 to -0.005
- 0.002 to -0.002
- 0.005 to 0.002
- 0.01 to 0.005
- 0.02 to 0.01
- 0.03 to 0.02
- 0.04 to 0.03
- > 0.04

1:600,000

0 20 km

SITE C CLEAN ENERGY PROJECT

RWDI BC hydro

Figure 5.4.6
Estimated changes in mixing ratio 2640 feet asl - monthly

DATE	Dec. 3, 2012	1016-C14-A5520-1	R 0

© BC Hydro 2012 - all rights reserved. This map is for information purposes only and accuracy is not guaranteed.

Construction of the Site C Clean Energy Project is subject to required regulatory approvals including environmental certification

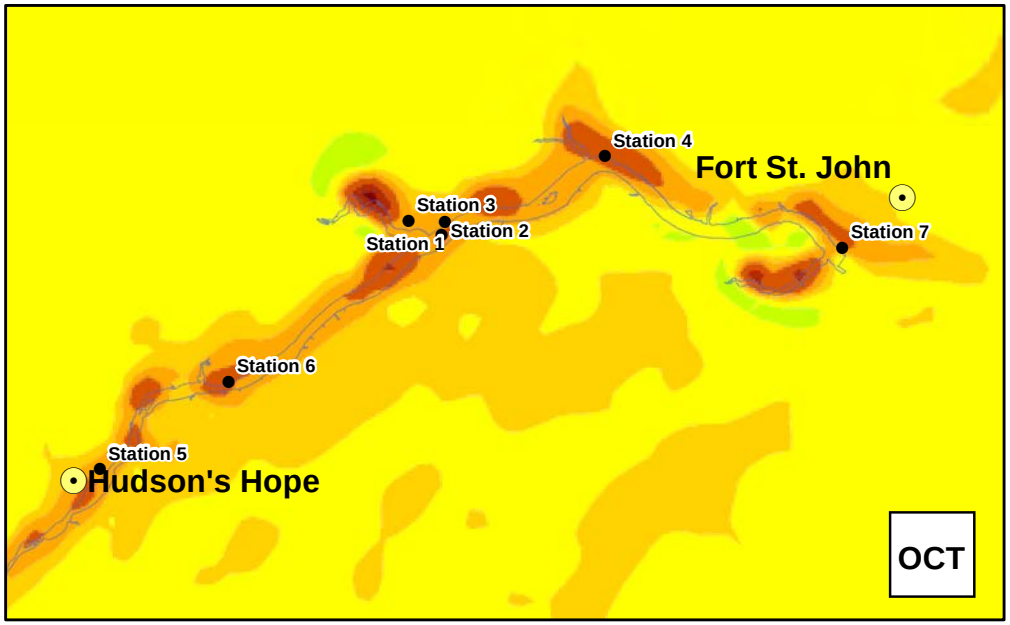

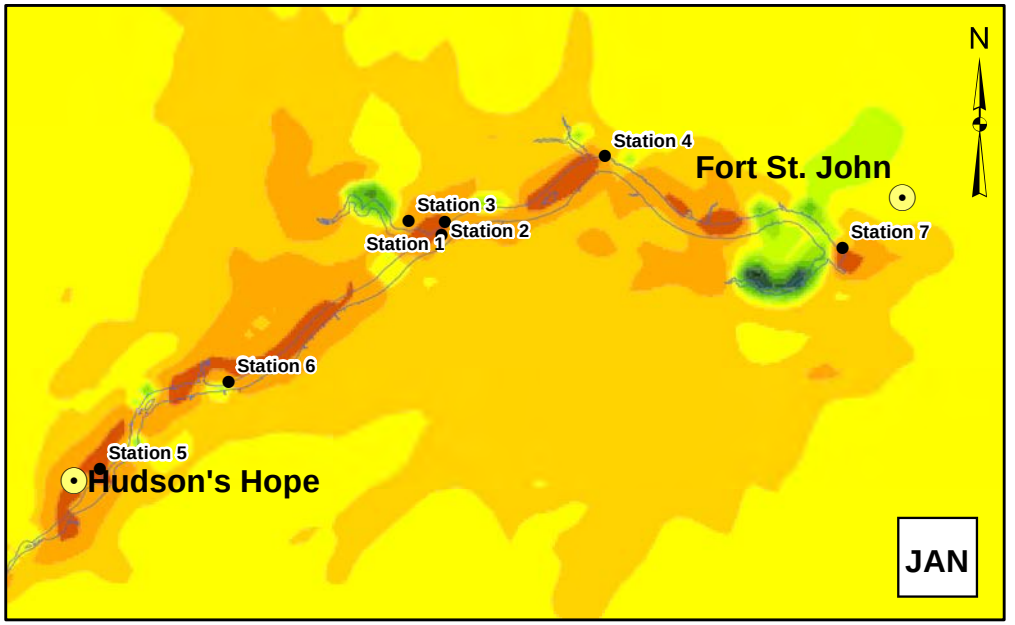

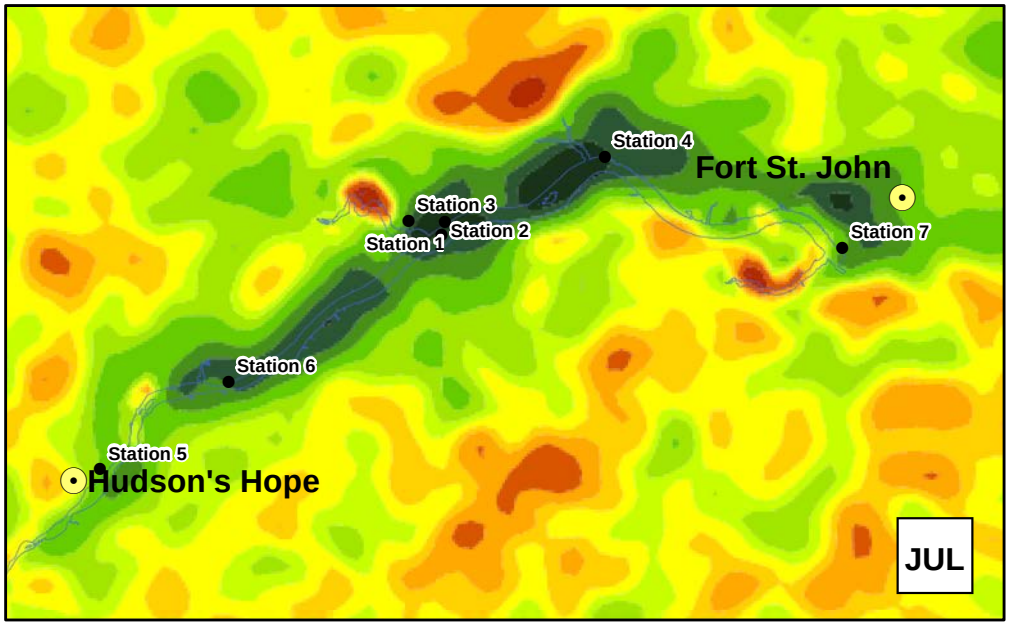

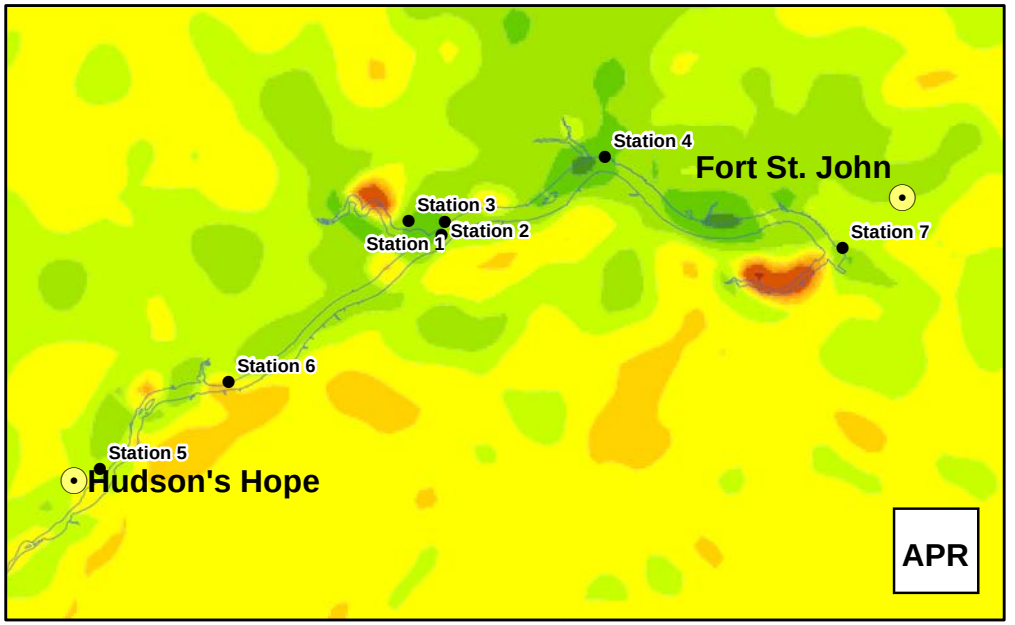

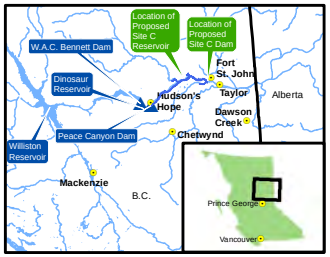

Weather Research and Forecasting (WRF) model-predicted changes in average monthly water vapour mixing ratio above ground level after formation of the reservoir (positive are increases) for four calendar months as labelled clockwise from top left: October, January, April, and July. Results are from WRF vertical grid level 7, corresponding to approximately 3000 feet above sea level.

Map Notes:
1. Datum/Projection: NAD83/UTM Zone 10N
2. Proposed Reservoir Area (461.8 m maximum normal elevation) from Digital Elevation Models (DEM) generated from LiDAR data acquired July/August 2006.

Legend

- BC Hydro - Site C Stations
- City / District Municipality
- Proposed Reservoir

Mixing Ratio Change (in g/kg)

- < -0.04
- -0.03 to -0.04
- -0.02 to -0.03
- -0.01 to -0.02
- -0.005 to -0.01
- -0.002 to -0.005
- 0.002 to -0.002
- 0.005 to 0.002
- 0.01 to 0.005
- 0.02 to 0.01
- 0.03 to 0.02
- 0.04 to 0.03
- > 0.04

1:600,000

0 20 km

SITE C CLEAN ENERGY PROJECT

RWDI BC hydro

Figure 5.4.7
Estimated changes in mixing ratio 3000 feet asl - monthly

DATE	Dec. 3, 2012	1016-C14-A5520-2	R 0

© BC Hydro 2012 - all rights reserved. This map is for information purposes only and accuracy is not guaranteed.

Construction of the Site C Clean Energy Project is subject to required regulatory approvals including environmental certification

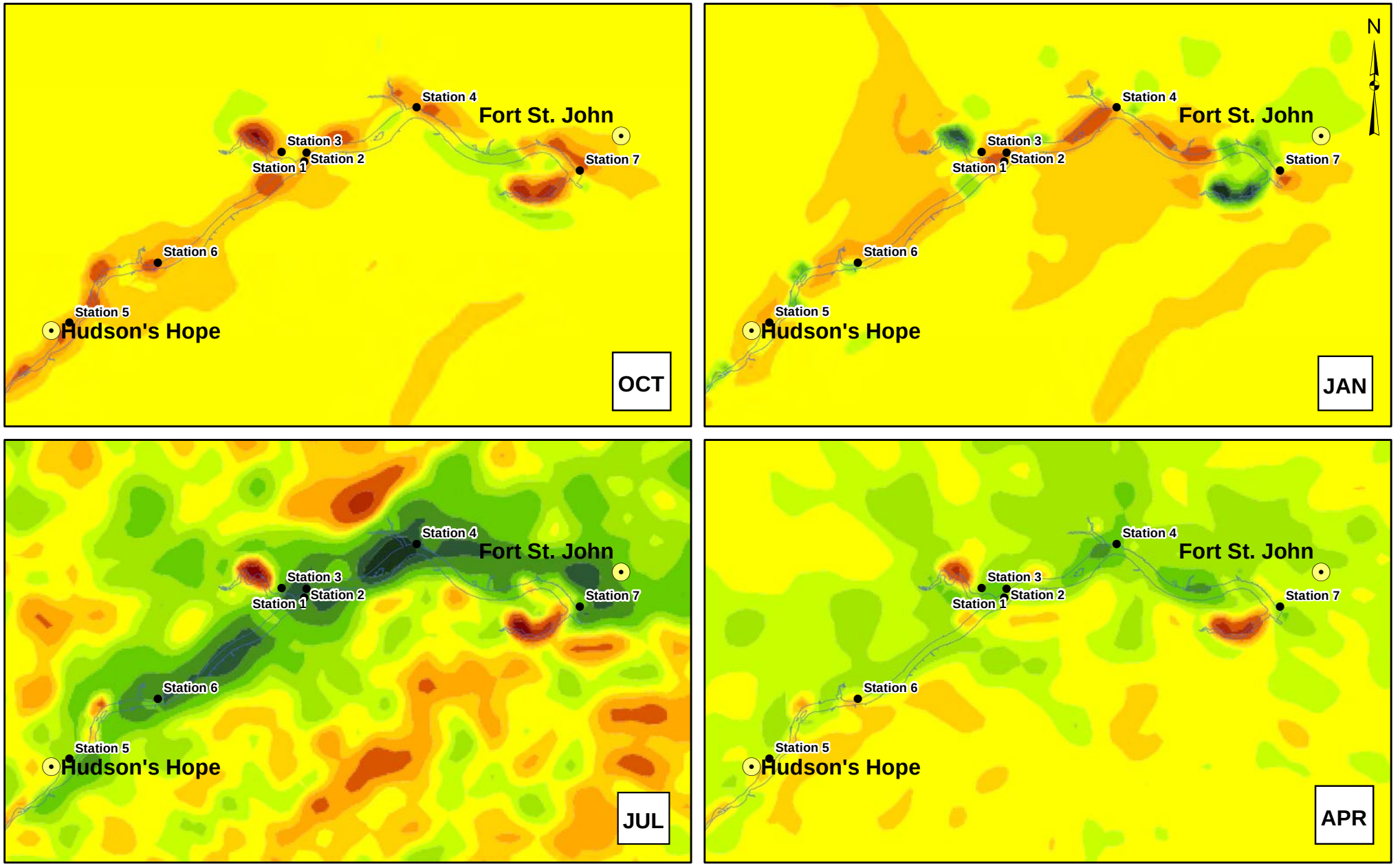

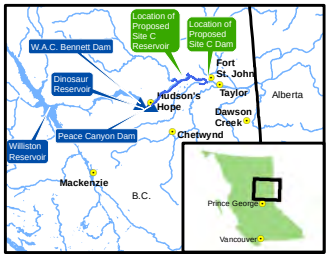

Weather Research and Forecasting (WRF) model-predicted changes in average monthly water vapour mixing ratio above ground level after formation of the reservoir (positive are increases) for four calendar months as labelled clockwise from top left: October, January, April, and July. Results are from WRF vertical grid level 8, corresponding to approximately 3300 feet above sea level.

Map Notes:
1. Datum/Projection: NAD83/UTM Zone 10N
2. Proposed Reservoir Area (461.8 m maximum normal elevation) from Digital Elevation Models (DEM) generated from LiDAR data acquired July/August 2006.

Legend

- BC Hydro - Site C Stations
- City / District Municipality
- Proposed Reservoir

Mixing Ratio Change (in g/kg)

- < -0.04
- -0.03 to -0.04
- -0.02 to -0.03
- -0.01 to -0.02
- -0.005 to -0.01
- -0.002 to -0.005
- 0.002 to -0.002
- 0.005 to 0.002
- 0.01 to 0.005
- 0.02 to 0.01
- 0.03 to 0.02
- 0.04 to 0.03
- > 0.04

1:600,000

0 20 km

SITE C CLEAN ENERGY PROJECT

RWDI BC hydro

Figure 5.4.8
Estimated changes in mixing ratio 3300 feet asl - monthly

DATE	Dec. 3, 2012	1016-C14-A5520-3	R 0

© BC Hydro 2012 - all rights reserved. This map is for information purposes only and accuracy is not guaranteed.

Construction of the Site C Clean Energy Project is subject to required regulatory approvals including environmental certification

5.5 FOG

For this study two intensities of fog were examined: normal and heavy fog. The criterion for occurrence of normal fog is the presence of cloud water and rainwater that reduces visibility to one kilometre or less. Heavy fog occurs when the visibility is reduced to 500 m or less. Table 5.5.1 shows the number of hours in which fog is predicted to occur for both the Baseline Case and Future Case with the Project. Hours of heavy fog are provided in Table 5.5.2. The frequency of fog is presented as total hours of predicted fog. The predicted change in fog as a result of the proposed Site C reservoir is given in terms of new fog events (increase) or fog events that are no longer predicted to occur (decrease).

The number of normal and heavy fog hours is predicted to decrease at most locations with the addition of the proposed Site C reservoir. The number of normal fog hours is predicted to decrease at five out of nine locations, with increases at Fort St. John Airport (seven hours per year), Taylor Bridge (eight hours per year), Hudson‘s Hope (one hour per year), and Attachie Flat Lower (nine hours per year) locations. The number of heavy fog hours decreases at most locations except Fort St. John Airport, where an increase of six hours per year is predicted, and Taylor Bridge where an increase of 118 hours is predicted.

The decrease in normal fog hours varies from four to 30 hours per year, with the higher decreases at Bear Flat (30 hours), Attachie Plateau (25 hours) and Site C Dam (18 hours) locations. The number of decreased heavy fog hours varies from two to 33 hours per year with five locations having a decrease greater than 10 hours.

At the Dam location, 18 and 20 fewer hours per year of normal and heavy fog are predicted, respectively. At Fort St. John Airport, seven additional hours per year of normal fog and six additional hours per year of heavy fog are predicted, respectively. The Taylor location experiences similar increases in fog hours, but a larger increase in heavy fog. This appears to be the result of more hours that were previously fog now becoming heavy fog than at other locations. e.g., an hour where the visibility was 550 metres in the Baseline Case that becomes 450 metres in the Future Case with the Project cause a change from fog to heavy fog, but a change from 650 metres to 550 metres still remains classified as fog.

Formation of fog depends on both temperature and water vapour mixing ratio. In general, increasing the annual average water vapour mixing ratio would suggest a concomitant increase in occurrence of fog. However, this is complicated by the fact that as air is warmed it can hold more water. As such, increases in water content alone are not necessarily enough to increase fog occurrence, particularly if the increase in water content is paired with a simultaneous increase in temperature that also increases the total water vapour holding capacity. For areas and periods where fog decreases, any increases in water content are dominated by a greater increase in vapour capacity from increased temperatures.

There is a general pattern of decreases in fog near the reservoir and increases in fog further away. Close to the reservoir, the increase in temperature is the dominant factor, so the air can hold more water and the number of fog hours is decreased, even though the total amount of

water in the air is increased. As the air moves away from the reservoir, the influence of the reservoir on temperature is lost and the air cools to be the same as without the reservoir. However, the increased water content remains and thus there is increased fog.

Even so, as the formation of fog is directly dependent on temperature and water vapour mixing ratio, if the changes in these underlying quantities are minimal, then changes in occurrence of fog, either increases or decreases, should also be minimal.

A statistical significance test was not performed on fog as the time series of prediction did not allow for an appropriate test to be performed. At all locations except Taylor Bridge the maximum change in either normal or heavy fog amount to less than 0.5% of the total hours in a year. The Fort St. John Airport and Taylor location do not coincide with areas where statistically significant changes in either precipitation or mixing ratio were predicted.

Table 5.5.1 Predicted change in fog from Baseline Case to Future Case with the Project

	Spring		Summer		Fall		Winter		Year	
Taylor Bridge	7	(151)	5	(136)	-3	(350)	-1	(496)	8	(1133)
Bear Flat	-18	(227)	2	(155)	-7	(393)	-7	(520)	-30	(1295)
Farrell Creek	-4	(210)	6	(178)	-14	(365)	-1	(492)	-13	(1245)
Fort St. John Airport	-6	(208)	4	(177)	16	(484)	-7	(692)	7	(1561)
Hudson's Hope	-8	(210)	0	(172)	9	(350)	0	(353)	1	(1085)
Attachie Flat Lower	4	(200)	-2	(179)	10	(353)	-3	(443)	9	(1175)
Attachie Plateau	-10	(229)	-14	(195)	3	(365)	-4	(462)	-25	(1251)
Site C	-8	(216)	-7	(171)	-7	(427)	4	(560)	-18	(1374)
Attachie Flat Upper	-7	(199)	-10	(177)	11	(359)	2	(437)	-4	(1172)

NOTES:
Shown are changes in normal fog hours with baseline hours given in parentheses.

Table 5.5.2 Predicted change in heavy fog from Baseline Case to Future Case with the Project

	Spring		Summer		Fall		Winter		Year	
Taylor Bridge	46	(130)	8	(124)	41	(329)	23	(475)	118	(1058)
Bear Flat	-16	(192)	-1	(133)	-6	(376)	-10	(508)	-33	(1209)
Farrell Creek	-3	(183)	6	(158)	-13	(354)	-1	(481)	-11	(1176)
Fort St. John Airport	-4	(188)	1	(155)	14	(468)	-5	(678)	6	(1489)
Hudson's Hope	-10	(187)	-4	(153)	9	(341)	1	(521)	-4	(1202)
Attachie Flat Lower	-5	(174)	-5	(151)	1	(336)	-5	(429)	-14	(1090)
Attachie Plateau	1	(197)	-6	(166)	0	(351)	-4	(453)	-9	(1167)
Site C	-14	(182)	-4	(142)	-7	(401)	5	(547)	-20	(1272)
Attachie Flat Upper	-9	(171)	-11	(156)	9	(338)	-4	(432)	-15	(1097)

NOTES:
Shown are changes in heavy fog hours with baseline hours given in parentheses.

The Taylor bridge location is also of concern due to potential changes in fog due to changes in river water temperature. The Peace River is too narrow to incorporate in the WRF simulation at one kilometre horizontal resolution. However the WRF model results provide a basis to infer potential changes in fog at Taylor bridge from River water temperature.

The left panel of Figure 5.5.1 shows the predicted monthly average change in water temperature of the Peace River at Taylor after construction of the Site C reservoir. The river temperature is expected to be about one degree warmer through the fall and about one degree cooler through the spring.

The upper right panel of Figure 5.5.1 shows the monthly surface water temperature of an example reservoir grid cell from the WRF simulation and the lower panel shows the monthly average simulated evaporation from the same location. Over the year, the WRF model suggests there tends to be more water vapour loading from the reservoir when the water temperature is higher, with lower values through the winter and spring and higher in summer and fall.

The WRF model results suggest that the reduction in river water temperature would result in less water vapour loading in the spring and more water vapour loading in the late summer and fall. One would thus expect less fog at Taylor in the spring and possibly more fog in the fall. However, Table 5.5.1 shows that the WRF modelling predicts fog would increase in spring. Thus changes in river temperature might actually mitigate the formation of fog from the reservoir. However, the increased river temperature in summer and fall may also offset the decrease in fog from the WRF model during those times.

In general, the formation of the reservoir, which would create a kilometre-wide water body with surface temperature changes up to 30 degrees different between Baseline Case and Future Case with the Project, represents a much greater geophysical change than a one degree increase or decrease change in river temperature. As such, one might reasonably expect that the changes in fog close to the reservoir surface would be greater than the changes in fog close to the river. By extension, the changes in fog predicted in Table 5.5.1 for locations close to the reservoir present an upper bound to the changes that might result from changes in river temperature.

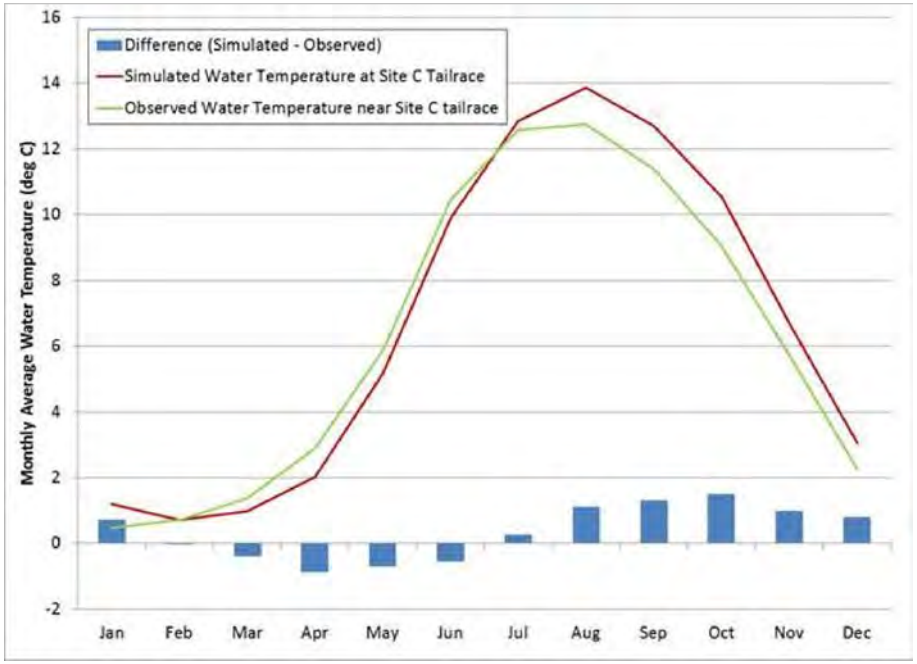

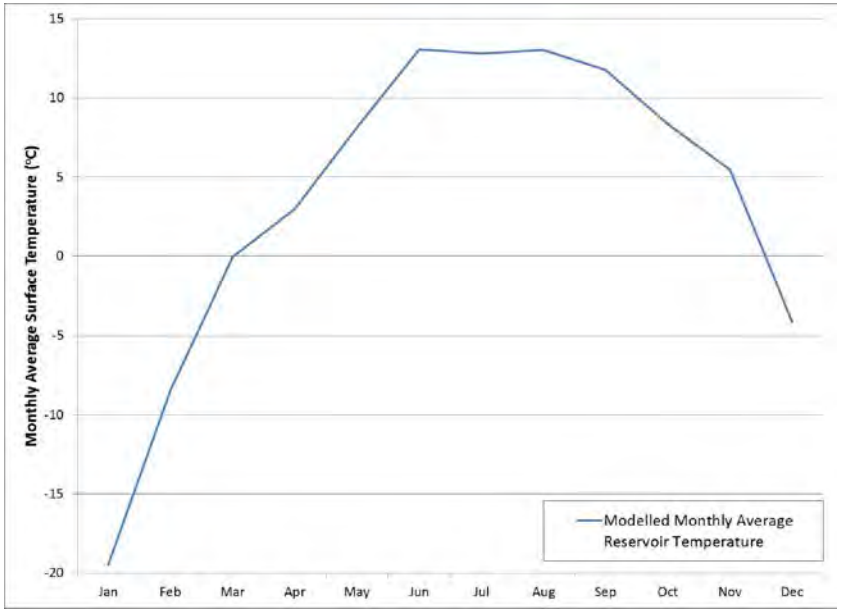

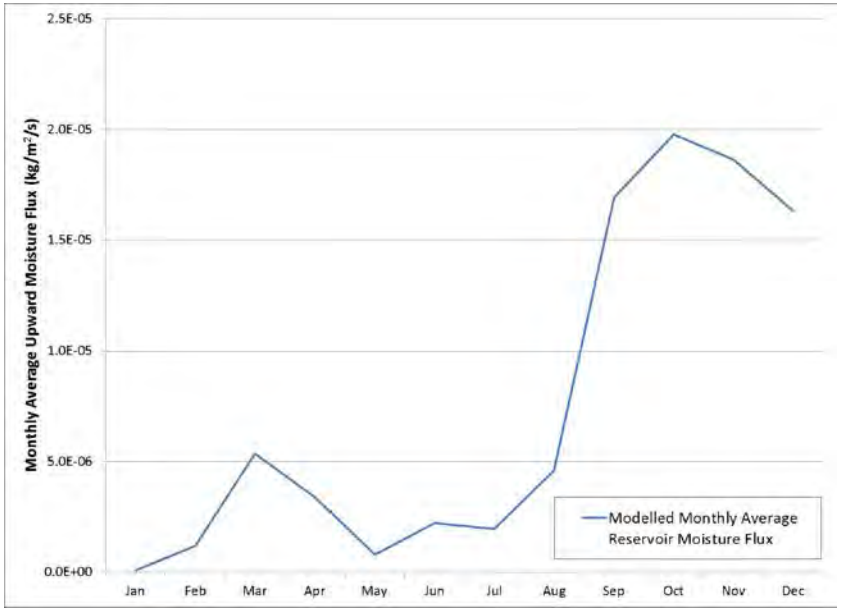

Predicted monthly average change in river temperature (left panel), predicted monthly average surface temperature (upper right panel), predicted monthly average reservoir evaporation rate.

SITE C CLEAN ENERGY PROJECT

RWDI BC hydro

Figure 5.5.1
Predicted changes in monthly river temperature, reservoir surface temperature and evaporation

DATE	Dec. 3, 2012		R 0

5.6 VISIBILITY AT FORT ST. JOHN AIRPORT

Fogging is closely associated with visibility as water droplets in the air can reduce the distance over which objects can be seen. The Fort St. John Airport location was examined to determine whether visibility would be altered due to the addition of the proposed Site C reservoir.

Visibility was categorized into the following distance groupings: greater than 20 kilometres, 10 to 20 kilometres, 5 to 10 kilometres, 1.0 to 5.0 kilometres, 0.5 to 1.0 kilometres, and less than 0.5 kilometres. Table 5.6.1 compares the numbers of hours, in which visibility falls into these categories for the Baseline Case and Future Case with the Project.

The number of clear hours (visibility greater than 20 kilometres and 10 to 20 kilometres) is predicted to be reduced with the addition of the proposed Site C reservoir, particularly in the summer and fall. The number of hours with visibility of 5 to 10 kilometres is also reduced whereas the number of hours with visibility of 1.0 to 5 kilometres increases. Overall, the number of hours in which poor visibility (0.5 to 1.0 kilometres and less than 0.5 kilometres) is predicted to occur is increased, most notably during the summer and fall. Changes in visibility are mostly strongly determined by changes in the amount of liquid water in the atmosphere. As explained above in Section 4.4, changes in liquid water content, or fog, are in turn determined by changes in temperature and water vapour mixing ratio. If the changes in the base quantities of temperature and water vapour are minimal, then changes in the derived quantities of fog and, by extension, visibility should also be minimal. This is as expected given that the changes in the quantities that determine fog and visibility, specifically temperature and humidity, are not predicted to be statistically significant at the airport.

Table 5.6.1 Predicted changes in visibility at Fort St. John Airport

	Visibility					
	Clear		Moderate		Poor	
	>20 km	10-20 km	5-10 km	1-5 km	0.5-1 km	<0.5 km
Spring						
Baseline Case	1914	9	16	37	20	188
Future Case with the Project	1919 (+5)	9 (0)	9 (-7)	45 (8)	18 (-2)	184 (-4)
Summer						
Baseline Case	1980	8	10	33	22	155
Future Case with the Project	1977 (-3)	5 (-3)	14 (4)	31 (-2)	25 (3)	156 (1)
Fall						
Baseline Case	1689	9	7	19	16	468
Future Case with the Project	1674 (-5)	7 (-2)	6 (-1)	21 (2)	18 (2)	482 (14)
Winter						
Baseline Case	1441	2	8	17	14	684
Future Case with the Project	1444 (3)	2 (0)	7 (-1)	22 (5)	12 (2)	679 (-5)
Year						
Baseline Case	7024	28	41	106	72	1495
Future Case with the Project	7014 (-10)	23 (-5)	36 (-5)	119 (13)	73 (1)	1501 (6)

NOTES:
Shown are hours per year within each visibility class. The change is given in parentheses

5.7 EVAPORATION FROM PROPOSED RESERVOIR

The predicted evaporation rates of the proposed reservoir spatially averaged over the entire reservoir and time averaged over each month and for the full year, are given in Table 5.7.1. Included is the maximum value at any one modelled cell. In general, the values are higher in the fall months and lower in the winter months. The reservoir average evaporation rate is lowest in January and February and is highest in October and there are lower average rates through the summer months. The maximum evaporation rate at any point on the reservoir is predicted to occur in December.

Table 5.7.1 Predicted evaporation from proposed reservoir for Future Case with the Project

Evaporation	Averaging Period (2004-2005)												
	Oct	Nov	Dec	Jan	Feb	Mar	Apr	May	Jun	Jul	Aug	Sep	Year
Ave (mm)	52.9	42.5	30.6	6.3	6.1	16.2	13.0	11.9	13.7	19.1	24.3	46.0	282.6
Max (mm)	62.7	57.0	68.4	50.0	25.0	24.1	46.2	52.8	38.1	49.3	45.3	55.0	365.5

For evaporation to occur from the proposed reservoir three things are necessary. There must be a moisture source, there must be a source of energy and there must be a water vapour gradient between the moisture source and the overlying atmosphere. The evaporation rates presented are a result of the interplay between these three components. Evaporation is also increased by turbulence in the atmosphere, which enhances transport along the water vapour gradient.

Over the course of the year the moisture source is present at all times that the proposed reservoir is not frozen over. During the winter months when large parts of the surface of the proposed reservoir freeze, the lowest evaporation rates are seen. This is purely a result of removing the moisture source. During other times of the year there is abundant moisture and evaporation is controlled by available energy and the water vapour gradient between the proposed reservoir and the overlying atmosphere.

The energy availability is controlled by the input of solar radiation to the proposed reservoir which is then reflected in the temperature of the water. During the model year, the temperature of the proposed reservoir in the WRF model never exceeds approximately 16 degrees Celsius and is below degrees Celsius for most of the year, as shown in Figure 2.5.4. Therefore, the evaporation is limited by this relatively low value. The solar radiation hits a maximum in the summer and the maximum water temperatures occur slightly later as there is a time lag between maximum solar radiation input and maximum temperature.

With the highest water temperatures occurring in late summer it would seem sensible to assume that maximum evaporation would occur at the same time. This does not occur. The reason is that during the summer the atmosphere is warm and moist. Therefore evaporation is limited at this time by the low temperature of the water and the higher moisture content of the atmosphere. The higher moisture content of the atmosphere limits evaporation by reducing the moisture gradient between the water surface and the overlying atmosphere.

The maximum evaporation rates occur in October when the proposed reservoir has not yet cooled dramatically but air temperatures have dropped significantly due to lower solar radiation input. The lower air temperatures and hence drier air allow for a strong water vapour gradient to occur between the water surface and overlying atmosphere. This large gradient and relatively warm water temperatures result in the largest evaporation rates of the year. From October until January, when ice forms on the proposed reservoir, the evaporation rate gradually drops as the water temperature drops and hence less energy is available to drive evaporation.

6.0 LIMITATIONS OF STUDY

This section describes the limitation of the microclimate study. There are two main issues to consider. The first is the magnitude of the influence of global climate change on the Peace River Valley. The second has to do within difficulties of fully describing all atmospheric physical processes, spatial and temporal scales of real-world phenomena with a numerical model simulation.

6.1 NON-PROJECT RELATED MICROCLIMATE CHANGES

Future global climate change is likely to alter the microclimate in the Technical Study Area, independent of the influence of the reservoir. On the regional scale of the Project's Technical Study Area, climate can be broken down into five components:

1. a mean state
2. trends due to global climate change
3. influence of land-cover changes
4. climate modes of variability (see Appendix A – Glossary of Terms), for example El Niño Southern Oscillation
5. stochastic processes such as non-linear interactions between adjacent regions or autocorrelations (basically noise)

Mesoscale models such as WRF are not yet capable of modelling all five components well enough to fully understand the interaction between them. It is assumed here that the five components are additive. This discussion therefore represents an upper bound for combined global and local climate changes in the Technical Study Area.

This study is concerned with the third component, specifically the influence of the filling of the reservoir, on the regional microclimate. Non-Project related land-cover changes would not be quantified. For example, vegetation might change as a result of temperature and precipitation changes, and logging, agriculture, and industrial and residential development might alter land cover. Averaged over twenty years, climate modes of variability and stochastic processes (points 4 and 5) usually become negligible. The only multi-decadal climate mode of variability that likely influences the Technical Study Area is the Pacific Decadal Oscillation. After averaging over twenty years, some residual influence of the Pacific Decadal Oscillation might remain within a single General Circulation Model (GCM). However, the literature suggests that current GCM still face challenges modelling this mode of variability (e.g., Furtado, et al. 2011; Lienert, et al. 2011). While current GCMs might reproduce its general characteristics, modelled Pacific Decadal Oscillations are likely not in phase with past observed variability. Therefore, over an ensemble of GCMs, any residual influence should average out. It is assumed here that, after taking the difference between a future and a past twenty-year period, only the regional trend due to global climate change remains.

One caveat of this approach is that current GCM results, including the most recent published in the scientific literature after the release of the IPCC's Fourth Assessment Report (2007), still show widely differing results for regional climate change. However, the range of regional climate projections from many different GCMs provides some indication of the changes that can be expected in the Technical Study Area without the filling of the reservoir. The left columns of the pairs of open boxes in Figure 6.1.1 and Figure 6.1.2 show the full range of predicted changes and 25th, 50th, and 75th percentiles from 21 GCM for daily mean temperatures and total precipitation, respectively, averaged over each of the four seasons and over the entire calendar year. These GCM results from Table 11.1 in IPCC (2007) are for the commonly used moderate SRES A1B emissions scenario (see Appendix A – Glossary of Terms) and for the Western North American domain (103-130°W, 30-75°N; note that there are typos in the domain

boundaries in IPCC, 2007). The difference is calculated between the future period from 2080 to 2099 and the past control period from 1980 to 1999. All changes, with the exception of summer (JJA) precipitation, are statistically significant at a 75% confidence level.

The right columns of the pairs of open boxes in Figure 6.1.1 and Figure 6.1.2 are based on an alternative dynamical downscaling approach. Schnorbus et al. (2011; Table 4-1) used GCM output as input to higher-resolution numerical models to achieve the high spatial resolution necessary for hydrologic modelling in the Peace River study area. Shown are 5th, 50th, and 95th percentiles of runs using output from different GCMs. Predicted temperature and precipitation changes from the 1961-1990 climate-normals period to the 2050s for the SRES A1B scenario were spatially averaged.

Smaller temperature changes are expected from Schnorbus et al. (2011) than IPCC (2007), because of the shorter period of change (60-90 versus 100 years). For precipitation, Schorbus et al. (2011) predict larger median (50%) changes than IPCC (2007) in all seasons. Dynamical downscaling substantially improves the spatial resolution of topography which tends to improve predictions of topographically enhanced precipitation. The predictions by Schnorbus et al. (2011) are likely more reliable than the coarse resolution results from IPCC (2007). It should be noted, however, that the wide ranges of predictions from both sources overlap substantially and the predictions therefore do not differ with great statistical significance.

The grey boxes in Figure 6.1.1 and Figure 6.1.2 show the Technical Study Area-wide full ranges and spatial means of the local grid-cell changes that the WRF model predicts due to the land-cover and elevation change associated with the formation of the reservoir, keeping everything else unchanged. Since the vast majority of grid cells in the Technical Study Area do not show statistically significant changes after formation of the reservoir (section 5.0), the Technical Study Area-wide spatial mean values are close to zero compared to the overall ranges of changes due to the reservoir (grey boxes) and due to globally driven climate change (open boxes).

The maximum annual average temperature changes due to the reservoir across all WRF model grid cells (1.2 degrees Celsius) is lower than the lowest temperature changes predicted due to climate change across all 21 GCMs (2.1 degrees Celsius) and the 5th percentile from dynamical downscaling (2.2 degrees Celsius). However, when WRF predictions are broken into seasons, there are grid cells for which the WRF model predicts reservoir-related temperature increases within the range of GCM-predicted temperature changes due to global climate change in the winter (DJF) and in the fall (SON). Figure 5.1.4 in section 5.1 shows that these large mean-temperature changes only occur in grid cells over the reservoir. It should also be noted that the WRF model predicts decreases of temperatures by up to 2.0 degrees Celsius at some of these grid cells in all seasons but fall (SON).

As pointed out in section 5.2, WRF predictions of precipitation increases and decreases on the order of 10-20% within the Technical Study Area (Figure 6.1.2) are statistically insignificant. The set of 21 GCM predicts precipitation increases of a few per cent up to about ten per cent in all seasons with 75% confidence with the exception of summer (JJA), where predicted changes are not statistically significant. Similarly, dynamical downscaling by Schnorbus et al. (2011) predicts

precipitation increases between 15 and 20 percent with more than 95% confidence in all seasons but summer. The GCM predictions of future precipitation changes in IPCC (2007) are averages over Western North America. The area is roughly three orders of magnitude larger than the Technical Study Area, which increases the signal-to-noise ratio but also ignores the influence of smaller-scale features like relief and land cover. The dynamical downscaling in Schnorbus et al. (2011) improves upon these limitations by resolving smaller-scale topographic features. However, the improved moisture budget of the higher-resolution model is lost every time boundary conditions are reset with GCM output. Therefore, any errors in the global GCM predictions could only partially be corrected by Schnorbus et al. (2011), and the reliability of the GCM predictions remains an open question. Note that within the Technical Study Area, there may be spatial variations in the magnitude and direction of global influences. Depending on the location within the Technical Study Area, global climate changes and local project changes may cancel or amplify each other.

In conclusion, the GCM modelling results provide statistically significant evidence that the Technical Study Area would experience increases in mean temperatures of two to four degrees Celsius degrees in all seasons and increases in precipitation roughly on the order of 10-20% in most seasons over the next 60 to 100 years for global GHG emissions similar to the A1B scenario. The WRF modelling results predict similar temperature increases only at a few grid cells over the proposed reservoir, and predictions of precipitation changes are statistically insignificant. The modelling results therefore provide statistically significant evidence that changes in microclimate that would be experienced within the Technical Study Area further than one kilometre (one grid cell) from the reservoir would be unrelated to the formation of the reservoir.

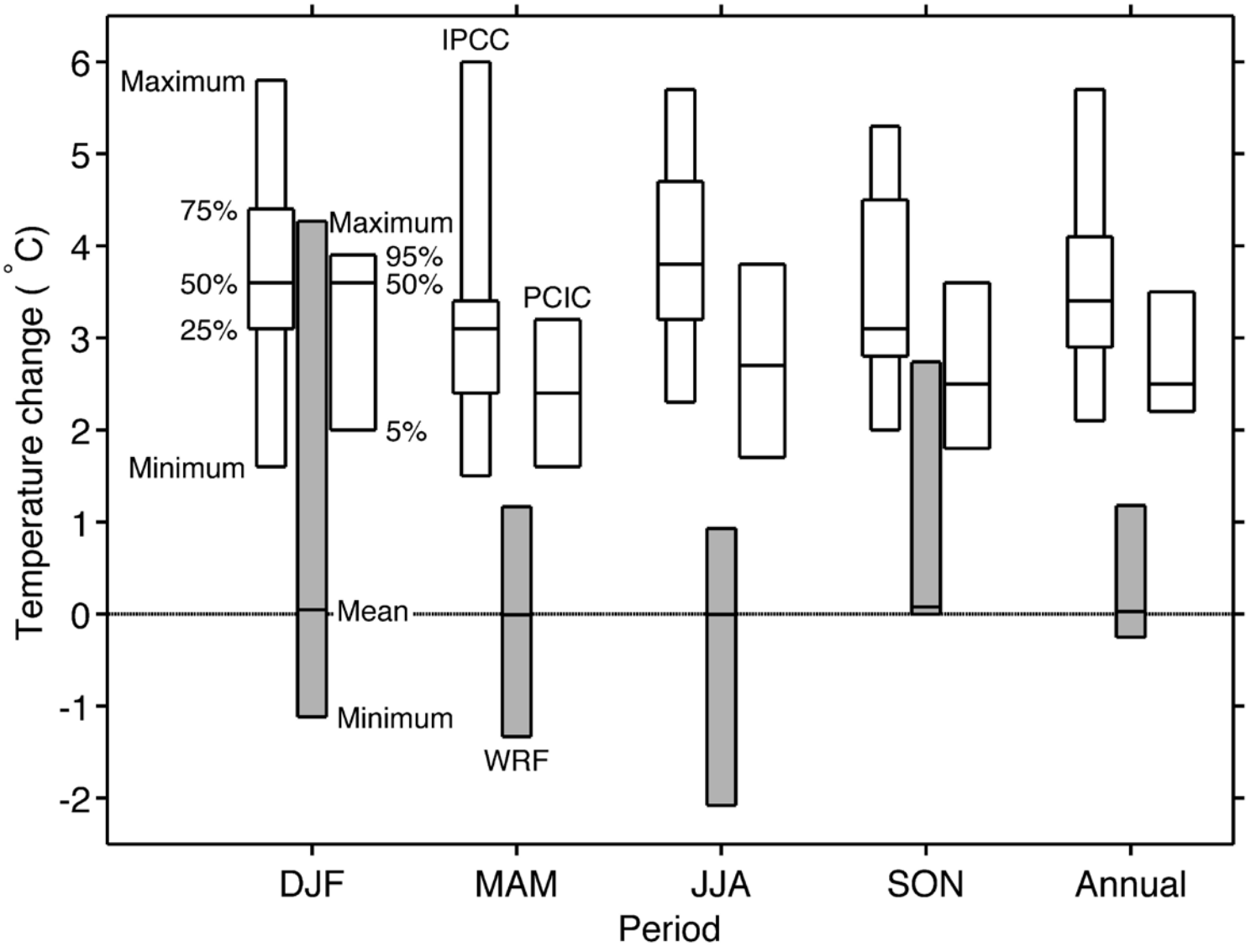

Pairs of open boxes (IPCC and PCIC) show statistics of regional climate-change projections of winter (DJF), spring (MAM), summer (JJA), fall (SON) and Annual mean temperatures for the A1B SRES scenario. Grey boxes (WRF) represent spatial statistics over the Technical Study Area of Weather Research and Forecasting (WRF) model-predicted daily mean temperature changes, caused by the filling of the reservoir, only. IPCC is based on Table 11.1, section WNA (Western North America) in IPCC (2007). These are changes projected by 21 GCM to occur from the control period 1980-1999 to the future period 2080-2099. PCIC is based on Table 4-1 in Schnorbus et al. (2011). It shows statistics of changes determined with dynamical downscaling of GCM ensemble output from the control period 1961-1990 to the 2050s. Box limits represent the statistics as labelled for DJF.

SITE C CLEAN ENERGY PROJECT

RWDI BC hydro

Figure 6.1.1
Project influences versus regional climate projections for temperature

DATE	Dec. 3, 2012		R 0

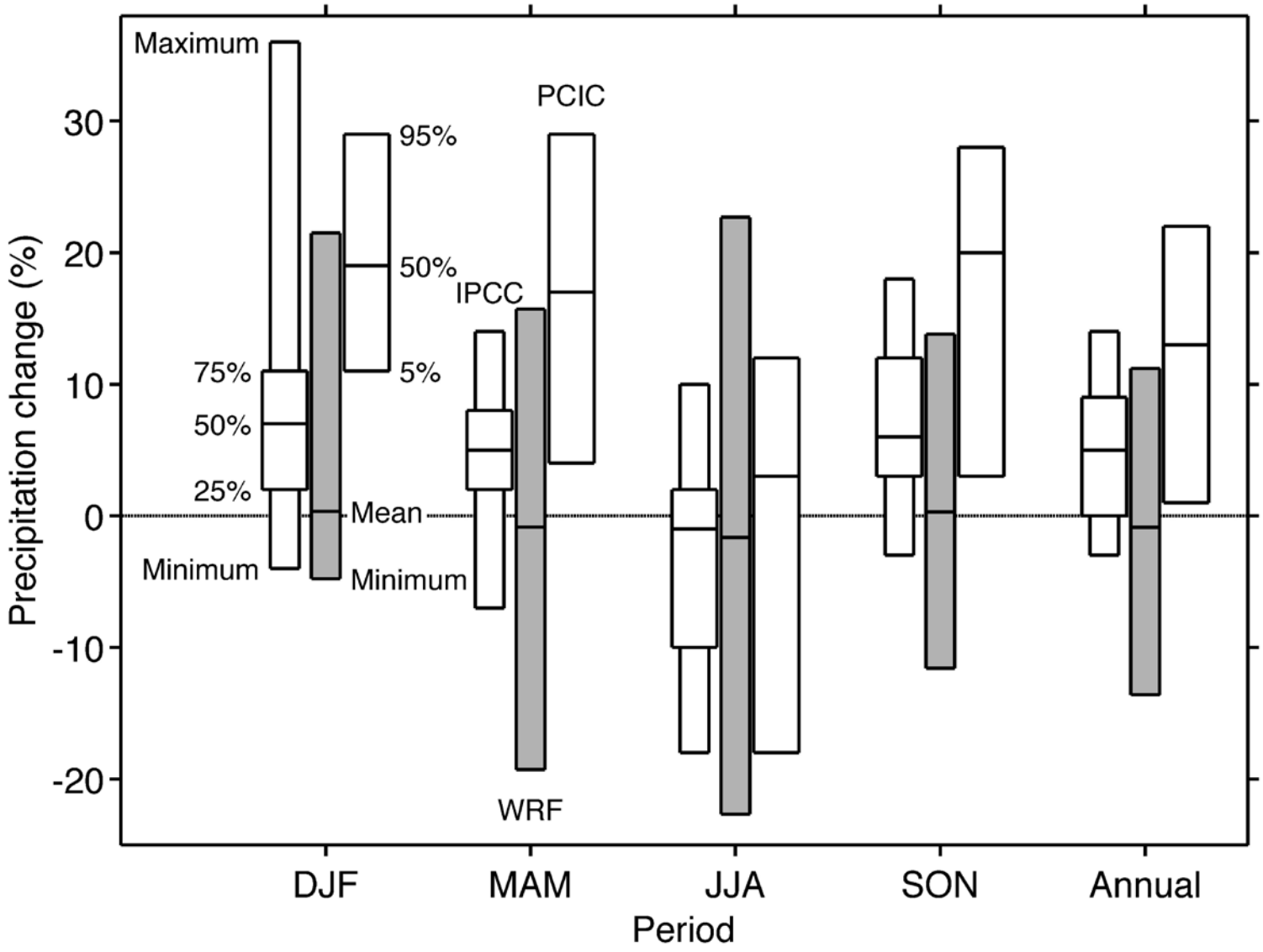

Pairs of open boxes (IPCC and PCIC) show statistics of regional climate-change projections of winter (DJF), spring (MAM), summer (JJA), fall (SON) and Annual total precipitation for the A1B SRES scenario. Grey boxes (WRF) represent spatial statistics over the Technical Study Area of Weather Research and Forecasting (WRF) model-predicted daily total precipitation changes, caused by the filling of the reservoir, only. IPCC is based on Table 11.1, section WNA (Western North America) in IPCC (2007). These are changes projected by 21 GCM to occur from the control period 1980-1999 to the future period 2080-2099. PCIC is based on Table 4-1 in Schnorbus et al. (2011). It shows statistics of changes determined with dynamical downscaling of GCM ensemble output from the control period 1961-1990 to the 2050s. Box limits represent the statistics as labelled for DJF.

SITE C CLEAN ENERGY PROJECT

RWDI BC hydro

Figure 6.1.2
Project influences versus regional climate projections for precipitation

DATE	Dec. 3, 2012		R 0

6.2 LIMITATIONS OF MODELLING APPROACH

This modelling study is limited by the difficulties in fully representing the phenomena of interest on adequate spatial and temporal scales. This is a common theme for all environmental models for which it is difficult if not impossible to accurately resolve all physical features on all scales of interest, particularly when faced with practical limitations of computing resources.

These limitations in model resolution and formulation do not undermine model results. Rather, acknowledgement and understanding of potential limitations allow one to place model results in the proper context and thus make informed decisions as to the information that the model provides.

For most of the physical features simulated by the model, systematic errors in the model formulation would be the same for both the Baseline Case and the Future Case with the Project and would cancel out when the difference between the two scenarios is calculated.

6.2.1 Spatial Scales

The model is limited on a spatial scale by the accuracy of defining the geophysical features, including the reservoir, using a grid size of one kilometre. For example, the model overestimates the surface area of the reservoir. This is due to the difficulty of using one kilometre ‘squares’ to estimate the long and narrow water surface that would result from filling of the reservoir. It would have been possible to limit the number of WRF model grid cells that were changed to water to a number that would more closely approximate the actual area, but this would have led to a discontinuous water surface in the model, with patches of water separated by scattered cells designated as land, and would have just substituted one source of error for another. Because the influence of the reservoir on microclimate is directly proportional to the size of the water surface, the overestimation of the water surface means that the model in turn represents a probable overestimation of the changes to microclimate that it would induce. In addition, the sensitivity of the model is likely of the same order as the scale of the overestimation, e.g., overestimating the reservoir width by 20% means that the distances from the reservoir, over which changes are observable in the model, are also likely overestimated by 20%.

The discretization of the model inputs over the one-kilometre grid can also introduce some discrepancy into direct model-to-observation comparisons. Averaged over the whole domain, or the whole reservoir valley, a mesoscale model such as WRF is able to capture and represent the broader-scale terrain features. However, for individual grid cells, choosing a single land-cover category or elevation can be overly simplistic. For example, a given grid cell might in reality be 55% forest and 45% grassland, with the local micrometeorology determined by the mixture of the two land-cover types. However, the WRF simulation can only have one of the two categories selected for the given grid. The result of this is to introduce more ‘noise’ into the model solution as the model condition changes quickly over the boundary from one grid cell to the next compared to reality where the changes occur more gradually. Over the entire domain,

these cases tend to average out, but for a given location this can be a source of disagreement between model predictions and observation. There is some evidence of this in the comparison of WRF model predictions to the observation at the climate stations.

Small-scale thermally driven flows are difficult to model, particularly at night. This is related to horizontal and vertical resolution limitations in the numerical model. These also affect the evaluation of model performance for wind speed and direction, because winds strongly depend on height above ground. These small-scale features can lead to some extreme observations that are not captured by the model. However, averaged over time and space, these discrepancies tend to be reduced.

Another consequence of the resolution limitations is that numerical mesoscale models have less skill in predicting precipitation in the warm season. It is much more difficult to accurately model warm season precipitation, which tends to be convective in nature. Convective precipitation is associated with individual storm cells while synoptic or frontal rainfall is characterized by large-scale cloud formations associated with frontal passage. The precipitation schemes within the WRF model are more able to resolve large-scale frontal features than to predict where individual storm cells may arise. Correspondingly, the WRF model is better able to predict precipitation amounts associated with large-scale wintertime synoptic condition than precipitation resulting from local scale warm weather cumulus clouds formation.

It should be noted that model-observation discrepancies are not only a shortcoming of model output. Station observations are point measurements, and model outputs are grid-cell averages. The station observation can be influenced by a sub-grid cell phenomenon that is not representative of the model grid cell. A local thunderstorm, for example, might lead to substantial average precipitation over the area of a model grid cell without any precipitation occurring at the station.

6.2.2 Temporal Scales

On a temporal scale, the model is limited by the use of a single year to estimate changes in climate, which is by definition a multi-year if not multi-decade average. The use of a single year of meteorology to estimate changes to climate means that real results on a longer-term average may differ. However, when multiple years are used, results would still be expected to fluctuate around what is seen for a ‘normal’ or typical year. The extra years are mostly useful to provide an estimate of year-to-year deviation from norm. The current study provides a reasonable estimate of how various meteorological parameters may be influenced by the proposed Site C reservoir in a typical year, but it does not provide information regarding the potential changes during non-typical years, such as a very wet or a very hot summer (i.e., extremes).

A specific temporal scale issue affects model evaluation of winds. Model predicted winds are hourly averages, while observations are measured for a few minutes once an hour. Winds can vary strongly over the course of an hour, mostly randomly. The numerical model performs calculations on sub-hourly time scales, but sub-hourly model output for wind is less representative of the short observation period than an hourly average.

CLOSURE

RWDI AIR Inc. has prepared this report for the sole benefit of BC Hydro for the purpose of documenting baseline conditions in anticipation of an environmental assessment under the British Columbia *Environmental Assessment Act* and the *Canadian Environmental Assessment Act*. The report may not be relied upon by any other person or entity, other than for its intended purposes, without the express written consent of RWDI AIR Inc. and BC Hydro. Any use of this report by a third party, or any reliance on decisions made based upon it, are the responsibility of such third parties.

The information provided in this report was compiled from existing documents and data provided by BC Hydro and by field data compiled by RWDI AIR Inc. (and others if applicable). This report represents the best professional judgment of the authors at the time of its preparation. RWDI AIR Inc. reserves the right to modify the contents of this report, in whole or in part, to reflect any new information that becomes available. If any conditions become apparent that differ significantly from our understanding of conditions as presented in this report, we request that we be notified immediately to reassess the conclusions provided herein.

BC Hydro has the right to reproduce, use and rely upon this Report for proper purposes in planning, operating and maintaining the electrical generation, transmission and distribution system in the Province of British Columbia, including, without limitation, the right to deliver this Report to regulatory authorities in support of or in response to regulatory inquiries and proceedings, including environmental assessment.

Respectfully submitted by:

RWDI AIR Inc.

Lead Author:
Jeff Lundgren, M.Sc.
Technical Director

Reviewer:
Christian Reuten, Ph.D.
Senior Engineer/Scientist

Reviewer:
Andres Soux, M.Sc.
Senior Engineer/Scientist

7.0 REFERENCES

7.1 LITERATURE CITED

ASTER GDEM, 2011. Ministry of Economy, Trade, and Industry (METI) of Japan and the United States National Aeronautics and Space Administration (NASA) (http://www.ersdac.or.jp/GDEM/E/3.htm)

EBA Engineering, Inc. June 2012. *Reservoir Water Temperature and Ice, Technical Data Report*, Rev. 1.Document Number 06-079. Submitted to BC Hydro Site C Clean Energy Project. June 2012.

EBA Engineering, Inc. 2011. *Stage 2 Baseline Water Temperature Modelling Report, Peace River Site C Hydro Project.* Prepared for BC Hydro, Vancouver, BC.

Furtado, J., E. Di Lorenzo, N. Schneider and N.A. Bond. 2011. *North Pacific decadal variability and climate change in the IPCC AR4 models*. Journal of Climate 24(12): 3049-3067.

Garratt J., R. 1992: The Atmospheric Boundary Layer, Cambridge University Press, Great Britain.

Gálvez J., M. and Douglas M., W. 2006: *Modulation of Rainfall by Lake Titicaca using the WRF Model*, Proceedings of 8 ICSHMO, Foz do Iguaçu, Brazil, April 24-28, 2006, INPE, p. 745-752.

Grossman-Clarke, S., Zehnder, J., A. Loridan, T.,C. and Grimmond, S., B. 2010: *Contribution of Land Use Changes to Near-Surface Air Temperatures during Recent Summer Extreme Heat Events in the Phoenix Metropolitan Area.* J. Appl. Meteor. Climatol., 49, 1649–1664.

Gultepe, I., J. Milbrandt, and S. Belair, 2006: *Visibility parameterization from microphysical observations for warm fog conditions and its application to the Canadian MC2 model*, AMS meeting, Atlanta, January 2006, USA.

Hong, S., Lakshmi, V., Chen, F., Tewari, M., and Manning, K., W: 2009: *Effects of vegetation and soil moisture on the simulated land surface processes from the coupled WRF/Noah model*, Journal of Geophysical Research, vol. 114, D18118, 13 pp., 2009 doi:10.1029/2008JD011249

Hudischewskyj, A. B., Douglas, S. G., Lundgren, J. R. 2001. *Meteorological And Air Quality Modeling To Further Examine The Effects Of Urban Heat Island Mitigation Measures On Several Cities In The Northeastern U.S.*. SYSAPP-01-001. San Rafael, CA: ICF Consulting/Systems Applications International, Inc. http://www.epa.gov/heatisland/resources/publications.html

IPCC. 2007. *Climate Change 2007: The Physical Science Basis. Contributions of Working Group I to the Fourth Assessment Report of the Intergovernmental Panel on Climate Change* [Solomon, S., D. Qin, M.

Jiang, X., Wiedinmyer, C., Chen, F., Zong-Liang, Y., Chun-Fung Lo, J., 2008: *Predicted impacts of climate and land use change on surface ozone in the Houston, Texas, area*, Journal of Geophysical Research, VOL. 113, D20312, 16 PP., 2008, doi:10.1029/2008JD009820

Lopez-Espinoza, E.D., Zavala-Hidalgo, J. and Gomez-Ramos, O. 2012: *Weather forecast sensitivity to changes in urban land covers using the WRF model for central México*, Atmósfera 25(2), 127-154 (2012)

Lienert, F., J.C. Fyfe and W.J. Marryfield. 2011. *Do climate models capture the tropical influences on North Pacific sea surface temperature variability?* Journal of Climate 24(23): 6203-6209.

Luhar, A.K., 1998: *An analytical slab model for the growth of the coastal thermal internal boundary layer under near-neutral onshore flow conditions.* Boundary-Layer Meteorology 88: 103-120.

Manning, Z. Chen, M. Marquis, K.B. Averyt, M. Tignor and H.L. Miller (eds.)]. Cambridge University Press, Cambridge, United Kingdom and New York, NY, USA.

Oke, T.R. 1987. *Boundary Layer Climates 2nd ed.* Routledge. London.

Reuten, C., R.D.(Dan) Moore and G.K.C. Clarke. 2011. *Quantifying differences between 2-m temperature observations and reanalysis pressure-level temperatures in Northwestern North America*. Journal of Applied Meteorology and Climatology 50(4): 916-929.

Reuten, C., B. Ainslie, D.G. Steyn, P.L. Jackson and I. McKendry. 2012. *Impact of climate change on ozone pollution in the Lower Fraser Valley*, Canada. Atmosphere-Ocean 50(1): 42-53.

Schaefer, D.C. 1976. *Climatologically Impacts of the Peace River Regulation and A Review of the Possible Effects of Climatic Change on Agriculture*. Report prepared for BCH&PA by Atmospheric Environment Services, Scientific Services Section. June 9, 1976.

Schnorbus, M.A., K.E. Bennett, A.T. Werner and A.J. Berland. 2011. *Hydrologic Impacts of Climate Change in the Peace, Campbell and Columbia Watersheds, British Columbia, Canada.* Pacific Climate Impacts Consortium, University of Victoria, BC.

Stoelinga, M. T., and T. T. Warner, 1999: *Nonhydrostatic, Mesobeta-scale Model Simulations of Cloud Ceiling and Visibility for an East Coast Winter Precipitation Event*. J. Appl. Meteor., 38, 385-404.

Thurber Consultants Ltd. 1977. *Site C Physical Environment, Climate, Interim Report to BC Hydro and Power Authority.* Prepared for BC Hydro and Power Authority. Burnaby, BC.

Tuller, S. 2008. *Site C Climate, Annotated Bibliography*. Prepared for BC Hydro. Burnaby, BC.

Tuller, S. 1991. *Review of Site C Climate Impacts*. Prepared for BC Hydro and Power Authority. Burnaby, BC.

7.2 INTERNET SITES

Adams, S., M. and Keith D., W., 2007: *A Wind Farm Parameterization for WRF*, presented to 2007 WRF users workshop, Boulder, Colorado.

Environment Canada. 2012. Canadian Climate Normals or Averages 1971-2000. Available at: http://www.climate.weatheroffice.gc.ca/climate_normals/index_e.html. Accessed: August 2012.

Epifanov, V. M.,2012, http://www.thermopedia.com/content/595/?tid=104&sn=1159, Accessed, November 2012.Grim, J., Knievel, J., and Crosman, E., 2012: *Effects of the Great Salt Lake's Temperature and Size on the Regional Precipitation in the WRF Model*, presented to 2012 WRF users workshop, Boulder, Colorado, http://www.mmm.ucar.edu/wrf/users/workshops/WS2012/ppts/4.5.pdf

NCEP, 2011. *North American Regional Reanalysis*. National Centers for Environmental Prediction, Camp Springs, Maryland.(http://www.emc.ncep.noaa.gov/mmb/rreanl).

Voogt, J, 2012, http://www.actionbioscience.org/environment/voogt.html, Accessed November 2012.

7.3 PERSONAL COMMUNICATIONS

Leung, R. 2009. Laboratory Fellow. Pacific Northwest National Laboratory. Presentation to BC Hydro. September 9, 2009.

APPENDIX A

Glossary of Terms

TABLE OF CONTENTS

1.0 Glossary of Terms A.1
2.0 References A.3

1.0 Glossary of Terms

A1B:
A particular SRES scenario (Nakićenović and Swart 2000) designed to represent an integrated world with a balanced emphasis on all energy sources.

β_ext:
Extinction of light by liquid water content of fog.

Climate Index, Pattern, and Mode of Variability:
Climate variables are divided into a climate index (time varying, constant in space) and a climate pattern (spatially varying, steady in time) with the objective to explain as much spatial and temporal variability as possible. The climate index is a time series of a single parameter that aggregates certain characteristics of the climate system of interest. An example is the difference of the Pacific Ocean sea surface temperature (SST) from the average value (called the SST anomaly) over the east-central tropical Pacific Ocean, which is used to define ENSO (El Niño Southern Oscillation). The climate pattern relates values of climate variables to the climate index at a given point in time. Usually, a climate mode of variability is the product of a climate pattern and a climate index. This is the most common decomposition of a climate variable into temporally and spatially varying components. The closer the climate modes of variability are to the actual climate variables, the more variance (i.e., temporal and spatial variability is explained).

GCM (General Circulation Model):
A numerical model of the global atmosphere used to model past and future climate, usually coupled with other physical, chemical, and biological components of the Earth's system that interact with the atmosphere, for example ocean, sea ice, and carbon cycle.

Liquid Water Content:
Atmospheric liquid water content expressed in grams of liquid water over kilograms of dry air.

Model Skill:
A meteorological model's ability to predict a parameter better than a forecast based on climate normals (long-term average) or persistence (previous value in a time series).

SRES (Special Report on Emissions Scenarios):
Emission scenarios developed by (Nakićenović and Swart 2000) for future emissions of greenhouse gases and other substances that might affect future climate.

Undercatch:
A lower precipitation measurement than actually occurs.

VIS:
Distance at which an illuminated object can no longer be seen.

Water Vapour Mixing Ratio:

Ratio of mass of water vapour and mass of dry air, typically expressed in grams of water vapour over kilograms of dry air.

2.0 References

Nakićenović, N., and R. Swart (eds.), 2000. Special Report on Emissions Scenarios. A Special Report of Working Group III of the Intergovernmental Panel on Climate Change. Cambridge University Press, Cambridge, United Kingdom and New York, NY, USA, 599 pp.

APPENDIX B

Bayesian Two-Sample Comparison

TABLE OF CONTENTS

1.0 Bayesian Two-Sample Comparison....B.1
2.0 References....B.6

Table of Tables

Table B.1 Statistically Significant differences of baseline period from climate normals....B.2

Table B.2 Odds in favour of a representative baseline period....B.5

Table of Figures

Figure B.1 Probabilities of differences between baseline period and climate normals....B.5

1.0 BAYESIAN TWO-SAMPLE COMPARISON

The evaluation period was chosen to be representative of average climate; therefore, for each month, values of the evaluation period should be close to the average over the climate-normal period. 'Close' here means 'small compared to the typical inter annual variability over the climate-normal period' as represented for example by the standard deviation.

If each calendar month could be treated independently, one would choose the year which the calendar month's value is closest to the climate average. The resulting twelve months, however, would not be consecutive. Ideally, a consecutive twelve-month period would be chosen such that the total differences between the monthly values and the climate averages are minimized by comparison with any other twelve-month period. A common measure to minimize is the sum of the squared differences ('least squares'). Additional constraints are imposed when several parameters simultaneously are expected to be representative of climate averages, for example precipitation and temperatures. At that point, the relative importance of one parameter over another might have to be taken into consideration.

To meet the requirement of representativeness, the twelve-month period needs to meet two conditions:

1. The twelve-month period should be unbiased, i.e. the mean should be statistically significantly the same as the climate average.

2. The twelve-month variability between evaluation period and climate average should be smaller than the thirty-year climate variability. This ensures that the evaluation year is closer to the climate average than a random sample drawn from the thirty-year climate normals.

In the main report, Figures 4.1.1 through 4.1.3 and 4.2.1 through 4.2.3 show observations and WRF output relative to the means and standard deviations of the climate normals. When a random sample is repeatedly drawn from a normal distribution, on average 68% of the values will be within one standard deviation of the mean and the remaining 32% outside. In other words, when twelve consecutive months are *repeatedly* randomly drawn from the 1971 through 2000 climate-normals period, then on average about four months will be more than one standard deviation from the climate mean.

For the evaluation period to be representative of the climate average, fewer than four months of observational data should be more than one standard deviation from the climate average. The figures in the main report indicate that this was indeed the case for all six parameters of interest (total monthly precipitation, snow, and rain and mean monthly daily minimum, mean, and maximum temperatures). This is summarized in Table B.1. However, if a small sample of only twelve months is randomly drawn from the climate-normals period, two or three outlier months (rather than the expected four) would actually occur quite often. Furthermore, not only does it matter how many months are more than one standard deviation from the mean but also how far each month lies from the mean. Finally, it is not clear from these figures if the means are unbiased.

Table B.1 Statistically Significant differences of baseline period from climate normals

Parameter	Oct. 2004	Nov. 2004	Dec. 2004	Jan. 2004	Feb. 2004	Mar. 2004	Apr. 2004	May 2004	Jun. 2004	Jul. 2004	Aug. 2004	Sep. 2004	Total
Monthly means of daily maximum temperatures		X						X					2
Monthly means of daily mean temperatures		X				X							2
Monthly means of daily minimum temperatures	X	X				X							3
Total monthly rain													0
Total monthly snow	X												1
Total monthly precipitation													0

NOTES:
Months (X) and their total numbers, in which observations during the Oct. 2004-Sep. 2005 evaluation year deviated more than one standard deviation from the corresponding 1971-2000 climate normals for the monthly means/totals of six parameters.

To address the caveats of only counting outlier months, RWDI implemented a Bayesian two-sample comparison (Gregory 2005) to calculate the appropriate probabilities associated with the two conditions for representativeness of the evaluation year above:

1. The probability that the observed parameter values for the October 2004 through September 2005 evaluation period are equal to the climate averages.

2. The probability that the observed parameter values during the evaluation period vary less from the climate averages than the thirty-year climate normals.

To apply the Bayesian approach, the data were prepared as follows. For mathematical convenience and to allow evaluating all twelve calendar months, the observations during the October 2004 through September 2005 evaluation period were standardized by subtracting each calendar month's 1971 through 2000 climate average and dividing by the 1971 through 2000 climate standard deviation. After standardization, the twelve monthly values for the evaluation period should meet the following conditions:

1. The mean should be zero with high probability.

2. The standard deviation should be less than one with high probability.

This was done individually for each of the six climate parameters. The Bayesian two-sample comparison was then performed for the following two data sets: the twelve monthly values of the evaluation period and 360 values randomly drawn from the standard normal distribution (representing thirty years of twelve-month standardized climate normals). The following four mutually exclusive and complementary probabilities were calculated:

1. Both data sets have equal means and equal standard deviations.
2. The two data sets have different means and equal standard deviations.
3. The two data sets have equal means and different standard deviations.
4. Both data sets have different means and different standard deviations.

This was repeated one thousand times to get a very robust representation of the climate normals, and finally the probabilities were averaged over the one thousand repetitions. The results are shown in Figure B.1 from top to bottom for the following parameters:

1. Monthly means of daily maximum temperatures.
2. Monthly means of daily mean temperature;
3. Monthly means of daily minimum temperatures;
4. Total monthly rain (all forms of precipitation except snow).
5. Total monthly snow.
6. Total monthly precipitation.
7. Combined monthly means of daily minimum and maximum temperatures.
8. Combined total monthly rain and snow.

An assumption underlying the Bayesian two-sample comparison is the independence of the individual values in each sample. Because daily mean temperatures are the mean of daily minimum and maximum temperatures and precipitation is the sum of rain and snow these two data sets were not included in the two combined data sets under points 7 and 8. It is worth noting that the two data sets in each of the combined data sets are typically slightly anti-correlated but not strongly enough to affect the conclusions drawn below.

The four probabilities in Figure B.1 add up to one and can be analyzed individually or in combinations to answer various questions. As described above, to meet the conditions for a representative evaluation year, means of zero and standard deviations of less than one are required. Table B.2 shows small mean values and standard deviations less than one. To evaluate the significance of these results, the following probabilities are of particular interest:

1. The probability of equal means and different standard deviations (yellow bars).

2. The probability of equal means (regardless of the standard deviations), which is the sum of the probability of equal means and equal standard deviations (dark blue bars) and the probability of equal means and different standard deviations (yellow bars).

3. The probability of different standard deviations (regardless of the means), which is the sum of the two probabilities for different standard deviations (yellow and brown bars).

A common measure used to amplify the probabilities in points 2 and 3 are the associated odds:

1. The odds in favour of equal means are the ratio of the probabilities of equal means and different means.

2. The odds in favour of different standard deviations are the ratio of the probabilities of different standard deviations and equal standard deviations.

As a rule of thumb, odds of more than three are considered statistically significant and roughly correspond to one standard deviation. Odds of more than 20 are considered statistically highly significant and roughly correspond to two standard deviations. The odds are shown in Table B.2.

Ideally, the yellow bars in Figure B.1 would dominate for all six parameters. This is true for rain, snow, and total precipitation. Also, the associated odds for equal means and for different standard deviations in Table B.2 are all statistically significant. Combining rain and snow into one data set doubles the length of the two samples (evaluation year and climate normals) and substantially improves the signal to noise ratio. The two odds for the combined data set are highly significant (Table B.2). Therefore, for rain, snow, and total precipitation, the evaluation year represents the average climate well.

For maximum, minimum, and mean temperature, the picture is more complicated. For the three individual data sets, the probabilities of equal means and different standard deviations (yellow bars in Figure B.1) do not dominate. Table B.2 shows significant odds for equal means but not for different standard deviations. For combined minimum and maximum temperatures, however, the probability of equal means and different standard deviations dominates in Figure B.1 (yellow bar), and the two odds in Table B.2 are significant.

Table B.2 Odds in favour of a representative baseline period

Parameter	[a] Standardized		[b] Odds in Favour of	
	Mean	Stdev	Equal Means	Different Stdev
Monthly means of daily maximum temperatures	0.13	0.86	3.8	(0.83)
Monthly means of daily mean temperatures	0.16	0.81	3.8	(0.98)
Monthly means of daily minimum temperatures	0.25	0.74	3.1	(1.2)
Total monthly rain	0.14	0.62	5.3	3.2
Total monthly snow	-0.07	0.54	7.3	7.7
Total monthly precipitation	0.13	0.58	5.8	4.7
Statistics for Combined Parameters				
Monthly means of daily minimum and maximum temperatures	0.19	0.79	17	6.9
Total monthly rain and snow	0.04	0.58	54	115

NOTES:
[a] Mean and standard deviations (Stdev) for the October 2004 to September 2005 baseline period after standardization with 1971-2000 climate averages and standard deviations for monthly averages/totals of the six parameters and two parameter combinations.
[b] Odds in favour of equal means and in favour of different standard deviations for evaluation year and climate normals. Statistically insignificant odds are shown in parentheses. High odds indicate a representative baseline period.

Given the need for the evaluation year to represent the average climate for several parameters simultaneously, the chosen October 2004 through September 2005 evaluation period can be considered a good choice.

Figure B.1 Probabilities of differences between baseline period and climate normals

2.0 REFERENCES

Gregory, P. 2005. *Bayesian Logical Data Analysis for the Physical Sciences: A Comparative Approach with Mathematica ® Support*. Cambridge University Press, Cambridge, United Kingdom and New York, NY, USA.

APPENDIX C

Climate and Air Quality Station Installation Summary

TABLE OF CONTENTS

1.0 INTRODUCTION C.1

2.0 DESCRIPTION OF STATIONS C.5

2.1 Station 1 – Attachie Flat Upper Terrace C.5

2.2 Station 2 – Attachie Flat Lower Terrace C.9

2.3 Station 3 – Attachie Plateau C.12

2.4 Station 4 – Bear Flat C.15

2.5 Station 5 – Hudson's Hope C.18

2.6 Station 7 – Site C Dam C.21

2.7 Station 8 – Old Fort C.24

3.0 OPERATION AND MAINTENANCE C.25

Table of Tables

Table C.1 Climate and Air Quality Stations Summary C.2

Table C.2 Site C Climate Stations C.5

Table C.3 Equipment Installed at Station 1 - Attachie Flat Upper Terrace C.8

Table C.4 Equipment Installed at Station 2 - Attachie Flat Lower Terrace C.11

Table C.5 Equipment Installed at Station 3 - Attachie Plateau C.14

Table C.6 Equipment Installed at Station 4 - Bear Flat C.17

Table C.7 Equipment Installed at Hudson's Hope C.20

Table C.8 Equipment Installed at Site C Dam C.23

Table C.9 Equipment Installed at Station 8 – Old Fort C.24

Table of Figures

Figure C.1 Map Showing the Locations of Climate and Air Quality Stations C.1

Figure C.2 Sample Wiring Diagram for Station 7 – Site C Dam C.3

Figure C.3 Sample Tower Footprint for Station 1 – Attachie Flat Upper Terrace C.4

Figure C.4 Station 1 – Attachie Flat Upper Terrace (Facing Northwest) C.6

Figure C.5 Location of Station 1 – Attachie Flat Upper Terrace (Denoted by Blue Box), Archaeological Sites (Denoted by Red Lines) Access Route (Denoted by Yellow Line) C.7

Figure C.6 Station 2 – Attachie Flat Lower Terrace (Facing North) C.9

Figure C.7 Location of Station 2 – Attachie Flat Lower Terrace (Denoted by Blue Box), Wash Station (Denoted by Red Circle) and Access Route (Denoted by Yellow Line) C.10

Figure C.8 Station 3 – Attachie Plateau (Facing East) C.12

Figure C.9 Location of Station 3 – Attachie Plateau (Denoted by Blue Box), Archaeological Sites (Denoted by Red Lines), Wash Station (Denoted by Red Dot) and Access Route (Denoted by Yellow Line) C.13

Figure C.10 Station 4 – Bear Flat (Facing Southeast) C.15

Figure C.11 Location of Station 4 (Denoted by Blue Box) and Access Route (Denoted by Yellow Line) C.16

Figure C.12 Station 5 – Hudson's Hope (Facing Northeast) C.18

Figure C.13 Location of Station 5 – Hudson's Hope (Denoted by Blue Box) and Access Route (Denoted by Yellow Line) C.19

Figure C.14 Station 7 – Site C Dam (Facing South) C.21

Figure C.15 Location of Station 7 – Site C Dam (Denoted by Blue Box), Archaeological Sites (Denoted by Red Lines), Vehicle Access Route (Denoted by Yellow Line) and Walking Access Route (Denoted by Dashed Blue Line) C.22

Figure C.16 Station 8 – Old Fort (Facing Southeast) C.24

1.0 INTRODUCTION

Site-specific climate and air quality data were deemed necessary to support baseline characterization, climate and air quality effects assessments, and erosion modelling along the shorelines of the reservoir potentially affected by the Site C dam. Given the lack of existing climate information available from the Peace River Valley, six climate stations and two air quality stations were installed downstream of Hudson's Hope to observe the micro-climate and air quality of the region. The stations are located north of the river, where road access is available, and are positioned to provide good spatial coverage along the Peace River between Hudson's Hope and Fort St. John as shown in Figure C.1.

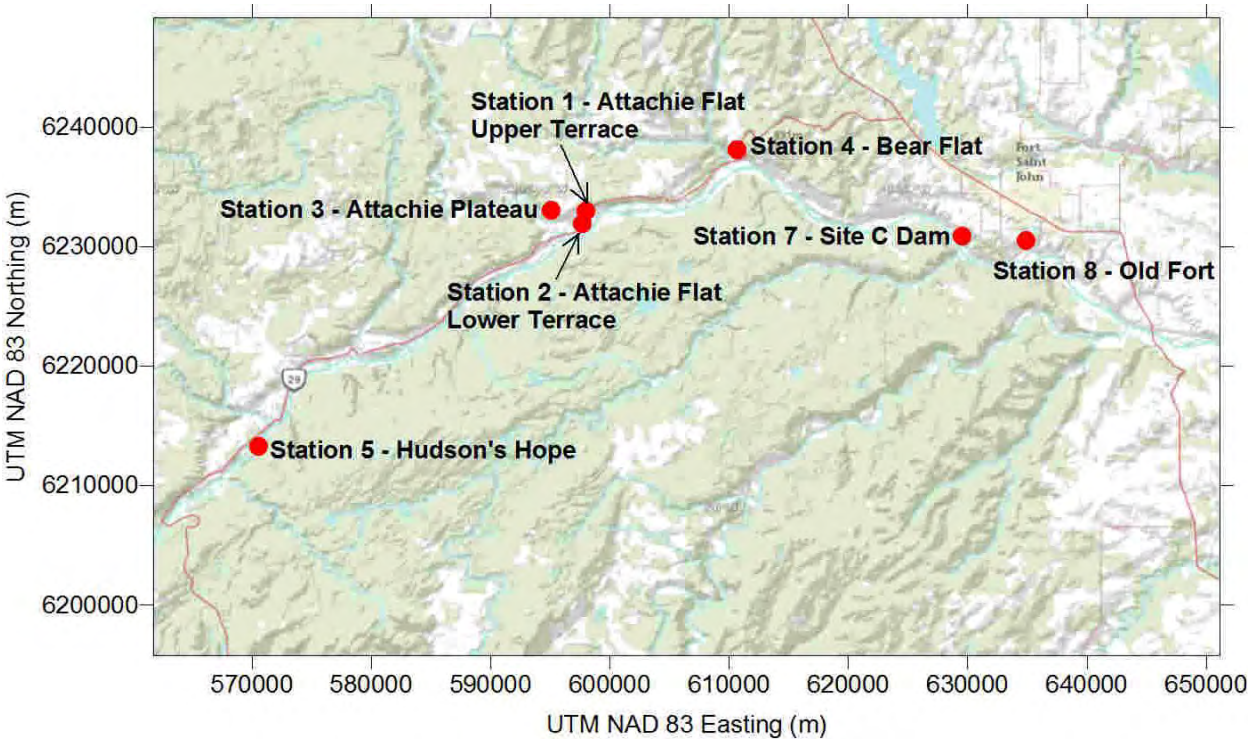

Figure C.1 Map Showing the Locations of Climate and Air Quality Stations

Three types of stations were installed: basic climate stations, research climate stations, and air quality stations. The basic climate stations measure wind speed and direction, relative humidity, precipitation, barometric pressure and incoming solar radiation. The research climate stations measure the parameters observed by the basic stations, as well as net radiation, soil heat flux, soil temperature, soil water content, sensible latent heat flux, wind speed in three dimensions and net radiation. Air quality stations measure two size fractions of particulate matter: less than 10 microns in diameter (PM_{10}) and less than 2.5 microns in diameter ($PM_{2.5}$). A summary of the stations is shown in Table C.1.

Table C.1 Climate and Air Quality Stations Summary

	Basic	Research	Air Quality	Other
Station 1 – Attachie Flat Upper Terrace		x	x	visibility
Station 2 – Attachie Flat Lower Terrace		x		
Station 3 – Attachie Plateau	x			
Station 4 – Bear Flat		x		
Station 5 – Hudson's Hope	x			
Station 7 – Site C Dam	x			
Station 8 – Old Fort			x	

Basic and research climate stations were installed between October 2010 and December 2010. The air quality stations were installed in December 2010 and February 2011.

A data logging program was written for each station to collect measurements from all instrumentation for selected averaging periods (30 minutes, hourly and daily). Instrumentation was tested in a controlled environment prior to installation to ensure each instrument was functioning properly with the data logger and the data logging program. A wiring diagram was also created for each station. An example of a wiring diagram is provided in Figure C.2.

Company:	RWDI
Project:	0920007A Station 7 - Site C Dam
Documented By:	MHW

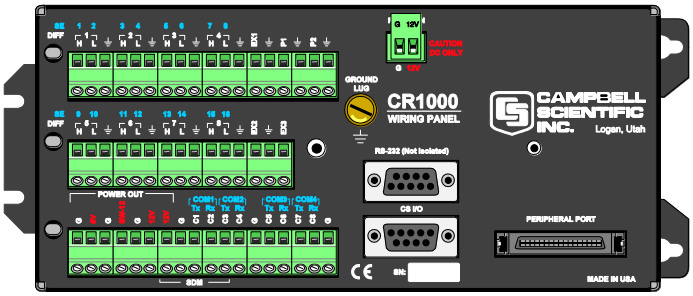

	G
	5V
	G
	SW-12
	G
61302V Power - Red, Crydom - Red(2)	12V
HMP45C212 Power - Red	12V
61302V Shield/Ground - Clr/Grn/Blk	G
	C1 (COM1 Tx)
	C2 (COM1 Red
	C3 (COM2 Tx)
	C4 (COM2 Red
	G
HMP45C212 Power Control - Yel	C5 (COM3 Tx)
	C6 (COM3 Red
	C7 (COM4 Tx)
Crydom - Red(3)	C8 (COM4 Red
	G

BP26 - Red (+), Crydom - Red(2)	12V
BP26 - Black (-), Crydom - Blk(4)	G
61302V Serial - Wht	5H (SE9)
	5L (SE10)
	6H (SE11)
	6L (SE12)
	7H (SE13)
	7L (SE14)
HMP45C212 Temp. Signal - Ora	8H (SE15)
HMP45C212 RH Signal - Grn	8L (SE16)
HMP45C212 Gnd/Ref- Clr, Prp, Wht	
HMP45C212 Ex - Blk	EX2
	EX3

05103 Signal - Grn	1H (SE1)
	1L (SE2)
05103 Ref - Wht	
CMP3 Signal - Wht	2H (SE3)
CMP3 Ref - Blu	2L (SE4)
CMP3 Shield - Clr	
	3H (SE5)
	3L (SE6)
	4H (SE7)
	4L (SE8)
05103 Ex - Blu	EX1
05103 - Red	P1
05103 - Blk & Clr	
TE525WS Signal - Blk	P2
TE525WS Shield/Ref - Clr, Wht	

Anemometer	**05103-10**	
EARTH GND	Clear	Clr
WS RedEF	Black	Blk
WD RedEF	White	Wht
WD SIG	Green	Grn
WD EXE	Blue	Blu
WS SIG	Red	Red

Barometric Prpressure	**61302V**	
TRIG/RX	Blue	Blu
REF	Green/Clea	Grn/Clr
-PWR	Black	Blk
+PWR	Red	Red
VOUT/TX	White	Wht

Rain Gauge	**TE525WS**	
	Black	Blk
	Clear	Clr
	White	Wht

Crydom - Modem	
To Modem Power (Red)	(1)
To Power	Red(2)
To Control Port 8	Red(3)
To Power Ground	Black(4)

Temperature and RedH	**HMP45C212**	
	Yellow	Yel
	Orange	Ora
	Black	Blk
	Clear	Clr
	White	Wht
	Purple	Prp
	Green	Grn
	Red	Red

Solar Redad'n (Pyranometer	**CMP3-L**	
	White	Wht
	Blue	Blu
	Clear	Clr

Figure C.2 Sample Wiring Diagram for Station 7 – Site C Dam

Prior to installing the stations, BC Hydro consulted with the affected land owners and leaseholders to get their input on the proposed station locations and accommodate, where possible, the schedule, approach, and siting of the stations to minimize impacts to their operations. Stations were installed between October 2010 and February 2011.

Stations were assembled on site in accordance with an Environmental Management Plan (EMP) approved by BC Hydro for each climate station. Concrete tower bases and guy wire anchors

were constructed for research climate station towers. Six-foot high chain-linked fencing was erected for all climate stations except Station 5 – Hudson's Hope where the existing fencing was used. Gates to each station were locked during installation and continue to be locked during station operation. All station equipment and materials were transported by truck to each site. Each station was installed following tower footprints. An example of a tower footprint is shown in Figure C.3.

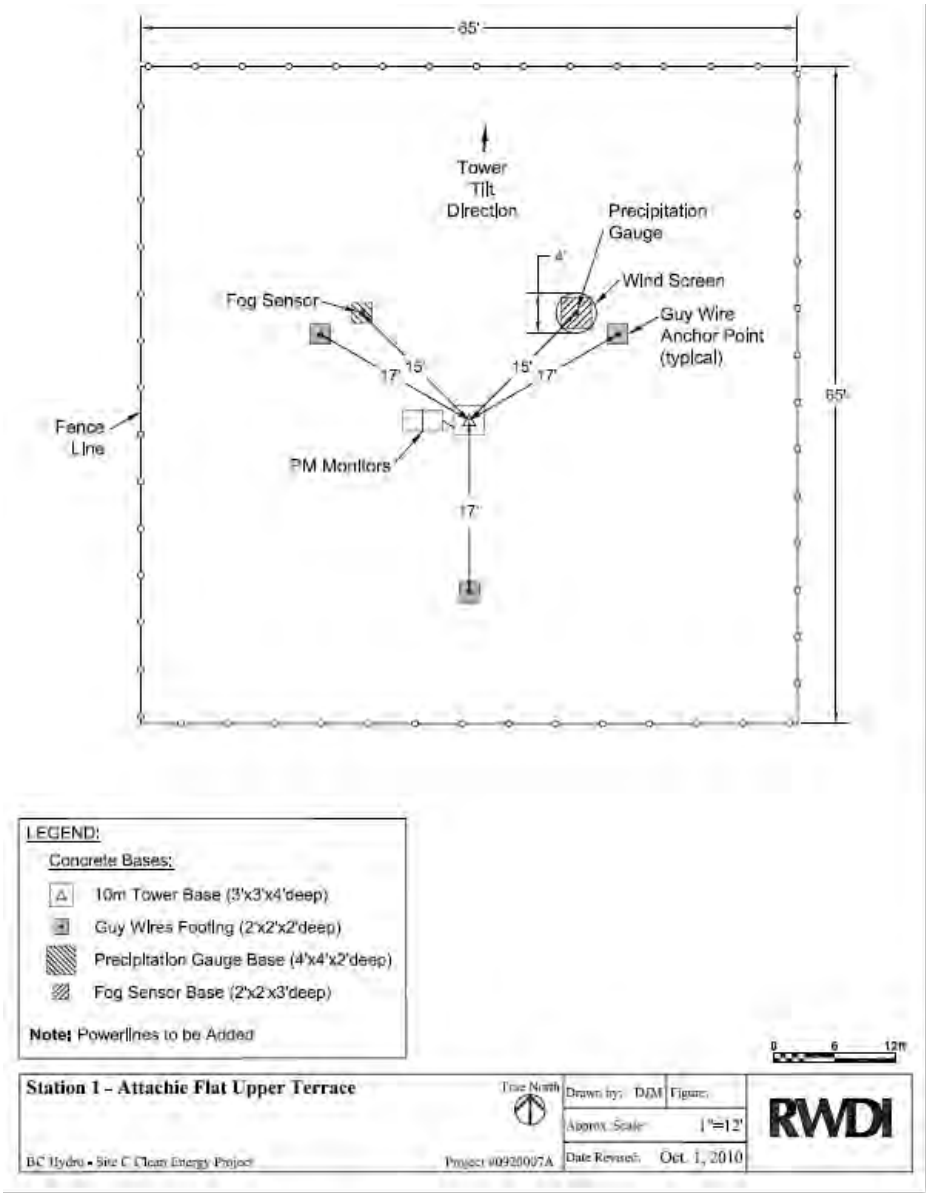

Figure C.3 Sample Tower Footprint for Station 1 – Attachie Flat Upper Terrace

2.0 DESCRIPTION OF STATIONS

Full descriptions of each station are provided in this section. Local terrain and land use around each site are presented using aerial and site photos. Station details including location, power supply, tower type and data range are summarized in Table C.2.

Table C.2 Site C Climate Stations

Station	Location UTM NAD 83 (m)	Power	Tower	Measurement Period
Station 1 – Attachie Flat Upper Terrace	597983 Easting 6232938 Northing	AC	In ground	January 15, 2011 to present
Station 2 – Attachie Flat Lower Terrace	597721 Easting 6231898 Northing	Batteries/Solar	In ground	January 13, 2011 to present
Station 3 – Attachie Plateau	595065 Easting 6233032 Northing	Batteries/Solar	Free standing	November 4, 2010 to present
Station 4 – Bear Flat	610669 Easting 6238135 Northing	AC	In ground	December 1, 2010 to present
Station 5 – Hudson's Hope	570577 Easting 6213303 Northing	Batteries/Solar	Free standing	December 12, 2010 to present
Station 7 – Site C Dam	629517 Easting 6230875 Northing	Batteries/Solar	Free standing	November 27, 2010 to present
Station 8 – Old Fort	634890 Easting 6230532 Northing	AC	No tower	February 28, 2011 to present

2.1 STATION 1 – ATTACHIE FLAT UPPER TERRACE

A research climate station and an air quality monitoring station were installed at Attachie Flat Upper Terrace. An in-ground tower with a concrete base replaced the existing free-standing tower that was used for the temporary wind station. The free-standing tower was disassembled and removed as it was not suitable for the proposed instrumentation.

A photograph of the location facing northwest and an aerial view of the area with the access route from the highway are presented in Figure C.4 and Figure C.5, respectively. The instruments and equipment installed at this station are outlined in Table C.3. Basic climate instrumentation and additional research instrumentation were installed at this station, as well as a visibility sensor. Two Thermo SHARP 5030 air quality monitors were installed to simultaneously measure PM_{10} and $PM_{2.5}$. The station is AC powered to accommodate the power required by all the instrumentation installed at this station.

Figure C.4 Station 1 – Attachie Flat Upper Terrace (Facing Northwest)

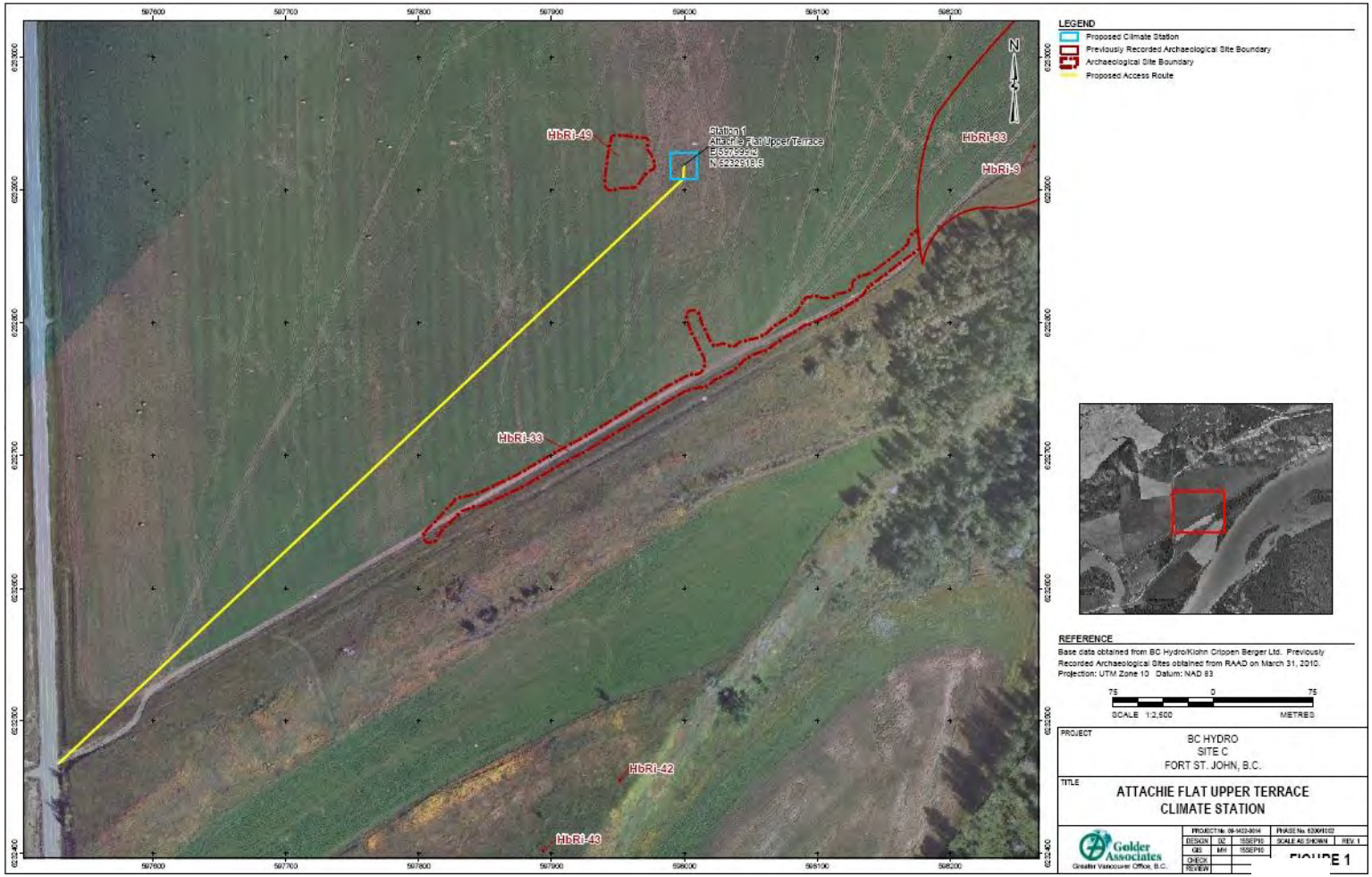

Figure C.5 Location of Station 1 – Attachie Flat Upper Terrace (Denoted by Blue Box), Archaeological Sites (Denoted by Red Lines) Access Route (Denoted by Yellow Line)

Table C.3 Equipment Installed at Station 1 - Attachie Flat Upper Terrace

Instrumentation/Equipment	Model	Parameter	Instrument Siting
Data Loggers	CR1000 -55 (two)	-	-
Data Logger Enclosures	Hammond Enclosure (two)	-	-
Modem	Raven X-Telus	-	-
Anemometer	RM Young 05103-10-L	Wind speed and direction	Ten metres
Barometric Pressure Sensor	RM Young 61302V	Barometric pressure	Screen level[1]
Relative Humidity and Temperature Probe	Vaisala HMP45C212 and 076B Aspirated Radiation Shield	Relative humidity and air temperature	Screen level
Precipitation Gauge	Texas Electronics TE525WS, CS705 and Alter Wind Screen 51	Precipitation	Screen level
Eddy-Covariance System	CSAT3 Sonic Anemometer and LI-COR H_2O analyzer LI-7500 A	Sensible and latent heat flux, wind speed and direction	Three metres
Net Radiometer	Kipp & Zonen CNR4	Net radiation and all components	Eight metres
PM monitors	Thermo SHARP 5030 (two)	PM_{10}, and $PM_{2.5}$	Screen level
Visibility Sensor	SVS1-AC-2-H Sentry	Visibility (fog)	Screen level
Soil Reflectometry	TDR Installation kit CS616 & CS615	Water Content and bulk electrical conductivity	Five centimetres below surface
Soil Temperature Probe	TCAV-L L10956	Soil Temperature	Surface level
Heat Flux Transducer	HFT3	Heat Flux	Surface level

[1] Screen level is between the surface and two metres above the surface

2.2 STATION 2 – ATTACHIE FLAT LOWER TERRACE

A research climate station with an in-ground tower was installed at Station 2 - Attachie Flat Lower Terrace. A photograph of the location facing north and an aerial view of the area with the access route from the highway are presented in Figure C.6 and Figure C.7, respectively. The instruments and equipment installed at this station are outlined in Table C.4. Basic climate instrumentation and additional research instrumentation were installed at this station. The basic instrumentation is powered by batteries charged by solar panels. Although this is a research station, AC power was not brought to this station because it was more cost effective to purchase larger solar panels with a large set of batteries than to install power poles, and also reduce the physical footprint on the property. A signal booster was also installed to provide the Raven-X modem at Station 2 with sufficient cellular signal for station connection and data retrieval.

Figure C.6 Station 2 – Attachie Flat Lower Terrace (Facing North)

Figure C.7 Location of Station 2 – Attachie Flat Lower Terrace (Denoted by Blue Box), Wash Station (Denoted by Red Circle) and Access Route (Denoted by Yellow Line)

Table C.4 Equipment Installed at Station 2 - Attachie Flat Lower Terrace

Instrumentation/Equipment	Model	Parameter	Instrument Siting
Data Loggers	CR1000 -55 (two)	-	-
Data Logger Enclosures	Hammond Enclosures (two)	-	-
Modem	Raven X-Telus	-	-
Anemometer	RM Young 05103-10-L	Wind speed and direction	Ten metres
Barometric Pressure Sensor	RM Young 61302V	Barometric pressure	Screen level
Relative Humidity and Temperature Probe	Vaisala HMP45C212 and 076B Aspirated Radiation Shield	Relative humidity and air temperature	Screen level
Precipitation Gauge	Texas Electronics TE525WS, CS705 and Alter Wind Screen 51	Precipitation	Screen level
Eddy-Covariance System	CSAT3 Sonic Anemometer and LI-COR H_2O analyzer LI-7500A	Sensible and latent heat flux, wind speed and direction	Three metres
Net Radiometer	Kipp & Zonen CNR4	Net radiation and all components	Eight metres
Soil Reflectometry	TDR Installation kit CS616 & CS615	Water Content and bulk electrical conductivity	Five centimetres below surface
Soil Temperature Probe	TCAV-L L10956	Soil Temperature	Surface level
Heat Flux Transducer	HFT3	Heat Flux	Surface level

2.3 STATION 3 – ATTACHIE PLATEAU

A basic climate station with a free-standing tower was installed at Station 3 - Attachie Plateau. A photograph of the location facing east and an aerial view of the area with the access route from the highway are presented in Figure C.8 and Figure C.9, respectively. The instruments and equipment installed at this station are outlined in Table C.5. Basic climate instrumentation was installed at this station. The basic instrumentation is powered by batteries charged by a solar panel. AC power is not needed at this site since the solar panel can provide sufficient power for basic instrumentation.

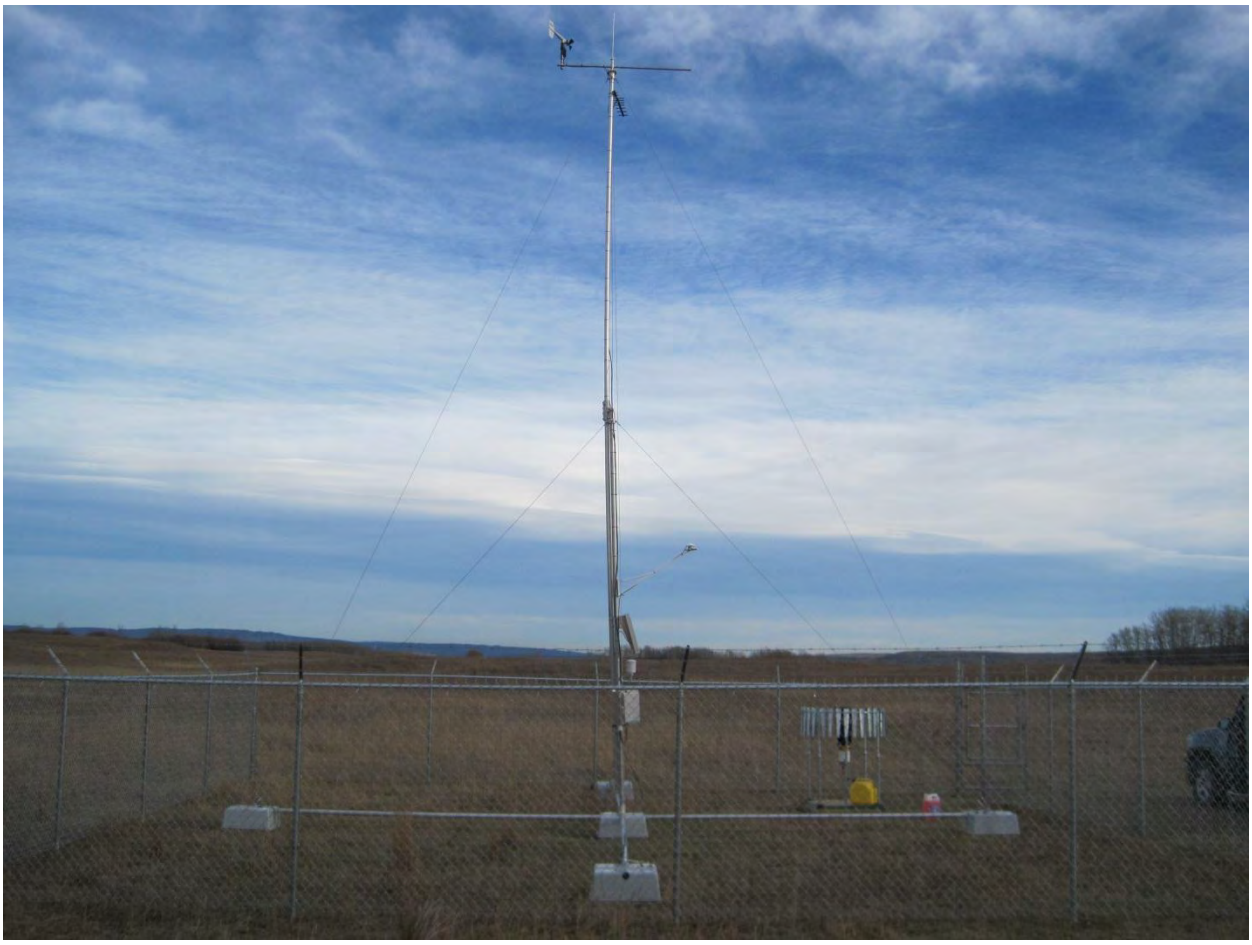

Figure C.8 Station 3 – Attachie Plateau (Facing East)

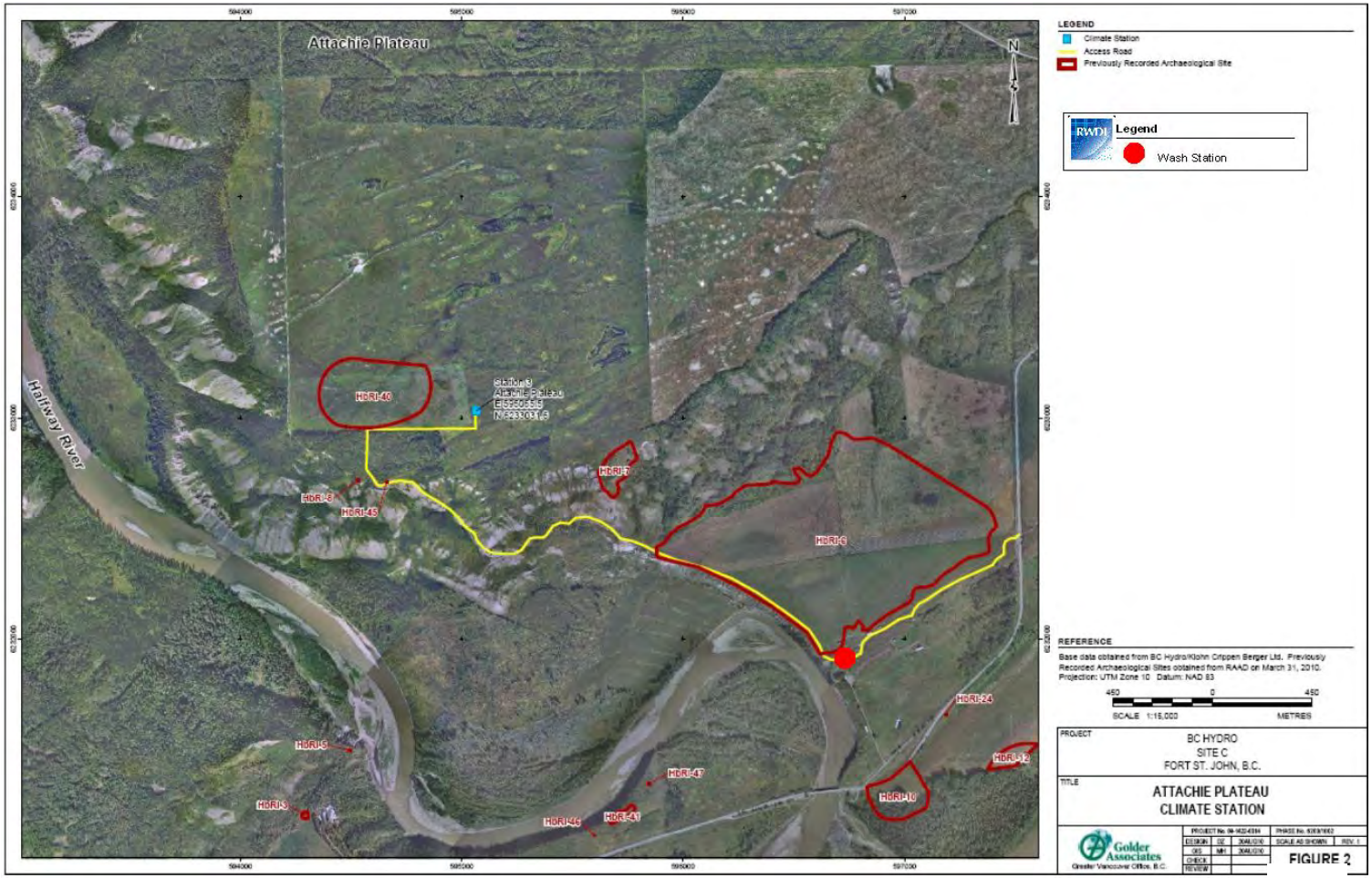

Figure C.9 Location of Station 3 – Attachie Plateau (Denoted by Blue Box), Archaeological Sites (Denoted by Red Lines), Wash Station (Denoted by Red Dot) and Access Route (Denoted by Yellow Line)

Table C.5 Equipment Installed at Station 3 - Attachie Plateau

Instrumentation/Equipment	Model	Parameter	Instrument Siting
Data Loggers	CR1000 -55	-	-
Data Logger Enclosures	Hammond Enclosures	-	-
Modem	Raven X-Telus	-	-
Anemometer	RM Young 05103-10-L	Wind speed and direction	Ten metres
Barometric Pressure Sensor	RM Young 61302V	Barometric pressure	Screen level
Relative Humidity and Temperature Probe	Vaisala HMP45C212 and RM Young 41003-X Radiation Shield	Relative humidity and air temperature	Screen level
Precipitation Gauge	Texas Electronics TE525WS, CS705 and Alter Wind Screen 51	Precipitation	Screen level
Pyranometer	Kipp & Zonen CMP3-L	Incoming Solar Radiation	Three and a half metres

2.4 STATION 4 – BEAR FLAT

A research climate station with an in-ground tower was installed at Station 4 - Bear Flat. A tower with a concrete base replaced the free-standing tower that was used for the temporary wind station at this location. The free-standing tower was disassembled and its components reused for Station 3 – Attachie Plateau. A photograph of the location facing southeast and an aerial view of the area with the access route from the highway are presented in Figure C.10 and Figure C.11, respectively. The instruments and equipment installed at this station are outlined in Table C.6. Basic climate instrumentation and additional research instrumentation were installed at this station. AC power was required at this site. The cellular signal at this station was not sufficient to establish a stable connection for remote data transfer; therefore, a satellite modem was installed.

Figure C.10 Station 4 – Bear Flat (Facing Southeast)

Figure C.11 Location of Station 4 (Denoted by Blue Box) and Access Route (Denoted by Yellow Line)

Table C.6 Equipment Installed at Station 4 - Bear Flat

Instrumentation/Equipment	Model	Parameter	Instrument Siting
Data Loggers	CR1000 -55 (two)	-	-
Data Logger Enclosures	Hammond Enclosure (two)	-	-
Satellite Modem	Iridium 9522B	-	-
Anemometer	RM Young 05103-10-L	Wind speed and direction	Ten metres
Barometric Pressure Sensor	RM Young 61302V	Barometric pressure	Screen level
Relative Humidity and Temperature Probe	Vaisala HMP45C212 and 076B Aspirated Radiation Shield	Relative humidity and air temperature	Screen level
Precipitation Gauge	Texas Electronics TE525WS, CS705 and Alter Wind Screen 51	Precipitation	Screen level
Eddy-Covariance System	CSAT3 Sonic Anemometer and LI-COR H_2O analyzer LI-7500A	Sensible and latent heat flux, wind speed and direction	Three metres
Net Radiometer	Kipp & Zonen CNR4	Net radiation and all components	Eight metres
Soil Reflectometry	TDR Installation kit CS616 & CS615	Water Content and bulk electrical conductivity	Five centimetres below surface
Soil Temperature Probe	TCAV-L L10956	Soil Temperature	Surface level
Heat Flux Transducer	HFT3-L	Heat Flux	Surface level

2.5 STATION 5 – HUDSON'S HOPE

The existing wind station with a free-standing tower at Hudson's Hope was converted to a basic climate station. A photograph of the location facing northeast and an aerial view of the area with the access route from the highway are presented in Figure C.12 and Figure C.13, respectively. The instruments and equipment installed at this station are outlined in Table C.7. Basic instrumentation was installed at this station. The basic instrumentation is powered by batteries charged by a solar panel. AC power is not needed at this site since the solar panel can provide sufficient power for basic instrumentation.

Figure C.12 Station 5 – Hudson's Hope (Facing Northeast)

Figure C.13 Location of Station 5 – Hudson's Hope (Denoted by Blue Box) and Access Route (Denoted by Yellow Line)

Table C.7 Equipment Installed at Hudson's Hope

Instrumentation/Equipment	Model	Parameter	Instrument Height
Data Logger	CR1000 -55	-	-
Data Logger Enclosure	Hammond Enclosure	-	-
Modem	Raven X-Telus	-	-
Anemometer	RM Young 05103-10-L	Wind speed and direction	Ten metres
Barometric Pressure Sensor	RM Young 61302V	Barometric pressure	Screen level
Pyranometer	Kipp & Zonen CMP3-L	Incoming solar radiation	Three and a half metres
Precipitation Gauge	Texas Electronics TE525WS, CS705 and Alter Wind Screen 51	Precipitation	Screen level
Relative Humidity and Temperature Probe	Vaisala HMP45C212 and RM Young 41003-X Radiation Shield	Relative humidity and air temperature	Screen level

2.6 STATION 7 – SITE C DAM

The temporary wind station with a free-standing tower at Site C Dam was converted to a basic climate station. A photograph of the location facing northeast and an aerial view of the area with the access route from the highway are presented in Figure C.14 and Figure C.15, respectively. The instruments and equipment installed at this station are outlined in Table C.8. Basic instrumentation was installed at this station. The basic instrumentation is powered by batteries charged by a solar panel. AC power is not needed at this site since the solar panel can provide sufficient power for basic instrumentation.

Figure C.14 Station 7 – Site C Dam (Facing South)

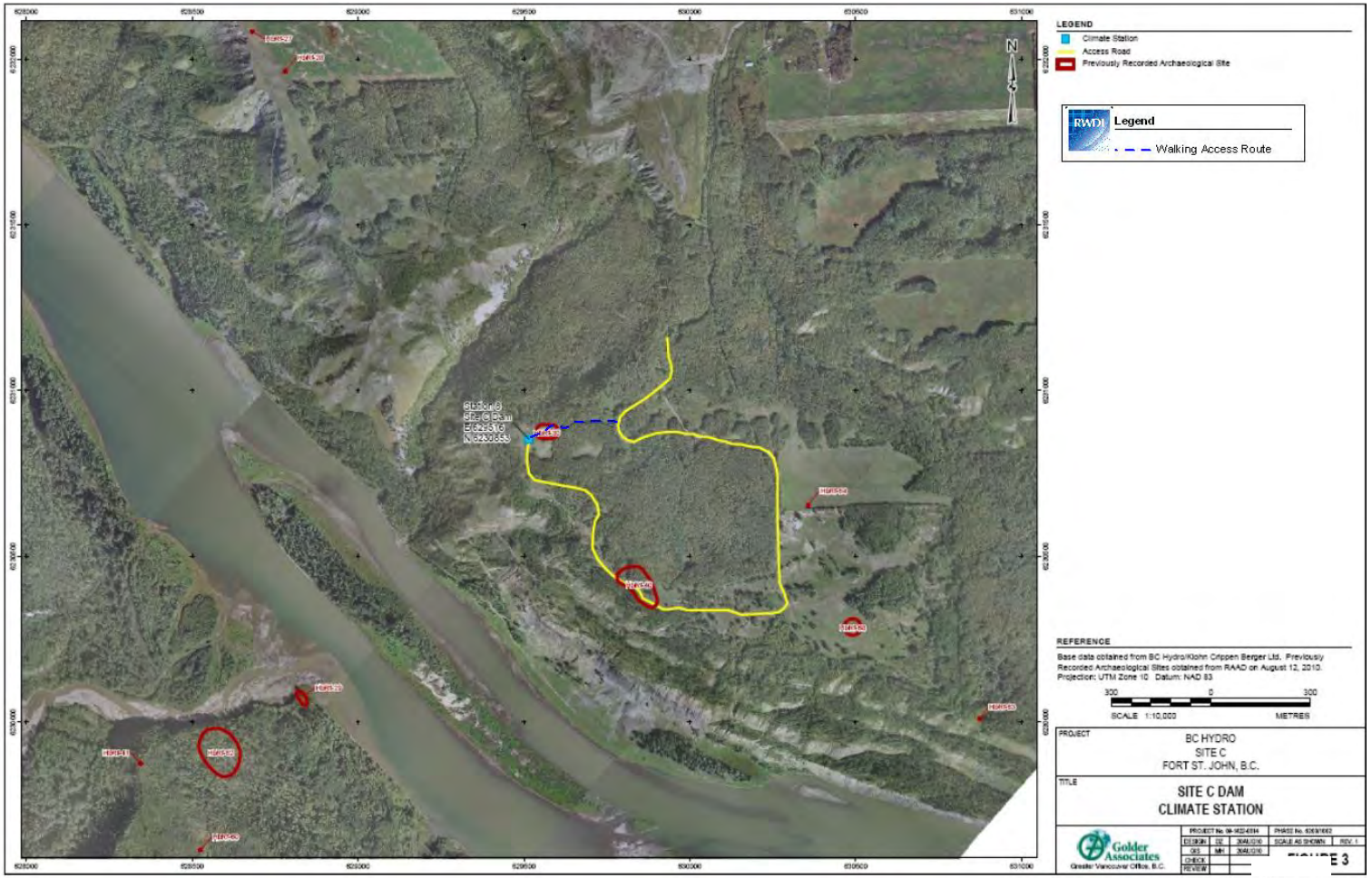

Figure C.15 Location of Station 7 – Site C Dam (Denoted by Blue Box), Archaeological Sites (Denoted by Red Lines), Vehicle Access Route (Denoted by Yellow Line) and Walking Access Route (Denoted by Dashed Blue Line)

Table C.8 Equipment Installed at Site C Dam

Instrumentation/Equipment	Model	Parameter	Instrument Height
Data Logger	CR1000 -55	-	-
Data Logger Enclosure	Hammond Enclosure	-	-
Modem	Raven X Telus	-	-
Anemometer	RM Young 05103-10-L	Wind speed and direction	Ten metres
Barometric Pressure Sensor	RM Young 61302V	Barometric pressure	Screen level
Pyranometer	Kipp & Zonen CMP3-L	Incoming solar radiation	Three and a half metres
Precipitation Gauge	Texas Electronics TE525WS, CS705 and Alter Wind Screen 51	Precipitation	Screen level
Relative Humidity and Temperature Probe	Vaisala HMP45C212 and RM Young 41003-X Radiation Shield	Relative humidity and air temperature	Screen level

2.7 STATION 8 – OLD FORT

Station 8 – Old Fort was installed downwind of the proposed Site C Dam near Fort St. John. It measures PM_{10} and $PM_{2.5}$ concentrations. The instruments and equipment installed at this station are outlined in Table C.9. This station does not measure climate parameters. The instrumentation is powered by AC power. A photograph of the station's instrumentation is shown in Figure C.16.

Table C.9 Equipment Installed at Station 8 – Old Fort

Instrumentation/Equipment	Model	Parameter	Instrument Siting
Data Loggers	CR800	-	-
Modem	Raven XT-Telus	-	-
PM monitors	Thermo SHARP 5030 (two)	PM_{10}, and $PM_{2.5}$	Screen level

Figure C.16 Station 8 – Old Fort (Facing Southeast)

3.0 OPERATION AND MAINTENANCE

Thirty-minute, hourly and daily averages are recorded by the data logger with a sampling period of 5 seconds for all climate parameters. Station 8 – Old Fort records hourly and daily average PM_{10} and $PM_{2.5}$ with a sampling period of 5 seconds. The timestamp given to observations collected is Pacific Standard Time (GMT-7:00) and there will be no adjustment for daylight savings time.

Field staff from Matrix Solutions will visit each station once every two weeks to check that the station is operating normally. Visits will be more frequent in the winter, as solar panels need to be cleared after a snowfall. Proper snow clearing to allow access to the stations in winter is extremely important. BC Hydro has arranged for snow clearing of the site access routes by local contractors/residents. Matrix is to report on any issues with respect to snow clearing or site access, so that RWDI can inform BC Hydro. Lack of ability to access the sites can result in station visits being extended or delayed, and could potentially disrupt proper operation of the stations.

Visits to the station will consist of a field staff accessing each site following the EMP, downloading data and visually checking the station for problems. Field staff will retrieve eddy covariance system data from research climate stations and upload the data onto an FTP site. The data will then be downloaded by RWDI staff for analysis. Field staff will also visually check that the station is operating normally and look for any tampering, damage or wear to the station instrumentation. Snow will be cleared from the equipment as required. The visual check will typically take less than 15 minutes. In total it is anticipated that field staff will spend a day to visit all stations unless there are problems with a station. All field staff must follow the EMP.

Stations powered by solar-panel-charged batteries will likely require fewer maintenance visits when snowfall is not expected. Research stations will, however, require biweekly visits by field staff to download eddy covariance data from the data loggers. Data will be automatically downloaded daily and checked for anomalies and errors three times per week. Potential issues that can be identified remotely include (but are not limited to):

- Unable to connect to a station remotely
- Data gaps
- Drop in battery voltage
- Erroneous measurements or data spikes

If a station is suspected to be malfunctioning, RWDI will contact field staff from Matrix Solutions to examine the station as soon as possible to address all potential issues.

The following maintenance will be performed on the Thermo Sharp 5030 particulate monitors:

- Sample inlets and radiation shields will be cleaned on a monthly basis and parts will be replaced as required.

- Every three months, each unit will be recalibrated.

- A pump rebuild will be performed annually.

Additional maintenance required at the stations will likely be minor.

APPENDIX D

Fort St. John Airport Climate Normals

Temperature	Jan	Feb	Mar	Apr	May	Jun	Jul	Aug	Sep	Oct	Nov	Dec	Year	Code
Daily Average (°C)	-14.2	-10.5	-4.4	4	10	13.8	15.7	14.6	9.9	3.9	-6.7	-12.1	2	A
Standard Deviation	5.7	5.6	3.6	2.2	1.7	1.1	1.1	1.5	2	2	4.5	5.3	1.3	A
Daily Maximum (°C)	-9.9	-6	0.3	9.3	15.7	19.2	21.2	20.2	15.1	8.2	-2.9	-8	6.9	A
Daily Minimum (°C)	-18.4	-15	-9.1	-1.3	4.1	8.2	10.2	8.9	4.6	-0.4	-10.4	-16.2	-2.9	A
Extreme Maximum (°C)	11.6	12.8	18	27.9	31.8	31.7	33.3	33.6	30	25.6	18.3	11.4		
Date (yyyy/dd)	1993/30	1943/17	1994/30	1977/25	1983/29	1969/17	1944/19	1981/09	1944/09	1943/02	1949/02	1980/15		
Extreme Minimum (°C)	-47.2	-42.2	-36.7	-28.9	-10.6	-0.6	0.7	-2.9	-12.8	-25	-39.2	-44.6		
Date (yyyy/dd)	1947/30	1947/01	1951/05	1954/01	1959/01	1951/25	1999/04	1992/22	1974/30	1984/31	1985/26	1992/29		
Precipitation														
Rainfall (mm)	0.4	0.5	0.7	8.8	35.5	70.9	83.2	56.1	41.1	11.5	3.4	0.6	312.6	A
Snowfall (cm)	32.2	28.3	25.3	10.6	4.1	0.4	0	0.8	4.8	16.5	30.3	32.4	185.6	A
Precipitation (mm)	26	21.9	21.4	18.8	39.7	71.4	83.2	56.9	45.7	25.8	28.5	26.5	465.6	A
Average Snow Depth (cm)	30	31	25	6	0	0	0	0	0	1	9	20	10	A
Median Snow Depth (cm)	30	30	25	4	0	0	0	0	0	0	10	20	10	A
Snow Depth at Month-end (cm)	31	29	16	0	0	0	0	0	0	2	13	23	10	A
Extreme Daily Rainfall (mm)	8.1	4	6.6	28.9	49.8	80.3	60.2	58.4	37.3	15.2	12.7	5.8		
Date (yyyy/dd)	1965/20	1995/01	1944/16	1994/22	1979/27	1965/27	1972/09	1972/10	1984/06	1970/04	1952/03	1989/27		
Extreme Daily Snowfall (cm)	21.4	27.3	31.5	20.8	47.8	11.7	0.4	18.5	18.5	34.5	24	28.7		
Date (yyyy/dd)	1988/27	1990/11	1954/10	1969/24	1960/22	1976/01	1999/04	1973/17	1972/21	1957/04	1996/09	1955/11		
Extreme Daily Precipitation (mm)	18.5	17.4	31.5	28.9	49.8	80.3	60.2	58.4	37.3	34.5	24.9	28.7		
Date (yyyy/dd)	1968/20	1990/11	1954/10	1994/22	1979/27	1965/27	1972/09	1972/10	1984/06	1957/04	1957/22	1955/11		
Extreme Snow Depth (cm)	99	107	112	99	23	0	0	5	10	61	67	90		
Date (yyyy/dd)	1967/30	1967/06	1974/28	1974/01	1960/23	1955/01	1955/01	1973/18	1972/22	1957/06	1995/30	1995/16		
Days with Maximum Temperature														
<= 0 °C	23.2	17.5	12.6	2	0.1	0	0	0	0.2	3.4	17	22.2	98.2	A

Temperature	Jan	Feb	Mar	Apr	May	Jun	Jul	Aug	Sep	Oct	Nov	Dec	Year	Code
> 0 °C	7.8	10.7	18.4	28	30.9	30	31	31	29.8	27.6	13	8.8	267.1	A
> 10 °C	0.1	0.2	1.4	14.7	27.6	29.4	30.9	30.4	25.3	12	0.6	0.1	172.8	A
> 20 °C	0	0	0	0.66	6.1	12.4	18.8	15.9	5.6	0.73	0	0	60.2	A
> 30 °C	0	0	0	0	0.03	0.03	0.23	0.33	0	0	0	0	0.62	A
> 35 °C	0	0	0	0	0	0	0	0	0	0	0	0	0	A
Days with Minimum Temperature														
> 0 °C	0.93	1.4	3.2	12.1	26.8	29.9	31	30.8	25.6	14.7	2.4	1.3	180.1	A
<= 2 °C	30.7	27.4	30.2	23.2	9	0.4	0.07	0.67	8.1	21.4	28.9	30.3	210.3	A
<= 0 °C	30.1	26.8	27.8	17.9	4.2	0.1	0	0.17	4.4	16.3	27.6	29.7	185.1	A
< -2 °C	28.7	25.4	24.4	10.3	1	0	0	0.03	1.8	10.5	24.8	28.2	155.3	A
< -10 °C	23.4	17.9	12.8	1.8	0	0	0	0	0.07	1.5	14.7	21.3	93.5	A
< -20 °C	13.9	9.5	3.7	0.07	0	0	0	0	0	0.1	4.3	11.9	43.4	A
< - 30 °C	4.9	2	0.13	0	0	0	0	0	0	0	0.23	3	10.3	A
Days with Rainfall														
>= 0.2 mm	0.57	0.4	0.6	3.6	8.4	11.5	13.1	10.6	9.7	5.5	1.6	0.43	66	A
>= 5 mm	0	0	0	0.62	2.3	4	5	3.3	2.6	0.67	0.17	0.03	18.7	A
>= 10 mm	0	0	0	0.14	1	2.2	2.5	1.6	1	0.03	0.07	0	8.5	A
>= 25 mm	0	0	0	0.03	0.1	0.57	0.57	0.43	0.13	0	0	0	1.8	A
Days With Snowfall														
>= 0.2 cm	11.3	9.7	8.5	4.1	1.3	0.07	0.03	0.13	1.2	5.1	10.3	10.8	62.6	A
>= 5 cm	2	1.6	1.9	0.72	0.34	0.03	0	0.03	0.37	1.3	1.8	2.1	12.2	A
>= 10 cm	0.37	0.53	0.23	0.14	0.1	0.03	0	0.03	0.07	0.3	0.3	0.5	2.6	A
>= 25 cm	0	0.03	0	0	0	0	0	0	0	0	0	0	0.03	A
Days with Precipitation														
>= 0.2 mm	10.8	9.4	8.5	6.9	9	11.5	13.1	10.6	10.2	9.2	10.9	10.7	120.9	A
>= 5 mm	1.5	1.1	1.5	1.2	2.6	4	5	3.3	3	1.5	1.6	1.5	27.8	A
>= 10 mm	0.27	0.27	0.13	0.31	1.1	2.2	2.5	1.6	1.4	0.37	0.33	0.37	10.8	A

Temperature	Jan	Feb	Mar	Apr	May	Jun	Jul	Aug	Sep	Oct	Nov	Dec	Year	Code
>= 25 mm	0	0	0.03	0.03	0.1	0.6	0.57	0.47	0.13	0.03	0	0	2	A
Days with Snow Depth														
>= 1 cm	30	27.5	25.6	9	0.52	0	0	0.03	0.57	5.6	21.2	28.6	148.8	A
>= 5 cm	27.8	25.2	22.5	6.1	0.14	0	0	0.03	0.33	2.8	16.1	23.4	124.4	A
>= 10 cm	25	21.2	19.1	4.6	0.07	0	0	0	0.13	1.3	12	19.3	102.7	A
>= 20 cm	18.5	16.3	14.2	2.6	0	0	0	0	0	0.07	4.7	13.2	69.5	A
Wind														
Speed (km/h)	13.7	14.3	13.8	14.4	14.3	13.6	12.3	11.9	13	15.4	13.8	13.7	13.7	A
Most Frequent Direction	SW	N	N	SW	SW	SW	SW	SW	SW	SW	SW	SW	SW	A
Maximum Hourly Speed (km/h)	89	84	68	77	77	64	80	58	64	80	74	97		
Date (yyyy/dd)	1963/06	1953/25	1959/17	1961/01	1965/12	1956/06	1955/19	1961/06	1956/23	1962/17	1956/19	1956/25		
Direction of Maximum Hourly Speed	SW	SW	SW	SW	SW	SW	SW	W	SW	SW	SW	SW	SW	
Maximum Gust Speed (km/h)	138	100	89	103	105	87	102	107	92	121	117	117		
Date (yyyy/dd)	1963/07	1976/07	1962/08	1961/01	1965/12	1960/01	1997/20	1996/30	1973/08	1966/24	1962/19	1959/05		
Direction of Maximum Gust	SW	SW	N	SW	SW	SW	SW	S	SW	S	SW	S	SW	
Days with Winds >= 52 km/h	1.2	1.1	0.5	0.5	0.4	0.2	0.2	0.2	0.3	0.9	0.6	0.7	6.6	A
Days with Winds >= 63 km/h	0.3	0.2	0	0	0.1	0	0.1	0	0	0.2	0	0.1	1.1	A
Degree Days														
Above 24 °C	0	0	0	0	0	0	0	0	0	0	0	0	0	A
Above 18 °C	0	0	0	0	1	3.1	11.7	10.4	0.8	0	0	0	27	A
Above 15 °C	0	0	0	0.3	6.6	20.7	47.6	39.7	6	0.9	0	0	121.7	A
Above 10 °C	0	0	0	5.3	49.1	117.3	178.6	148.3	49.4	10.9	0	0	558.9	A
Above 5 °C	0.3	1	2.4	43.3	161	262.6	333	297.9	156.7	50.7	2.2	0.8	1311.9	A
Above 0 °C	7.5	12.9	33.2	145.4	309.6	412.5	488	452.7	297	147.9	19.4	10.1	2336.2	A

Temperature	Jan	Feb	Mar	Apr	May	Jun	Jul	Aug	Sep	Oct	Nov	Dec	Year	Code
Below 0 °C	446.7	309.6	169.7	22.2	0.6	0	0	0	1.4	26.7	220.3	384.4	1581.6	A
Below 5 °C	594.5	439	293.9	70.1	7	0.1	0	0.2	11.1	84.5	353	530.1	2383.6	A
Below 10 °C	749.2	579.4	446.5	182.1	50.1	4.8	0.6	5.7	53.8	199.7	500.8	684.3	3457	A
Below 15 °C	904.2	720.7	601.5	327.1	162.7	58.3	24.6	52	160.3	344.7	650.8	839.3	4846.1	A
Below 18 °C	997.2	805.5	694.5	416.8	250	130.6	81.7	115.7	245.2	436.8	740.8	932.3	5847.2	A
Bright Sunshine														
Total Hours	76.2	106.2	171.1	230.4	280.9	283.3	294.9	267.8	174.5	139.9	78.6	60.8	2164.8	D
Days with measureable	21.6	22.2	28.2	28.1	29.4	27.3	29.9	28.9	27	26.5	20.3	19.7	309.1	D
% of possible daylight hours	32.2	39.5	46.7	54.2	55.5	53.8	55.9	57.2	45.4	43.2	31.6	27.9	45.3	D
Extreme Daily	8	10.2	11.4	15	15.8	17	16.2	15.6	13.2	10.2	9	7		D
Date (yyyy/dd)	1973/26	1971/19	1994/29	1975/29	1988/30	1994/25	1989/10	1974/01	1988/02	1976/14	1971/04	1987/14		
Humidex														
Extreme Humidex	11.3	12.4	17.3	27.4	31.5	34.3	37.4	34.5	32.6	24.9	16.2	11.2		
Date (yyyy/dd)	1993/30	1992/28	1994/30	1977/25	1983/29	1969/17	1960/31	1971/01	1988/04	1980/03	1978/01	1980/15		
Days with Humidex >= 30	0	0	0	0	0	0.1	1.6	1.4	0	0	0	0	3.2	A
Days with Humidex >= 35	0	0	0	0	0	0	0.1	0	0	0	0	0	0.1	A
Days with Humidex >= 40	0	0	0	0	0	0	0	0	0	0	0	0	0	A
Wind Chill														
Extreme Wind Chill	-59.5	-59.3	-48.7	-37.8	-19.9	-6.2	-4.4	-7.8	-18.4	-35.3	-58.3	-53.9		
Date (yyyy/dd)	1969/26	1975/12	1955/03	1954/01	2002/03	1976/01	1999/04	1973/17	1974/30	1984/30	1985/25	1992/30		
Days with Wind Chill < -20	19.9	15.1	9.3	1.2	0	0	0	0	0	0.7	10.6	17	73.8	A
Days with Wind Chill < -30	12.4	8.3	2.9	0	0	0	0	0	0	0.1	3.8	9.6	37.2	A
Days with Wind Chill < -40	5.2	2.6	0.2	0	0	0	0	0	0	0	0.2	3.2	11.5	A
Humidity														
Average Vapour Pressure (kPa)	0.2	0.2	0.3	0.4	0.6	0.9	1.2	1.1	0.8	0.6	0.3	0.2	0.6	A
Average Relative Humidity - 0600LST (%)	73	73.4	73.8	69.3	69	75.6	81.2	84.9	84.1	77.3	78.9	74.4	76.2	A

Temperature	Jan	Feb	Mar	Apr	May	Jun	Jul	Aug	Sep	Oct	Nov	Dec	Year	Code
Average Relative Humidity - 1500LST (%)	69.1	63.8	55	42.6	40.6	47.3	51.3	52.7	53.6	56.9	71.8	71.6	56.4	A
Pressure														
Average Station Pressure (kPa)	93.1	93.2	93.1	93.1	93.1	93.1	93.3	93.3	93.3	93	93	93.1	93.1	A
Average Sea Level Pressure (kPa)	101.8	101.7	101.5	101.5	101.4	101.3	101.5	101.5	101.5	101.4	101.5	101.7	101.5	A
Visibility (hours with)														
< 1 km	14.5	6.5	5.2	2.7	3.3	3.9	7.6	13	14	15.4	25.7	18.5	130.3	C
1 to 9 km	92.4	76.6	59	25.5	16	20.4	18.8	29	31.3	39	82.1	92.5	582.7	C
> 9 km	637.1	595.1	679.7	691.8	724.7	695.7	717.6	702	674.8	689.6	612.2	633	8053.2	C
Cloud Amount (hours with)														
0 to 2 tenths	194.4	169.4	191	180	168.4	150.5	175.6	203.7	172.6	176.6	171.7	185.6	2139.5	C
3 to 7 tenths	147	139.8	170.9	201.5	216.4	229	242.3	220.4	184.1	172.3	143.9	157.5	2225.1	C
8 to 10 tenths	402.6	369.1	382.1	338.5	359.3	340.5	326	319.9	363.3	395.1	404.5	400.8	4401.5	C